SSC-SR-1006

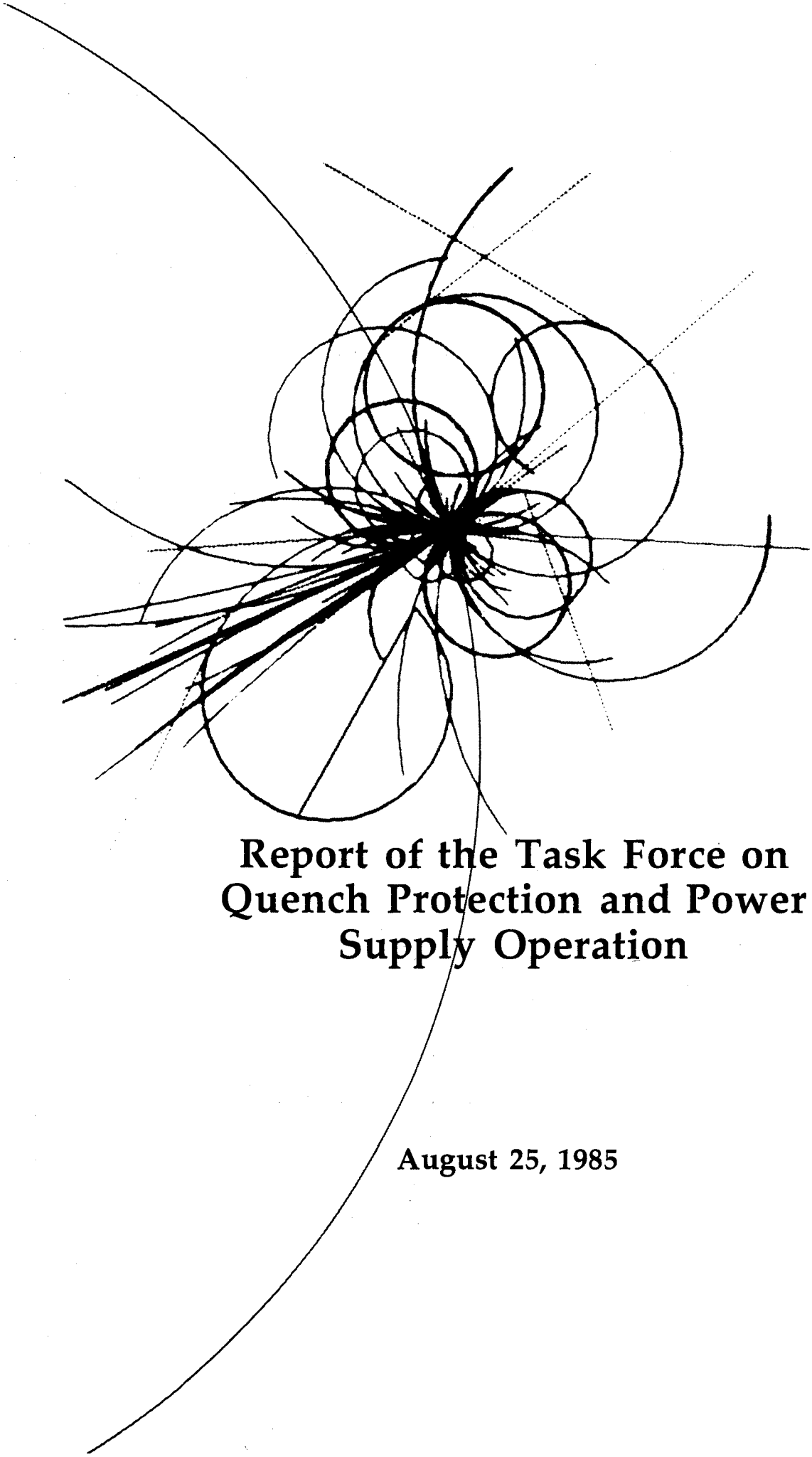

Report of the Task Force on Quench Protection and Power Supply Operation

August 25, 1985

TABLE OF CONTENTS

		Page
I.	INTRODUCTION	1
II.	QUENCHES IN THE DESIGN C MAGNET	3
III.	QUENCHES IN THE 40 MM BORE DESIGN D DIPOLE	13
IV.	POWER SUPPLY CONSIDERATIONS	16

APPENDICES

A. Quench Velocity Measurements on TAC005
J. Zeigler

B. Results From Heater-Induced Quenches of a 4.5 m Tow-in-One Superconducting R&D Dipole for the SSC
G. Ganetis and A. Prodell

C. Quench Computer Analysis for the 3T SSC Superferric Dipole Cold Iron Magnet
G. Lopez

D. Quench Simulation of a 3 T SSC Dipole Magnet
T. Tominaka

E. A Brief Analysis of Quenches in the Three Tesla, TAC SSC Magnets
W. Hassenzahl

F. A Simulation of Quenches in SSC Magnets with Passive Quench Protection
K. Koepke

G. Computer Studies of the Quench Behavior of an SSC Model-Dipole
G. Moritz and W. Hassenzahl

H. Quench Protection for SSC Design D Magnets
J.G. Cottingham

I. Magnet Power Supplies "Appendix 7.2 of SSC-SR-1005"
D. Hartell

J. ACSL Study of Mutually Coupled Loop Regulation for TAC SSC Design
G. Tool and O. Calvo

K. Dipole Power Supply System
J. Zeigler

L. Participants

I. INTRODUCTION

This report presents the results of discussions during and work subsequent to a Workshop on Quench Analysis and Power Supply Operation held at the SSC-CDG on April 1-4, 1985. The major portion of this volume addresses quenches in the Design C and D magnets, as described in detail in Appendices A through H. Some work has been carried out on the power supply operation and the appropriate control philosophy as described in Appendices I through K. Further work will be required for a complete understanding of the quenches and of power supply operation, in particular of the response under transient conditions. A list of participants is included as Appendix L.

The results of the appendices are presented in the main test of the report along with enough of the figures to verify the conclusions. Some of the effort on power supply operation can be found in the Commissioning and Operations Workshop report, SSC-SR-1005.

The first topic is the analysis of quenches in the Design C, superferric magnet in Section II. Analysis using four different programs are presented, and the differences, which are in some cases significant, are discussed. The detailed results of each of these programs are presented in Appendices C through F. In addition, subsequent to the workshop, quench velocities were measured on a 1-m long Design C magnet at the Texas Accelerator Center (TAC). The results of these measurements, which form the basis of much of the input to the analysis of the type C magnets, are given in Appendix A. When longer magnets are tested, it will be instructive to induce quenches to determine if our extrapolations from 1-m models are correct.

Quenches in the Design D magnets are considered in Section III. These have been evaluated with three different computer codes. Again, the results are quite similar when the initial hypotheses are the same; however, there is

some disagreement as to the exact initial conditions that should be used for the calculations.

In general, slower initial quench velocities give higher temperatures. At present, the only quench data are on 1-m models of Designs C and D, a 4.5-m long, 30 mm bore magnet, and short samples. Additional data on quenches in longer model magnets are recommended to aid in further extrapolations of these results to full-scale magnets. At this point it should be noted that the quench data on the Design C magnet were taken subsequent to (in fact the effort was stimulated by) the April 1-4 workshop, and the results have considerably lowered the expected quench temperature. The major issue is the number of diodes required for passive protection. Eventually a tradeoff between passive and active protection will have to be made after the diode requirement for passive protection is established precisely. At present, the group is leaning toward the use of a passive protection system for both magnet designs because of the inherent reliability and simplicity relative to the active protection system.

Simulations of the transient response of the two principal magnet types, Designs C and D are described in Section IV. The preliminary analysis considered the elements as lumped circuit elements using the program SPICE. Some part of this effort has been reported elsewhere and is included here as Appendix I. Subsequent efforts have been to try to understand the implications of the transformer coupling in the Design C magnets on the current regulation limits and the effects of the delay line character of the magnet strings on the use of differential transductors to insure tracking between the 12 sectors of the ring. A simulation program, ACSL (Advanced Continuous Simulations Language), has been used to model the coupling (see Appendix J). A preliminary report of the new Design C power supply is given in Appendix K. In this design, at present, the trim coil will quench during a dump because of

excessive dI/dt due to transformer coupling. The increased thermal load on the cryogenic system implies longer recovery times. Because of the lower inductance of the design C magnet, the delay time from the power supply to the far end of a quadrant in the new design is comparable to the delay time of a sector (1/12) of Design D.

II. QUENCHES IN THE DESIGN C MAGNET

The Design C magnet is shown in Figs. 1 and 3 of Appendix A, and the conductor is shown in Fig. 3 of Appendix F. The three coils are independently powered in such a way as to produce a uniform field across the bore for all beam energies. These coils are magnetically coupled so that when the current in one changes rapidly a voltage will be induced in the others. Of course, the induced current will depend on the external connections of the magnets, the number and placement of diodes, the cause for the initial voltage variation, etc.

Recently, some quench velocity data have been obtained on the Design C magnet. These data are used in the quench analysis and are described in Appendix A. The critical observation is the rather slow propagation of the quench from turn-to-turn and coil-to-coil. The slow transition times are a result of the insulation, which, at 0.008 inches of Kapton, is much thicker than that used in the other proposed SSC dipoles.

The Design C conductor, which is described in some detail in the Appendices, contains solder that melts at about 500 K. There is some concern for the long term safety of a magnet in which the solder melts repeatedly during

* During the tests of the ISABELLE magnets, which were made with a braided conductor saturated with solder, some spectacular low-temperature burnouts were observed. These coils were not insulated as throughly as the present generation of magnets so the experience there may not be relevant. However, these results do suggest some caution in the use of solder.

quenches. Because there is little experience* with this situation, we cannot be certain there is a problem. On the other hand, until some hard data are available in terms of many quenches on a long coil where the solder can be forced to melt, there can be no assurance that the system will be safe. The prudent course to follow at present is to choose a magnet length and protection scheme that will give a maximum temperature that is below 500 K for the worst case quench.

Here we consider the temperature during a quench, and its variation with length, for several different cases. A simple analysis of the temperature development for a single coil is described initially. Then a more complicated analysis that includes the mutual inductances among the three coils is presented.

The Design C magnets are 105-m long and consist of three 35 m long sections. Because of the double conductor thickness in the joints at the ends of the magnet sections, and near the diode, quenches are not likely to propagate across these regions. The doubling up of the conductor in a long joint tends to reduce the quench velocity considerably. Theoretically the ratio would be on the order of

$$v_{joint}/v_{wire} = \frac{C_{wire}}{C_{joint}} \cdot \sqrt{\frac{T_{marg\ wire}}{T_{marg\ joint}}} \cdot \varepsilon$$

where the C's are the specific heat per unit length, is a number less than 1 and reflects the expected resistive heating in the joint, and the T_{marg} are the temperature margins for the two regions. The net velocity ratio can easily be as high as 5. As a result, the propagation in this region is so slow that the involvement of a second 35 m length of magnet in a quench can only be relatively minor. Further, this dramatically affects the maximum temperature,

which is set, in essence, by the part of the volume of material that goes normal in the first 200 ms or so. If a quench begins near one of these joints, it will only propagate in a single conductor and in only one direction for a significant length of time.

Aside from a possible quench near the end, the worst case condition for the Design C magnets is a quench that starts in the outer coil along the straight section. Only two conductors of the outer coil are involved significantly in such a quench, at least until very late, around 300 ms or so. As a result, it is possible to analyze the quench as if only two conductors participate and to obtain a reasonable estimate of the energy deposited if the effective inductance of the outer coil alone is used.

The temperatures for the outer coil quenches using the single coil version of the computer program QUENCH are shown in Fig. 1 as a function of time for four different magnet lengths. These curves suggest that, with some reservation, magnets up to about 100 m long could be safe with a single-diode, passive protection system. The temperatures calculated by QUENCH may be low because the magnetic coupling among the coils are not included.

For a more complete analysis of the quenches in the superferric magnets, we need to include the mutual inductances of the three different coils and the effect of quench propagation from one coil to another. This propagation occurs both by thermal effects in the case of the inner and outer layers, and inductively for the trim coil. Details of the circuits and solutions are given in appendices C, D, and F, and a summary is given below.

The circuit for the 3 T superferric, Design C magnet is shown in Fig. 1 of Appendix C and is described in detail in Appendix K. The values of the self and mutual inductances vary with field due to the saturation of the iron. These inductances are given at several field levels in Table 3 of Appendix D.

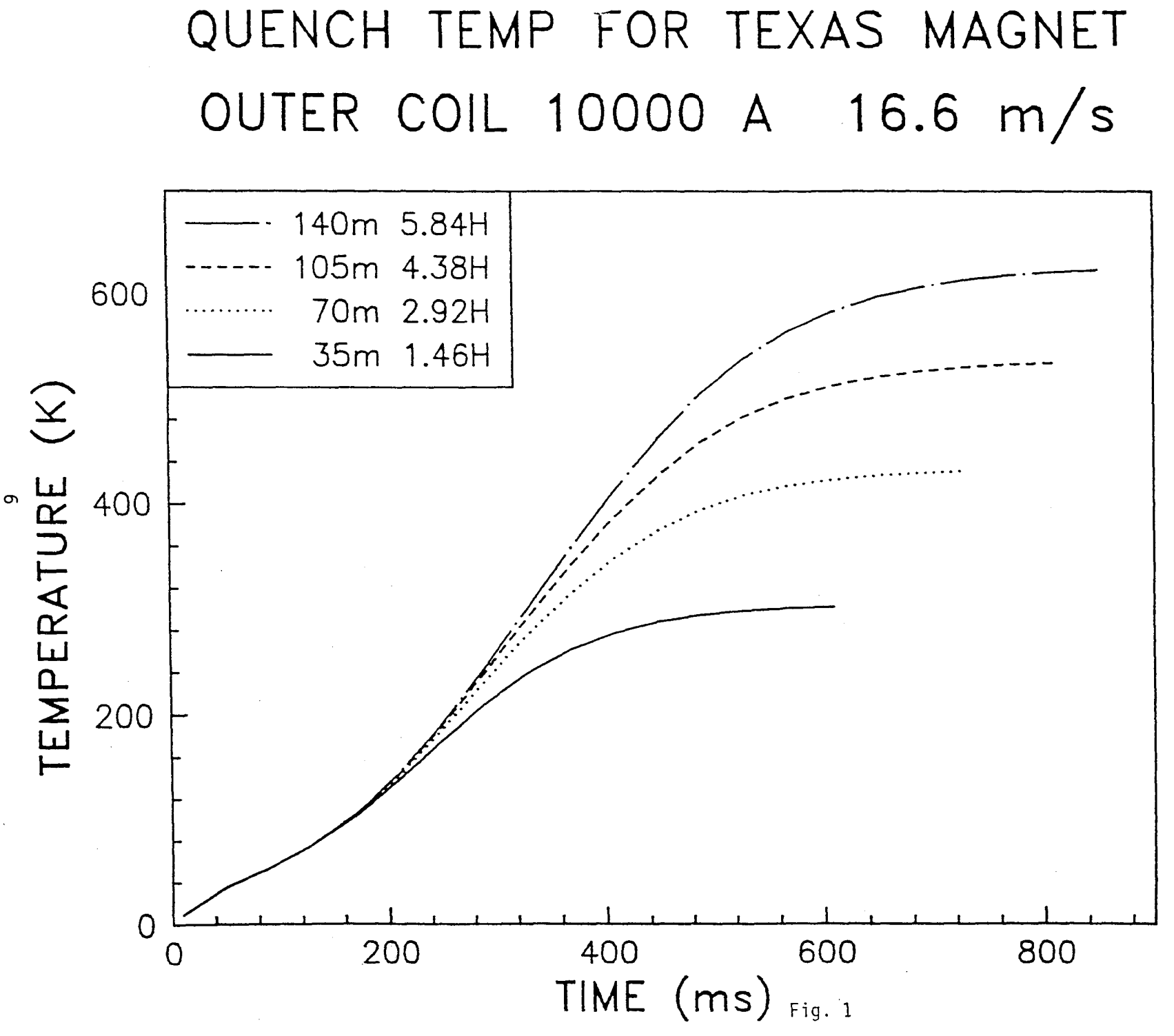
QUENCH TEMP FOR TEXAS MAGNET
OUTER COIL 10000 A 16.6 m/s
140m 5.84H
105m 4.38H
70m 2.92H
35m 1.46H
TEMPERATURE (K)
0
200
400
600
0
200
400
600
800
TIME (ms)

Fig. 1

Using the inductances at peak field gives an erroneously low value of the total stored energy, and thus predicts a low temperature.

The computer code SSC* models the individual conductors of the SSC superferric magnet and includes transitions of the quench from conductor to conductor and from coil-to-coil. It does not model a general coil with some averaged parameters as does QUENCH. Rather it requires a specific description of the inductor and then calculates the temperature accordingly. (Note that the estimate of temperature along the conductor assumes that thermal conductivity dominates the temperature development whereas the program QUENCH assumes that thermal conductivity is zero.) The SSC* code probably gives a slightly low peak temperature because of this assumption.

The development of the three currents in the superferric design as estimated by the computer code SSC* are shown in Fig. 2 for a quench that begins in the outer coil. A similar set of currents for a quench that begins in the inner coil are shown in Fig. 3. In both cases, the entire trim coil is driven normal fairly early in the quench due to inductive coupling, and reaches a modest temperature.

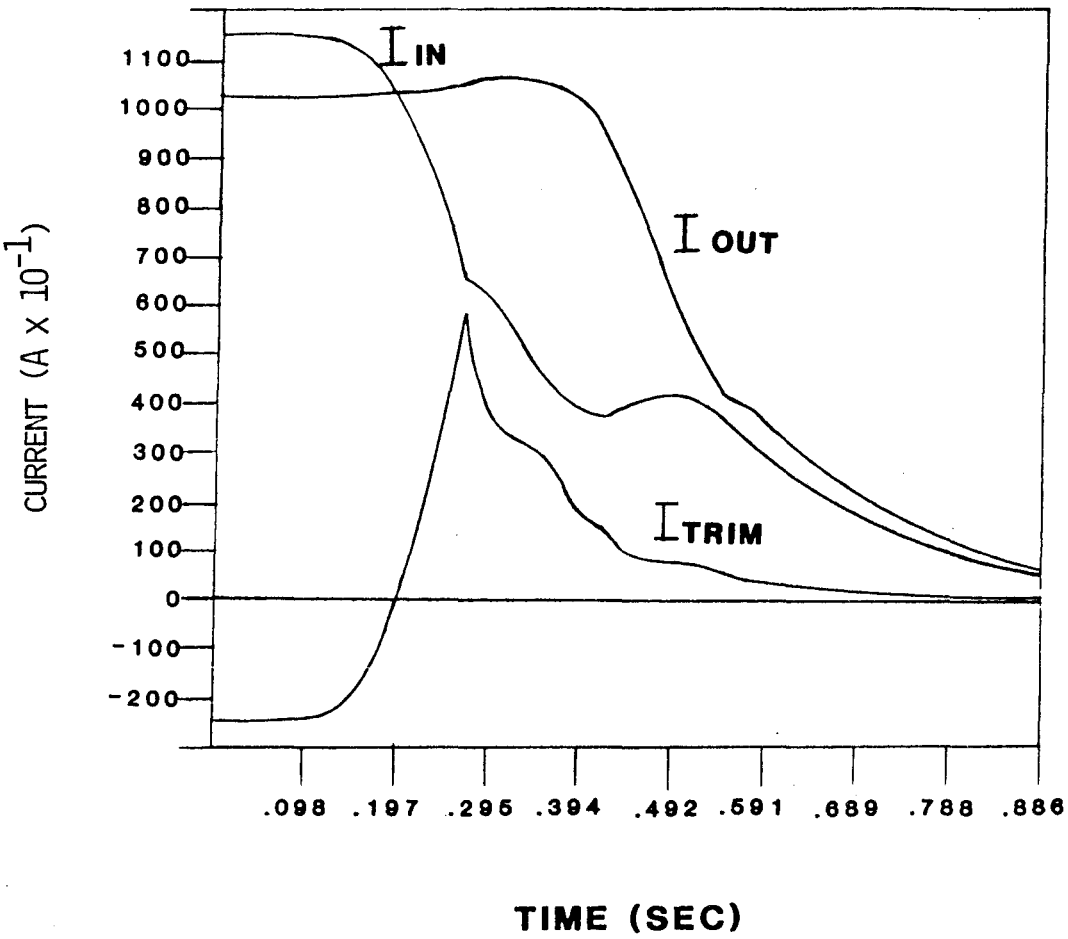
CURRENT (A x 10^-1)
1100
1000
900
800
700
600
500
400
300
200
100
0
-100
-200
I IN
I OUT
I TRIM
.098
.197
.295
.394
.492
.591
.689
.788
.886
TIME (SEC)

Fig. 2

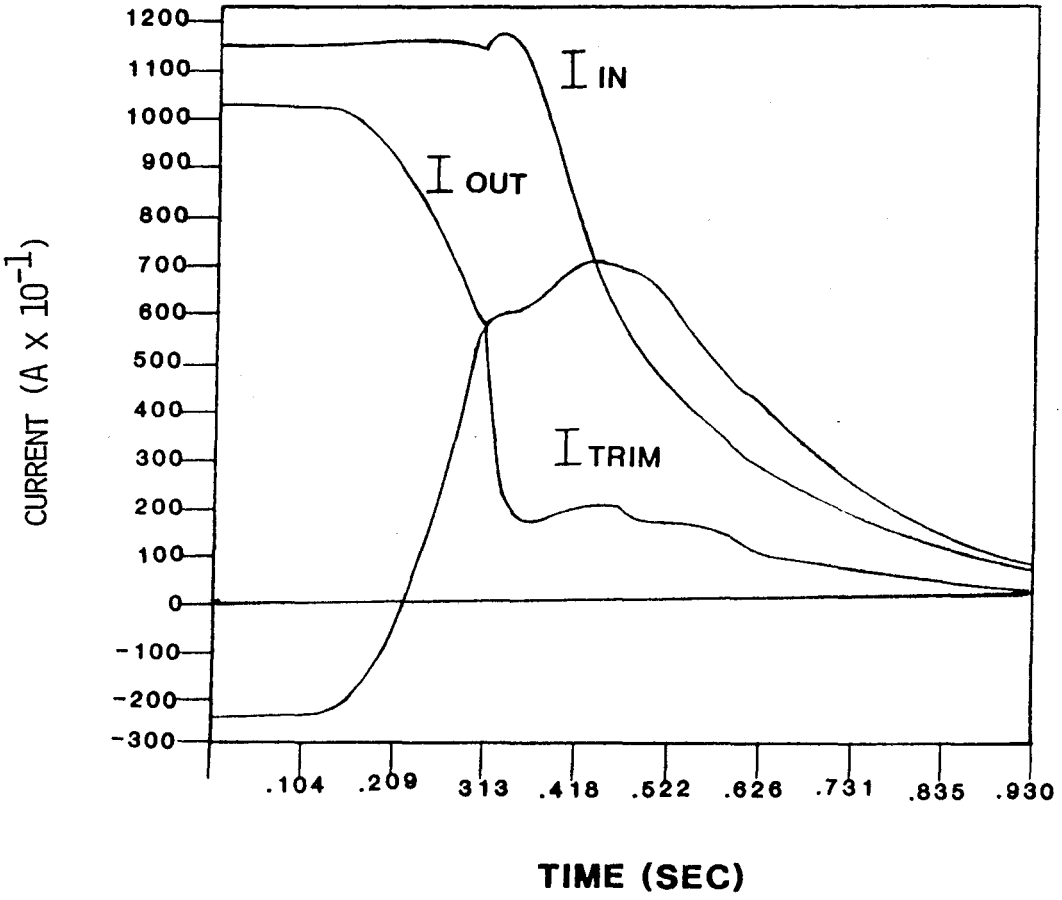
1200
1100
1000
900
800
700
600
500
400
300
200
100
0
-100
-200
-300
CURRENT (A x 10^-1)
I IN
I OUT
I TRIM
.104
.209
313
.418
.522
.626
.731
.835
.930
TIME (SEC)

Fig. 3

Two effects cause the trim coil to quench more rapidly when the inner coil quenches than when the outer coil quenches.

The first is the fact that all four turns of the inner coil become involved in a quench, so that dB/dt is greater.

The second is the closer coupling between the trim and the inner coil than between the trim and the outer coil.

Note that the mutual inductances used as input to in the program SSC* are the same between the trim and both main coils so this effect is not included.

One version of the computer code QUENCH is capable of simulating quenches in inductively and thermally coupled systems. This code has also been used to model quenches in the Design C dipoles as described in Appendix D. A plot of one of these quenches is included here as Fig. 4 because the variation of temperature with time is shown along with the currents. Note that the currents in the quenched coil are shown as dashed lines while the currents in the rest of the magnets in the string are shown as solid lines. These magnets are discharged into the dump resistors and the current in them decays much more slowly.

The discussion above describes quenches that occur in the body of one of the 35 m long coils that make up the Design C magnet. If a quench begins at an end, either between 35 m sections, or at a diode, there will be a delay of the propagation into other turns. This delay will result in a higher temperature and is probably the true worst case condition.

An estimate of peak temperatures is described in Appendix F for quenches that start in different regions of the superferric magnet. These are based on a computer code TMAX and are summarized in Table I. This computer code models each conductor in much the same fashion as the code SSC*. However, the

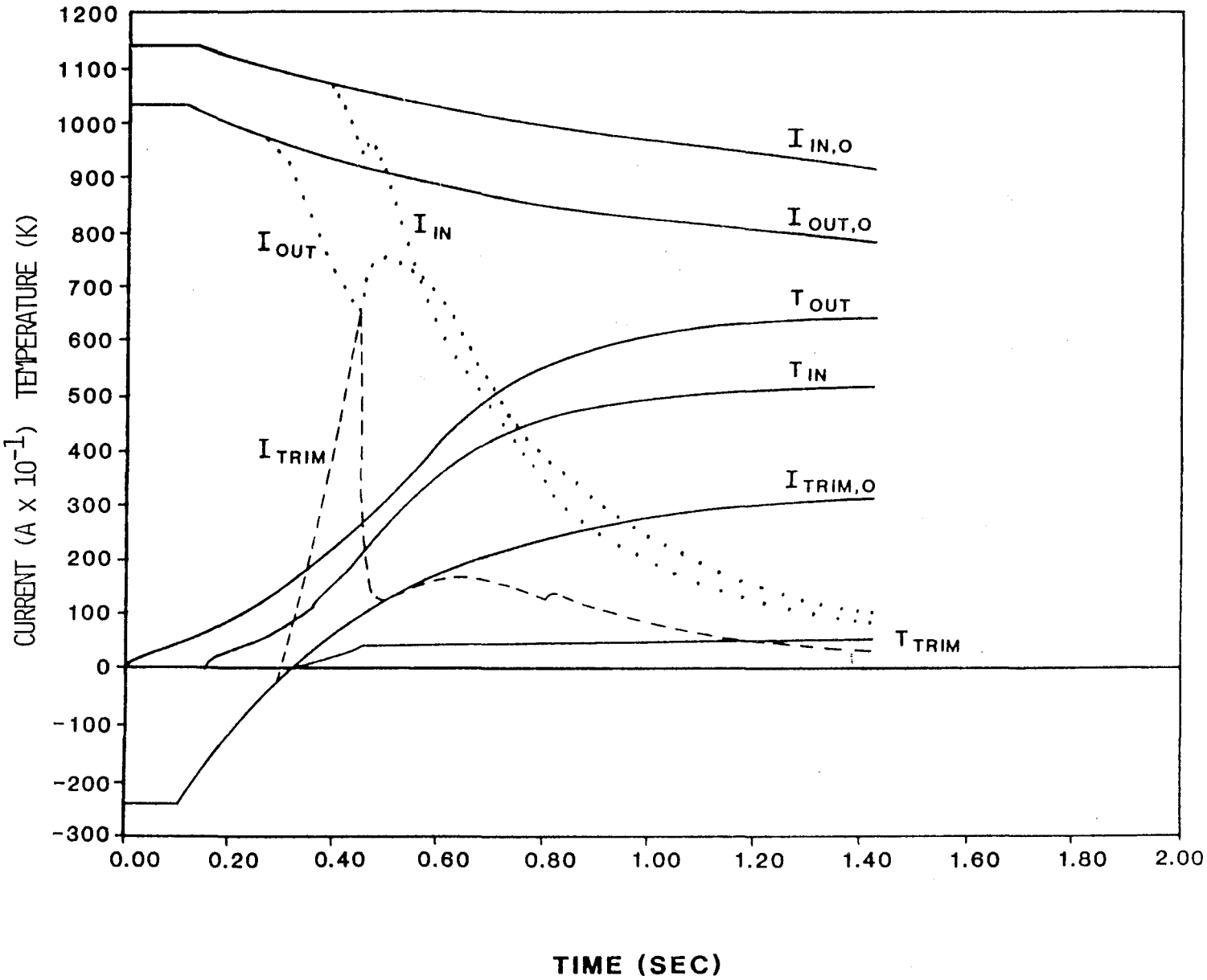
1200
1100
1000
900
800
700
600
500
400
300
200
100
0
-100
-200
-300
CURRENT (A x 10^-1) TEMPERATURE (K)
0.00
0.20
0.40
0.60
0.80
1.00
1.20
1.40
1.60
1.80
2.00
TIME (SEC)
I IN,O
I OUT,O
I OUT
I IN
T OUT
T IN
I TRIM
I TRIM,O
T TRIM

Fig. 4

turn-to-turn propagation time and the quench velocity are inputs to this code rather than being calculated. To the extent that empirical data is better than the theoretical estimates, a point which is debatable at this time, this code should give the best results. We are still not certain of the exact values of the quench velocity and the turn-to-turn propagation times in a long coil, even though we have some data from tests on shorter coils.

Table I

Peak Quench Temperature in the 3T Superferric Magnet

Length (m)	Peak Conductor Temperature (K)			
	Outer	Outer End	Inner	Inner End
140	796	1050	799	981
70	520	679	529	648
35	355	457	365	446
	Δt = 90 ms		Δt = 70 ms 3rd & 4th turn at 140 ms	

III. QUENCHES IN THE 40 MM BORE DESIGN D DIPOLE

The Design D magnet is shown in cross section in Fig. 5. As for the Design C magnet of the previous section, the quench phenomenon in this coil has been studied with several programs and for several conditions, such as temperature, number of diodes, critical current of the conductor, etc.

The critical question to ask of a quench in the Design D coil is what is the maximum temperature reached by the conductor. Because there is no solder in this conductor it can be expected to safely reach some higher temperature, say 800 K. Some magnets have even been tested and showed no apparent damage after having experienced local quench temperatures of 800 to 900 K. However, it is not clear that this temperature range is acceptable for a coil that is operated over a long period of time and is subjected to many quenches. The ultimate temperature the coils can withstand for a few quenches, which may occur anywhere in the SSC, may be higher than is possible in those coils that may be frequently quenched during a beam dump or due to beam excursions near interaction regions. At present, we can only guess at the effects of multiple quenches on magnet performance. A conservative approach is recommended here, with a relatively low temperature, 700 K or so, considered to be acceptable.

Those quenches induced by beam dumps are likely to involve a large portion of the magnet rather than the small regions that the worst case quench calculations suggest. In fact, the beam will likely cause an extensive area to be heated close to the critical temperature before one spot goes normal. The resulting velocity of quench propagation may be 3 to 10 times higher than the worst case estimates. As a result, the final magnet temperature in these "susceptible" regions may only be 400 to 500 K, rather than 700 to 800 K. The life expectancy in this case would be improved considerably.

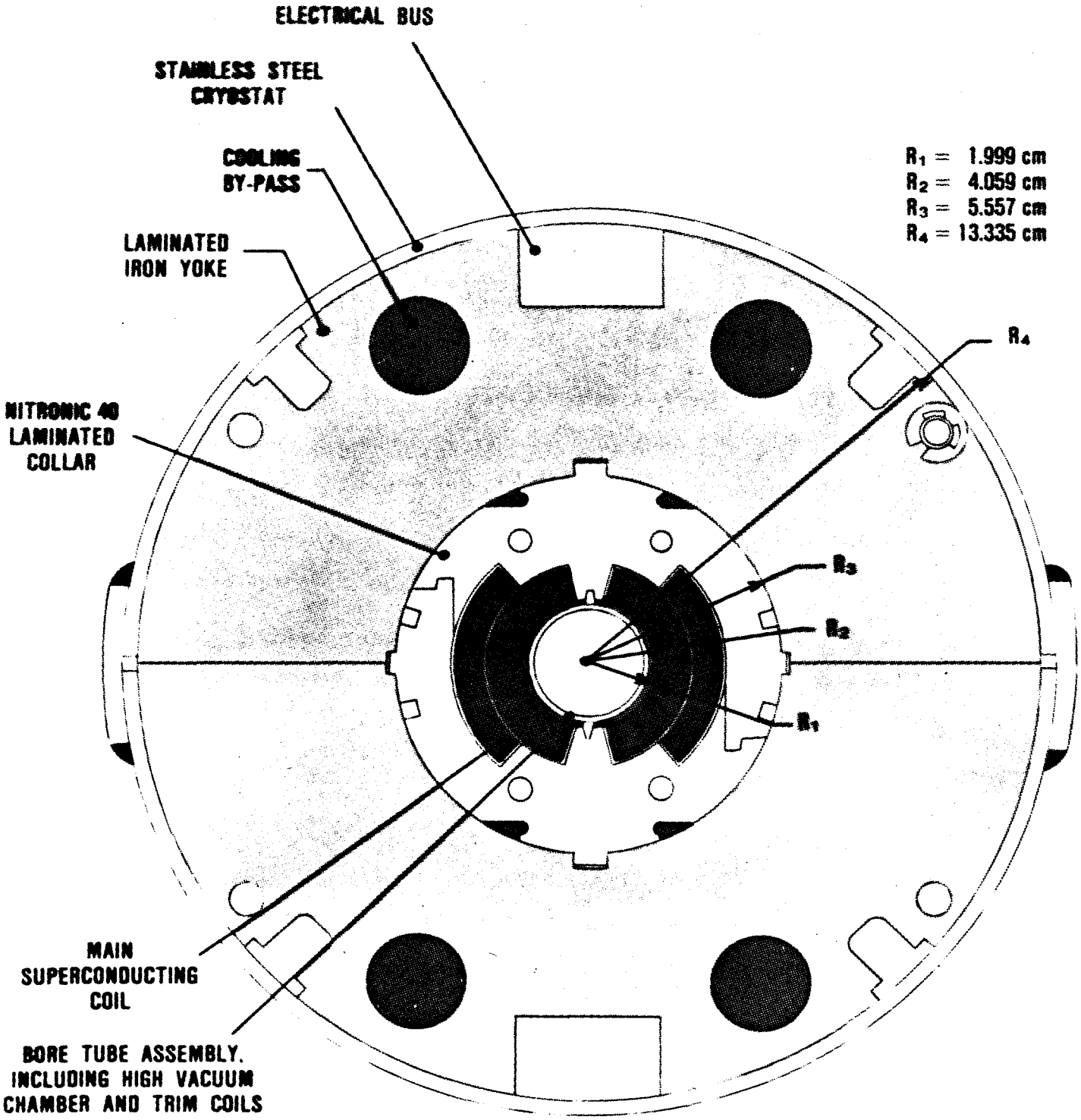

Fig. 5. The new type D magnet, is essentially a one-bore version of the evolved Design A.

The effect of operating (not peak) current on quench temperature has been observed for some CBA magnets. Quenches near short sample, which have high-quench velocities, generate lower peak temperatures than those occurring at 70 to 80% of short sample, (see Appendix G). These conditions can be compared to calculations of CBA quenches and then used to predict the results of quenches in magnets of different designs and having different conductors.

Not all models of the quenches give the same results. We compare below some different predictions that give different results. These comparisons are summaries of results described in detail in Appendices F, G, and H. The major causes of the differences in final temperatures are the different input conditions, in particular quench velocities and the resistivities of the copper.

Data taken on LBL developed inner coil conductor, in a short sample apparatus at BNL, gave a velocity of 9.18 m/s at 6 T and 5900 A. Data on training quenches in a model dipole at LBL for this same conductor gave velocities for similar, but not identical, conditions of current and field of about 25 m/s. The latter velocity is in agreement with other "in situ" measurements and also with the formula used in the program QUENCH. The short sample data is suspect, but it cannot be ignored. This difference in velocity, with all other characteristics held constant and using a single diode per dipole, leads to a very different ultimate temperature for a given magnet length. A conservative approach, if one is to base the protection system on the slow velocity, would be to put two or four diodes in each magnet rather than one.

One possible suggestion for a 16.6 m magnet is to have 4 small diodes, one across each quarter of the coil and to have 1 large diode across the total magnet. These would all be in a single heat sink. The small diodes would

never carry the entire current, and, by mechanically connecting the diodes together, only one heat sink is needed. This heat sink must be sized for the single diode protection system.

Some calculations that are based on the higher velocity, about 25 m/s, are shown in Fig. 6. This prediction is from Appendix G. An even lower temperature is given by an extrapolation from 30 mm bore, 4 m dipole test data, Appendix H. The lower quench velocity of 12 m/s, gives an unsafe temperature for Design D dipoles longer than 4 m if only one diode is used. This result is described in Appendix F.

The conclusions one can draw from these calculations is that the Design D dipole will be safe with a passive protection scheme at some length and with some indeterminate number of diodes. Additional measurements, in particular on long magnets, will be needed to select the appropriate length and number of diodes needed for protection.

IV. POWER SUPPLY CONSIDERATIONS

Simulations of the transient response of the two principal magnet types, Designs C and D, as lumped circuit elements were carried out during the week of the workshop using the program SPICE running on the VAX used by the CDG. During this time the main focus was on understanding the magnet systems as circuit elements. The voltage waveforms required for a linear field ramp from 1 TeV to 20 TeV in 1000 seconds were generated for the designs.

As expected, Design D had no surprises. The transformer coupling of the three separate windings for the Design C requires larger voltages to compensate for the mutual inductance between the windings and, in the case of the trim winding, a +20 V power supply capable of currents from -3 kA to +3 kA. This latter power supply provides an interesting design challenge. The main conclusions of this workshop have already been presented as Appendix 7.2

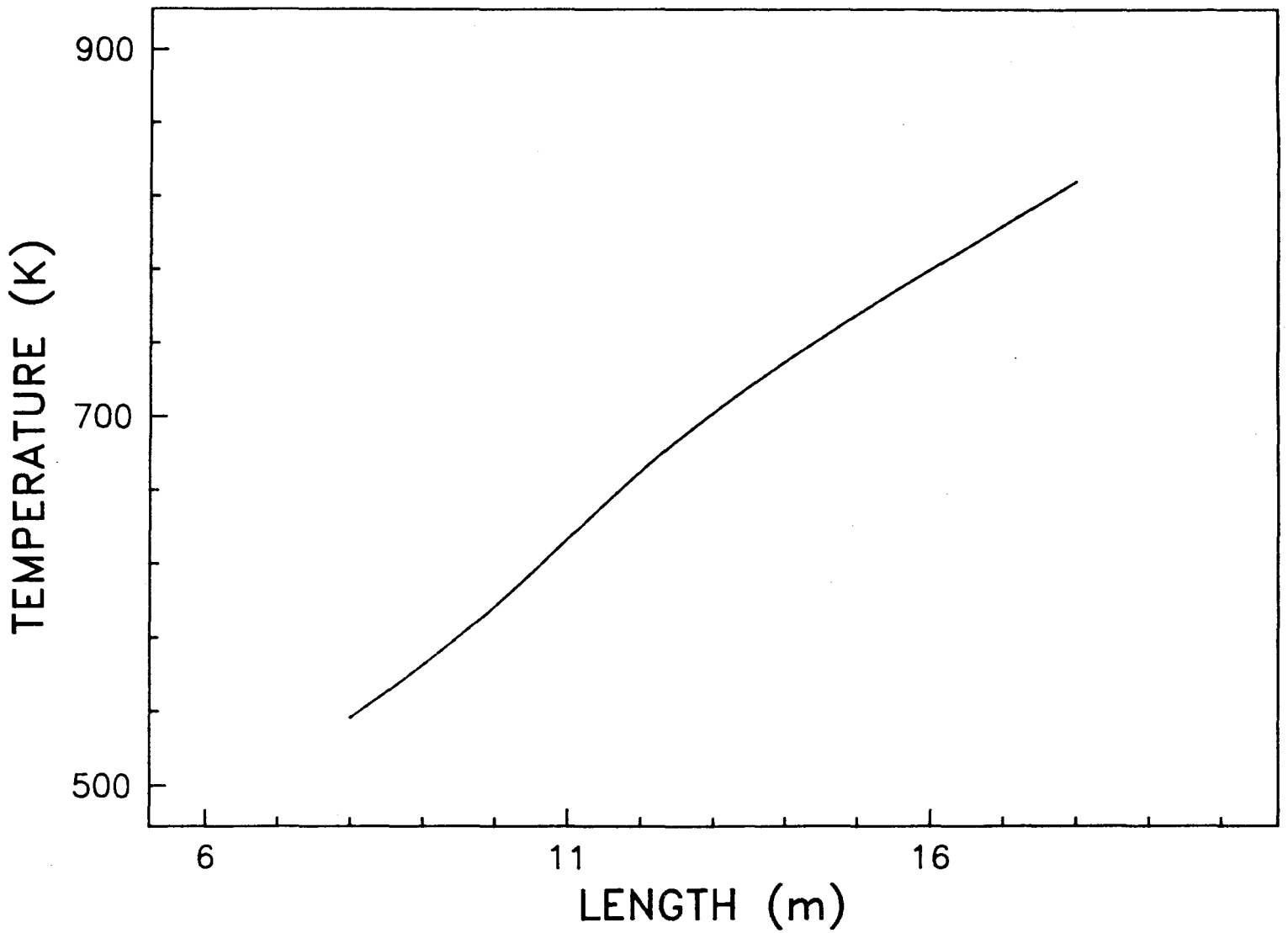

XBL 852-1277

Fig. 6. Peak temperature as a function of magnet length for 5000A quenches.

of the Report of the Task Force on SSC Commissioning and Operations (SSC-SR-1005), which is included here as Appendix I. This Appendix, along with the original Reference Designs Study, gives an overview of the magnet power supply system for the SSC.

Since the workshop, the efforts of the group have been to try to understand the implications of the transformer coupling in the TAC design concerning the limits on current regulation and to understand the effect of the delay line character of the magnets in using the differential transductor approach to insure tracking between the 12 sectors of the ring. A simulation program, ACSL (Advanced Continuous Simulations Language), was used to model the coupling. In this process it was necessary to make a first pass design of the regulator loops for one sector of Design C. The preliminary report of this work is given in Appendix J.

In response to the observation that there was substantial power consumption in the room temperature components of the output filter networks in the high current power supplies proposed for the original design C circuit, that supply has evolved into a 4-sector circuit, which reduces power consumption by a factor of 3. A preliminary report of the new Design C power supply is given in Appendix K. This new design has not received the same level of scrutiny as the previous design and Design D. In particular, with the present choice of dump resistor values, the trim coil will quench because of excessive dI/dt due to transformer coupling during a dump. The increased thermal load on the cryogenic system implies longer recovery times.

Little progress has been made in actually simulating the effect of the delay line character of the magnet system on the tracking of the magnetic field in the different sectors of the ring. Because of the lower inductance of the design C magnet, the delay time from the power supply to the far end of

a quadrant in the new design is comparable to the delay time of a sector (1/12) of Design D.

As mentioned above, two simulation programs were used to study the proposed SSC magnet power supply characteristics. The program SPICE has been around for many years and simulates the response of an arbitrary network made up of linear discrete components. The lumped constant equivalent circuit of an SSC 6 T magnet half cell is shown in Fig. 7. The transient response of a sector of 6 T magnets to a voltage step at the power supply is shown in Fig. 8.

The program ACSL was used to understand the dynamics of the coupled regulation loops within a sector of Design C magnets. It is much more powerful than SPICE and can handle linear, nonlinear, and discrete step digital systems simultaneously. The problem to be solved can be formulated by specifying either: (1) the complete set of differential equations, (2) the set of state vectors (variables and their first derivatives) and the system transform matrix, or (3) the Laplace Transforms for all the elements connecting the system variables. The studies outlined in Appendix J specified the problem by using the Laplace Transform approach. The model for the Design C three current regulator is shown in Fig. 9. The transformer couplings of the three windings are included in the output by the appropriate Laplace Transforms. In these coupling studies, the transmission line behavior of the magnet string was ignored, i.e., the load was assumed to be an inductance with a time constant T_E. After the model is set up. the program then finds the time response of the system by numerical integration starting from the specified initial conditions. As a check of the programs, the transient response to a voltage step at the output of the power supply of one of the windings was calculated both by ACSL and SPICE and the results agreed. As a further check,

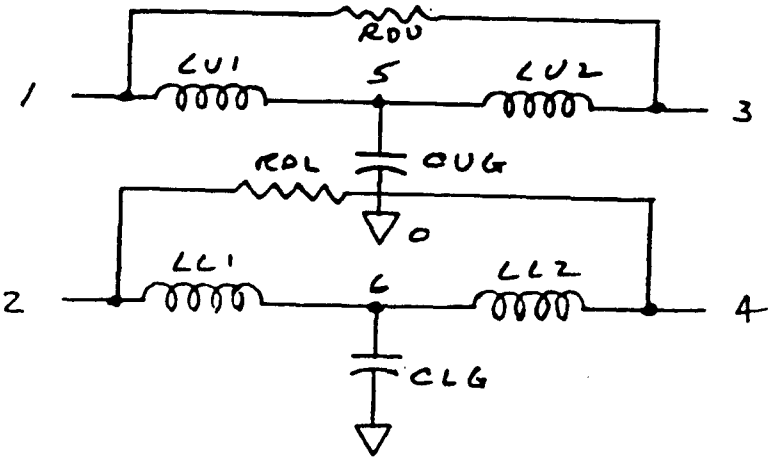

Fig. 7. Lamped Constant equivalent circuit for a SSC, 6T magnet.

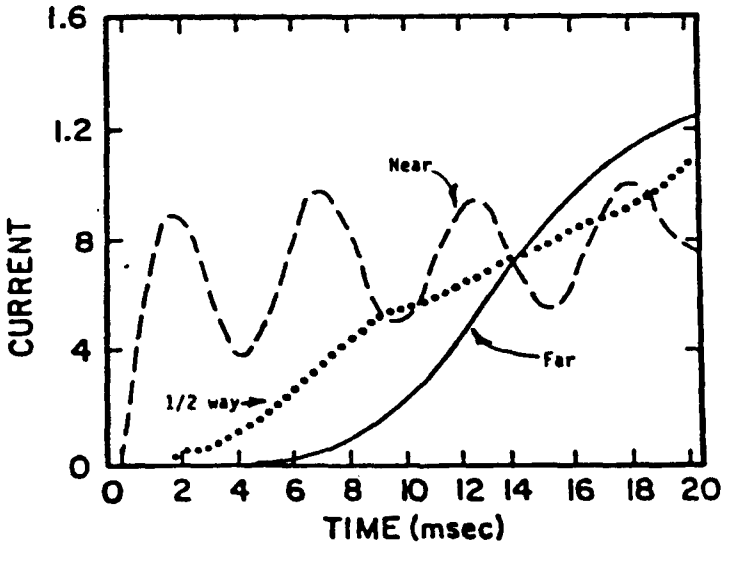

Fig. 8. Transient Response of 6 T magnet sector to a power supply voltage step.

the Tevatron power supply was modeled and the performance predicted by ACSL agreed with the empirically observed regulation level, stability margin and transient response of the accelerator magnet system.

The results presented in Appendix J illustrate the coupling problem of the superferric magnet by applying an appropriate voltage step at the voltage program input to give a 1 V step at the output of the power supply. The gains for the forward current amplifiers and the forward voltage amplifiers were determined by a lengthy trial-and-error effort looking for stable solutions.

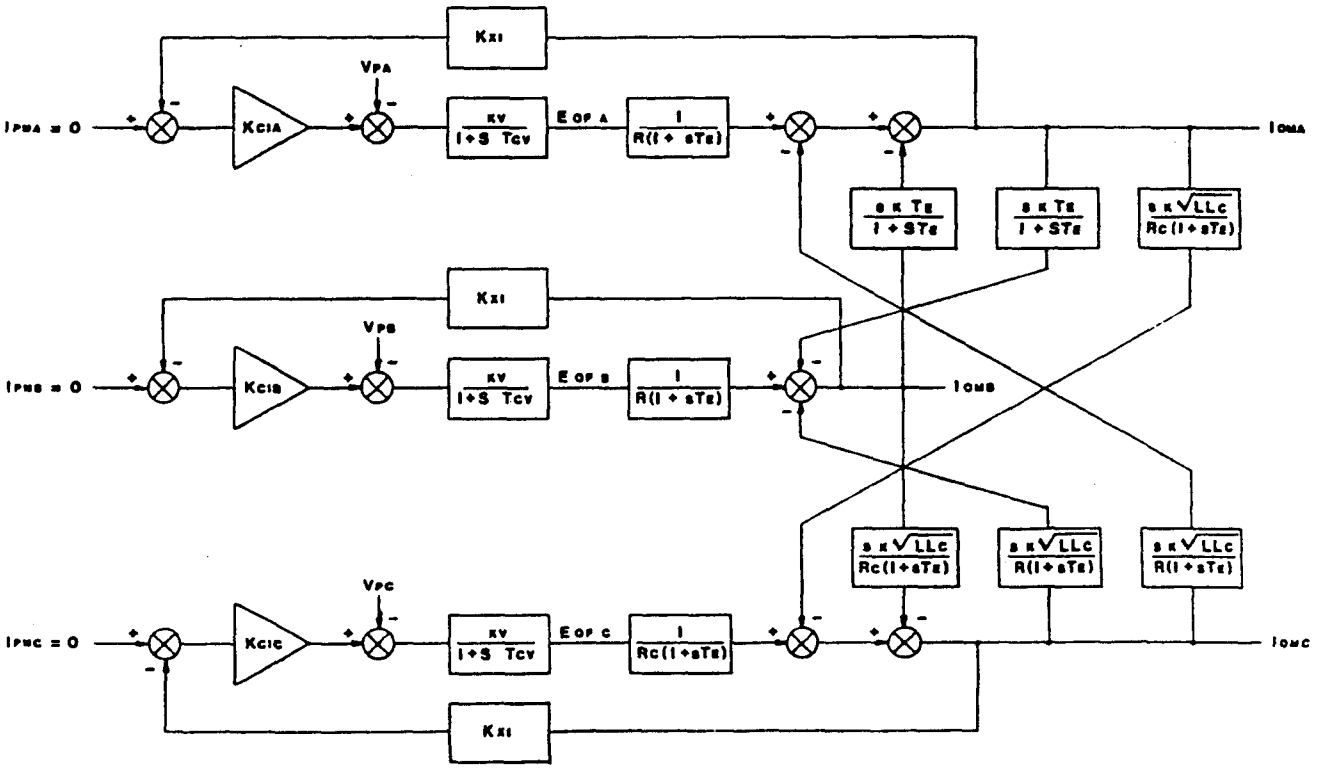

Fig. 9. Regulation loops for the 3T magnet power supply.

The values noted on the graphs in Appendix J represent the maximum gains that do not lead to oscillations. Lower gains lead to poorer regulation and a larger current error. As can be seen from the graphs in Appendix J, a 1 V step leads to 10 mA peak current pulses in the other windings. Experience with the Tevatron power supply indicated that 80 V steps, which would scale to 8 to 10 V steps for this power supply, are not uncommon due to SCR misfiring, for example. This variation would lead to 100 mA current pulses or current errors at the 10^{-5} level due to coupling. It is possible to compensate for the coupling by including a compensation network at the power supply output. A two winding example (Appendix J) shows that the effect of the coupling can be reduced by at least an order of magnitude making it negligible in comparison to other sources of regulation error. The penalty paid for this solution is added power dissipation in room temperature components and a higher output voltage requirement for the power supply.

The other distinction between the 6 T and 3 T magnets from a power supply point of view is their different transmission line characteristics due to their different inductances per unit length. The 6 T magnet has a larger inductance per unit length and the propagation velocity of signal along the magnet string, which acts as a delay line, is smaller, leading to larger delays. Because of time limitations, and our feeling that addressing the transformer coupling problem was more important, little progress has been made in determining the details of this delay line characteristic on the level of the entire ring. It should be noted however that this behavior is well understood and completely reproducible so that feed-forward techniques using smart regulators can reduce the tracking error to the negligible level. The next modeling project should be to demonstrate that this form of regulation will function in a real system.

The main conclusion at this point with respect to the power supply systems is that acceptable designs can be made for both the superferric (3 T) and the design D (6 T) magnets. It appears possible to build power supply systems that will provide the necessary part-in-10^5 regulation and tracking accuracy using present day techniques. There will be operational differences having to do both with the complexity and the current levels required by the two different magnet types. The 6 T magnet power supply, since it provides only one current at 6 kA, is somewhat simpler and thus will be cheaper to operate.

APPENDIX A

QUENCH VELOCITY MEASUREMENTS ON TAC005

6/19/85
JCZ

QUENCH VELOCITY MEASUREMENTS ON TAC005

A series of quenches was initiated with a heater installed in dipole magnet TAC005 to study its quench properties. This dipole is a 1m 1-in-1 prototype using the three coil design optimized to eliminate sextupole and decapole error components. The quench response of this multi-coil magnet must be understood to verify that the proposed passive quench protection scheme is feasible.

The cross-section of TAC005 in Figure 1 shows the turns corresponding to the inner, outer, and trim coils. A top view of the outer coil in Figure 2 shows the placement of the heater and voltage taps used in the quench velocity measurements. Since these components were retrofitted to an existing magnet, they were only added to the outer coil to minimize the amount of disassembly required. Thus, their placement allowed the measurement of longitudinal and transverse quench velocity in the outer coil only. The field values in Figure 3 show that the heater was placed on the conductor that is in the lowest field region in the coil assembly. Thus, the quench velocities measured in this test are the minimum values which may be expected for this magnet.

The quenches were initiated by firing a Minco thermofoil heater taped to the outside of the superconductor. Since the heater was installed in a retrofit operation, the Kapton insulation on the conductor was not removed. Thus, the heat produced by the thermofoil heater had to travel through four layers of Kapton tape, a total of 0.008 inches. All quenches were initiated by passing a 0.58 amp current pulse through the 10 ohm heater. The length of the current pulse was varied to produce the minimum amount of heat required to initiate a quench. In some instances multiple pulses were required before the conductor was quenched.

The quench measurements were performed with the test circuit shown in Figure 4. This configuration was chosen for safety considerations rather than to provide proper dipole field quality. The design currents for the inner and outer coils are roughly equal at high fields, so the test circuit provides a reasonable approximation for the outer coil under those conditions.

Each measurement consisted of initiating a quench with the heater and then monitoring the voltage taps to determine the rate of quench growth. The automatic quench detection circuitry was prevented from tripping the power supply so that the full current could be maintained until the quench resistance forced the power supply to its voltage compliance limit. During the quench development, the power supply current and the voltage between each pair of taps were recorded on a strip chart recorder. These oscillographic traces were then analysed to determine the time delay between the quench inception and the appearance of quench resistance between each pair of voltage taps.

A series of quenches was initiated at coil currents of 9 kA, 7.5 kA, and 5.0 kA. Figure 5 lists the time required for the quench to propagate from the heater location (tap 6) to each of the other tap locations for each test. The table also lists the corresponding average quench velocities calculated by using the distance between the center points of the voltage tap pairs listed in the path. For the tests run at 5 kA, the path notation "(6-) 3-4" denotes the quench velocity from tap 3 to tap 4 after the time required for transverse propagation from tap 6 to tap 3 has been subtracted.

In general, the quench velocity in the conductor outside the laminations (6 - 5) was faster than the quench velocity in the conductor inside the laminations (6 - 7). The first test was the exception, but it was run at a bath temperature of approximately 4.42 K as compared to approximately 4.44 K for the remaining tests. Thus, the extra cooling on the exposed end blocks may have slowed the quench velocity around the end during the first test.

The dependence of longitudinal quench velocity on coil current for each of the propagation paths is shown in Figure 6. Due to the short length of the magnet, the propagation path from tap 6 to tap 4 changed as a function of coil current. At high currents, the quench propagated from tap 6 around the end of the magnet to tap 5, down the inside turn on that side, and around the far end of the magnet to tap 4. At lower currents, however, the quench propagated transversely from tap 6 to tap 3 and down the inside turn to tap 4. As expected, the quench velocity in the inside turn is much higher than in the outside turn since the conductor is in a higher magnetic field. As a comparison, the quench velocity in the outside turn (6 - 7) is approximately 6.5 m/s at 5 kA while the quench velocity in the inside turn (3 - 4) is approximately 9.4 m/s at the same current.

The transverse quench propagation time is shown in Figure 7 as a function of coil current. The propagation times range from approximately 115 ms at 9 kA to approximately 250 ms at 5 kA. These relatively long propagation times are due to the .016 inch layer of Kapton insulation between conductors.

The quench velocity measurements on TAC005 provide an initial set of data for use in understanding the quench behavior of this type of magnet. Further studies of the quench properties of the outer coil as well as the inner and trim coils will be performed on future dipoles. The propagation of a quench from one coil to the other coils will also be studied to give a complete analysis of the quench response.

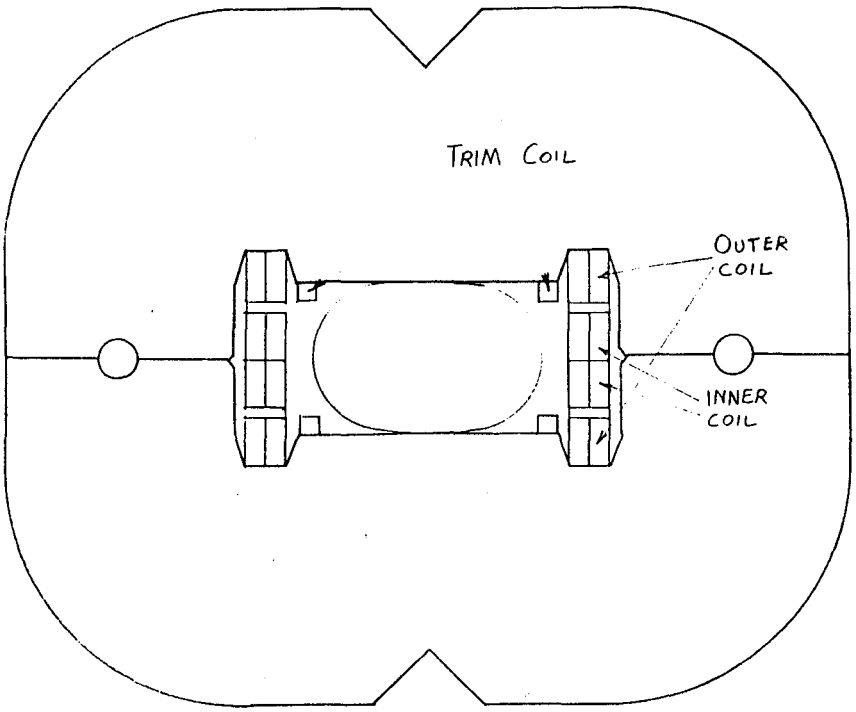

FIGURE 1. CROSS-SECTION OF TAC005

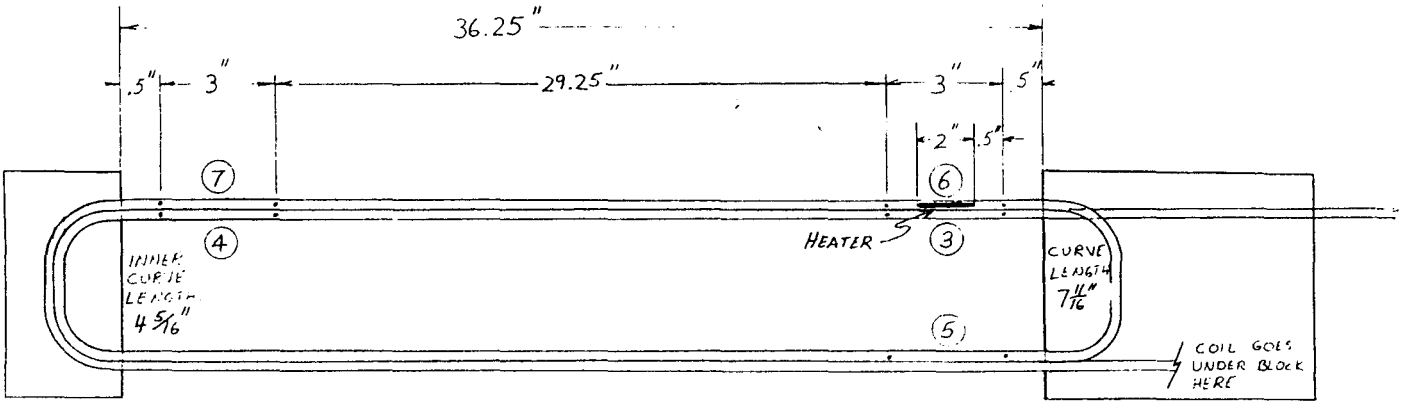

FIGURE 2. LOCATION OF HEATER AND VOLTAGE TAPS

LOW FIELD, B=0.5021T

LOCATION	B(X)	B(Y)
1	71.1	-5128.1
2	102.1	-3778.1
3	1761.1	-1337.9
4	37.2	- 803.5
5	-333.2	- 92.6
6	-521.6	-5047.6
7	-781.9	-2130.5
8	-885.2	- 26.9

COORDINATES

LOCATION	X	Y
1	0.732	0.41
2	0.832	0.41
3	0.9283	0.528
4	1.0443	0.528
5	1.1443	0.528
6	0.9283	0.18114
7	1.0443	0.18114
8	1.1443	0.18114

MID FIELD, B=1.6288T

LOCATION	B(X)	B(Y)
1	497.1	-16380.1
2	505.7	-12270.1
3	3756.6	- 5078.2
4	- 594.4	- 2666.2
5	-1690.3	- 341.4
6	-1910.5	-16666.1
7	-2858.4	- 6983.0
8	-3290.8	249.6

HIGH FIELD, B=2.98T

LOCATION	B(X)	B(Y)
1	972.5	-27980.0
2	1795.2	-31147.7
3	2104.5	-23723.2
4	-1347.5	-11082.8
5	-1979.2	535.6
6	-1035.1	-30388.1
7	-1338.3	-13315.3
8	-1495.3	196.1

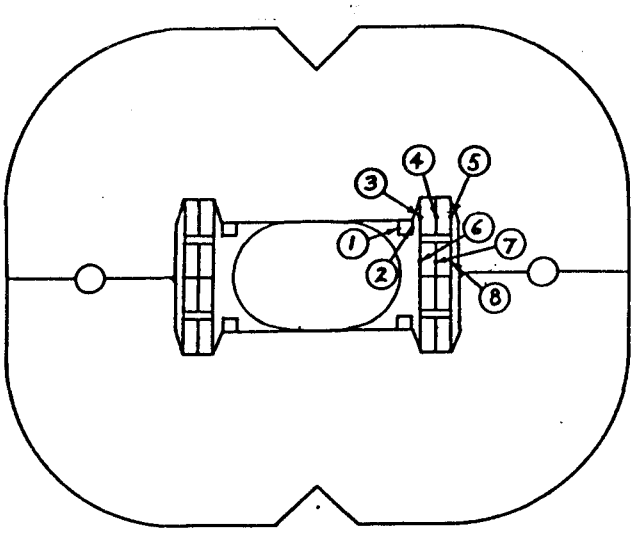

Figure 3. Magnetic field values near conductors

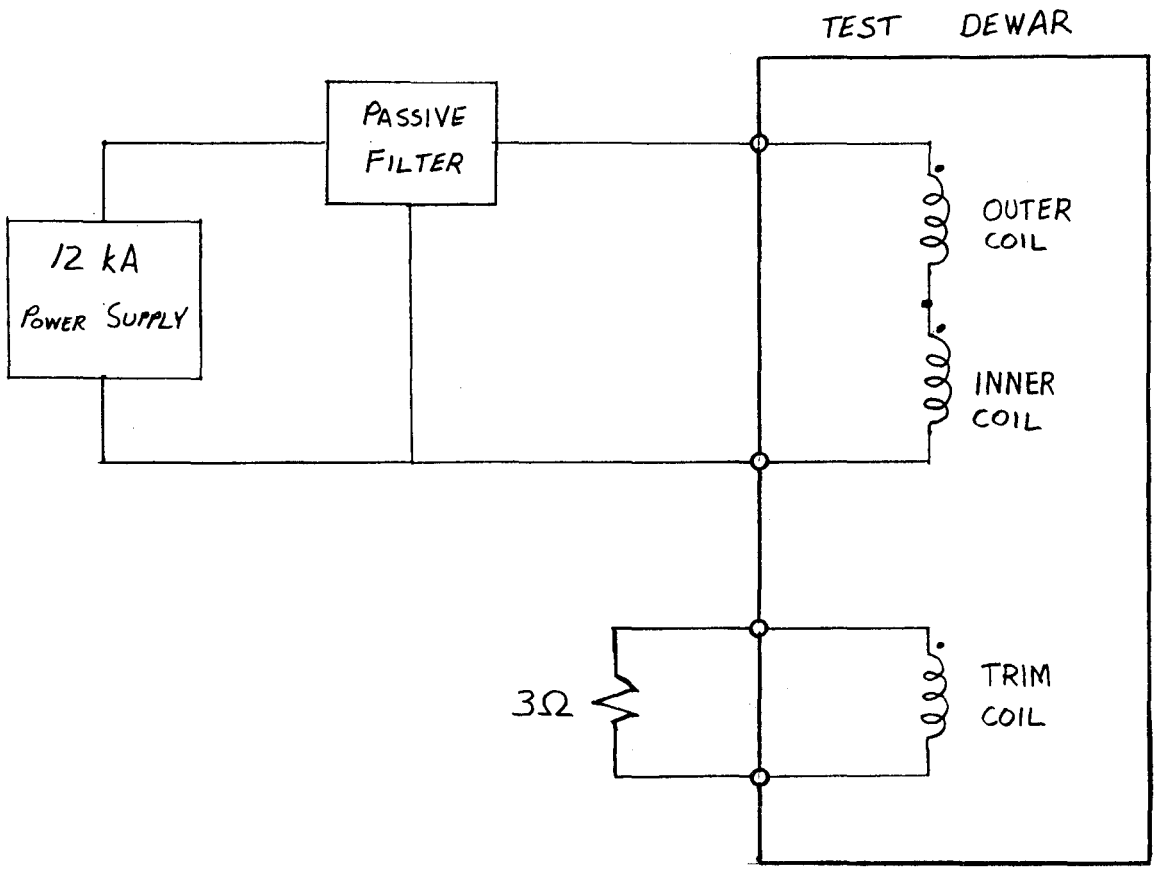

FIGURE 4. TEST CIRCUIT FOR QUENCH VELOCITY MEASUREMENTS

QUENCH PROPAGATION VELOCITIES

TEST #	CURRENT (KA)	HEATER PULSE (SEC)	TAP LOCATION	DELAY TIME (MS)	PATH	AVERAGE VELOCITY (M/S)
11	9	0.70	7	60.8	6-7	13.47
			5	23.2	6-5	12.80
			4	85.2	6-5-4	15.58
			3	118.8		
12	9	0.70	7	62.4	6-7	13.13
			5	21.6	6-5	13.75
			4	80.4	6-5-4	16.51
			3	113.4		
13	9	0.70	7	62.6	6-7	13.09
			5	21.8	6-5	13.62
			4	80.2	6-5-4	16.55
			3	113.0		
15	7.5	0.96	7	94.2	6-7	8.70
			5	30.4	6-5	9.77
			4	133.6	6-5-4	9.93
			3	177.0		
16	7.5	0.96	7	100.4	6-7	8.16
			5	30.2	6-5	9.83
			4	131.4	6-5-4	10.10
			3	173.0		
17	7.5	0.96	7	103.0	6-7	7.95
			5	29.0	6-5	10.24
			4	130.4	6-5-4	10.18
			3	175.4		
19	5.0	2 @ 1.54	7	195.2	6-7	4.20
			5	45.6	6-5	6.51
			4	344.8	(6-) 3-4	9.14
			3	255.2		
20	5.0	2 @ 1.73	7	193.2	6-7	4.24
			5	45.6	6-5	6.51
			4	338.8	(6-) 3-4	9.14
			3	249.2		
21	5.0	2 @ 2.21	7	188.0	6-7	4.36
			5	49.2	6-5	6.03
			4	336.0	(6-) 3-4	8.75
			3	242.4		
22	5.0	3.00	7	198.4	6-7	4.13
			5	43.6	6-5	6.81
			4	325.6	(6-) 3-4	10.56
			3	248.0		

Figure 5. Results of quench velocity tests

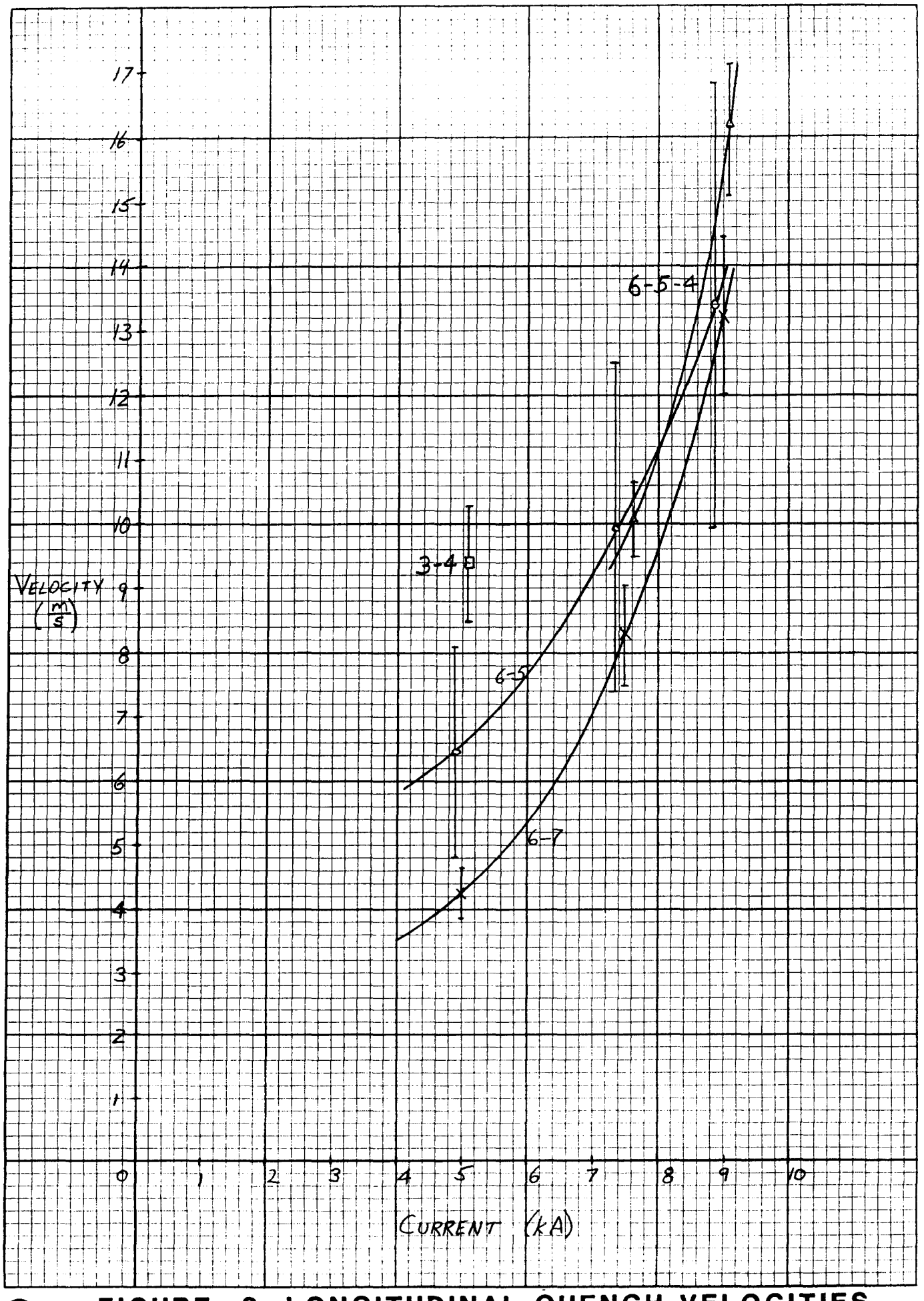

FIGURE 6. LONGITUDINAL QUENCH VELOCITIES

AMPAD 22-115 CROSS SECTION 10 SQUARES TO INCH

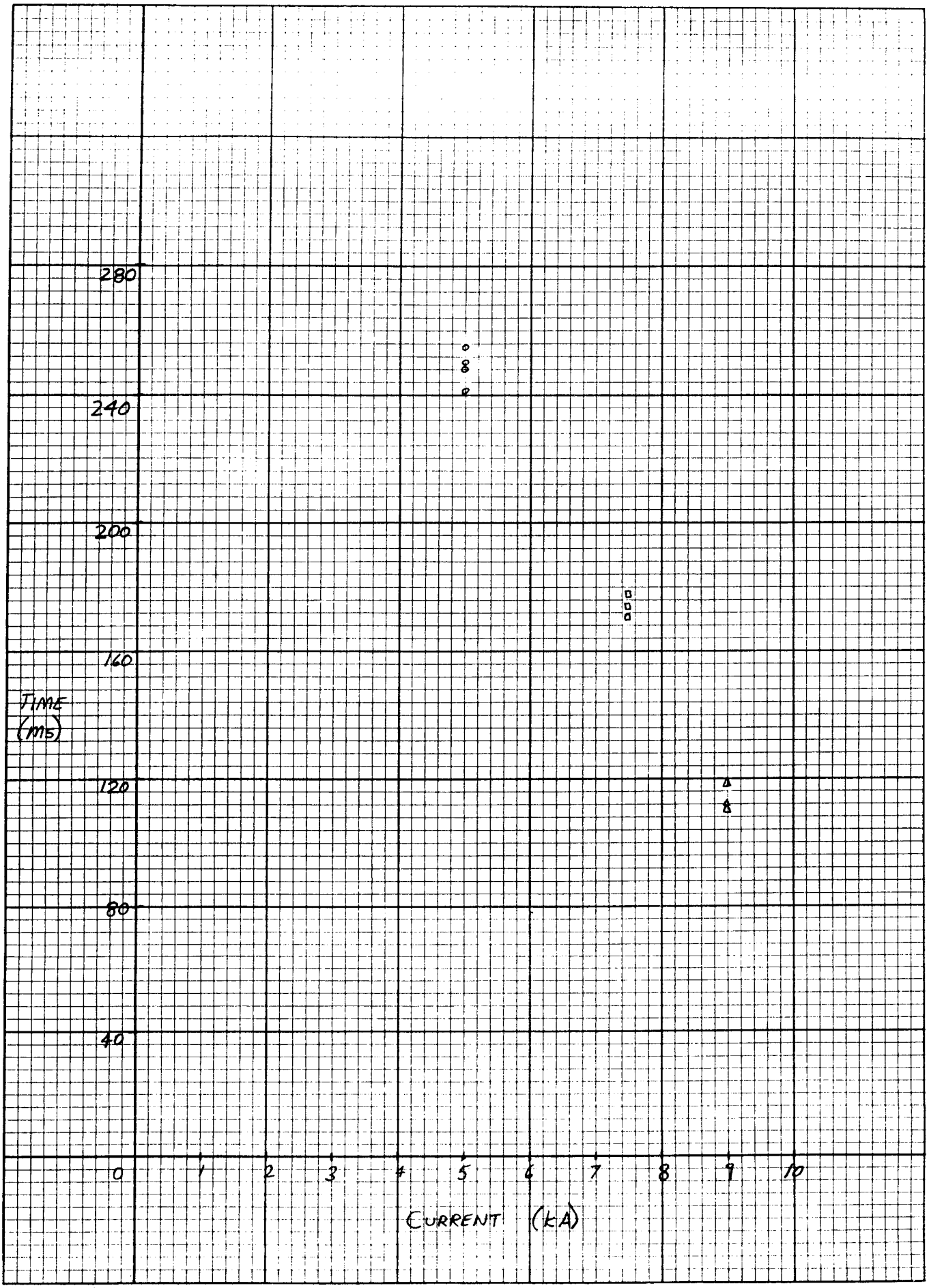

FIGURE 7. TRANSVERSE QUENCH PROPAGATION TIMES

AMPAD 22-115 CROSS-SECTION 10 SQUARES TO INCH

APPENDIX B

RESULTS FROM HEATER-INDUCED QUENCHES OF A 4.5m TWO-IN-ONE SUPERCONDUCTING R&D DIPOLE FOR THE SSC

Submitted to the 1985 Particle Accelerator Conference
Vancouver, B.C. May 13-16, 1985

BNL-36624

RESULTS FROM HEATER-INDUCED QUENCHES of a 4.5 m TWO-IN-ONE SUPERCONDUCTING R&D DIPOLE FOR THE SSC*

G. Ganetis and A. Prodell
Brookhaven National Laboratory
Upton, NY 11973

Abstract

Quench studies were performed using a 4.5 m long SSC R&D dipole to determine the temperature rise during a quench by measuring the resistance of the conductor cable in the immediate vicinity of the quench. The 2-in-1 magnet was wound with improved "high homogeneity" NbTi conductor in a 2-layer cosine θ coil configuration of 3.2 cm inner diameter with each layer powered separately to simulate graded conductor. Twelve pairs of voltage taps were installed at various locations in the coils around one bore of the magnet. "Spot" heaters were placed between the voltage taps of 8 of these pairs to initiate magnet quenches. The resistance of the conductor was obtained from observations of the current and voltage during a magnet quench. The temperature of the conductor was then determined by comparing its resistance to an R vs T curve measured independently for the conductor. The quantity $\int I^2 dt$ is presented as a function of current and location, and the maximum conductor temperature is shown as a function of $\int I^2 dt$ and location. Measured longitudinal and azimuthal quench propagation velocities are also presented.

Introduction

This paper reports on tests conducted with the third of a series of four 2-in-1, 4.5 m long superconducting dipoles built to specifications similar to those for SSC Reference Design A. This magnet, which is described in detail elsewhere in these proceedings[1], was wound with improved "high homogeneity" NbTi conductor in a 2-layer cosine θ coil configuration of 3.2 cm inner diameter. To simulate graded conductor each layer was powered separately with the current in the outer layer always set 35% higher than the current in the inner layer as the currents were varied during these tests. The temperature of the liquid helium bath in which the magnet was suspended was also decreased from 4.5° to 2.4°K during the course of these tests to increase the magnet currents at which the heater quenches could be initiated.

Experimental Arrangement

The parameters of the conductor with which the magnet was wound are given in Table I. Eight heaters were installed in different locations in the inner and outer coils around one bore of the magnet, 4 in the inner coil and 4 in the outer coil. Each heater consisted of a 0.0635 mm thick strip of stainless steel with an overall length of 30.5 mm and width of 7.62 mm with the width reduced to 2.54 mm over the 17.8 mm long center section of the heater. By varying the voltage from 5.0 to 7.5 V, about 1 to 2 j of energy could be delivered to the heater in approximately 60 millisec. The heaters were wrapped with one layer of 0.0508 mm thick Kapton and positioned against the inner surface of the insulated mid-plane turns of the inner and outer coils in the locations shown in Fig. 1. At each heater position a pair of voltage taps, separated nominally by 12.7 cm, was connected to the conductor with the heater located centrally between the taps. Four additional pairs of similar voltage taps were installed on the third turn on the left and right sides of both the inner and outer coils next to the heaters positioned on the straight sections of the coils. These pairs of taps, which are designated in Fig. 1 by the numbers 5 and 6 on each coil, were used to determine the azimuthal quench velocity. The leads from each pair of voltage taps were carefully twisted to minimize any induced voltage in the voltage tap signal due to a change in magnetic field.

Table I. Conductor Parameters for the SSC R&D Dipole

Multifilamentary Wire	
Superconductor	Nb 46.5 wt % Ti High Homogeneity Alloy
Diameter	.0681 mm
Filament Diameter	19 microns
No. of Filaments	528
Cu to SC Ratio	1.3 to 1
Cabled Conductor	
Width (bare)	7.823 mm
Mean Thickness (bare)	1.257 mm
Keystone Angle	2.8°
No. of Wires	23
Filling Factor	88%
Insulation Thickness	
Kapton	0.0508 mm
Fiberglass-epoxy	0.0762 mm

Experimental Results

Since one of the objectives of the tests was to measure the highest temperature to which the conductor could be raised before the magnet was damaged, the first heater quenches were made at a constant bath temperature of 4.4°K at different values of magnet current to determine the current, Im, at which $\int I^2 dt$ was maximum. This procedure was repeated for each heater and the curves for two of the heaters in the outer coil are shown in Fig. 2. The heater locations, OEL and OMPL, are identified using the key in Fig. 1. The points plotted as x's are measurements made by firing the heaters on the right side of the coil in equivalent locations, OER and OMPR. Throughout these tests the heaters on the left side of the inner and outer coils were used since occasional firings of the heaters on the right side indicated that the results from these heater quenches were essentially the same as those from the left. From the curves in Fig. 2 it was determined that $\int I^2 dt$ was a maximum when Im was about 76% of the non-heater induced magnet quench current, Iq, of the outer coil. The points marked with a "C" in Fig. 2 were obtained at a temperature less than 4.4°K indicating that as the magnet quench current increased with decreasing temperature, the current at which $\int I^2 dt$ was a maximum also increased, maintaining the relationship, Im = 0.76 Iq. Each time the bath temperature was changed the magnet current was increased until a quench occurred to determine Iq and permit the resetting of Im for the subsequent heater quenches. Curves similar to those in Fig. 2 were also obtained for the heaters on the inner coil.

The temperature rise of the conductor cable during a heater-induced quench was measured by monitoring the magnet current and the voltage across the 12.7 cm section of cable where the heater was fired. The re-

*Work performed under the auspices of the U.S. Department of Energy.

sistance of this length of cable was calculated from which the average temperature over the 12.7 cm length between voltage taps could be determined by using the R vs T calibration curve. A correction to obtain the "hot spot" temperature was made by calculating an incremental ΔR following the procedure of Ganetis and Stevens.[2] From the trace of the voltage across the section of cable where the heater was fired as a function of time and knowledge of the magnet current the slope $d(\int I^2dt)/dR$ may be obtained. The trace in Fig. 3 shows that when the heater is fired the voltage and thus the resistance increase rapidly as the quench propagates away from the heater toward the voltage taps as both ρ and ℓ are increasing in the relationship, $R = \rho\ell/A$. The slope changes when the normal quench fronts reach the voltage taps since ℓ is now constant between the taps and R is a function only of ρ. From such traces, for each heater quench the time from the beginning of the quench to the time when the entire 12.7 cm length is resistive can be measured. Half this time multiplied by I^2 gives $\Delta\int I^2dt$, the difference in $\int I^2dt$ between the hot spot and the length of 6.35 cm which, to first approximation, is the position corresponding to Tave. R is then corrected by adding ΔR where $\Delta R = \Delta\int I^2dt/d(\int I^2dt)/dR$ and with this addition the hot spot temperature is found. The corrections for these tests varied from less than 1°K to 15°K.

The curves in Fig. 4 show the temperature rise of the section of conductor where a heater quench was initiated as a function of $\int I^2dt$ for locations OMPL and OEL. The curves for the inner coil, IMPL and IEL, not shown, followed closely the curve for OMPL to a maximum of 345°K for IEL and 280°K for IMPL. As mentioned above, the current in the outer coil (curves OMPL and OEL) was 35% greater than that in the inner coil. It was apparent from Fig. 2 that larger values of $\int I^2dt$ for a given current could be obtained during a heater quench by firing the heater (OEL) near the end of the outer coil. This heater was then used in the final series of heater quenches at reduced liquid He bath temperatures in an attempt to damage the magnet coil. After each heater quench in this series the magnet current was increased until a quench occurred to ascertain if there had been any deterioration in the magnet performance. For the last heater quench which caused no damage, $\int I^2dt$ = 8.72 MIITS and T ≈ 920°K. For the next and last heater quench which damaged the magnet, $\int I^2dt$ = 9.04 MIITS and T reached an estimated 1170°K. The He bath temperature for these last quenches was 2.4°K.

Measurements were also made of longitudinal and azimuthal quench velocities by measuring the distance between pairs of voltage taps and recording the time when a voltage signal would appear at the several pairs of taps after a heater quench had been initiated at a particular location. The longitudinal quench velocities as a function of current are shown for the outer coil in Fig. 5 (OMPL) and Fig. 6 (OEL), for the inner coil in Fig. 7 (IMPL) and Fig. 8 (IEL), and the azimuthal quench velocities for both the outer and inner coils in Fig. 9. The numbers next to the curves in each of the figures are the locations between which the velocities were measured (see Fig. 1). The quench velocities given by these curves were measured in a He bath at 4.5°K. Additional data, not shown here, indicate a dependence of the quench velocities on temperature for the same magnet current.

References

1. P. Dahl et al., "Performance of Four 4.5 m Two-in-One Superconducting R & D Dipoles for the SSC", these proceedings.
2. G. Ganetis and A. Stevens, "Results of Quench Protection Experiment on DM1-031," SSC Technical Note No. 12, Brookhaven National Laboratory.

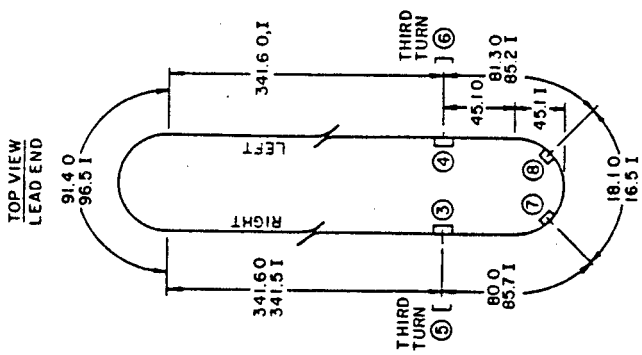

Key:
Coil Dimensions in cm: O-Outer, I-Inner
Heater + Voltage Taps: 3,4,7,8. Taps only: 5,6
Mid Plane Right: OMPR-Outer, IMPR-Inner Coil
Mid Plane Left: OMPL-Outer, IMPL-Inner Coil
End Right: OER-Outer, IER-Inner Coil
End Left: OEL-Outer, IEL-Inner Coil

Figure 1. Location of heaters and voltage taps on the magnet coils.

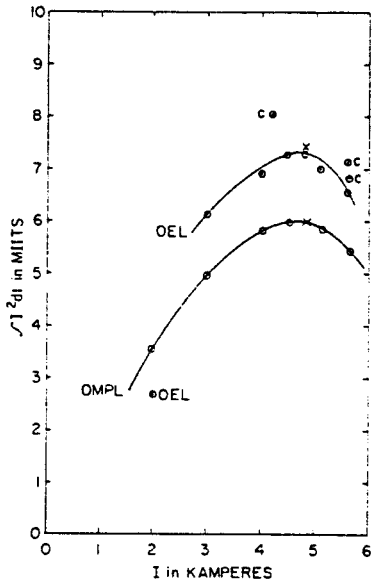

Figure 2. $\int I^2dt$ vs I for Outer Coil at 4.4°K.

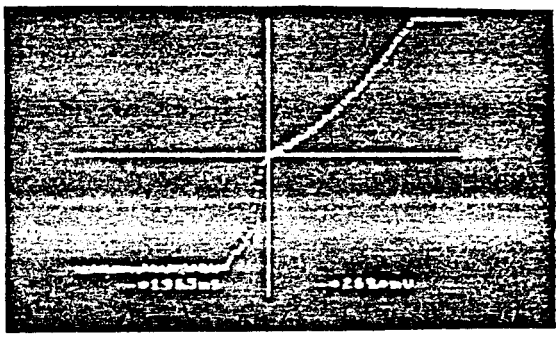

Figure 3. Voltage vs Time across a 12.7 cm section of conductor cable where a heater quench was initiated.

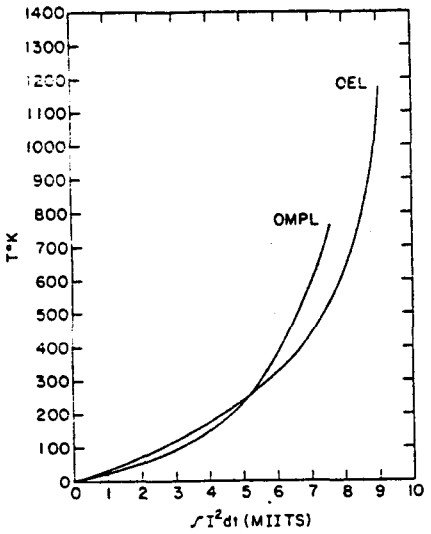

Figure 4. T vs $\int I^2 dt$ for OMPL and OEL.

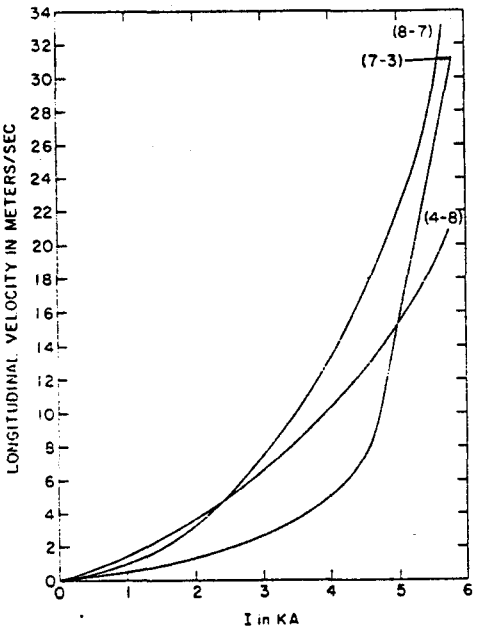

Figure 5. OMPL: Longitudinal Quench Velocity vs I at 4.5°K.

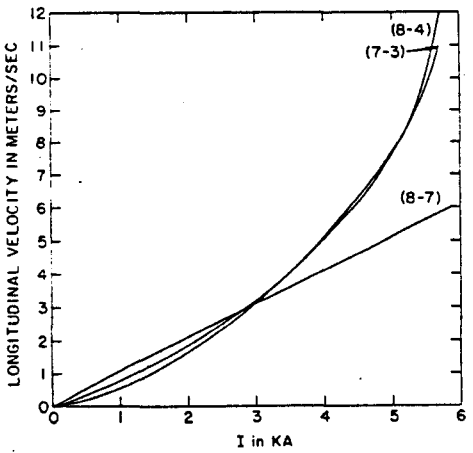

Figure 6. OEL: Longitudinal Quench Velocity vs I at 4.5°K.

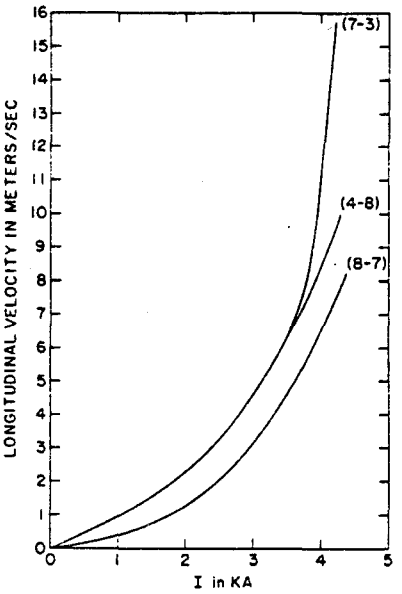

Figure 7. IMPL: Longitudinal Quench Velocity vs I at 4.5°K.

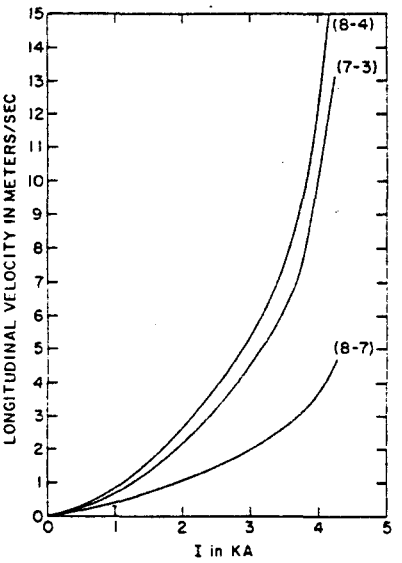

Figure 8. IEL: Longitudinal Quench Velocity vs I at 4.5°K.

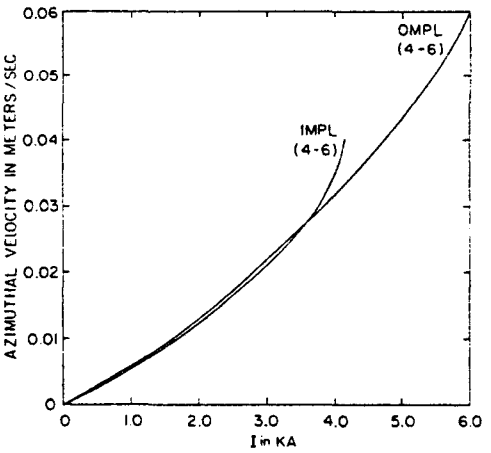

Figure 9. IMPL and OMPL: Azimuthal Quench Velocity vs I at 4.5°K.

APPENDIX C

QUENCH COMPUTER ANALYSIS FOR THE 3T SSC SUPERFERRIC DIPOLE COLD IRON MAGNET

G. LOPEZ
TEXAS ACCELERATOR CENTER

QUENCH COMPUTER ANALYSIS FOR THE 3T SSC SUPERFERRIC DIPOLE COLD IRON MAGNET

G. LOPEZ

TEXAS ACCELERATOR CENTER
2319 TIMBERLOCH PLACE
THE WOOODLANDS,TEXAS 77380

ABSTRACT

The principal quench parameters such as decay time ,maximum temperature,etc. are calculated for 105m dipole magnet unit proposed for the 3T Superconducting Super Collider (SSC). This simulation was achieved with the SSC* computer programs developed specifically for few conductor coils . Special cases are presented for possible active quench protection considerations. Finally the possibility of having higher magnetic field than 3T-field is studied.

INTRODUCTION

The most important parameters for coil protection , once quench has started, are the ultimate temperature reached and the characteristic decay time. We shall deal here with these quench parameters [1].

In the first part of this report, the characteristics of the superferric magnet, the conductors, quench velocity, are shown for a single magnet.

In the second part, the global circuit for one of the four main sectors of the accelerator , is shown with the equivalent circuit equations. Results are presented at the end . Also the operation of the program is explain, and the quench of a single, independent, magnet is described.

In the third part of this work we address some special cases for posible quench protection , and higher field considerations . All of these cases are considered for a single magnet.

The approach followed here for a quench is based on the distribution of the resistivity along the quenched region, in the fourth part we make some detailed derivation of the distribution used here . We also consider other resistivity distributions and their 'the quench' implications. The thermal and electrical data of the materials are shown at the end (RRR=97 is the copper used in this calculation).

1. QUENCH APPROACH.

The superferric dipole magnet proposed for use in the Superconducting Super Collider has a maximum central field of 3 tesla. This field is determinated by three coils carrying 10.1 kA , 11.3kA ,-2.25kA and by the steel which provides approximatly 1.7 tesla. The 105m magnet has a passive quench protection system with one diode per coil per three 35m magnets, as is shown in FIG.1 :

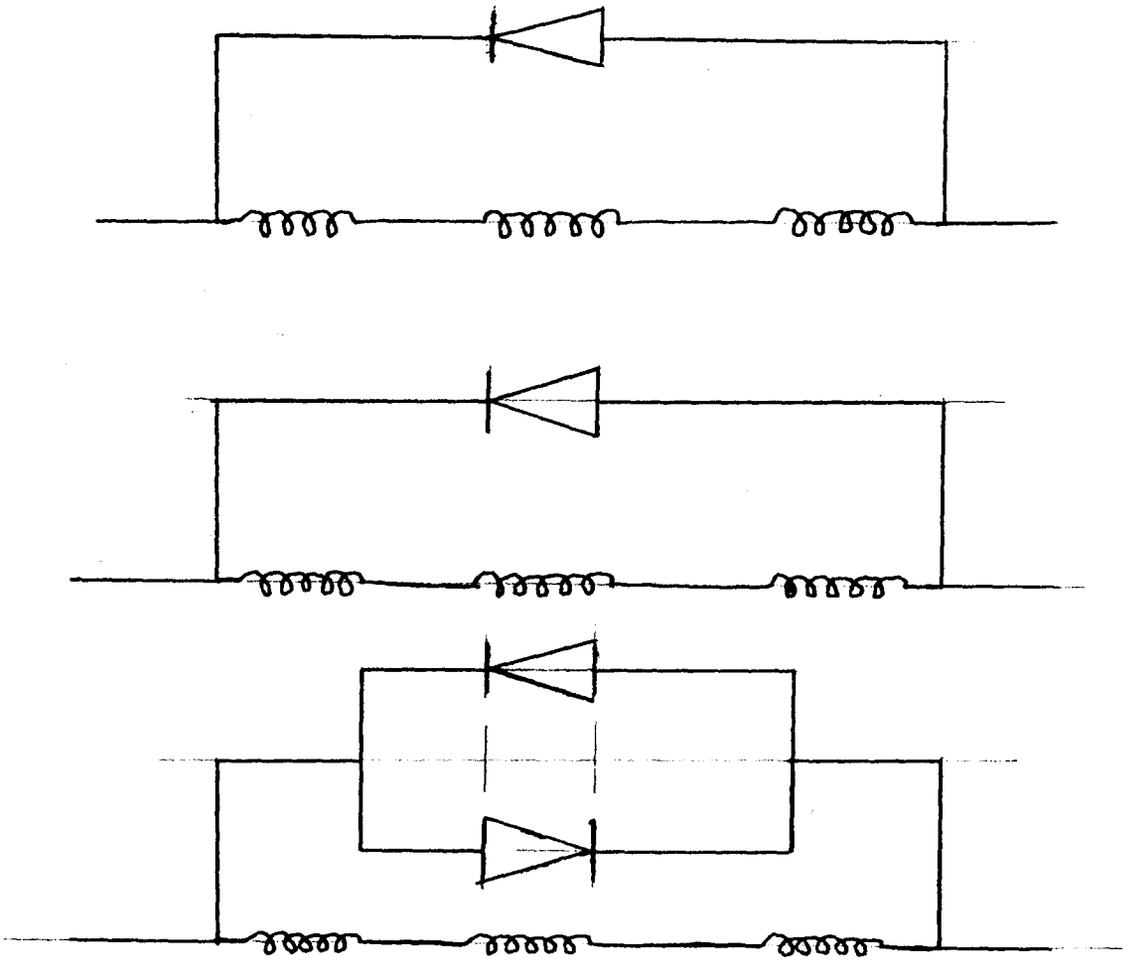

FIG.1 Passive Protection System for Cold Iron Dipole Magnet

The cross section of a single dipole magnet is shown in the next figure 2:

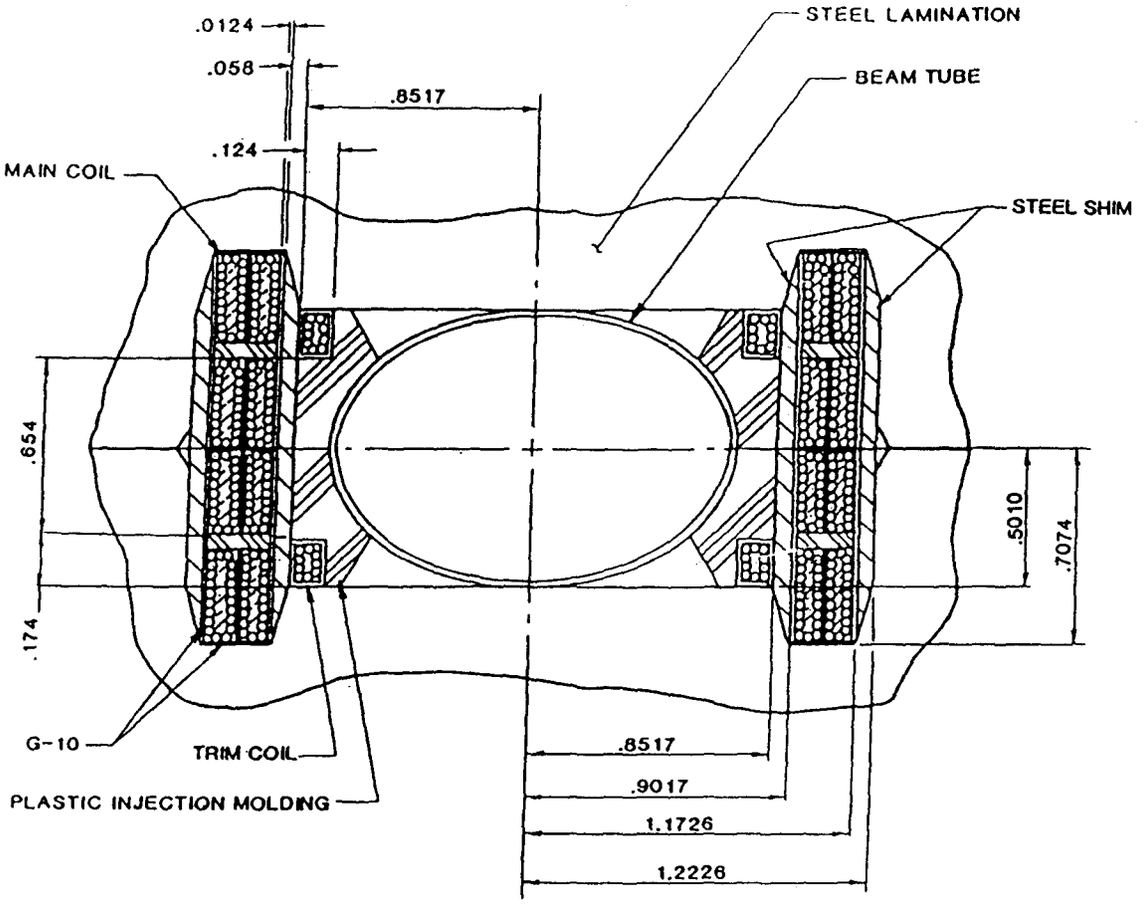

FIG.2 Cross Section of Cold Iron Dipole Magnet

The inner and outer coils have one kind of conductor while the trim coil has another one. The inner and outer conductors have 24 superconducting strands. Each strand has 367 filaments of NbTi(46.7%) imbedded in a copper matrix . The conductor has a copper stabilizer among the strands and solder SnAg(5%) between the strands. The total copper area (Acu), solder area (Asol), superconducting area (As.c.), andd kapton (Ak)area are given by:

$$
\begin{aligned}
Acu &= 0.1281E-04\ m*m \\
Asol &= 0.2556E-05\ m*m \\
As.c. &= 0.3985E-05\ m*m \\
Ak &= 0.4294E-05\ m*m
\end{aligned}
\qquad (a)
$$

The trim coil conductor is made of a similar superconductor but of with 12 strands of 500 filaments each. The areas are given below:

```
Acu   =0.5708E-05 m*m
Asol  =0.2085E-05 m*m
As.c.=0.1885E-05 m*m                                    (b)
Ak    =0.2147E-05 m*m
```

It is known that the final temperature reached, within the quench region, depends on how the stored energy is distributed in the conductors, and this depends on the increase of the resistance of the conductors. The increase of the resistance depends in turn on the temperature along the conductor (axial quench velocity) and the propagation of the quench to the adjacent conductors.

The axial quench velocity we are going to use is the known [2] Cherry & Gittleman and Broom & Rhoderick expression:

$$v_Q = \frac{j}{(\delta C_p)_s}\sqrt{\frac{L_0\,\theta_s}{\theta_s-\theta_0}}\;\frac{1-\dfrac{2(\theta_s-\theta_0)}{\theta-\theta_0}}{\sqrt{1-\dfrac{\theta_s-\theta_0}{\theta-\theta_0}}} \qquad (1)$$

The adiabatic version of (1) is :

$$v_Q' = \frac{j}{(\delta C_p)_s}\sqrt{\frac{L_0\,\theta_s}{\theta_s-\theta_0}} \qquad (1')$$

Where j is the current density, L_0 is the Lorentz number, θ_c is the critical temperature of the superconductor in magnetic field B, θ is the maximum temperature in the quench region, $(\delta C_p)_s$ is the average heat capacity at the transition temperature θ_s given by $\theta_s = (\theta_g + \theta_c)/2$, and θ_0 is the bath temperature.
The temperatures θ_g and θ_c depend on the field B and the current density in the following way (linear assumption):

$$\theta_g = \theta_0 + (\theta_c - \theta_0)(1 - j/j_{c0}) \qquad (2a)$$

$$\theta_c = \theta_{co} - (\theta_{co} - \theta_{oo})\, B/11.3 \tag{2b}$$

The critical current density J_{co} at the temperature of 4.5 K is given by:

$$J_{co} = J_{oo} \frac{\theta_c - \theta_o}{\theta_c - \theta_{oo}} \tag{2c}$$

Where j_{oo} the critical current density at 4.2 K, is given by:

$$J_{oo} = -550 \times 10^6 B + 4950 \times 10^6 \tag{2d}$$

The current densities are given in units of A/m^2 and θ_{co} is the critical temperature at B=0.

The propagation of the normal region to the adjacent conductors is based on the experimental results of short magnets.

A. Single Magnet Quench and programs description.

Let us assume the quench appears in one of the coils (say the outer one), and consider the 3X35m magnets represented by three independent current sources feeding the coils, as is shown in the circuit model below, FIG.3 :

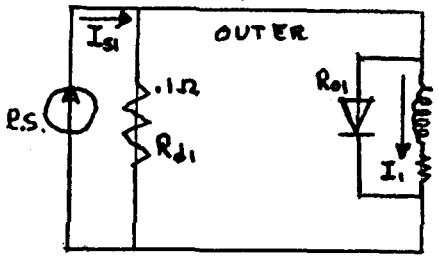

(3a)

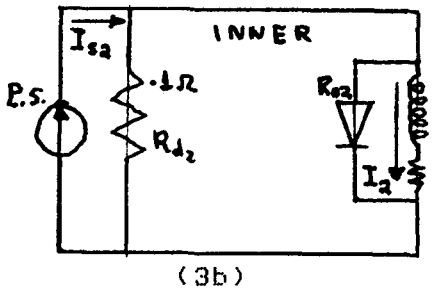

(3b)

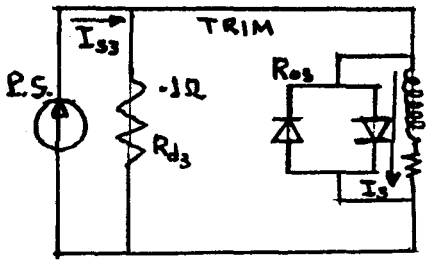

(3c)

FIG.3 Circuit Coils View

Once the quench starts and the voltage across any diode reaches four volts, the diode begin to conduc and the current bypasses the magnet, causing the current inside the magnet to fall off. In FIG.3 the L1 , L2 , and L3 variables are the outer , inner, and trim self inductances respectively .Rq1 , Rq2 , and Rq3 are the quench resistances, and Roi i=1,2,3 are the external diode resistances (considered here with constant value .0001Ω in the conducting stated).

The equations for the above circuit and the increasing temperature of the quenched regions are :

$$\frac{d}{dt}\begin{bmatrix} L_1 & M & m \\ M & L_2 & m \\ m & m & L_3 \end{bmatrix}\begin{bmatrix} I_1 \\ I_2 \\ I_3 \end{bmatrix} + \begin{bmatrix} R_{q_1} I_1 + R_{e_1}(I_1 - I_{s_1}) \\ R_{q_2} I_2 + R_{e_2}(I_2 - I_{s_2}) \\ R_{q_3} I_3 + R_{e_3}(I_{s_3} - I_3) \end{bmatrix} = \begin{bmatrix} 0 \\ 0 \\ 0 \end{bmatrix} \tag{3}$$

$$\begin{bmatrix} (\delta C_p)_1 & 0 & 0 \\ 0 & (\delta C_p)_2 & 0 \\ 0 & 0 & (\delta C_p)_3 \end{bmatrix} \frac{d}{dt}\begin{bmatrix} \theta_1 \\ \theta_2 \\ \theta_3 \end{bmatrix} - \begin{bmatrix} \rho_1 J_1^2 & 0 & 0 \\ 0 & \rho_2 J_2^2 & 0 \\ 0 & 0 & \rho_3 J_3^2 \end{bmatrix} = \begin{bmatrix} 0 \\ 0 \\ 0 \end{bmatrix} \tag{4}$$

The subindexes 1 , 2 , and 3 mean outer , inner , and trim coils respectively, " M " is the mutual inductance between inner and outer coils, " m " is the mutual inductance between the trim and both the inner and outer coils; " A " is the conductor area. The quench resistance is given by:

$$R = \frac{1}{A}\int_{-l}^{l} \rho(x)\, dx \tag{5}$$

with "l" being the normal length calculated by:

$$l = \int_0^t v_Q(t)\, dt \tag{6}$$

here $\rho(x)$ is the distribution of the resistivity along the quenched region, which is taken in first approximation as :

$$\rho(x) = \rho(\theta) \cos \frac{\pi x}{2l} \quad , \tag{7a}$$

which is derived in the section 4.

and $\rho(\theta)$ is the resistivity at the initial quench point given by:

$$\frac{1}{\rho(\theta)} = \sum_i \frac{\lambda_i}{\rho_i(\theta)} \tag{7b}$$

λ_i is the fraction of the i-conductor component. The average specific heat includes kapton insulation.

We solve the equations (3) and (4) by the Runge-Kutta's method with the program SSCEX (outer case) and SSCIN (inner case) with the initial conditions:

$$I_1(0) = 10.1\ kA$$
$$I_2(0) = 11.3\ kA \qquad \theta_1(0) = \theta_2(0) = \theta_3(0) = 4.5°K \tag{8}$$
$$I_3(0) = -2.25\ kA$$

In both programs we use the adiabatic expression (1') for the quench velocity. The resistivities and specific heats are approximated by polinomials of the form $A\theta^{\alpha} + B\theta^{\beta}$,where θ the temperature ; the data used can be seen in the F. L1 and L2 . The resistances of the quenched conductors are estimated in the following way. Let $\tau_i^{(1)}$, $i = 1,2,3$ be the times the quench arrives at the conductors 02, 03, 04 respectively for a quench that stants in 01 , let $\tau_i^{(2)}$, $i = 1,2,3$ be the delay time to propagate from I1 to of I2, I3, I4 respectively, and τ_{10} be the delay time to propagate from 01 to I1.

$$R_{q_1} = R_{q_1}(t) + \tilde{R}_{q_1}(t) \quad , \quad R_{q_2} = R_{q_2}(t - \tau_{10}) + \tilde{R}_{q_2}(t) \tag{9a}$$

Where R_{q_1} and R_{q_2} are the total outer and inner resistances, $R_{q_1}(t)$ and $R_{q_2}(t-\tau_{10})$ are the resistances of the first outer and inner conductors quenched , $\tilde{R}_{q_1}(t)$ and $\tilde{R}_{q_2}(t)$ are the constribution to the resistance of the other outer and inner conductors which are going to quench later, defined by:

$$\tilde{R}_{q_1}(t) = \begin{cases} 0 & t < \tau_i^{(1)} \quad i=1,2,3 \\ \sum_{i=1}^{k-1} R_{q_1}(t - \tau_i^{(1)}) & \tau_1^{(1)} \leq t < \tau_k^{(1)} \\ \sum_{i=1}^{3} R_{q_1}(t - \tau_i^{(1)}) & t \geq \tau_3^{(1)} \end{cases} \tag{9b}$$

$$R_{q_2}(t-\tau_{co}) = \begin{cases} 0 & t < \tau_{co} \\ R_{q_2}(t) & t \geq \tau_{co} \end{cases} \tag{9c}$$

$$\tilde{R}_{q_2}(t) = \begin{cases} 0 & t < \tau_i^{(2)},\ i=1,2,3 \\ \sum_{i=1}^{K-1} R_{q_2}(t-\tau_{co}-\tau_i^{(2)}) & \tau_1^{(2)} \leq t < \tau_K^{(2)} \\ \sum_{i=1}^{3} R_{q_2}(t-\tau_{co}-\tau_i^{(2)}) & t \geq \tau_3^{(2)} \end{cases} \tag{9d}$$

Because of the iron's constribution to the magnetic field, the self and mutual inductances are field dependent. The variation of L1 , L2 , M , L3 , and , m with respect the magnetic field can be seen in the FIG.5. The way these inductances are determined is : given a desired magnetic field value Bo, this can be set up by different combination of the outer, inner, and trim currents (we can select one of these zero, for example). For every combination (ℓ), the stored energy per volume ($\mathcal{E}_\ell$) is calculated with the Poisson's program and the expression:

$$\mathcal{E}_\ell = \frac{1}{2} \sum_{i,j>i}^{3} A_{ij} I_i I_j \tag{9e}$$

Where (A_{ij}) is the symmetric inductance matrix ($A_{ij} = A_{ji}$); $A_{ii} = L_i$, $i=1,2,3$ are the self inductances , and $A_{12} = 2M$ and $A_{13} = A_{23} = 2m$ are the mutual inductances. The coupling coefficients are of course less than one. This increasing of the inductances can be show that has the same effect like the reduction in the inductances themselves or an faster increasing in the resistance of the conductors (depending if we see the inductances as a function of the total current (2Iout+2Iin +Itrim) or if we see these as a function of the magnetic field (B), respectively), see appendix A.

The calcultions are made for two cases, when the quench appears in the outer coil (more exactly in the conductor O1 of FIG. 2), and when the quench appears in the inner coil (conductor I1 FIG.2). The distribution of the magnetic field on the conductors for the inner coil is very high from 100% near the beam tube to 50% near the yoke. In the outer coil changes from 93% to 20% . In this work, we chose the average of the field in the conductor.

Program description:

The initial condition include a quenched length ($\ell^{(0)}$), heat capacity ($\mathcal{C}_p^{(0)}$), inductances ($L_i^{(0)}$, $M^{(0)}$, $m^{(0)}$), resistivity ($\rho_0^{(0)}$), quench resistance ($R^{(0)}$), current ($I_i^{(0)}$), and quench velocity ($vq^{(0)}$) defined at the bath temperature $\theta^{(0)}$ and at the initial time ($t=t_0$). After a time Δt using equation (4), the temperature rises to $\theta^{(1)}$ in the point where quench appeared . New values are read for $A_{ij}^{(1)}$, $\rho_0^{(1)}$, and $\mathcal{C}_p^{(1)}$, with these values and the relations (5,9), (6), and (7) we obtain the values for $R^{(1)}$, $\ell^{(1)}$, and $\rho_0^{(1)}$. Once we have these, with the relation (3) we calculate the new value of the current ($I_i^{(1)}$). The process continues to the next time step.

I must point out the fact that for a given step, $\rho_0^{(0)}$ is the resistivity

at the point where the quench appeared (this value is from a table, once the temperature at that point is calculated from (4)), while $\rho(\,)$ is the distribution of the resistivity along the length quenched (is calculated by (6) and (7)).

The evolution of quenches can be seen in the FIG. 6 , and 7 , for quenches starting in the outer or in the inner coil. The meaning of the variables that appear are : T(s) is the characteristic time decay of the field in seconds , O is maximum temperature reached, NM is the number of Miits ($10^{-6}\int I^2 dt$ (A^2s)), and R is the maximum quench resistance. All of these quantities are taken when the magnetic field has fallen off 90% of its highest value (3 tesla) ; the maximum voltage across the normal region is V, and the maximum quench velocity is VQ(m/s) reached during the quench .

From the experimental results, we have that the time delay quench propagation from the conductor O1 to the conductor I1 (FIG.2) is 158ms, from O1-O2 and I1-I2 is 80ms, and from I1 to I3 is 200ms (see FIG. E3-E5 (Quench expeirmental results)).

2. Quenches including real circuit performance.

The main ring circuit proposed for the SSC involves 4 sectors of 332 dipoles units, each unit with 3 35m-long magnets with a diode in parallel for each of the inner and outer coils , and two way diodes for the trim coil (without taking account the quadrupoles) as can be seen in the next FIG. 8 :

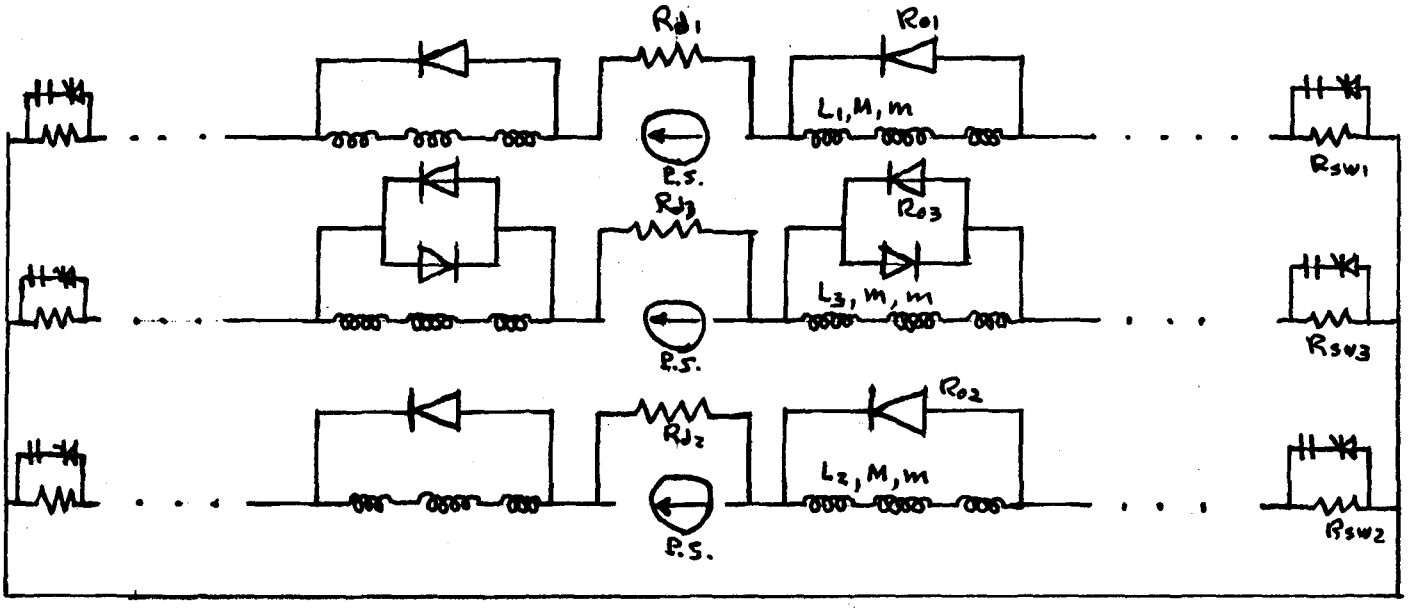

FIG.8 GLobal Circuit Sector for the SSC

The equation to be solved for this circuit are:

$$\begin{bmatrix} L_{1f} & M_f & m_g \\ M_f & L_{2f} & m_g \\ m_g & m_g & L_{3f} \end{bmatrix} \begin{bmatrix} I_{s1} \\ I_{s2} \\ I_{s3} \end{bmatrix} + \begin{bmatrix} R_{d1}(I_{s1}-I_\alpha) + R_{sw1} I_{s1} + R_{o1}(I_{s1}-I_1) \\ R_{d2}(I_{s2}-I_\beta) + R_{sw2} I_{s2} + R_{o2}(I_{s2}-I_2) \\ R_{d3}(I_{s3}-I_\gamma) + R_{sw3} I_{s3} + R_{o3}(I_{s3}-I_3) \end{bmatrix} = \begin{bmatrix} 0 \\ 0 \\ 0 \end{bmatrix} \quad (11)$$

3. SPECIAL CASES FOR SINGLE MAGNET QUENCHES

The FIG.11 shows the variation of the tempeRatures in the coils as a function of the length of the magnet when quench appears in the outer coil.

The FIG.12 shows the variation of the temperatures (when quench appears in the outer coil) with respect the variation of normalized area enclose by the resistivity distribution (see FIG.13), giving by the integral $\gamma = \frac{1}{\ell \rho_0} \int_0^{\ell} \rho(x)\, dx$, γ =1 is the uniform distribution, γ =.636 is the cosine distribution, γ =.5 ,and γ =.3333 is the distribution (21) with n=1, and n=2 respectively.

The TABLE 1 shows the results when quench appears in the outer or in the inner coil but with a reduction of time delay for quenching between outer and inner coil . This can be achieve putting a layer of Copper (but without forming a loop) in bettween the inner coil and the outer one instead of the insulator G-10 we have in the calculations A.

The results presented in the TABLE 2 correspond to induction of total quenchig along the whole inner and outer coils (by heating it) when the voltage across the diode is 4 volts.

TABLE 3 and TABLE 4 correspond to have a copper layer coils in between the main coils(4). The coupling inductance between the layer copper coil and the outer (inner) coil is "M" (see page 8). The assumed self inductances of the layer copper coils is 1.5*L1 . The quench evolution of this particular cases can be seen in the FIG.14 and 15.

Finally TABLE 5 represents quenches at 3.25T. For this case the kind of superconductor strand used (outer and inner coils) has 709 NbTi filaments of 20 μm diameter, each one, the strand's diameter is 0.0268 inches. The conductor is made up of 24 strands and copper stabilizer among the strands of .05X.25 inches square of cross section area. Solder (SnAg(5%)) is also used to make good contact with the stabilizer. The total areas of the metal components are:

As.c. =0.5345734E-05 m*m
Acu =1.145327E-05 m*m
Asolder=0.2555798E-05 m*m

The currents at high field are:

Iout = 14900 A
Iin = 11300 A
Itrim= -4000 A

$$\begin{bmatrix} L_1 & M & m \\ M & L_2 & m \\ m & m & L_3 \end{bmatrix} \begin{bmatrix} I_1 \\ I_2 \\ I_3 \end{bmatrix} + \begin{bmatrix} R_{q_1} I_1 + R_{o1}(I_1 - I_{s1}) \\ R_{q_2} I_2 + R_{o2}(I_2 - I_{s2}) \\ R_{q_3} I_3 + R_{o3}(I_3 - I_{s3}) \end{bmatrix} = \begin{bmatrix} 0 \\ 0 \\ 0 \end{bmatrix} \qquad (12)$$

Where Rswi, i=1,2 are the switch resistances that are connected once a quench is detected . L1f , L2f , Mf , and Mg are defined by L1f=331*L1 ; L2f=331*L2 ; Mf=331*M ; and Mg=331*m. All other variables have the same meaning as before. The above equations are solved by Runge-Kutta method with the programs SSCX (outer) and SSCY (inner case).

The results can be seen in the FIG. 9 and 10 ,which represent the quench appearing in the outer and inner coils . The protection circuit fired when the voltage across the diode reaches one volts. These and the "QUECH" program's results [5] shows that an outer coil quench is the more dangerous. If we use current detection for the coil protection (i.e. the quench is not detected until the voltage across the diode reaches four volts) the peak temperatures are only larger by about 10 K.

The above results point out that the magnets studied quench safely in the sense that they will not reach the melting point of the Cu or NbTi . We should worry about the SnAg solder because the temperatures are above of the 494 K melting point of this material.

4. DISTRIBUTION OF THE RESISTIVITY

Given a quench length ℓ there are not experimental results about the distribution of the resistance along this length yet[4]. To determinate this distribution analytically or numerically would require solving a highly non linear differential equation. Instead an approximation is used here to bypass this difficulty.

a) Diffusion approximation.

The one dimensional diffusion equation with heat source ρJ^2 is given by:

$$(\delta C_p)\frac{\partial \theta}{\partial t} = \frac{\partial}{\partial x} k \frac{\partial \theta}{\partial x} + \rho J^2 \tag{13}$$

The resistivity is not constant, we assume, as a first approximation,

$$\rho = \Gamma \theta \tag{14}$$

Where Γ is a positive constant. With this assumption, at any given time equation (13) becomes :

$$\frac{k}{\Gamma}\frac{d^2\rho}{dx^2} + \rho J^2 = 0 \tag{15a}$$

or

$$\frac{d^2\rho}{dx^2} + \lambda^2 \rho = 0 \tag{15b}$$

Where λ^2 is the positive quantity $\lambda^2 = \rho\Gamma/k$ (16)

Clearly the solution of the equation (15b) is:

$$\rho = A e^{i\lambda x} + B e^{-i\lambda x} \tag{17}$$

With the condition: $\rho(0) = \rho_0$, ρ_0 is the resistivity in the point where quench appeared, we have:

$$\rho = i(2A - \rho_0)\,\mathrm{sen}\,\lambda x + \rho_0 \cos \lambda x \tag{18}$$

because ρ must be a real function and with the condition $\rho(\ell) = 0$, the value of the other constants are $A = \rho_0/2$ and $\lambda\ell = (2n+1)\frac{\pi}{2}$. The harmonic solutions are :

$$\rho = \rho_0 \cos(2n+1)\frac{\pi x}{2\ell} , \tag{19}$$

and the only non negative solution is :

$$\rho = \rho_0 \cos \frac{\pi x}{2\ell} \tag{20}$$

This is finally the formula (7a) used in the calculations.

(20)

b) Adiabatic approximation give us less resistivity than the distribution (20), for this case we can make a polinomia assumption for the resistive distribution:

$$\rho = \rho_0 \left(1 - \frac{x}{\ell}\right)^n \qquad n > 0 \tag{21}$$

In the next figure we plot some distributions:

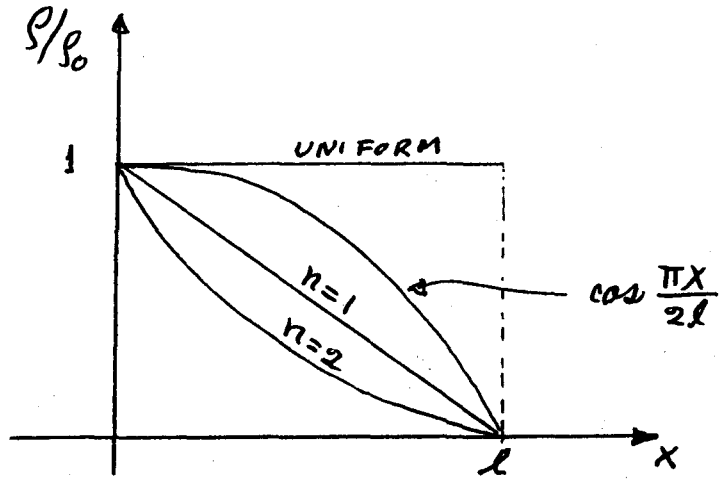

FIG.4 Some Resistivity Distributions

5.DISCUTION

As I said above the results in A. and B. point out the fact that the solder (SnAg) is going to melt if the passive diodes are used as protection only. But we need an estimation of how much solder is melted off the total quenched region.

With approximation made for the distribution of the resistivity, the radius of resistivities corresponds to the radius of temperatures so, the distribution of temperatures along the normal zone is :

$$\theta = \theta_0 \cos \frac{\pi X}{2l}$$

If the maximun temperature reached is about 690 K and the melting point is about 494 K then the fraction of solder melt is about 49 % of the normal region . Of course this fraction goes to zero when the maximun temperature reached goes to this melting point. In this way, if we have 20m of normal region then we would expect about 10m of solder melt. Any way this fact does not damage our conductor , even if the resistivity distribution is adiabatic (n=1,2 in the FIG.4 above) as can be seen from the FIG.12 (see also ref.6).

In these calculations , the absorbtion of the stored energy in the magnet because of the eddy currents induced in the iron and beam tube has not been taken account. These eddy currents could be simulated with another coil coupling to the main and trim coils through certain mutual inductances. This fact, as we have seen in the TABLES 3, 4, 5B, and 5C and FIG. 14, 15 reduce the peak temperature on the normal region, I expect this reduction not to be higher than 50 K.

From the TABLES 3, 4, 5B, 5C and FIG. 14 ,15 we see the copper coil between the main coils work like a good consumer of energy when quench appears. This fact reduce the peak temperature of the normal region about 170 K at 3 Tesla and about 260 K at 3.25 Tesla. This is so beacuse of the high eddy current induced in the copper coil. This eddy current does not make trables during exitation according with the next estimation :
The maximum induced current on the copper coil (Icm) is proportional to the change of the magnetic field with the time (B), so :

$I_{cmq} \sim \dot{B}_q$ during quench

$I_{cme} \sim \dot{B}_e$ during exitation

Then, the maximum eddy current during exitation is given by :

$I_{cme} = \dot{B}_e * I_{cmq} / \dot{B}_q$

From the data of the TABLES 3 and 4, and form the FIG. F1 and F2, we have the values Icmq=4400 A, $\dot{B}_q$=3/.83 (T/s), and assuming $\dot{B}_e$=3/150 (T/s), Icme has the small value Icme= 25 A. In this case we must have care with the maximum voltage between the outer and inner coil since a posible arking can appear . I need to mention here another possible advantageous of this case, the heating on the copper layer coils (because of the eddy currents) is more or less uniform, and can induced quenches on other parts of the superconductor (or even quench it completelly) , increasing the normal zone and then speeding the falling off the current.

Finally, from the FIG.D we obseve that the peak temperature reached in the normal zone, depends critically of the distribution of the resistivity along the normal region. Although we predict the 105m magnet will quench safely, it is important to determinate experimentally the resistivity distribution to improve the predictions of the QUENCH programs.

This calculation will need to be confirmed experimentaly on the model magnets.

APPENDIX A

The equation (3) can be written as :

$$\frac{d}{dt}(\mathbb{L}\mathbb{I}) + \mathbb{R}\mathbb{I} = 0 \tag{22}$$

Where $\mathbb{L}$ is the inductances matrix, $\mathbb{I}$ is the column current vector, and $\mathbb{R}$ is the resistances matrix. I shall omit their explicit difinition here.

If we see the inductances matrix $\mathbb{L}$ as a function of the total current "It" defined by :

$$It=2*Iout+2*Iin+Itrim \tag{23}$$

we have for the term involving the variation of the inductances:

$$\frac{d\mathbb{L}}{dt}\mathbb{I} = \frac{d\mathbb{L}}{dI_T}\mathbb{I}\left(2\frac{dI_{OUT}}{dt} + 2\frac{dI_{IN}}{dt} + \frac{dI_{TRIM}}{dt}\right) = \Omega\frac{d\mathbb{I}}{dt} \tag{24}$$

Where Ω is the matrix defined by:

$$\Omega = \begin{bmatrix} 2\sum_{\ell}\frac{dL_{1\ell}}{dI_T}I_\ell & 2\sum_{\ell}\frac{dI_{1\ell}}{dI_T}I_\ell & \sum_{\ell}\frac{dI_{1\ell}}{dI_T}I_\ell \\ 2\sum_{\ell}\frac{dL_{2\ell}}{dI_T}I_\ell & 2\sum_{\ell}\frac{dL_{2\ell}}{dI_T}I_\ell & \sum_{\ell}\frac{dL_{2\ell}}{dI_T}I_\ell \\ 2\sum_{\ell}\frac{dL_{3\ell}}{dI_T}I_\ell & 2\sum_{\ell}\frac{dL_{3\ell}}{dI_T}I_\ell & \sum_{\ell}\frac{dL_{3\ell}}{dI_T}I_\ell \end{bmatrix} \tag{25}$$

So the equation (22) can be written as :

$$\mathbb{L}_{ef}\frac{d\mathbb{I}}{dt} + \mathbb{R}\mathbb{I} = 0 \tag{26}$$

$\mathbb{L}_{ef}$ is the effective inductance matrix defined by:

$$\mathbb{L}_{ef} = \mathbb{L} + \Omega \tag{27}$$

the effect of having a increase of the inductance from high to low field imply that the effective inductance matrix $\mathbb{L}_{ef}$ has lower value than the original $\mathbb{L}$ (the elements of the matrix Ω are non positive).

If we see the inductance matrix $\mathbb{L}$ as a function of the magnetic field B , in this case we have :

$$\frac{d\mathbb{L}}{dt}\mathbb{I} = \dot{B}\,\frac{d\mathbb{L}}{dB}\mathbb{I} \tag{28}$$

and the equation (22) can be written like :

$$\mathbb{L}\frac{d\mathbb{I}}{dt} + \mathbb{R}_{ef}\mathbb{I} = 0 \tag{29}$$

Where the effective resistance matrix $\mathbb{R}_{ef}$ has a higher value than $\mathbb{R}$ and is given by:

$$\mathbb{R}_{ef} = \mathbb{R} + \dot{B}\,\frac{d\mathbb{L}}{dB} \tag{30}$$

so the effect is to have an increment in resistance.

AKNOWLEDGEMENT

I want to thank W. Schmidt for his help in calculating the stored energy and his numerous computer asistances; to F.R. Huson, P. McIntyre, M. Kobayashi, J. Zeigler, W. Hassenzahl, S. Heifets, and T. Tominaka for their valuable discutions; to R. Wolgast and M. Kobayashi for the data provided ; to F.R. Huson , C. Avilez, and TAMU for their support; to the whole T.A.C. persons for their hospitality.

REFERENCES

1) Conference Proceeding no.105. PHys. of High Energy Particle Accelerators (SLAC Summmer School, 1982).

2) Superconducting Magnets, M. N. Wilson, Oxford University Press (1983).

3) W. Schmidt. Internal Comunication (12-1984).

4) W. V. Hassenzahl (LBL). Internal Comunication (12-1985).

5) T. Tominaka. Quench Simulation on 3T Dipole Magnet (Report IAC June 17-85).

TIME DELAY TURN TO TURN
QUENCH PROPAGATION

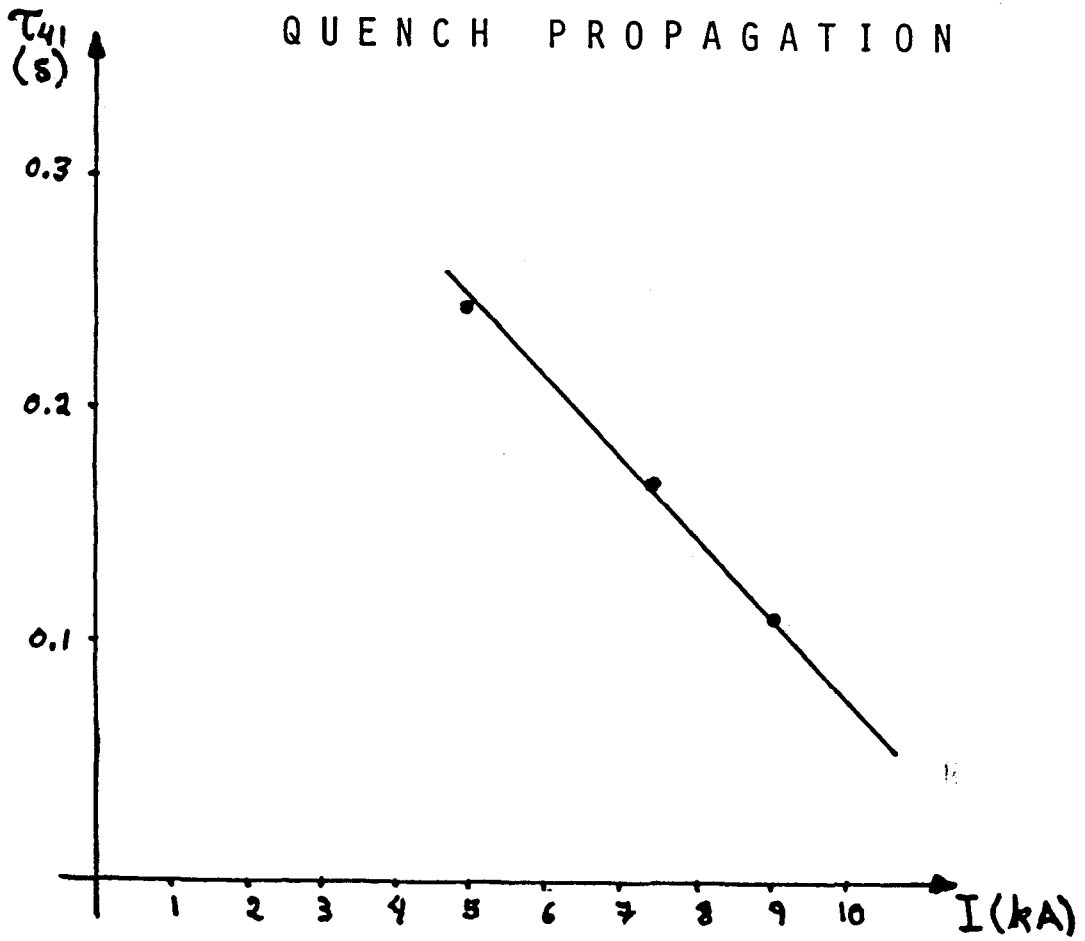

4.43°K

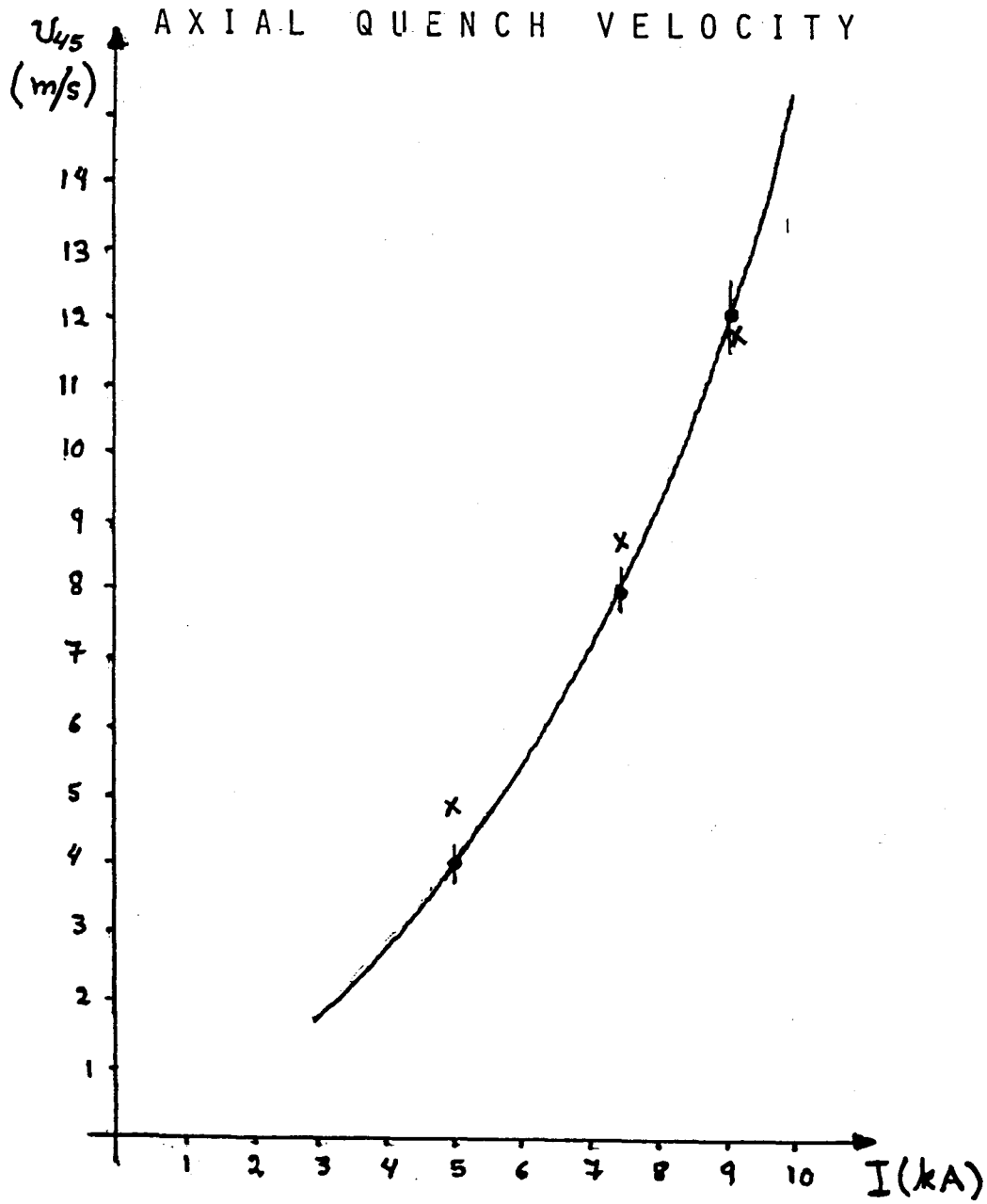
AXIAL QUENCH VELOCITY
v_{45} (m/s)
14
13
12
11
10
9
8
7
6
5
4
3
2
1
1
2
3
4
5
6
7
8
9
10
I(kA)

4.43 °K

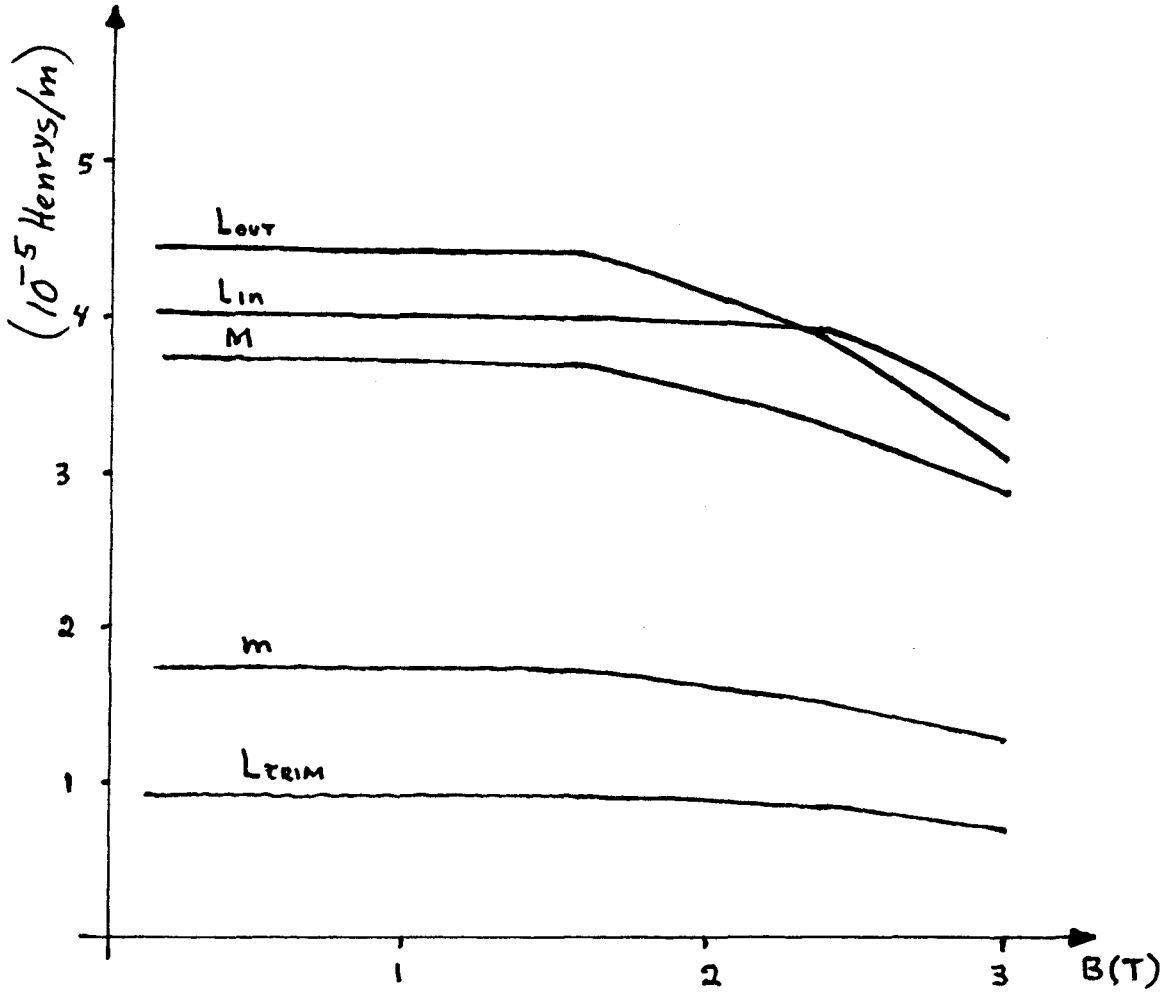

FIG 5 SELF AND MUTUAL INDUCTANCES FIEL DEPENDING

3.0 TESLA MAGNET

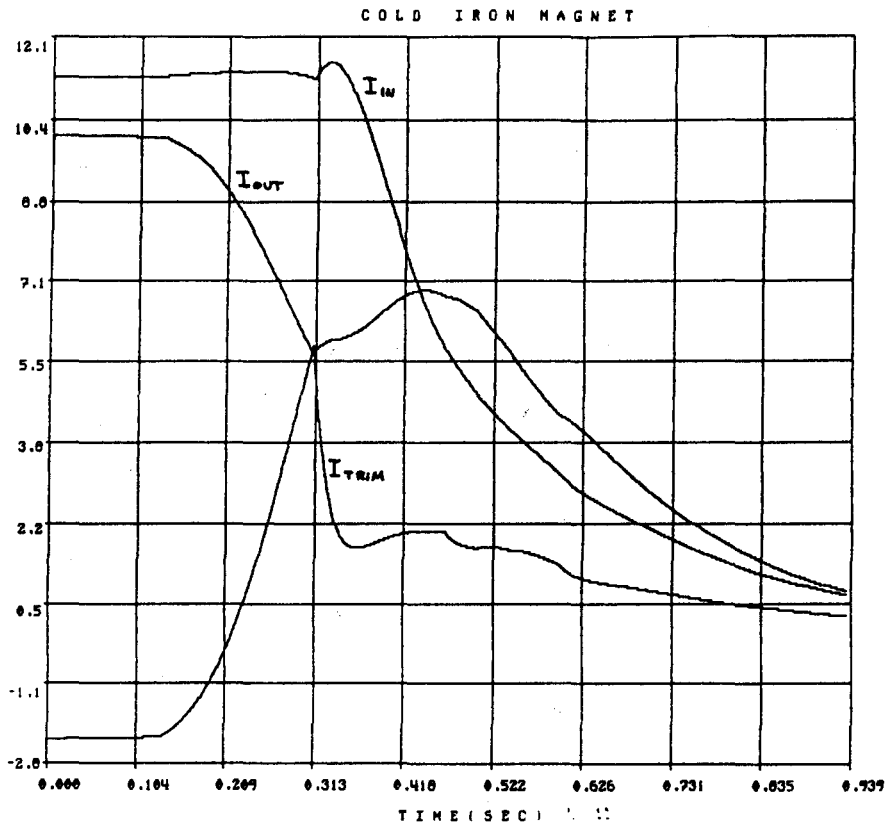

FIG. 6 3X35 SINGLE MAGNET VIEW
OUTER COIL QUENCH

	T(s)	Q(K)	NM	R(Ohm)	V(volts)	VQ(m/s)	FRACTION
OUTER	.93	548	39	.0501	126	15	.088
INNER		445	36	.0500	135	21	.102
TRIM		48	1.7	.0463	96	5	1.000

3.0 TESLA MAGNET

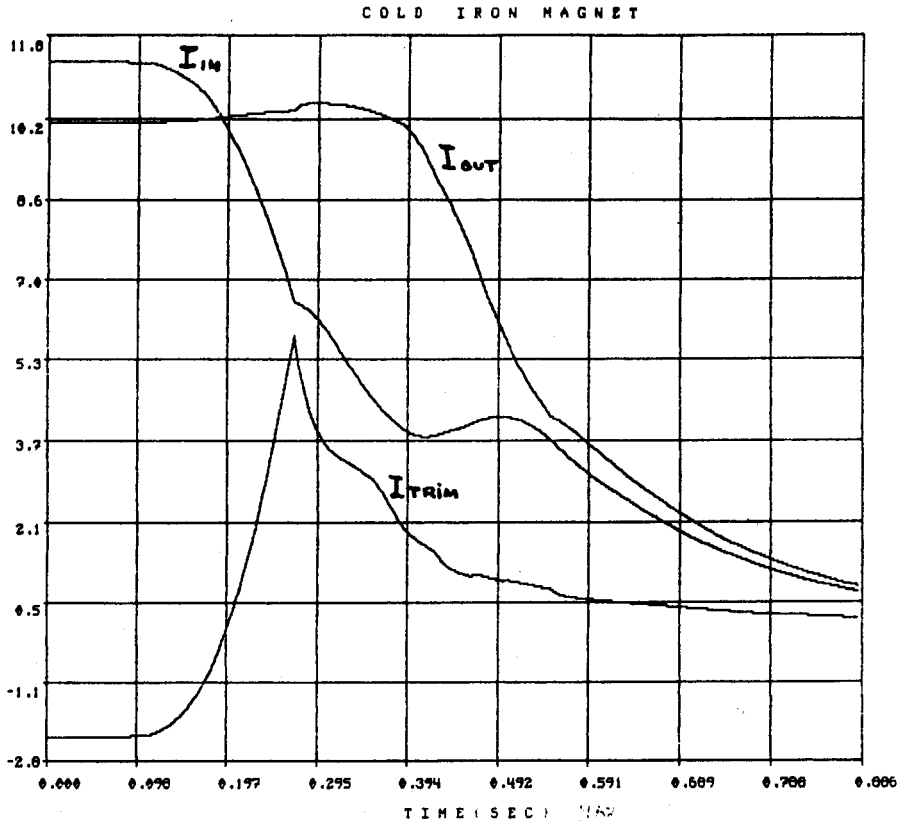

FIG. 7 3X35 SINGLE MAGNET VIEW
INNER COIL QUENCH

	T(s)	Θ(K)	NM	R(Ohm)	V(volts)	VQ(m/s)	FRACTION
OUTER	.88	356	33	.0428	145	17	.100
INNER		386	34	.0478	136	20	.102
TRIM		61	2.4	.0799	78	5	1.000

3.0 TESLA MAGNET

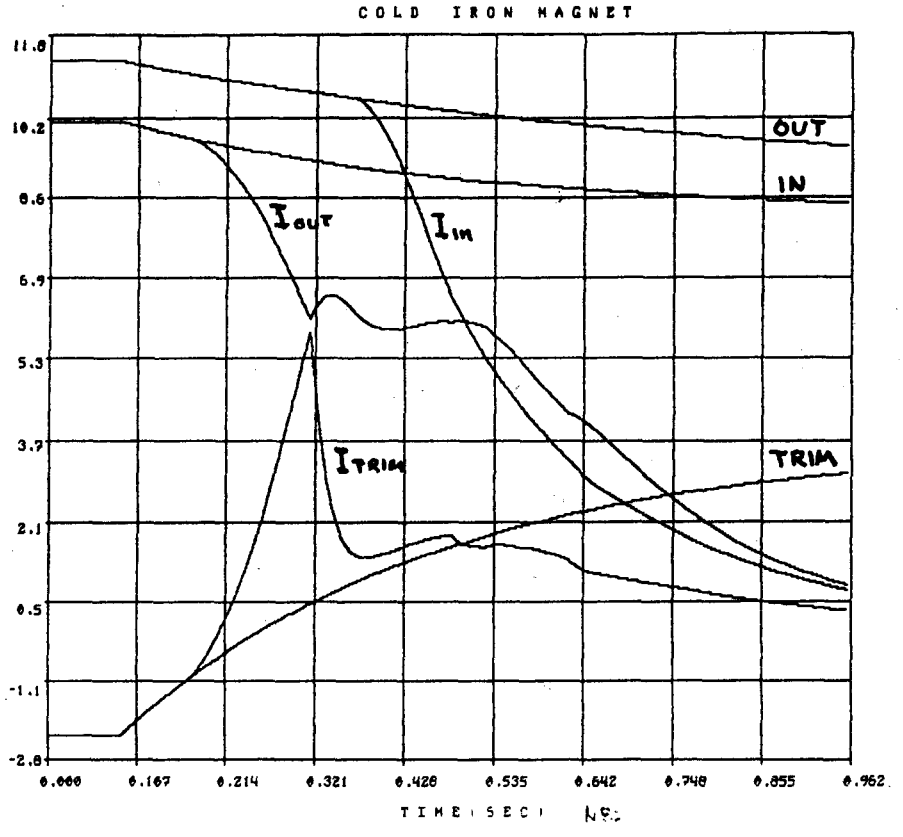

FIG. 9 3X35 GLOBAL CIRCUIT VIEW
OUTER COIL QUENCH

	T(s)	θ(K)	NM	R(Ohm)	V(volts)	VQ(m/s)	FRACTION
OUTER		552	41	.0485	121	15	.093
INNER	.95	462	39	.0525	133	19	.104
TRIM		46	1.7	.0423	85	5.2	1.000

3.0 TESLA MAGNET

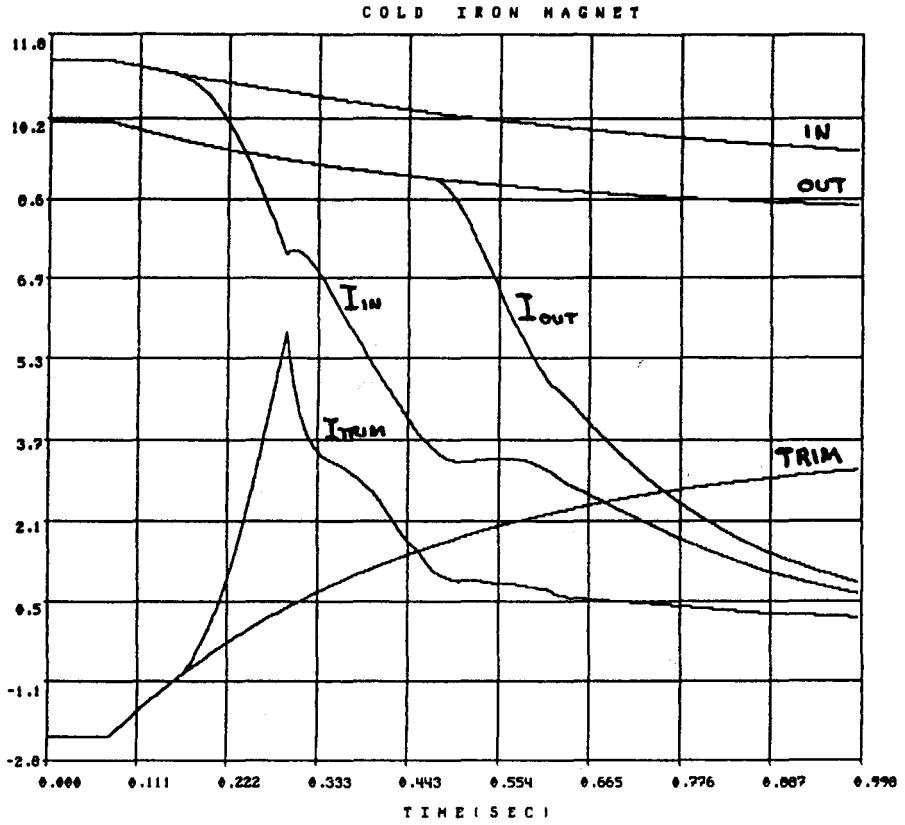

FIG. 10 3X35 GLOBAL CIRCUIT VIEW
INNER COIL QUENCH

	T(s)	θ(K)	NM	R(Ohm)	V(volts)	VQ(m/s)	FRACTION
OUTER	.99	264	36	.0359	118	17	0.12
INNER		326	39	.0470	111	23	0.12
TRIM		57	2.7	.0695	79	5	1.00

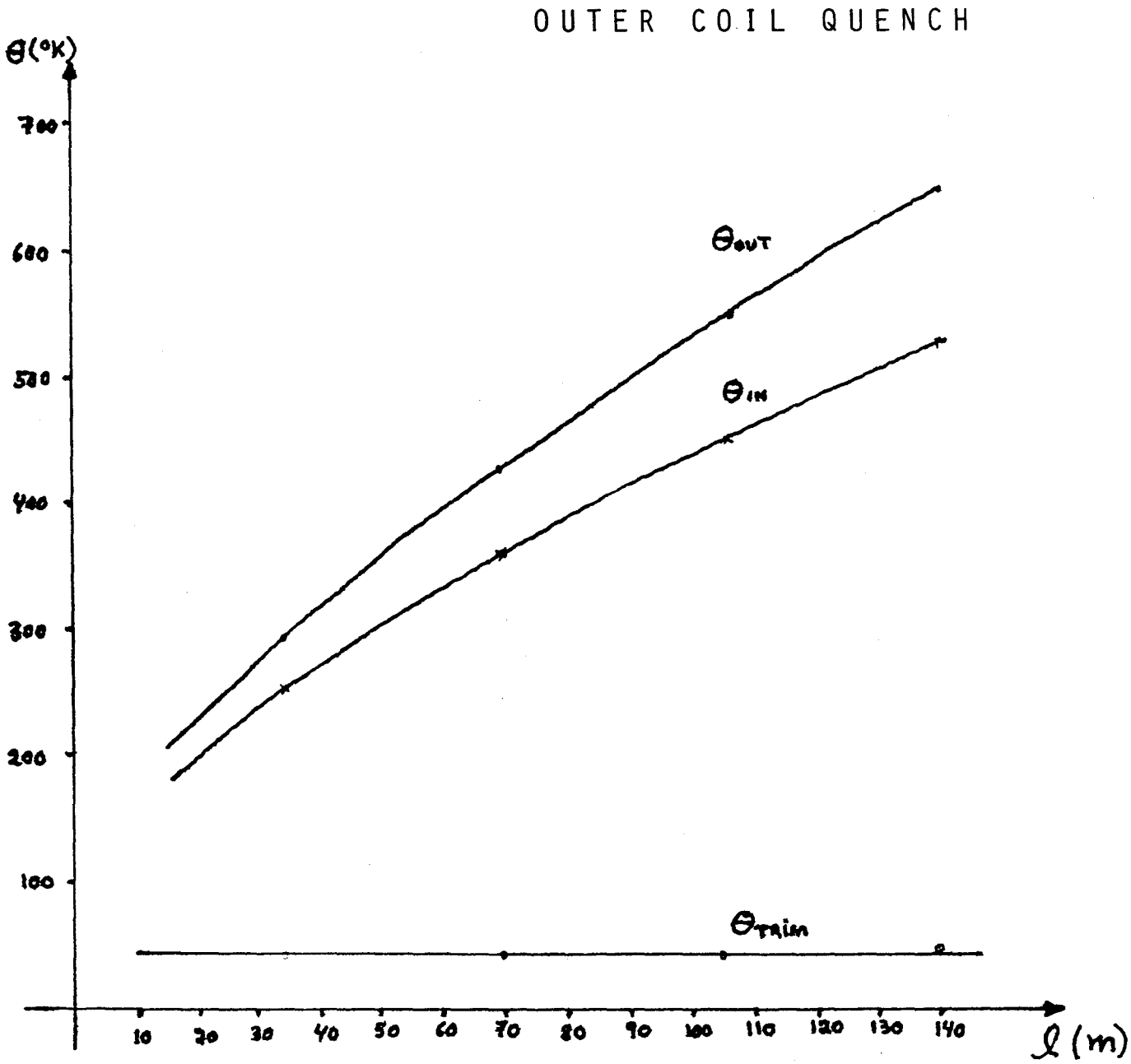

FIG. 11 MAGNET LENGTH DEPENDENCY OF MAXIMUM TEMPERATURE RISE

QUENCH APPEARS IN THE OUTER COIL

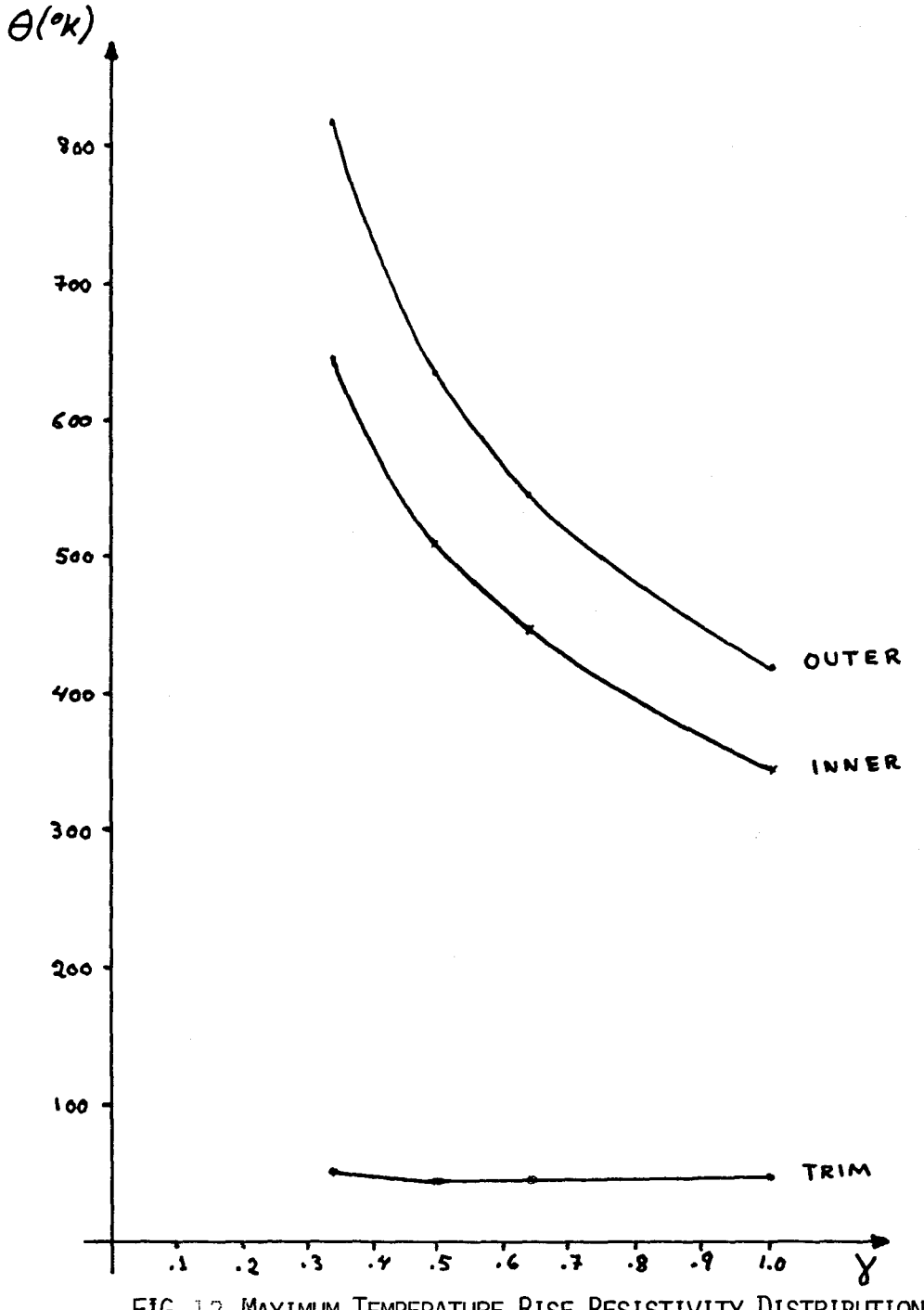

FIG. 12 MAXIMUM TEMPERATURE RISE RESISTIVITY DISTRIBUTION DEPENDING

3.0 TESLA COLD IRON MAGNET

QUENCH APPEAR	T(S)	COIL	Q(K)	NM	R(Ohm)	V(volts)	VQ(m/s)	FRACTION
OUTER COIL	1.5	OUTER	364	34	.0291	77	16	.075
		INNER	271	30	.0286	96	20	.097
		TRIM	38	2	.0281	98	4	1.000
INNER COIL	1.36	OUTER	387	35	.0334	79	16	.11
		INNER	290	31	.0371	86	21	.07
		TRIM	41	1.3	.0315	86	5	1.00

TABLE 1 . 3X35 SINGLE MAGNET VIEW WITH
A REDUCTION TIME QUENCHING
TURN TO TURN

3.0 TESLA COLD IRON MAGNET

QUENCH APPEAR	T(S)	COIL	Q(K)	NM	R(Ohm)	V(volts)	VQ(m/s)	FRACTION
OUTER COIL	.42	OUTER	115	19	.2610	281	14	1.0
		INNER	60	10	.0748	303	15	1.0
		TRIM	54	2.1	.0614	136	4.8	1.0
INNER COIL	.41	OUTER	58	9	.0652	279	14	1.0
		INNER	125	20	.3079	303	15	1.0
		TRIM	55	2	.062	137	5	1.0

TABLE 2 . 3X35 SINGLE MAGNET VIEW WITH
THE INDUCTION OF TOTAL
QUENCHING

3.0 TESLA COLD IRON MAGNET

QUENCH APPEAR	T(S)	COIL	Q(K)	NM	R(Ohm)	V(volts)	VQ(m/s)	FRACTION
OUTER COIL	1.0	OUTER	481	37	.0523	124	15	.095
		INNER	356	33	.0447	195	19	.116
		TRIM	69	3	.1089	80	7	1.000

MAXIMUN INDUCED CURRENT IN THE COPPER LAYER (Icu)= 5612 A
MAXIMUM TEMPERATURE RISE IN THE COPPER LAYER = 72 K
CROSS SECTION AREA OF THE COPPER LAYER = .1313E-04 m*m

TABLE 3 . 3X35 SINGLE MAGNET VIEW WITH A COPPER LAYER COIL BETWEEN THE OUTER AND INNER COILS

3.0 TESLA COLD IRON MAGNET

QUENCH APPEAR	T(S)	COIL	Q(K)	NM	R(Ohm)	V(volts)	VQ(m/s)	FRACTION
OUTER COIL	.94	OUTER	376	34	.0359	95	15	.085
		INNER	266	30	.0277	80	19	.095
		TRIM	66	3	.0978	83	7	1.000

MAXIMUN INDUCED CURRENT IN THE COPPER LAYER 1 (Icu1)= 4363 A
MAXIMUM TEMPERATURE RISE IN THE COPPER LAYER 1= 56 K
CROSS SECTION AREA OF THE COPPER LAYER 1= .1313E-04 m*m

MAXIMUN INDUCED CURRENT IN THE COPPER LAYER 2 (Icu2)= 2432 A
MAXIMUM TEMPERATURE RISE IN THE COPPER LAYER 2 = 57 K
CROSS SECTION AREA OF THE COPPER LAYER 2 = .578E-05 m*m

TABLE 4 . 3X35 SINGLE MAGNET VIEW WITH COPPER LAYER COILS BETWEEN OUTER AND INNER COILS AND BETWEEN THE TWO PAIR OF INNER CONDUCTORS

3.0 TESLA MAGNET

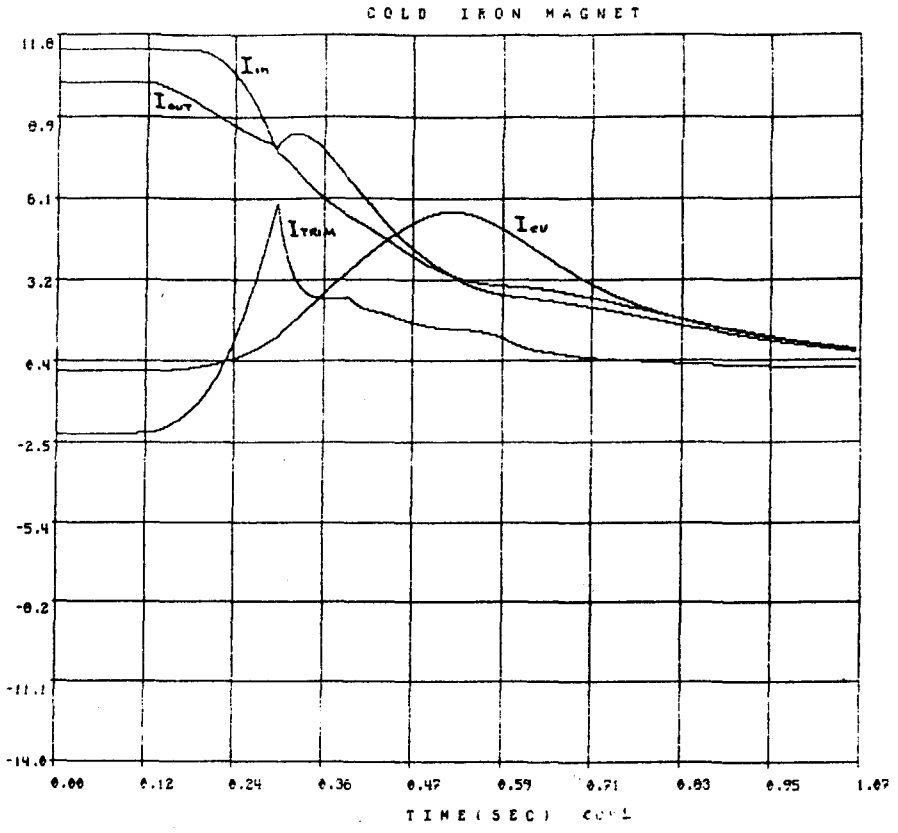

FIG.14 3X35 SINGLE MAGNET VIEW "OUTER" COIL QUENCH WITH ONE COPPER LAYER COIL BETWEEN THE OUTER AND INNER COILS

3.0 TESLA MAGNET

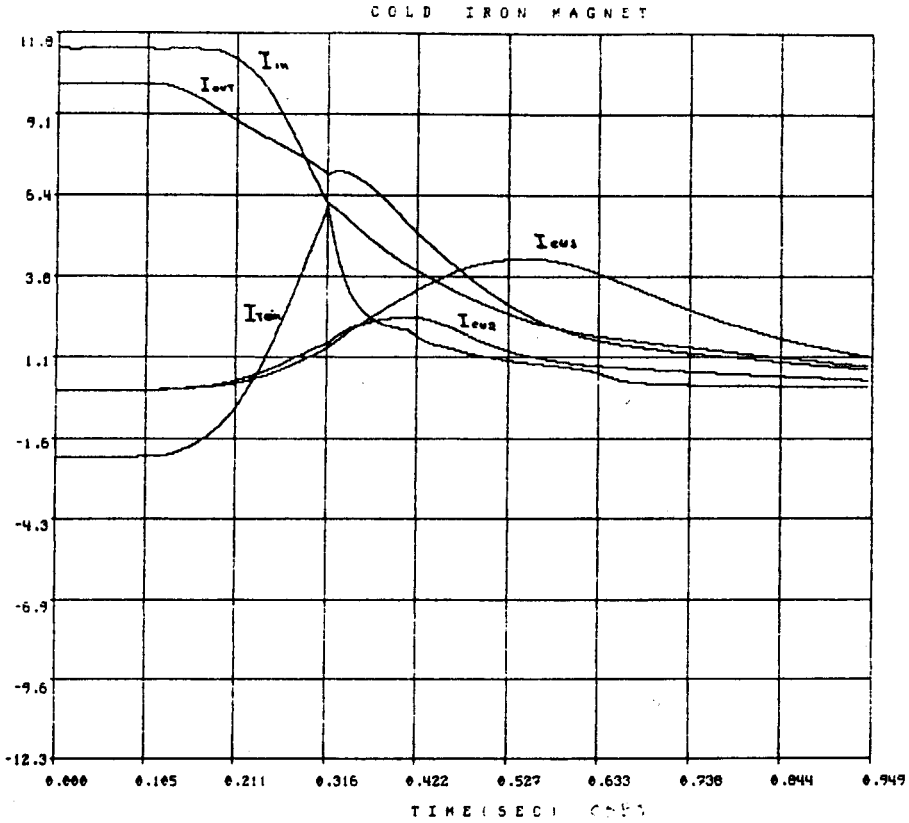

FIG.15 3X35 SINGLE MAGNET VIEW 'OUTER' COIL QUENCH WITH ONE COPPER LAYER COIL BETWEEN THE OUTER AND INNER COILS AND OTHER ONE BETWEEN THE TWO PAIR OF CONDUCTOR OF THE INNER COIL

3.25 TESLA COLD IRON MAGNET

QUENCH APPEAR	T(S)	COIL	Q(K)	NM	R(Ohm)	V(volts)	VQ(m/s)	FRACTION
OUTER COIL	.92	OUTER	776	41	.0452	113	19	.048
		INNER	613	38	.0472	133	12	.062
		TRIM	48	2	.0447	80	6	1.000
INNER COIL	.82	OUTER	415	38	.0466	153	26	.095
		INNER	527	42	.0613	173	16	.071
		TRIM	111	5	.2868	88	6	1.000

TABLE 5A . 3X35 SINGLE MAGNET VIEW
AT 3.25 TESLA

3.25 TESLA COLD IRON MAGNET

QUENCH APPEAR	T(S)	COIL	Q(K)	NM	R(Ohm)	V(volts)	VQ(m/s)	FRACTION
OUTER COIL	.81	OUTER	671	38	.0743	164	22	.090
		INNER	399	32	.0671	185	22	.134
		TRIM	55	2	.0606	73	6.5	1.000

MAXIMUN INDUCED CURRENT IN THE COPPER LAYER (Icu)= 6789 A
MAXIMUM TEMPERATURE RISE IN THE COPPER LAYER = 81 K
CROSS SECTION AREA OF THE COPPER LAYER = .1313E-04 m*m

TABLE 5B . 3X35 SINGLE MAGNET VIEW WITH A COPPER LAYER COIL
BETWEEN THE OUTER AND INNER COILS

3.25 TESLA COLD IRON MAGNET

QUENCH APPEAR	T(S)	COIL	Q(K)	NM	R(Ohm)	V(volts)	VW(m/s)	FRACTION
OUTER COIL	.94	OUTER	516	34	.0489	124	22	.076
		INNER	296	30	.0419	141	22	.116
		TRIM	44	1.4	.0354	74	7	1.000

MAXIMUN INDUCED CURRENT IN THE COPPER LAYER 1 (Icu1)= 5524 A
MAXIMUM TEMPERATURE RISE IN THE COPPER LAYER 1= 64 K
CROSS SECTION AREA OF THE COPPER LAYER 1= .1313E-04 m*m

MAXIMUN INDUCED CURRENT IN THE COPPER LAYER 2 (Icu2)= 2845 A
MAXIMUM TEMPERATURE RISE IN THE COPPER LAYER 2 = 64 K
CROSS SECTION AREA OF THE COPPER LAYER 2 = .578E-05 m*m

TABLE 5C . 3X35 SINGLE MAGNET VIEW WITH COPPER LAYER COILS BETWEEN OUTER AND INNER COILS AND BETWEEN THE TWO PAIR OF INNER CONDUCTORS

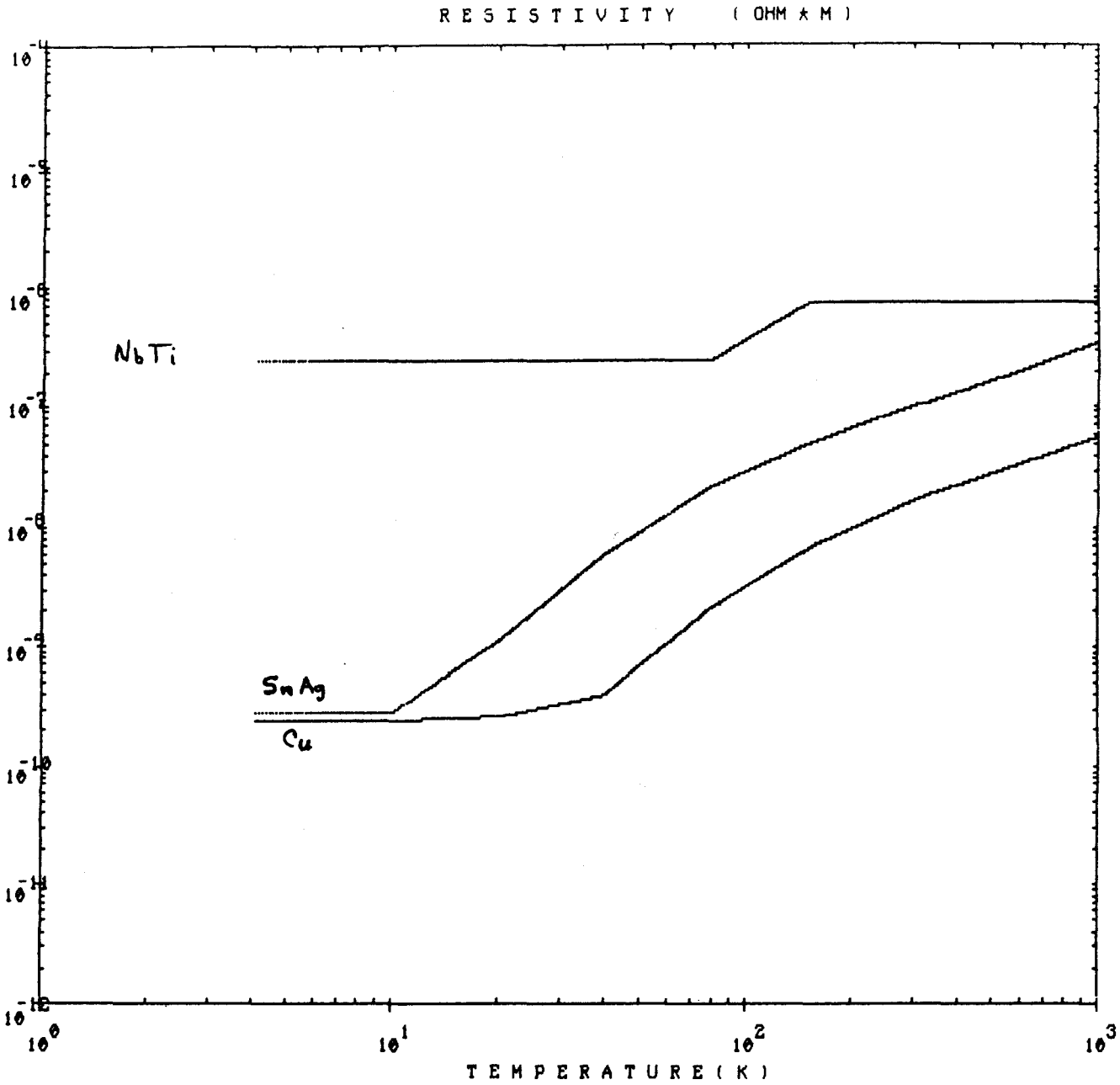
RESISTIVITY (OHM * M)
NbTi
SnAg
Cu
TEMPERATURE (K)

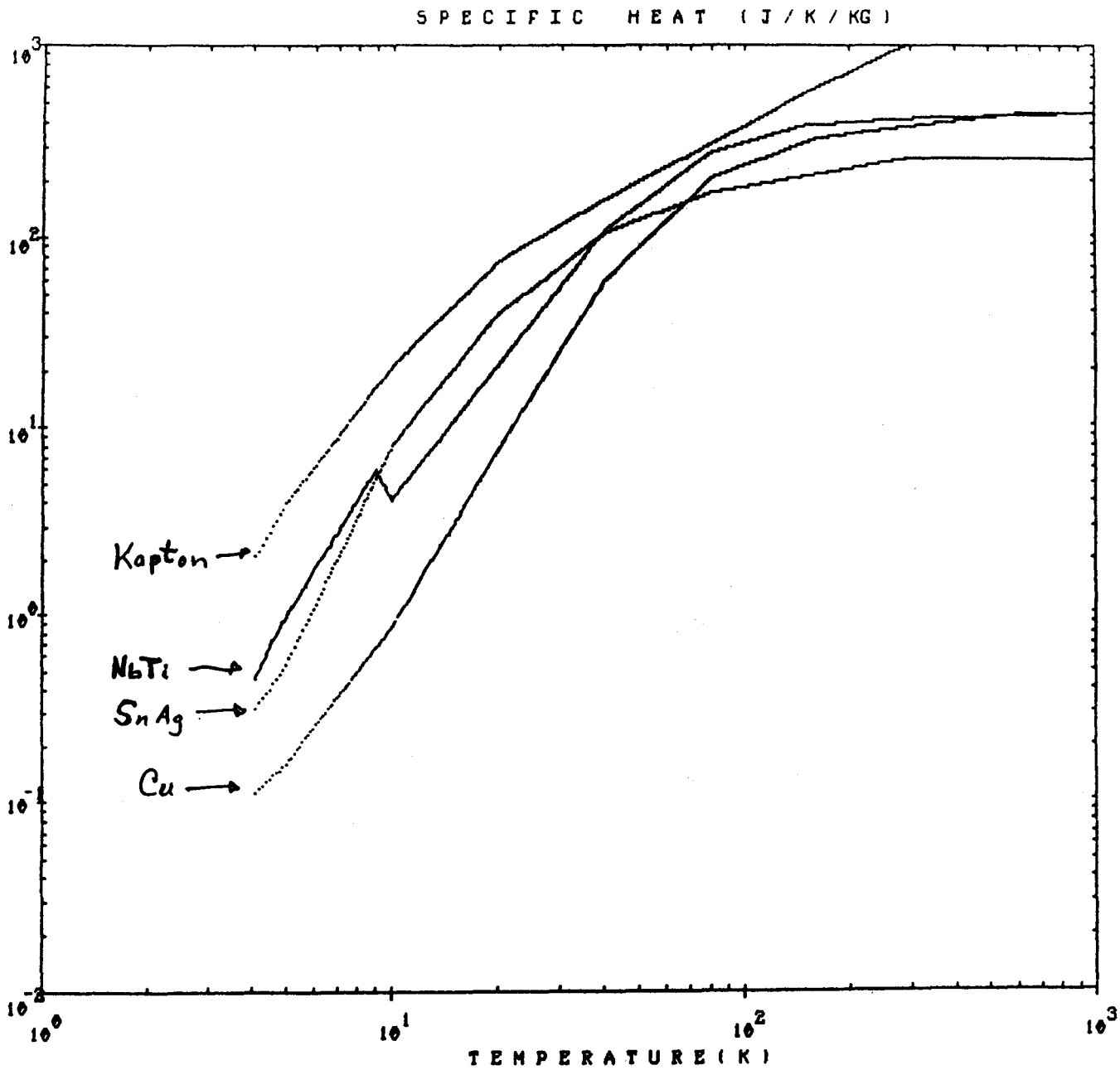
SPECIFIC HEAT (J/K/KG)
10^3
10^2
10^1
10^0
10^{-1}
10^{-2}
Kapton
NbTi
SnAg
Cu
10^0
10^1
10^2
10^3
TEMPERATURE (K)

APPENDIX D

QUENCH SIMULATION OF 3T SSC DIPOLE MANGET

TOSHI TOMINAKA
TEXAS ACCELERATOR CENTER

Preliminary 6/17 '85

Quench Simulation of 3 T SSC Dipole Magnet

Toshi Tominaka
Texas Accelerator Center
2319 Timberloch Place
The Woodlands, TX 77380

June 17, 1985

Abstract

The quench of the 3 T Superconducting Super Collider (SSC) dipole magnet is simulated by using the modified 'QUENCH' program.

(1) Introduction

As the magnet must be designed to quench safely, we calculate the quench characteristics of the magnet, that is, the current decay, the coil temperature rise, the coil voltage development, etc. applying the program developed from the 'QUENCH' program.[1-5] This program is developed and modified mainly from a version of 'QUENCH' program which takes account of the secondary coil's effect and was applied for the design of some large solenoids for high energy physics experiments.[4]

(2) Quench Calculation by the Modified 'QUENCH' Program

Input Data for the Program

About the materials of the superconducting cable, the cross section and fractional percent of each material are listed in Table 1, and the specific heat and the resistivity are assumed as shown in Fig.1 and 2. In addition, the relation between the current and the field, the relation between the inductance and the field, and the relation between the central field and the field at each coil are listed in Table 2-4. These values are estimated by 'POISSON'.[6,7]

Quench Velocity

With the adiabatic approximation, the quench velocity (or the propagation velocity of normal zone) is given by the following equation [2],

$$V_{ad} = \frac{J}{\gamma C}\sqrt{\frac{L_0 T_t}{T_t - T_0}} \qquad (1)$$

where J is the current density, γC is the heat capacity per unit volume of the conductor, L_0 (= 2.45×10^{-8} W*ohm*K^{-2}) is the Lorentz number, T_t is the transition temperature, and T_0 is the operating temperature.

With the assumption of the critical current density in the superconductor, J_C (A/cm^2) $= -5.50\times10^4 \cdot B$ (T) $+ 4.95\times10^5$, we got the good agreement between the calculated results and the experimental ones, as shown in Table 5.

Subsequent Quench of Adjacent Coil

The temperature of the quenched coil arises by the joule heat generation, especially near the point where the quench occurred. This heat flows through the insulation layer between the quenched coil and the adjacent coil, and rises the temperature of the adjacent coil. This temperature T(t) is estimated by the following equation,

$$T(t+\Delta t) = T(t) + k\frac{\{T_{max}(t) - T(t)\}\cdot\Delta t}{d\cdot\gamma C[T(t)]\cdot w} \qquad (2)$$

where k is the effective thermal conductivity ~~of the insulation spacer (G-10)~~, d is the thickness of the insulator, $T_{max}(t)$ is the temperature of the quench point in the quenched coil, γC is the averaged heat capacity per unit volume of the adjacent coil, and w is the width of the conductor of the adjacent coil.

With the value of $2\sim3 \times 10^{-5}$ W/cm*K as the effective thermal conductivity, we also got the good agreement as shown in Table 5.

Effective Inductance Matrix

As the self and mutual inductances of this superferric magnet depend on the exitation current (or the magnetis field), we assumed that the inductance is a function of the total current, $I_t = 2(I_{IN} + I_{OUT}) + I_{COR}$ through the magnetic field at the center, B_0. Then, the effective inductance for the current decay was calculated as follows, where $I_{IN} = I_1$, $I_{OUT} = I_2$, and $I_{COR} = I_3$ is defined.

$$\begin{aligned}
&\frac{d}{dt}(L_1 I_1) + \frac{d}{dt}(M_{12} I_2) + \frac{d}{dt}(M_{13} I_3) \\
&= L_1\frac{dI_1}{dt} + I_1\frac{dL_1}{dt} + M_{12}\frac{dI_2}{dt} + I_2\frac{dM_{12}}{dt} + M_{13}\frac{dI_3}{dt} + I_3\frac{dM_{13}}{dt} \\
&= L_1\frac{dI_1}{dt} + I_1\frac{dL_1}{dI_t}\left\{2\left(\frac{dI_1}{dt}+\frac{dI_2}{dt}\right)+\frac{dI_3}{dt}\right\} \\
&\quad + M_{12}\frac{dI_2}{dt} + I_2\frac{dM_{12}}{dI_t}\left\{2\left(\frac{dI_1}{dt}+\frac{dI_2}{dt}\right)+\frac{dI_3}{dt}\right\} \\
&\quad + M_{13}\frac{dI_3}{dt} + I_3\frac{dM_{13}}{dI_t}\left\{2\left(\frac{dI_1}{dt}+\frac{dI_2}{dt}\right)+\frac{dI_3}{dt}\right\} \\
&= \left\{L_1 + 2\left(I_1\frac{dL_1}{dI_t} + I_2\frac{dM_{12}}{dI_t} + I_3\frac{dM_{13}}{dI_t}\right)\right\}\frac{dI_1}{dt} + \left\{M_{12} + 2\left(I_1\frac{dL_1}{dI_t} + I_2\frac{dM_{12}}{dI_t} + I_3\frac{dM_{13}}{dI_t}\right)\right\}\frac{dI_2}{dt} \\
&\quad + \left\{M_{13} + \left(I_1\frac{dL_1}{dI_t} + I_2\frac{dM_{12}}{dI_t} + I_3\frac{dM_{13}}{dI_t}\right)\right\}\frac{dI_3}{dt} \\
&= L_{1,eff}\frac{dI_1}{dt} + M_{12,eff}\frac{dI_2}{dt} + M_{13,eff}\frac{dI_3}{dt} \qquad (3)
\end{aligned}$$

As a result, the effective inductance matrix is given as follows,

$$[\mathbb{L}_{eff}] = \begin{pmatrix} L_1 + 2\alpha_1 & M_{12} + 2\alpha_1 & M_{13} + \alpha_1 \\ M_{21} + 2\alpha_2 & L_2 + 2\alpha_2 & M_{23} + \alpha_2 \\ M_{31} + 2\alpha_3 & M_{32} + 2\alpha_3 & L_3 + \alpha_3 \end{pmatrix} \tag{4}$$

where,

$$\begin{aligned} \alpha_1 &= I_1 \frac{dL_1}{dI_t} + I_2 \frac{dM_{12}}{dI_t} + I_3 \frac{dM_{13}}{dI_t}, \\ \alpha_2 &= I_1 \frac{dM_{21}}{dI_t} + I_2 \frac{dL_2}{dI_t} + I_3 \frac{dM_{23}}{dI_t}, \\ \alpha_3 &= I_1 \frac{dM_{31}}{dI_t} + I_2 \frac{dM_{32}}{dI_t} + I_3 \frac{dL_3}{dI_t}. \end{aligned} \tag{5}$$

A typical variation of inductance is shown in Fig.3.

(3) Simplified Calculation for One Magnet on the Whole Circuit

The simplified electric circuits are shown in Fig.4 for one magnet on the whole circuit and the equations of three coil's currents (I_1, I_2 and I_3) are as follows,

$$(\mathbb{L}_{eff}) \begin{pmatrix} \frac{dI_1}{dt} \\ \frac{dI_2}{dt} \\ \frac{dI_3}{dt} \end{pmatrix} = \begin{pmatrix} -R_{n1}(t) \cdot I_1 + R_d (I_{01} - I_1) \\ -R_{n2}(t) \cdot I_2 + R_d (I_{02} - I_1) \\ -R_{n3}(t) \cdot I_3 + R_d (I_{03} - I_1) \end{pmatrix} \tag{6}$$

where L_{eff} is the effectve inductance matrix, $R_n(t)$ is the resistance due to the normal zone in the coil, R_d is the ~~parallel~~ resistance due to the diode ~~and the dump resistor~~, and I_0 is the initial operating current. The resistance of diode is approximately assumed to be infinite on the 'OFF' state and 0.1 milli-ohm on the 'ON' state.

Calculation Result

The quench calculation is carried out for the magnet of 35 m long, 70 m long, 105 m long (35 m long × 3), and 140 m long. The calculational results are compiled in Table 6-7, and the plots of the current decay and the temperature rise are shown in Fig.6-11, respectively.

(4) Detailed Calculation for a Whole Circuit of One Power Supply System

The electric circuit is shown in Fig.5 for one array of ring magnets. The equations of currents are as follows,

$$
\left\{
\begin{aligned}
&\frac{d}{dt}(L_1' I_1') + \frac{d}{dt}(M_{12}' I_2') + \frac{d}{dt}(M_{13}' I_3') + (N-1)\left\{\frac{d}{dt}(L_1 I_1) + \frac{d}{dt}(M_{12} I_2) + \frac{d}{dt}(M_{13} I_3)\right\} \\
&+ R_{n1} I_1' + R_{dump1}(I_1 - I_{01}) = 0 \\
&\frac{d}{dt}(M_{21}' I_1') + \frac{d}{dt}(L_2' I_2') + \frac{d}{dt}(M_{23}' I_3') + (N-1)\left\{\frac{d}{dt}(M_{21} I_1) + \frac{d}{dt}(L_2 I_2) + \frac{d}{dt}(M_{23} I_3)\right\} \\
&+ R_{n2} I_2' + R_{dump2}(I_2 - I_{02}) = 0 \\
&\frac{d}{dt}(M_{31}' I_1') + \frac{d}{dt}(M_{32}' I_2') + \frac{d}{dt}(L_3' I_3) + (N-1)\left\{\frac{d}{dt}(M_{31} I_1) + \frac{d}{dt}(M_{32} I_2) + \frac{d}{dt}(L_3 I_3)\right\} \\
&+ R_{n3} I_3' + R_{dump3}(I_3 - I_{03}) = 0 \\
&-\frac{d}{dt}(L_1' I_1') - \frac{d}{dt}(M_{12}' I_2') - \frac{d}{dt}(M_{13}' I_3') - R_{n1} I_1' + R_d i_1 = 0 \\
&-\frac{d}{dt}(M_{21}' I_1') - \frac{d}{dt}(L_2' I_2') - \frac{d}{dt}(M_{23}' I_3') - R_{n2} I_2' + R_d i_2 = 0 \\
&-\frac{d}{dt}(M_{31}' I_1') - \frac{d}{dt}(M_{32}' I_2') - \frac{d}{dt}(L_3' I_3') - R_{n3} I_3' + R_d i_3 = 0
\end{aligned}
\right.
$$

, where $I_1' = I_1 - i_1$, $I_2' = I_2 - i_2$, and $I_3' = I_3 - i_3$ are defined.

$$
[L_{eff}]
\begin{bmatrix}
\frac{dI_1}{dt} \\ \frac{dI_2}{dt} \\ \frac{dI_3}{dt} \\ \frac{di_1}{dt} \\ \frac{di_2}{dt} \\ \frac{di_3}{dt}
\end{bmatrix}
=
\begin{bmatrix}
-R_{n1}(I_1 - i_1) - R_{dump1}(I_1 - I_{01}) \\
-R_{n2}(I_2 - i_2) - R_{dump2}(I_2 - I_{02}) \\
-R_{n3}(I_3 - i_3) - R_{dump2}(I_3 - I_{03}) \\
R_{n1}(I_1 - i_1) - R_d i_1 \\
R_{n2}(I_2 - i_1) - R_d i_2 \\
R_{n2}(I_3 - i_3) - R_d i_3
\end{bmatrix}
\qquad (7)
$$

, where

$$
[L_{eff}] =
\begin{bmatrix}
(N-1)(L_1+2\alpha_1)+(L_1'+2\alpha_1'), & (N-1)(M_{12}+2\alpha_1)+(M_{12}'+2\alpha_1'), & (N-1)(M_{13}+\alpha_1)+(M_{13}'+\alpha_1'), & -(L_1'+2\alpha_1'), & -(M_{12}'+2\alpha_1'), & -(M_{13}'+\alpha_1') \\
(N-1)(M_{21}+2\alpha_2)+(M_{21}'+2\alpha_2'), & (N-1)(L_2+2\alpha_2)+(L_2'+2\alpha_2'), & (N-1)(M_{23}+\alpha_2)+(M_{23}'+\alpha_2'), & -(M_{21}'+2\alpha_2'), & -(L_2'+2\alpha_2'), & -(M_{23}'+\alpha_2') \\
(N-1)(M_{31}+2\alpha_3)+(M_{31}'+2\alpha_3'), & (N-1)(M_{32}+2\alpha_3)+(M_{32}'+2\alpha_3'), & (N-1)(L_3+\alpha_3)+(L_3'+\alpha_3'), & -(M_{31}'+2\alpha_3'), & -(M_{32}'+2\alpha_3'), & -(L_3'+\alpha_3') \\
-(L_1'+2\alpha_1'), & -(M_{12}'+2\alpha_1'), & -(M_{13}'+\alpha_1'), & (L_1'+2\alpha_1'), & (M_{12}'+2\alpha_1'), & (M_{13}'+\alpha_1') \\
-(M_{21}'+2\alpha_2'), & -(L_2'+2\alpha_2'), & -(M_{23}'+\alpha_2'), & (M_{21}'+2\alpha_2'), & (L_2'+2\alpha_2'), & (M_{23}'+\alpha_2') \\
-(M_{31}'+2\alpha_3'), & -(M_{32}'+2\alpha_3'), & -(L_3'+\alpha_3'), & (M_{31}'+2\alpha_3'), & (M_{32}'+2\alpha_3'), & (L_3'+\alpha_3')
\end{bmatrix}
$$

(8)

where L' and L are the self inductance of a quench coil and a non-quench coil, respectively, M' and M are the mutual inductance of a quench coil and a non-quench coil, respectively, N is the total number of magnet, I_0 is the initial operating current, $R_n(t)$ is the resistance due to the normal zone in the coil, R_{dump} is the resistance of the dump (or protection) resistor in the circuit, and R_d is the resistance of the diode.

Calculation Result

The quench calculation is carried out for one section (1/4) with the 332 magnets of 105 m long (35 m long × 3). The calculational results are compiled in Table 8, and the plots of the current decay and the temperature rise are shown in Fig.12-16, respectively.

(5) Discussions

The melting temperature of the solder (Sn-5%Ag) of the superconducting cable is 494 - 518 K (430 - 473 F), and the operatable temperature of Kapton is up to 673 K. Therefore, the maximum temperature of the superconducting coil ~~must~~ should be lesser than 500 K.

The calculation result by the modified 'QUENCH' program shows that the maximum temperature of the 105 m (35 m × 3) long magnet is little bit high.

As this calculation involves many uncertain parameters, this calculation will need to be confirmed experimentally on the small model magnet.

Acknowledgements

I would like to thank my colleagues for their comments and assistance, particularly M. Kobayashi, G. Lopez, W. Schmidt, J. Zeigler and W. Hassenzahl (LBL).

References

[1] M. N. Wilson, Rutherford Laboratory Report, RHEL/M151 (1968).

[2] M. N. Wilson, 'Superconducting Magnets', chapter 9, Oxford University Press (1983).

[3] W. Hassenzahl, CEN Saclay, SUPRA/78-61 CEN.

[4] D. Andrews, Cornell Ins Internal Report CBX-77-1 (1977).

[5] T. Tominaka, TAC Internal Report (1985).

[6] W. Schmidt, TAC Internal Report (1984).

[7] G. Lopez, Private communication.

Table 1.

Details of the TAC SSC 3-T Dipole Conductor

		Inner or Outer Coil	Trim Coil
Conductor dimentions with insulation	(mm*mm)	2.95*8.03	3.15*4.42
Conductor cross section	(mm^2)	23.6 (100 %)	13.9 (100 %)
Superconductor cross section	(mm^2)	3.80 (16.1%)	1.90 (13.7%)
Copper cross section	(mm^2)	12.99 (55.0%)	5.70 (40.9%)
Solder cross section	(mm^2)	2.56 (10.8%)	2.08 (14.9%)
Insulation cross section	(mm^2)	4.29 (18.1%)	4.24 (30.5%)
H_c at 4.2K	(T)	11.3	
T_c at B=0	(K)	9.3	

Table 2.

Relation between the Total Current* and the Central Field

I_t (kA)	0.	1.55	5.10	10.8	12.1	16.6	19.3	21.0
B_0 (T)	0.	.152	.502	1.06	1.21	1.63	1.88	2.04

I_t (kA)	24.3	26.7	32.0	35.1	40.6
B_0 (T)	2.28	2.42	2.66	2.79	2.98

* The total current is defined as $I_t = 2*(I_{IN} + I_{OUT}) + I_{COR}$

Table 3.

Inductances for the 3-T TAC SSC Dipole

B_0	(T)	0.0	0.5	1.6	2.4	3.0
L in	(H/m)	5.24(*E-5) 10^{-5}	5.24*E-5	4.40*E-5	4.04*E-5	3.42*E-5
L out	(H/m)	5.88*E-5	5.88*E-5	4.78*E-5	3.95*E-5	3.16*E-5
L trim	(H/m)	9.10*E-6	9.10*E-6	8.88*E-6	8.11*E-6	7.03*E-6
M in,out	(H/m)	4.64*E-5	4.64*E-5	3.91*E-5	3.36*E-5	2.86*E-5
M in,trim	(H/m)	1.86*E-5	1.86*E-5	1.70*E-5	1.49*E-5	1.24*E-5
M out,trim	(H/m)	1.86*E-5	1.86*E-5	1.70*E-5	1.49*E-5	1.24*E-5

Table 4

Relation Between the Central Field and Typical Fields at Each Coil*

B_0 (T)	0.0	0.50	1.6	3.0
B in (T)	0.0	0.27	0.92	1.5
B out (T)	0.0	0.11	0.36	1.2
B trim (T)	0.0	0.45	1.4	3.0

* ~~B = (Bx + By)**(1/2)~~

$B = \sqrt{B_x^2 + B_y^2}$

Table 5.

Quench Velocities and Turn-to-Turn Transition Times
for the Outer Coil of TAC Magnet

Current	Quench Velocities Measured	Quench Velocities Calculated
(kA)	(m/s)	(m/s)
9.0	12.4 + 0.4	12.8
7.5	7.9 + 0.3	9.7
5.0	4.1 + 0.1	5.5

Current	Turn to Turn Propagation Time Measured	Calculated ($\cancel{2\times E-5}$ 2×10^{-5} W/cm*K)	Calculated ($\cancel{3\times E-5}$ 3×10^{-5} W/cm*K)
(kA)	(ms)	(ms)	(ms)
9.0	116 + 3	122	92
7.5	176 + 2	186	142
5.0	249 + 5	---	278

Table 6.

QUENCH STARTS	MAGNET LENGTH (m)	COIL	Tmax (K)	Rmax (milli-ohm)	Vmax (V)	Veli (m/s)	Frac. of Normal (%)
INNER -COIL Fig. 6	35 * 3 (=105)	IN	570.	22.	64.	23.	8.1
		OUT	500.	19.	68.	18.	4.2
		COR	51.	23.	110.	8.6	100.
OUTER -COIL Fig. 7	35 * 3 (=105)	IN	530.	24.	88.	23.	7.3
		OUT	610.	20.	70.	18.	4.7
		COR	58.	26.	160.	7.6	100.
COR. -COIL Fig. 8	35 * 3 (=105)	IN	520.	23.	78.	23.	7.6
		OUT	530.	21.	75.	18.	4.5
		COR	320.	21.	32.	7.5	11.

Table 7.

QUENCH STARTS	MAGNET LENGTH (m)	COIL	Tmax (K)	Rmax (milli-ohm)	Vmax (V)	Veli (m/s)	Frac. of Normal (%)
OUTER -COIL Fig. 9	35 * 4 (=140)	IN	600.	30.		23.	6.0
		OUT	730.	26.		18.	3.7
		COR	59.	35.		6.0	100.
OUTER -COIL Fig. 7	35 * 3 (=105)	IN	530.	24.	88.	23.	7.3
		OUT	610.	20.	70.	18.	4.7
		COR	58.	26.	160.	7.6	100.
OUTER -COIL Fig. 10	35 * 2 (= 70)	IN	390.	17.		23.	9.9
		OUT	510.	14.		18.	6.4
		COR	53.	18.		8.6	100.
OUTER -COIL Fig. 11	35 * 1 (= 35)	IN	280.	9.1		22.	13.
		OUT	330.	8.2		18.	11.
		COR	140.	7.7		11.	19.

Table 8. In the case of $t_{sw} = 0.1$ sec

QUENCH STARTS	MAGNET LENGTH (m)	COIL	Tmax (K)	Rmax (milli-ohm)	Vmax (V)	Veli (m/s)	Frac. of Normal (%)	
INNER -COIL Fig. 13	35 * 3 (=105)	IN	560.	21.	69.	23.	8.0	$K = 3\times10^{-5}$ w/cm·K
		OUT	420.	16.	52.	15.	4.1	
		COR	45.	26.	160.	9.0	100.	
OUTER -COIL Fig. 14	35 * 3 (=105)	IN	500.	22.	83.	21.	7.1	
		OUT	610.	20.	60.	18.	4.7	
		COR	49.	26.	160.	9.0	100.	
INNER -COIL Fig. 15	35 * 3 (=105)	IN	560.	23.	69.	23.	8.2	≈ Gustavo's Assumption
		OUT	380.	21.	70.	17.	7.3	
		COR	52.	24.	110.	2.9	100.	
OUTER -COIL Fig. 16	35 * 3 (=105)	IN	510.	25.	89.	22.	8.0	
		OUT	640.	22.	79.	18.	6.5	
		COR	56.	24.	110.	0.22	100.	

Input Data A

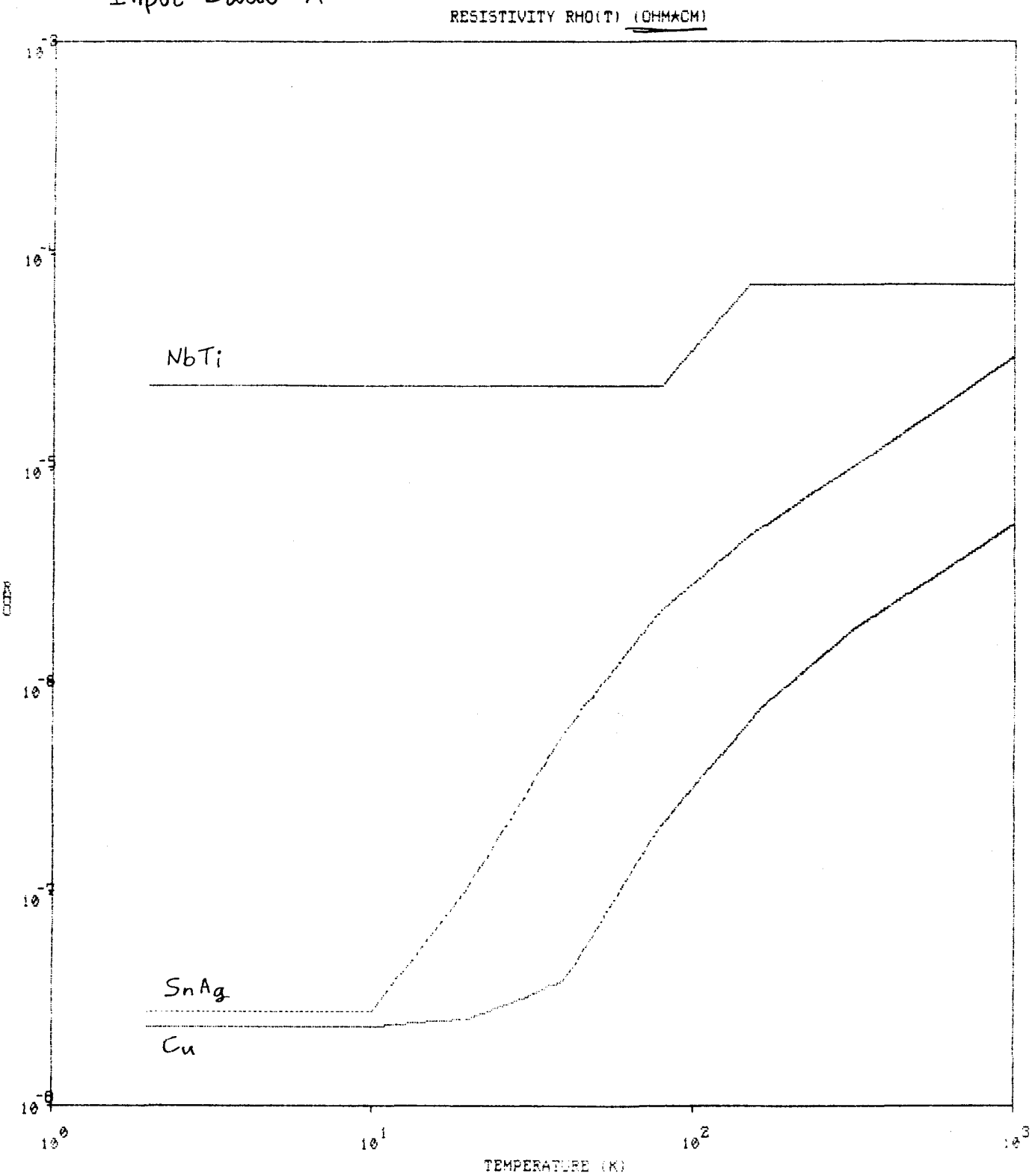

Fig. 1

Input Data B′

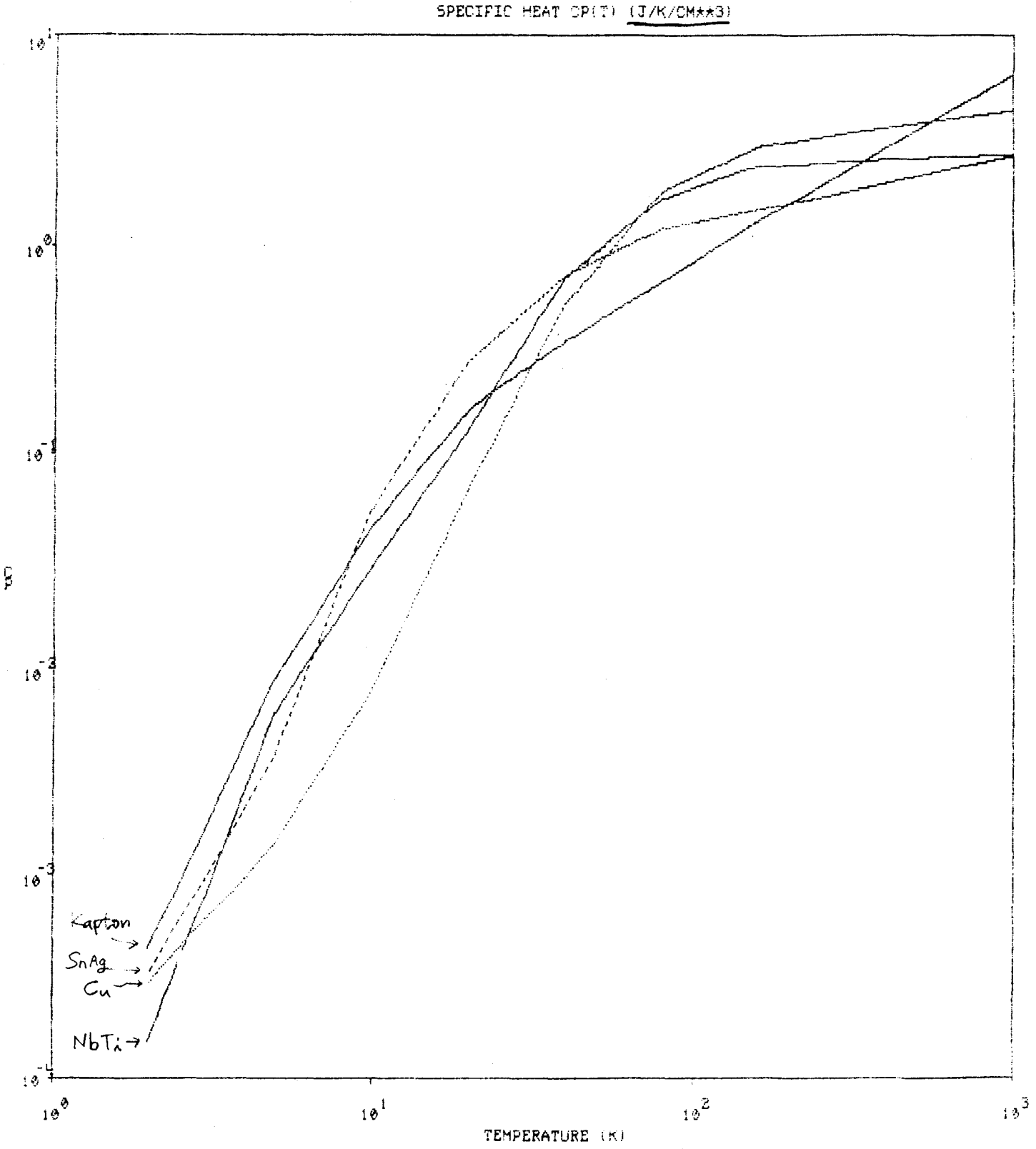

Fig. 2

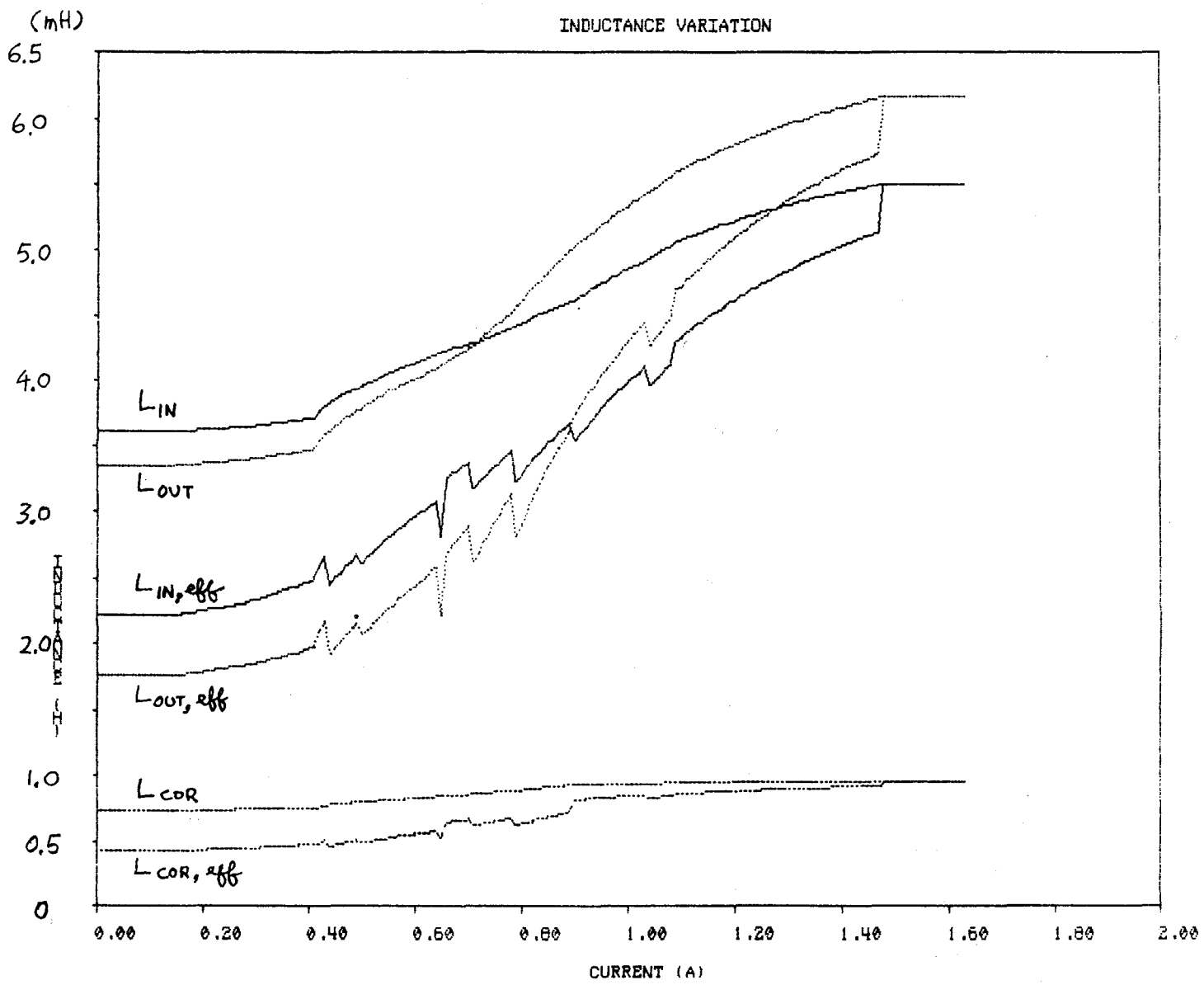

Fig. 3
(in the case of Fig. 6)

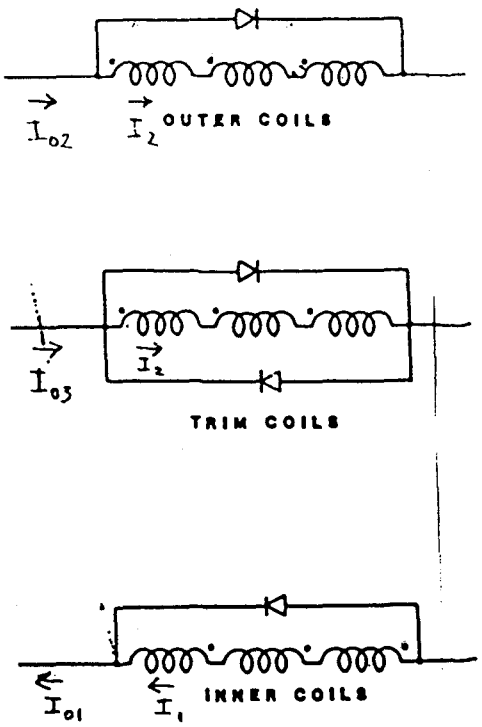
I_{02}
I_2
OUTER COILS
I_{03}
I_2
TRIM COILS
I_{01}
I_1
INNER COILS

Fig. 4

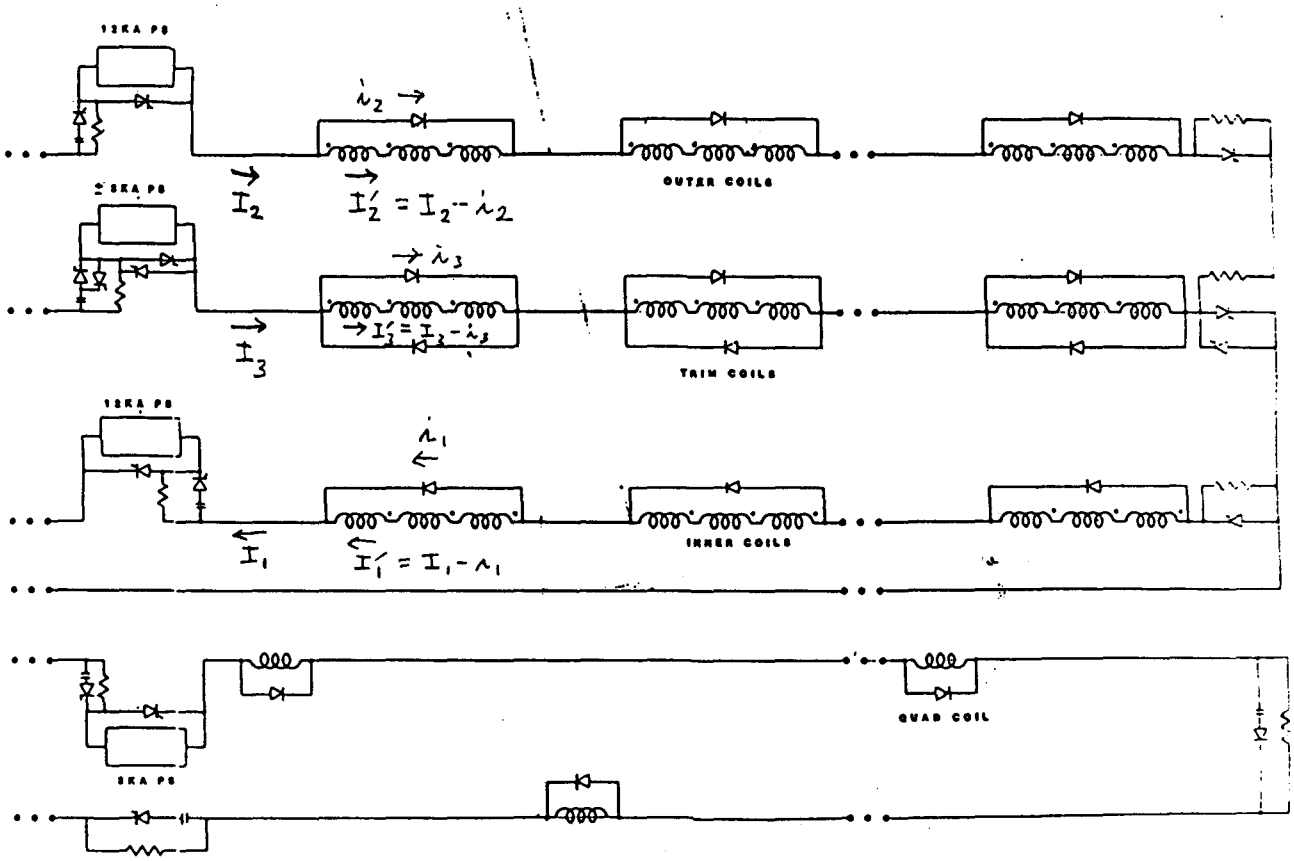
12KA PS
i_2
I_2
$I_2' = I_2 - i_2$
OUTER COILS
i_3
I_3
$I_3' = I_3 - i_3$
TRIM COILS
12KA PS
i_1
I_1
$I_1' = I_1 - i_1$
INNER COILS
QUAD COIL
5KA PS

Fig. 5

Symbols of the Table attached to the Figure

Rext : Dump resistance
L : Self inductance and (effective inductance)
Ii : Initial coil current
If : Final coil current
Rmax : Final coil resistance due to the normal zone
(including the volume per cent of the normal zone in the coil)
Tmax : Maximum temperature in the coil
Vmax : Maximum resistive voltage in the coil
Veli : Initial quench velocity and (including the quench time)
Es,i : Initial magnetic stored energy of the coil
Es,f : Final magnetic stored energy of the coil
Ein : Thermally dissipated energy in the coil
Eext : Thermally dissipated energy in the external resistor (or diode)

105 m Magnet
Inner Coil Quench

	R_{ext}	L	I_i	I_f	R_{max}	T_{max}	V_{max}	Vel_i	$E_{s,i}$	$E_{s,f}$	E_{in}	E_{ext} Diode
Coil in	—	3.6~5.5 (2.2~5.5) mH	11275A	800 A	22mΩ (8.1%)	570 K	64 V	23 m/sec	3.9×10^5 J	3.9×10^3 J	2.3×10^5 J	9.5×10^3 J
Coil out	—	3.3~6.2 (1.8~6.2) mH	10225A	990 A	19 mΩ (4.2%)	500 K	68 V	18 m/sec (0.31 sec)	3.3×10^5 J	5.2×10^3 J	2.1×10^5 J	5.4×10^3 J
Coil trim	—	0.74~0.96 (0.43~0.96) mH	-2400A	270 A	23mΩ (100%)	51 K	110 V	8.6 m/sec (0.33 sec)	-3.2×10^4 J	5.0×10^3 J	2.5×10^4 J	1.8×10^3 J
Total	(52'… U.H.), e = 0 , Δt = 0.01 sec								6.9×10^5 J	9.7×10^3 J	4.6×10^5 J	1.7×10^4 J

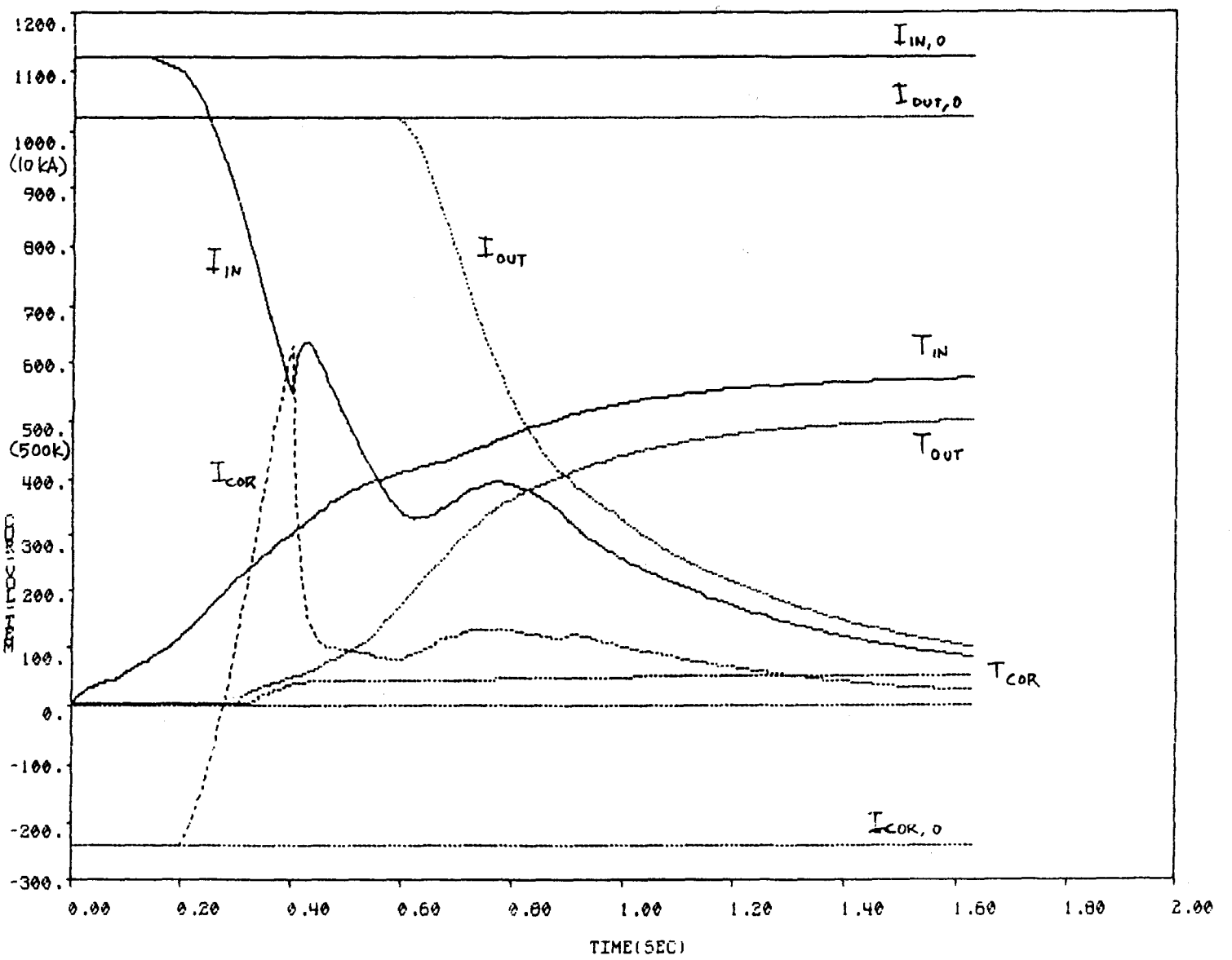

Fig. 6.

105 m Magnet

Outer Coil Quench

	R_{ext}	L	I_i	I_f	R_{max}	T_{max}	V_{max}	Vel_i	$E_{s,i}$	$E_{s,f}$	E_{in}	E_{ext} Diode
Coil in	—	3.6~5.5 (2.2~5.5) mH	11275A	800A	24mΩ (7.3%)	530K	88V	23 m/sec (0.29 sec)	3.9×10^5J	3.9×10^3J	2.5×10^5J	7.2×10^3J
Coil out	—	3.3~6.2 (1.8~6.2) mH	10225A	1000A	20mΩ (4.7%)	610K	70V	18 m/sec	3.3×10^5J	5.3×10^3J	2.3×10^5J	5.6×10^3J
Coil trim	—	0.74~9.6 (0.43~9.6) mH	-2400A	250A	26mΩ (100%)	58K	160V	7.6 m/sec (0.39 sec)	-3.2×10^4J	4.7×10^2J	2.3×10^4J	1.7×10^3J
Total	(52'… U.H.), e = 0 , Δt = 0.01 sec								6.9×10^5J	9.7×10^3J	5.1×10^5J	1.5×10^4J

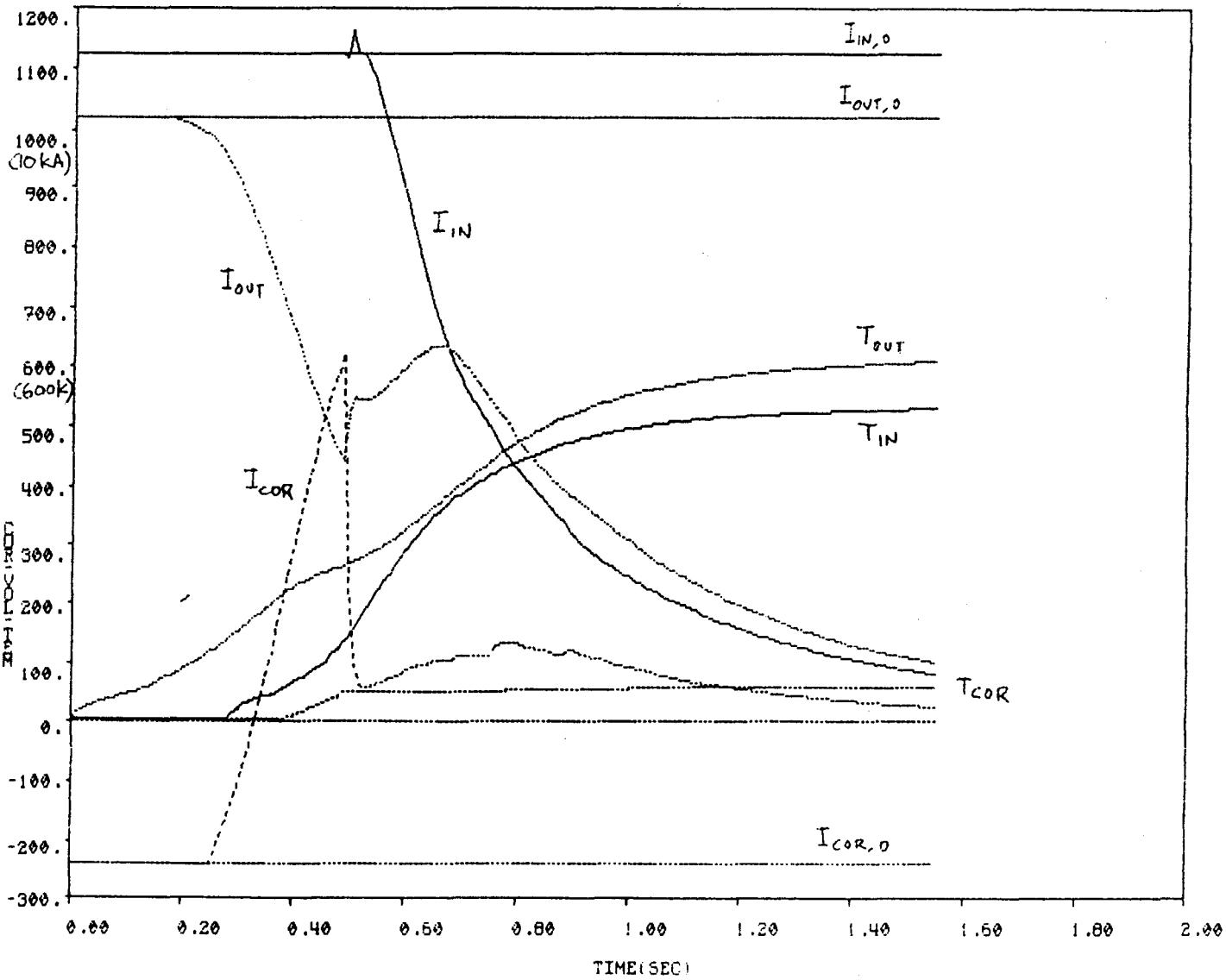

Fig. 7

105 m Magnet
Cor. Coil Quench

	R_{ext}	L	I_i	I_f	R_{max}	T_{max}	V_{max}	Vel_i	$E_{s,i}$	$E_{s,f}$	E_{in}	E_{ext} (Diode)
Coil in	—	3.6~5.5 (2.2~5.5) mH	11275 A	850 A	23 mΩ (7.6%)	520 K	78 V	23 m/sec (0.35 sec)	3.9×10^5 J	4.3×10^3 J	2.5×10^5 J	7.8×10^3 J
Coil out	—	3.3~6.2 (1.8~6.2) mH	10225 A	1000 A	21 mΩ (4.5%)	530 K	75 V	18 m/sec (0.48 sec)	3.3×10^5 J	5.4×10^3 J	2.3×10^5 J	5.1×10^3 J
Coil trim	—	0.74~0.96 (0.43~0.96) mH	−2400 A	330 A	21 mΩ (~~10.7%~~ 11%)	320 K	32 V	7.5 m/sec	-3.2×10^4 J	6.4×10^2 J	4.5×10^4 J	2.4×10^3 J
Total	(1:15'… U.H.), e = 0 , Δt = 0.01 sec								6.9×10^5 J	1.0×10^4 J	5.3×10^5 J	1.5×10^4 J

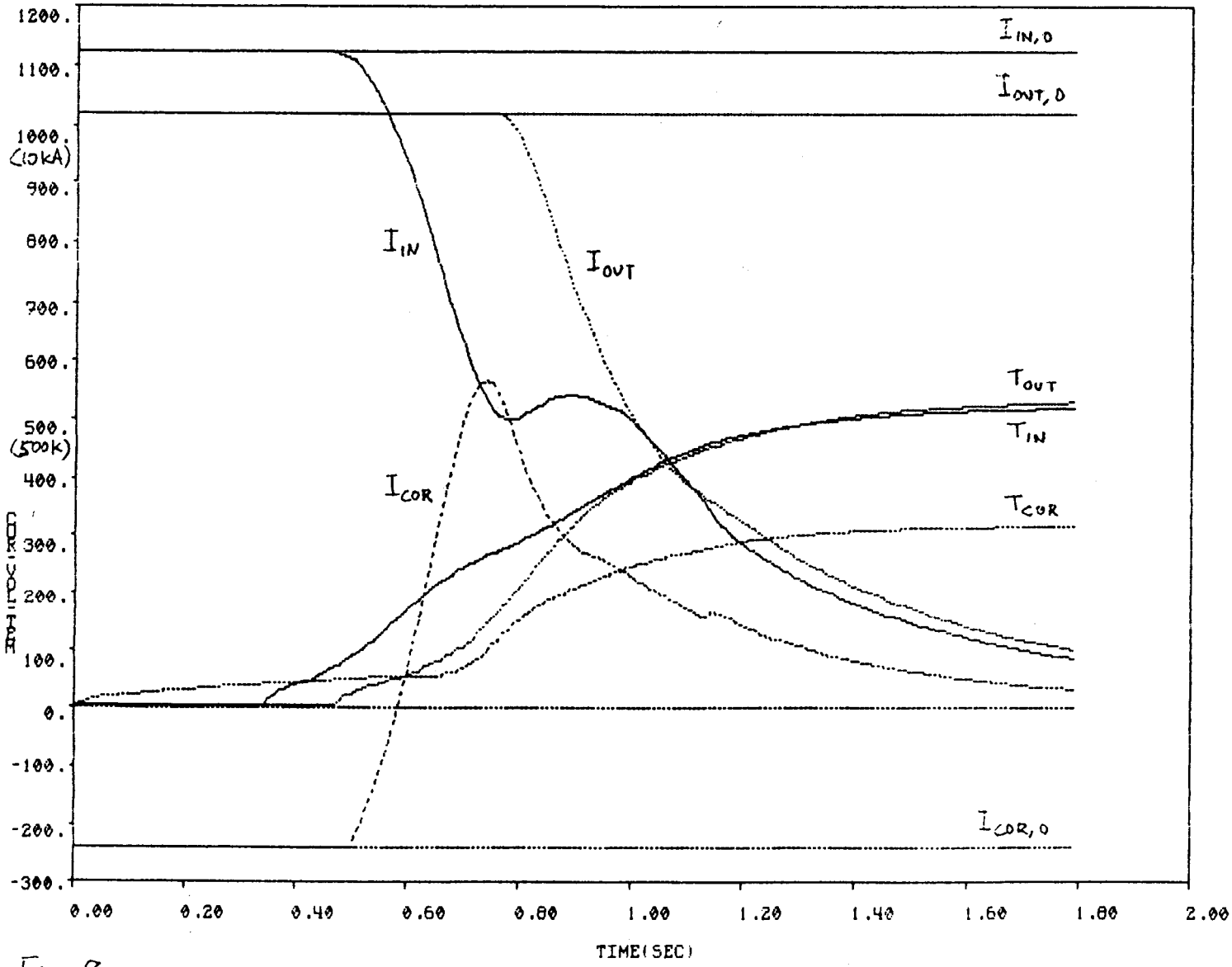

Fig. 8

140 m Magnet
Outer Coil Quench

	R_{ext}	L	I_i	I_f	R_{max}	T_{max}	V_{max}	Vel_i	$E_{s,i}$	$E_{s,f}$	E_{in}	E_{ext} Diode
Coil in	—	4.8 ~ 7.3 (3.0 ~ 7.3) mH	11275A	800 A	30 mΩ (6.0 %)	600 K		23 m/sec (0.29 sec)	5.1×10^5 J	5.2×10^3 J	3.4×10^5 J	7.6×10^3 J
Coil out	—	4.6 ~ 8.2 (2.3 ~ 8.2) mH	10225A	990 A	26 mΩ (3.7 %)	730 K		18 m/sec	4.4×10^5 J	6.9×10^3 J	3.1×10^5 J	5.8×10^3 J
Coil trim	—	0.99 ~ 1.3 (0.58 ~ 1.3) mH	-2400 A	240 A	35 mΩ (100 %)	59 K		6.0 m/sec (0.40 sec)	-4.2×10^4 J	6.0×10^2 J	3.2×10^4 J	1.7×10^3 J
Total	(1:01'… U.H.), e = 0 , Δt : 0.01 sec								9.2×10^5 J	1.3×10^4 J	6.8×10^5 J	1.5×10^4 J

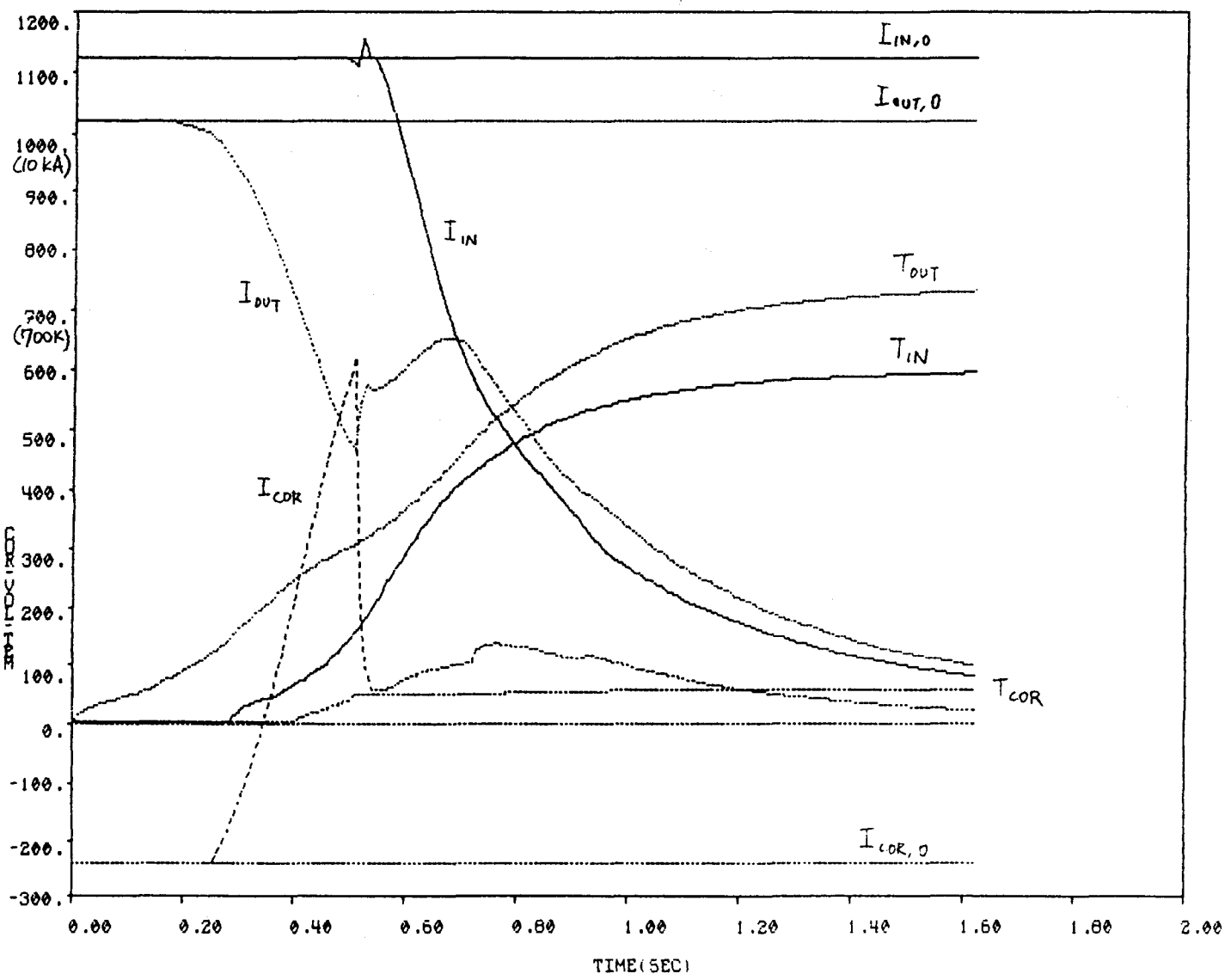

Fig. 9

70 m Magnet

Outer coil Quench

	R_{ext}	L	I_i	I_f	R_{max}	T_{max}	V_{max}	Vel_i	$E_{s,i}$	$E_{s,f}$	E_{in}	E_{ext} Diode
Coil in	—	2.4~3.7 (1.5~3.7) mH	11275A	810 A	17 mΩ (9.9%)	390 K		23 m/sec (0.29 sec)	2.6×10^5 J	2.6×10^3 J	1.7×10^5 J	6.8×10^3 J
Coil out	—	2.2~4.1 (1.2~4.1) mH	10225A	1000 A	14 mΩ (6.4%)	510 K		18 m/sec	2.2×10^5 J	3.5×10^3 J	1.5×10^5 J	5.5×10^3 J
Coil trim	—	0.49~0.64 (0.29~0.64) mH	-2400A	260 A	18 mΩ (100%)	53 K		8.6 m/sec (0.37 sec)	-2.1×10^4 J	3.2×10^2 J	1.6×10^4 J	1.6×10^3 J
Total	(5:29 … TAC), e = 0 , Δt = 0.01 sec								4.6×10^5 J	6.5×10^3 J	3.3×10^5 J	1.4×10^4 J

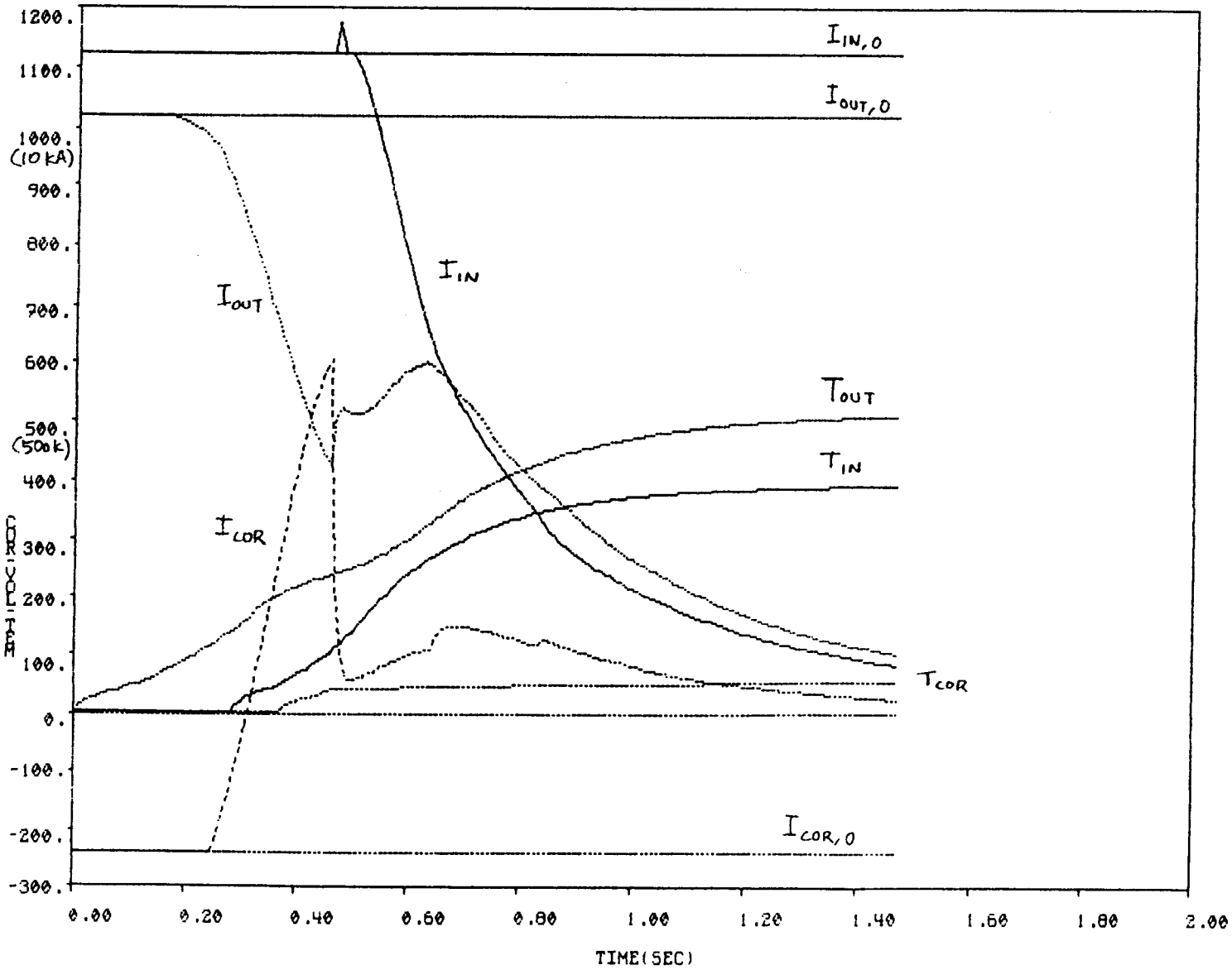

Fig. 10.

35 m Magnet
Outer Coil Quench

	R_{ext}	L	I_i	I_f	R_{max}	T_{max}	V_{max}	Vel_i	$E_{s,i}$	$E_{s,f}$	E_{in}	E_{ext} Diode
Coil in	—	1.2~1.8 (0.74~1.8) mH	11275A	850 A	9.1 mΩ (13%)	280 K		22 m/sec (0.29 sec)	1.3×10^5 J	1.4×10^3 J	8.3×10^4 J	6.3×10^3 J
Coil out	—	1.1~2.1 (0.59~2.1) mH	10225A	1000 A	8.2 mΩ (11%)	330 K		18 m/sec	1.1×10^5 J	1.8×10^3 J	7.5×10^4 J	5.5×10^3 J
Coil trim	—	0.25~0.32 (0.14~0.32) mH	-2400A	300 A	7.9 mΩ (19%)	140 K		11 m/sec (0.35 sec)	-1.1×10^4 J	2.0×10^2 J	1.4×10^4 J	2.3×10^3 J
Total	(33'… U.H.), e = 0 , Δt = 0.01 sec								2.3×10^5 J	3.5×10^3 J	1.7×10^5 J	1.4×10^4 J

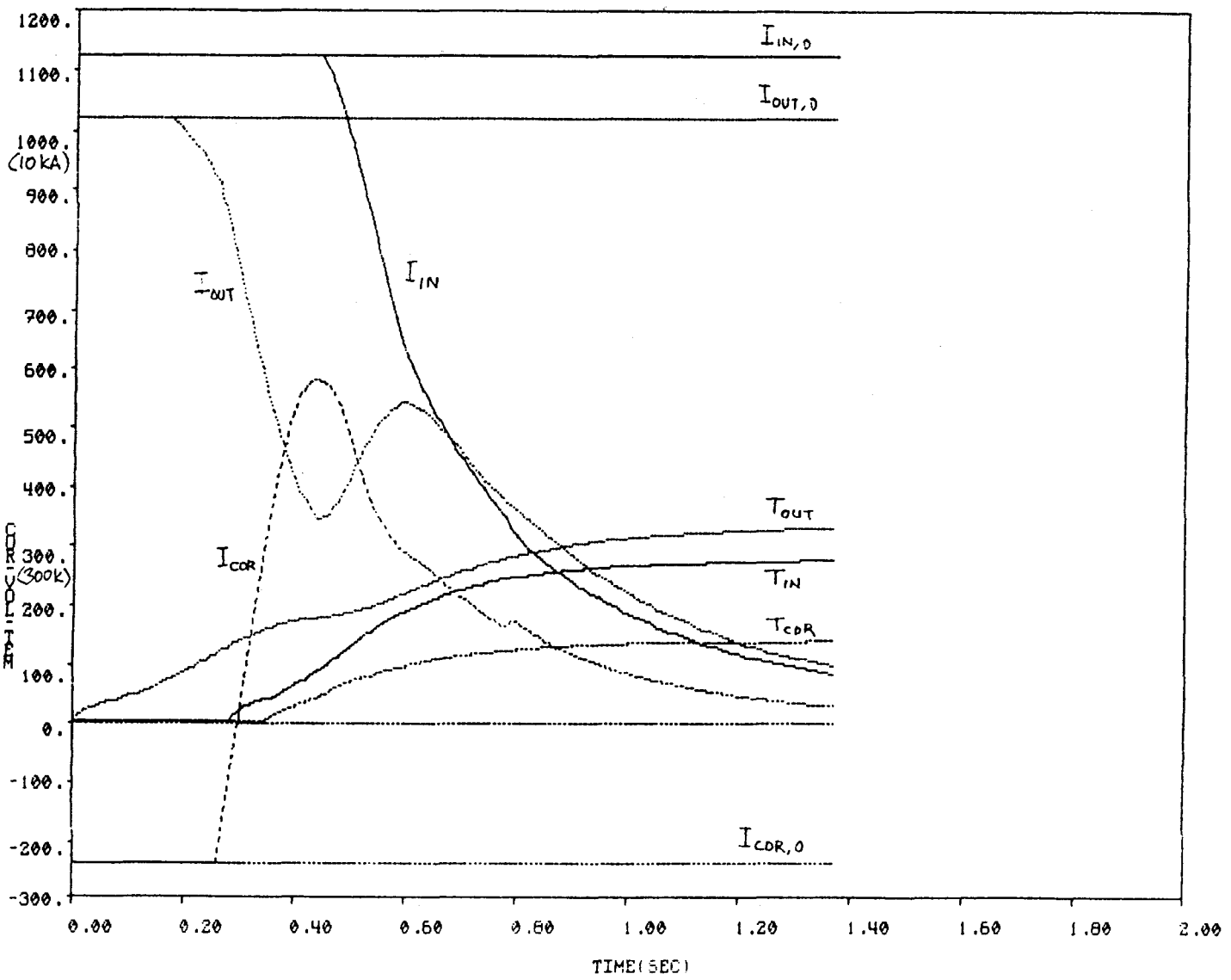

Fig. 11

105 m Magnet × 332
Inner Coil Quench
$k = 3.0 \times 10^{-5}$ W/cm·K

	R_{ext}	L (L_{eff})	I_i	I_f	R_{max}	T_{max}	V_{max}	Vel_i	$E_{s,i}$	$E_{s,f}$	E_{in}	E_{ext} Diode
Coil in	0.15 Ω	3.6~5.5 (2.2~5.5) mH	11275 A	800 A	22 mΩ (8.1%)	570 K	64 V	23 m/sec	3.9×10^5 J	3.9×10^3 J	2.3×10^5 J	9.5×10^3 J
Coil out	0.15 Ω	3.3~6.2 (1.8~6.2) mH	10225 A	990 A	19 mΩ (4.3%)	500 K	68 V	18 m/sec (0.31 sec)	3.3×10^5 J	5.3×10^3 J	2.1×10^5 J	5.4×10^3 J
Coil trim	0.15 Ω	0.74~0.96 (0.43~0.96) mH	-2400 A	270 A	23 mΩ (100%)	51 K	110 V	8.5 m/sec (0.33 sec)	3.2×10^4 J	5.0×10^2 J	2.5×10^4 J	1.8×10^3 J
Total									6.9×10^5 J	9.7×10^3 J	4.6×10^5 J	1.7×10^4 J

effective inductance

(56'... U.H.), e = 0, Δt = 0.01 sec

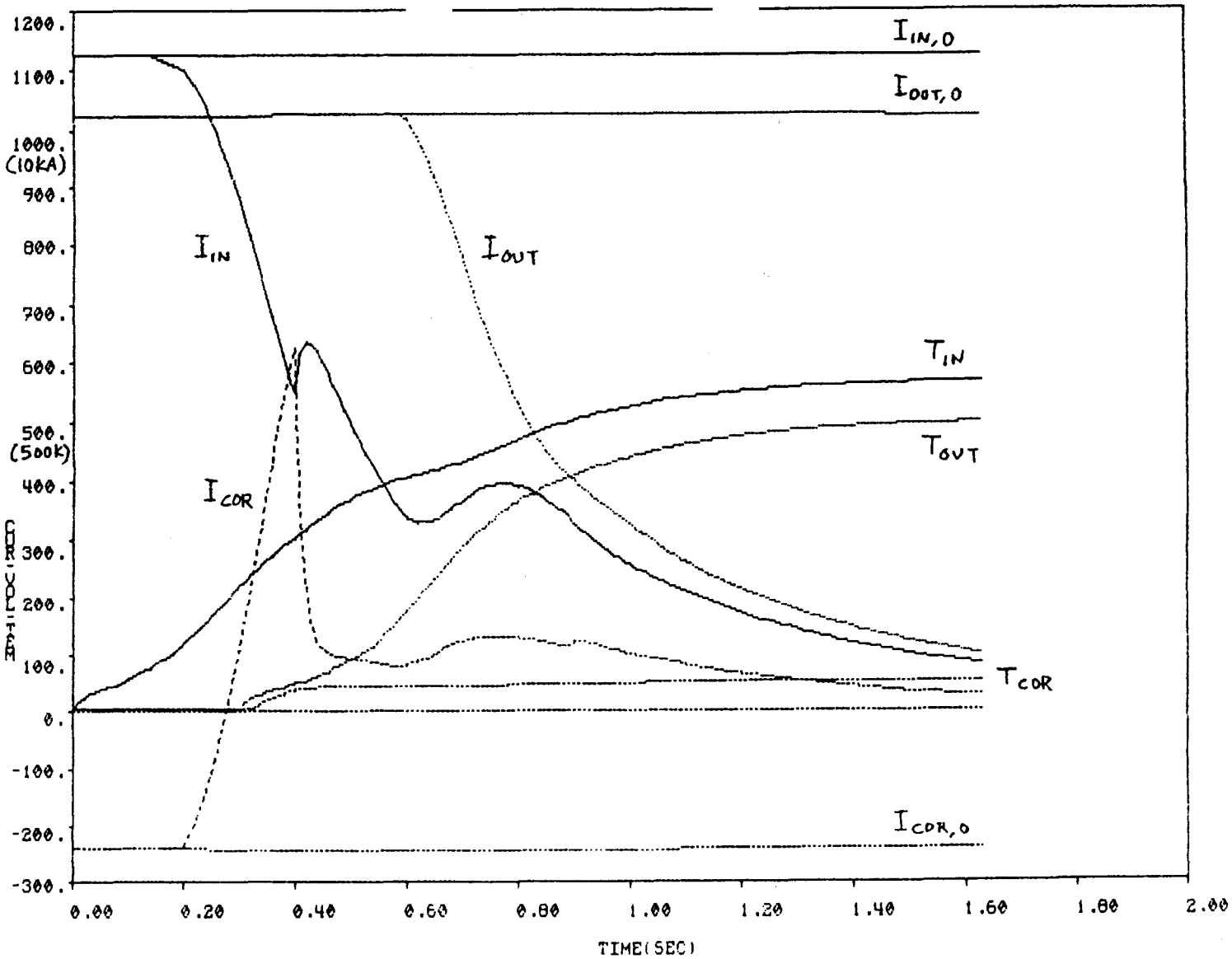

Fig. 12

105 m Magnet × 332

Inner Coil Quench

$t_{sw} = 0.1$ sec

$k = 3.0 \times 10^{-5}$ W/cm·K

	R_{ext}	L	I_i	I_f	R_{max}	T_{max}	V_{max}	Vel_i	$E_{s,i}$	$E_{s,f}$	E_{in}	E_{ext} Diode
Coil in	0.15 Ω	3.6~5.5 (2.2~5.5) mH	11275A	700 A	21 mΩ (8.0%)	560 K	69 V	23 m/sec	3.9×10^5 J	3.2×10^3 J	2.2×10^5 J	7.3×10^3 J
Coil out	0.15 Ω	3.3~6.2 (1.8~6.2) mH	10225A	990A	16 mΩ (4.1%)	420 K	52 V	15 m/sec (0.33 sec)	3.3×10^5 J	5.0×10^3 J	1.7×10^5 J	2.8×10^3 J
Coil trim	0.15 Ω	0.74~0.96 (0.43~0.96) mH	-2400A	220 A	26 mΩ (100%)	45 K	160 V	9.0 m/sec (0.31 sec)	-3.2×10^4 J	3.9×10^2 J	2.2×10^4 J	8.0×10^2 J
Total									6.9×10^5 J	8.6×10^3 J	4.1×10^5 J	1.1×10^4 J

(59'·· U.H.), $\epsilon = 0$, $\Delta t = 0.01$ sec

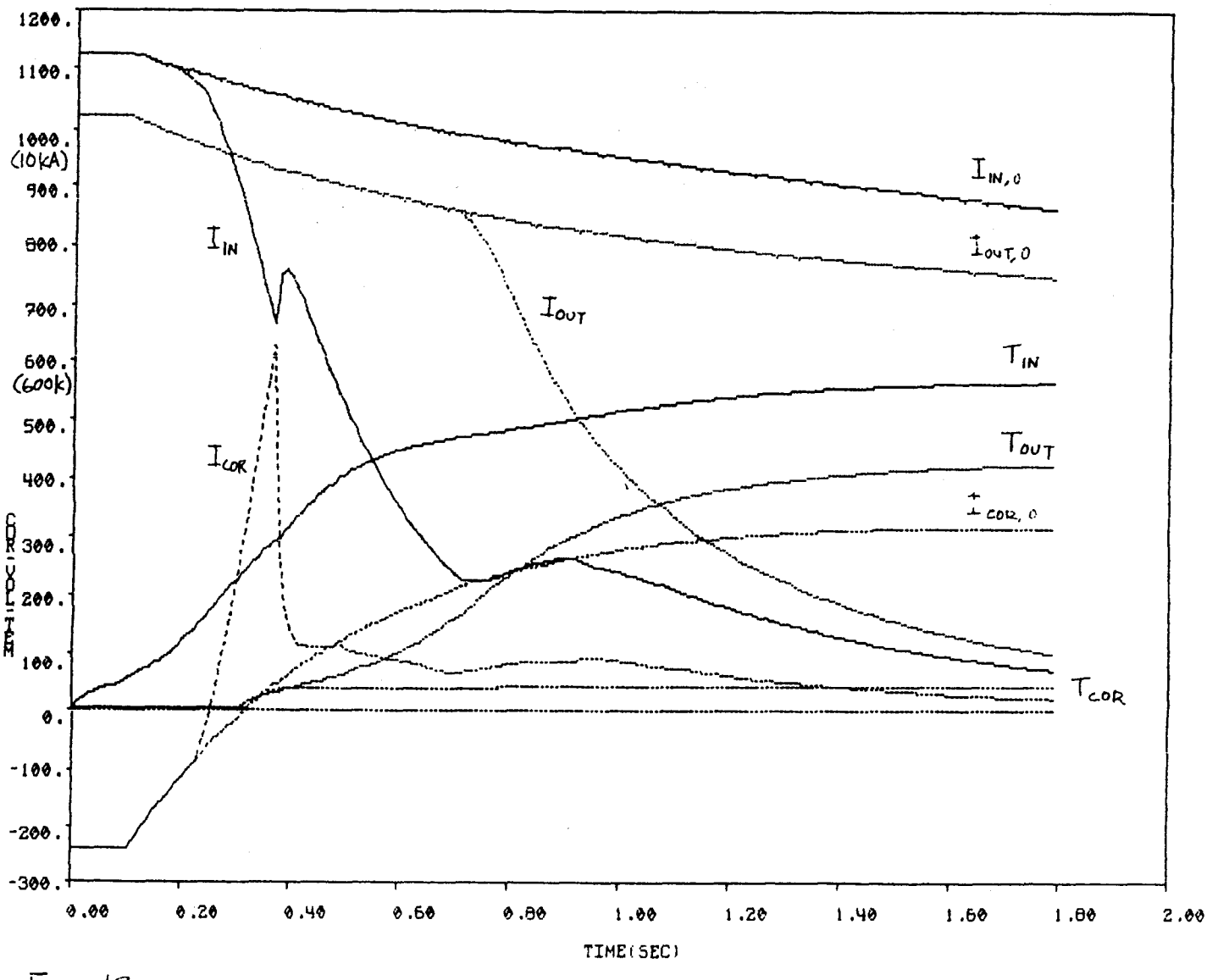

Fig. 13.

105 mMagnet × 332
Outer Coil Quench
$t_{sw} = 0.1$ sec
$k = 3.0 \times 10^{-5}$ W/cm·K

5 mMagnet × [illegible]
Outer Coil Quench
Along conductor
$k = 3.0 \times 10^{-5}$ W/cm·K
$t_{sw} = 0.1$ sec

6/11 '85

24

	R_{ext}	L	I_i	I_f	R_{max}	T_{max}	V_{max}	Vel_i	$E_{s,i}$	$E_{s,f}$	E_{in}	E_{ext} Diode
Coil in	0.15 Ω	3.6~5.5 (2.2~5.5) mH	11275 A	830 A	22 mΩ (7.1%)	500 K	83 V	21 m/sec (0.32 sec)	3.9×10^5 J	4.1×10^3 J	2.3×10^5 J	4.4×10^3 J
Coil out	0.15 Ω	3.3~6.2 (1.8~6.2) mH	10225 A	990 A	20 mΩ (4.7%)	610 K	60 V	18 m/sec	3.3×10^5 J	5.3×10^3 J	2.2×10^5 J	3.1×10^3 J
Coil trim	0.15 Ω	0.74~0.96 (0.43~0.96) mH	-2400 A	260 A	26 mΩ (100%)	49 K	160 V	9.0 m/sec (0.37 sec)	-3.2×10^4 J	5.0×10^5 J	2.4×10^5 J	6.3×10^2 J
Total	(57'…U.H.), e = 0, Δt = 0.01 sec								6.9×10^5 J	9.9×10^3 J	4.8×10^5 J	8.1×10^3 J

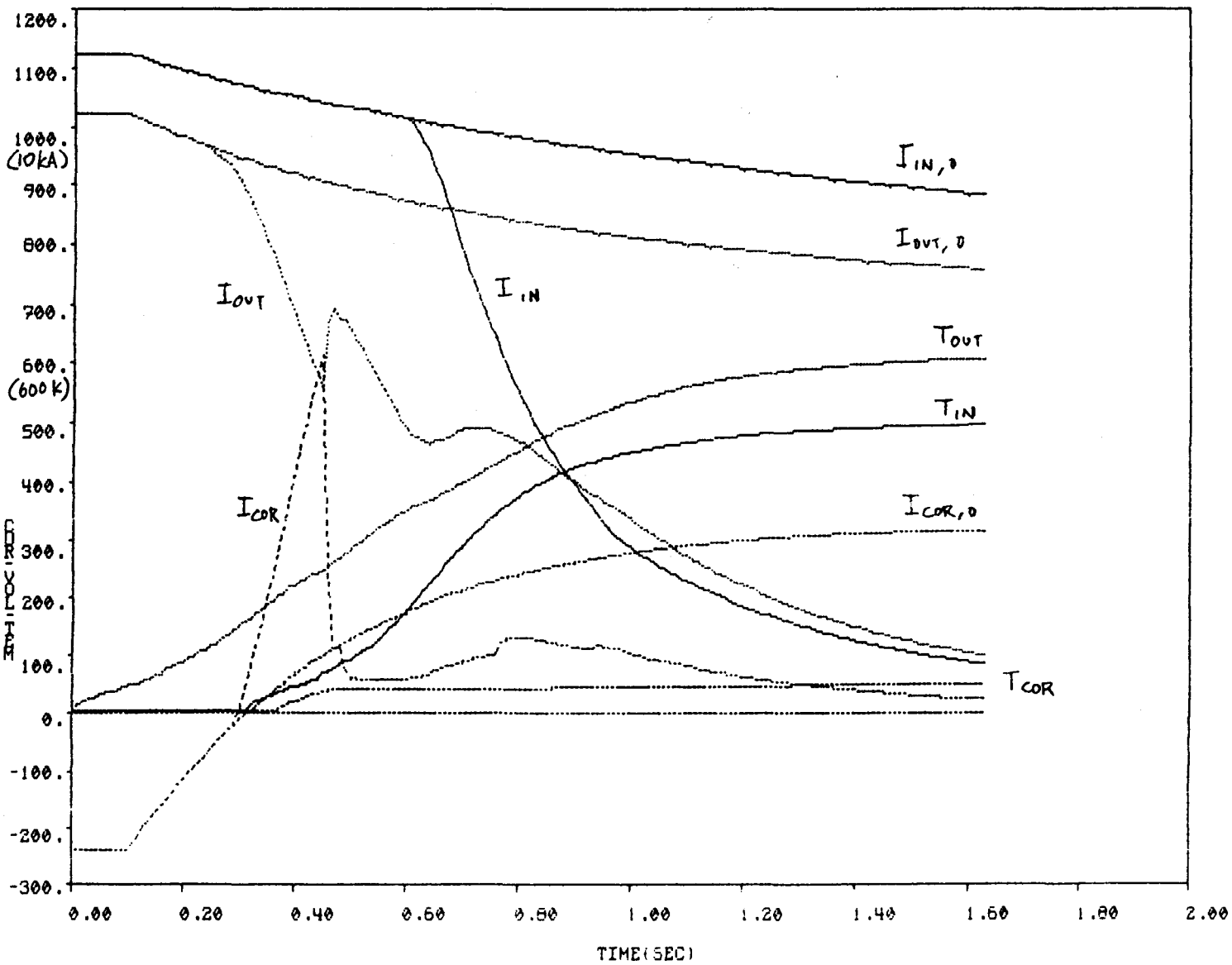

Fig. 14

105 m Magnet × 332
Inner Coil Quench
$t_{sw} = 0.1$ sec
≈ Gustavo's Assumption

[illegible] Magnet [illegible]
Inner Coil Quench
Along Conductor
I_{sw} [illegible] sec

[illegible] '85
25

	R_{ext}	L	I_i	I_f	R_{max}	T_{max}	V_{max}	Vel_i	$E_{s,i}$	$E_{s,f}$	E_{in}	E_{ext} (Diode)
Coil in	0.15 Ω	3.6~5.5 (2.2~5.5) mH	11275 A	830 A	23 mΩ (8.2%)	560 K	69 V	23 m/sec	3.9×10^5 J	4.1×10^3 J	2.4×10^5 J	5.3×10^3 J
Coil out	0.15 Ω	3.3~6.2 (1.8~6.2) mH	10225 A	1000 A	21 mΩ (7.3%)	380 K	70 V	17 m/sec (0.20 sec)	3.3×10^5 J	5.4×10^3 J	2.0×10^5 J	2.5×10^3 J
Coil trim	0.15 Ω	0.74~9.6 (0.43~9.6) mH	-2400 A	310 A	24 mΩ (100%)	52 K	110 V	2.9 m/sec (0.20 sec)	-3.2×10^4 J	6.0×10^2 J	2.8×10^4 J	5.3×10^2 J
Total	(1:04 … U.H.), e = 0, Δt = 0.01 sec								6.9×10^5 J	1.1×10^4 J	4.7×10^5 J	8.4×10^3 J

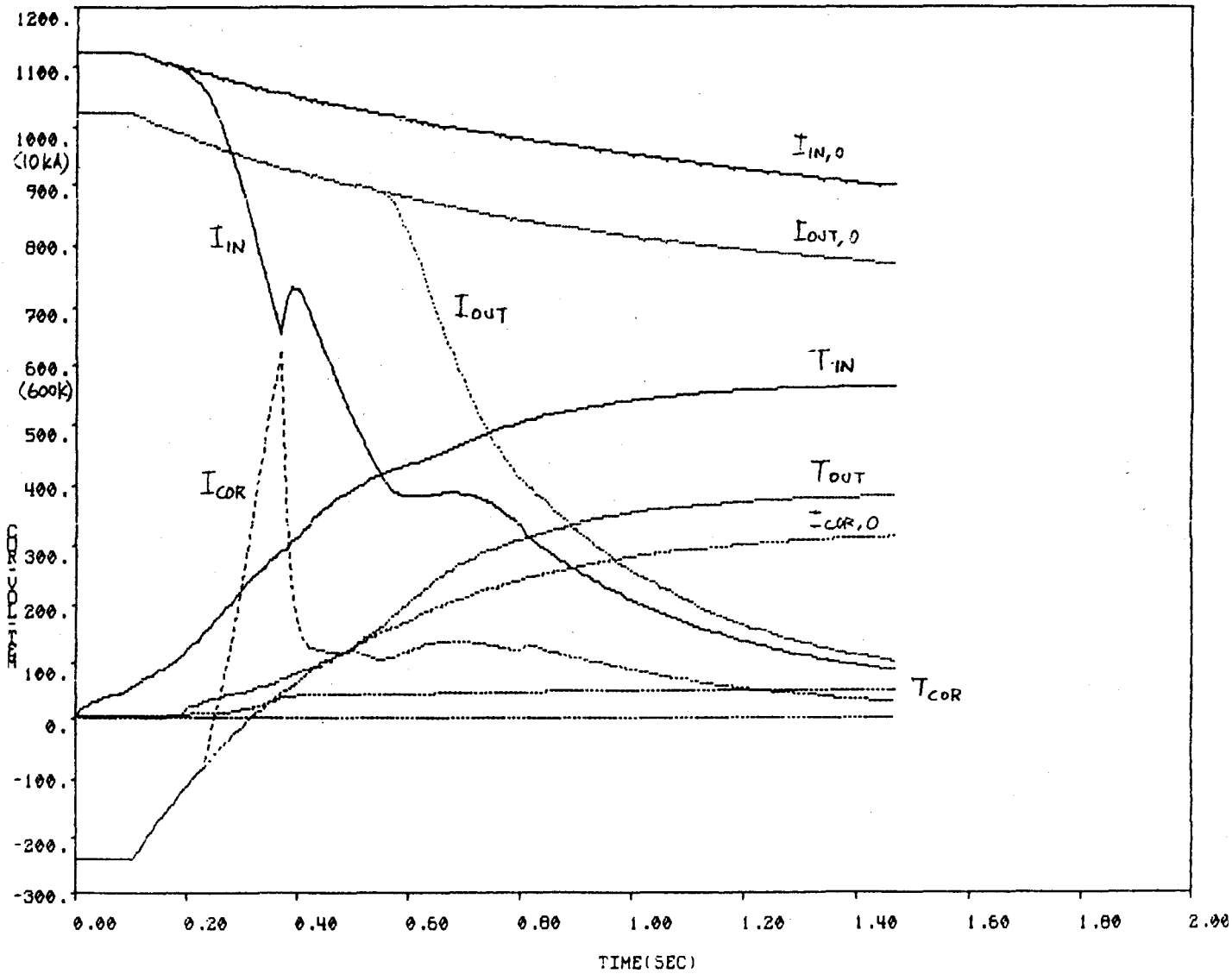

Fig. 15.

105 m Magnet × 332
Outer Coil Quench
$t_{sw} = 0.1$ sec
≈ Gustavo's Assumption

	R_{ext}	L	I_i	I_f	R_{max}	T_{max}	V_{max}	Vel_i	$E_{s,i}$	$E_{s,f}$	E_{in}	E_{ext} Diode
Coil in	0.15 Ω	3.6~5.5 (2.2~5.5) mH	11275A	800A	25 mΩ (8.0%)	510 K	89 V	22 m/sec (0.16 sec)	3.9×10^5 J	3.9×10^3 J	2.6×10^5 J	4.4×10^3 J
Coil out	0.15 Ω	3.3~6.2 (1.8~6.2) mH	10225A	980A	22 mΩ (6.5%)	640K	79 V	18 m/sec	3.3×10^5 J	5.2×10^3 J	2.4×10^5 J	2.6×10^3 J
Coil trim	0.15 Ω	0.74~0.96 (0.43~0.96) mH	-2400A	320A	24 mΩ (100%)	56 K	110 V	0.22 m/sec (0.30 sec)	-3.2×10^4 J	6.0×10^2 J	3.1×10^4 J	4.5×10^2 J
Total									6.9×10^5 J	9.8×10^3 J	5.4×10^5 J	7.4×10^3 J

(1:03'... U.H.), C = 0 , Δt = 0.01 sec

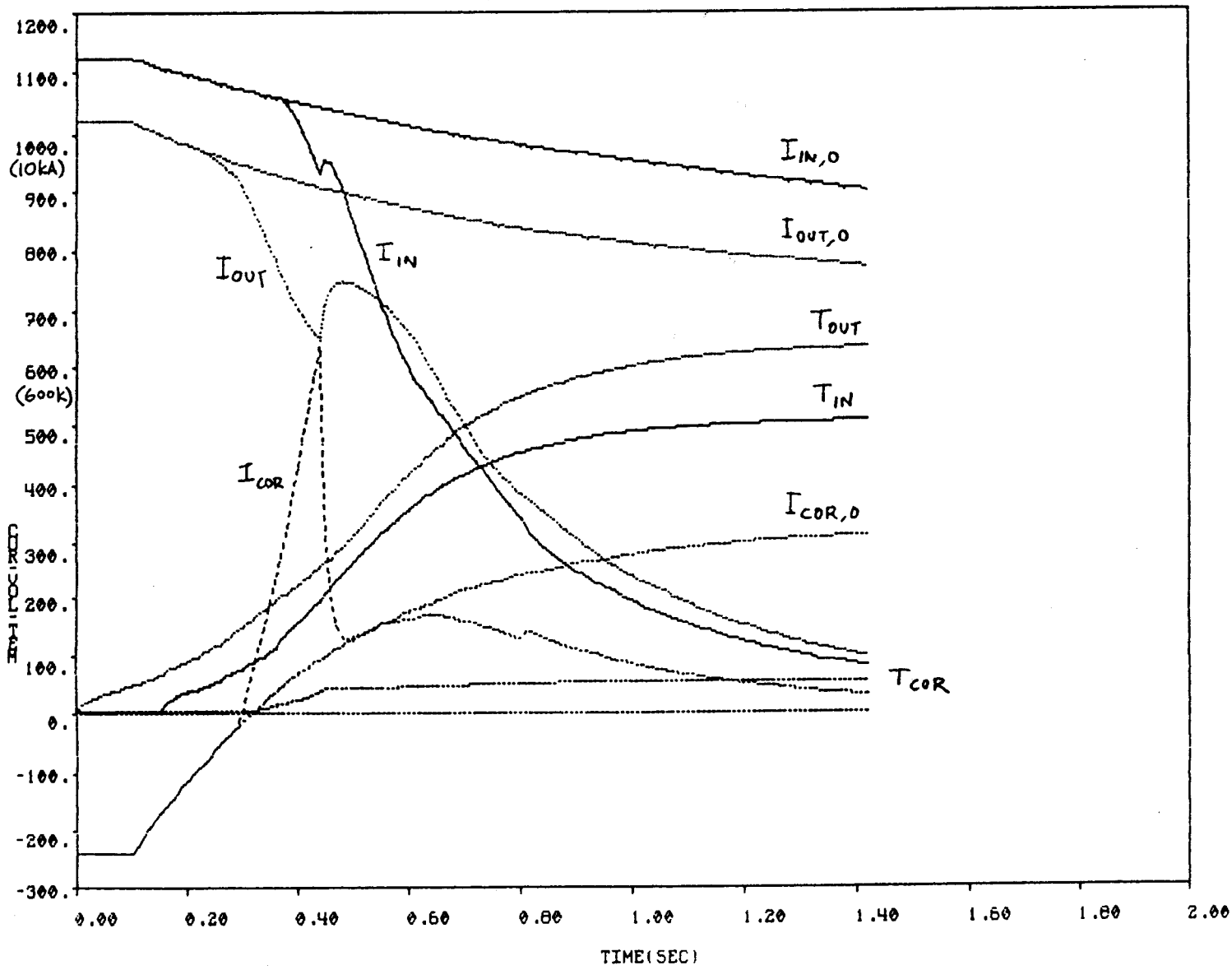

Fig. 16.

APPENDIX E

A BRIEF ANALYSIS OF QUENCHES IN THE THREE TESLA, TAC SSC MAGNETS

W.V. HASSENZAHL
LAWRENCE BERKELEY LABORATORY

A BRIEF ANALYSIS OF QUENCHES IN THE THREE TESLA, DESIGN C SSC MAGNETS*

W.V. Hassenzahl

Lawrence Berkeley Laboratory
University of California
Berkeley, CA 94720

Quenches in the 3 T, superferric magnets proposed by the Texas Accelerator Center[1] have been analyzed by using the computer program QUENCH[2]. The version of QUENCH used here models only one coil so the two and three coil geometries that are proposed cannot be analyzed explicitly. However, the inductances of each single coil circuit allows this version of the program to give good estimates of the final temperature because the energy dump in a quenched coil must occur in a time much shorter than the discharge by the external protection circuit.. In addition, an estimate of the "worst case" temperature, when a large fraction of the energy goes into one or the other of the two main coils, can be calculated directly.

Description of the 3-T Magnet

The 3-T Superferric magnet has been described in great detail elsewhere.[1] The salient features for the analysis presented here relate to the conductor and the details of the coil and conductor placement. As a reference point the cross section of the magnet is shown in Fig. 1 and the details of the conductor region is shown in detail in Fig. 2. There are three independent coils that are driven with different currents to produce very uniform fields within the bore. The discharge circuits that protect these coils in the event of a quench in another coil are not addressed here. Rather, we consider the effect of a quench in either the inner coil or the outer coil that causes a

*This work was supported by the Director, Office of Energy Research, Office of High Energy and Nuclear Physics, High Energy Physics Division, U.S. Dept. of Energy, under Contract No. DE-AC03-76SF00098.

dump of the energy associated with a certain length into the winding selected. The energy deposited in a normal region is controlled by changing the inductance and current, which are an input to the program. This does not allow a simulation of the case where the quench begins in one coil winding and propagates to another.

The parameters of the conductor for the inner and outer windings, which we study here, are presented in Table I and the conductor is shown in Fig. 3.. The two different coil windings have slightly different inductances, and, because the iron saturates the differential inductance is somewhat different from the integrated or net inductance at a given field/current. Some of these inductances are given in Table II.

The field within the windings at the positions 1, 2, 3, 4, 5, and 6 of Fig. 4 are given in this same figure for three different values of central field.

The critical current curve for the conductor, as proposed by Texas Accelerator Center is shown in Fig. 5. This curve was used to obtain the quench velocities in the inner and outer coils shown in Fig. 6. These velocities are calculated in the program quench and are based on the conductor cross section given in Fig. 3 and Table I. They are quite similar to the velocities observed by Zeigler in magnet TAC005. These velocities are also given in Fig. 5 in the low field region, which represents the field in the region of the conductor in the superferric design. The information on this coil suggested that the transverse quench propagation velocity was quite small. We begin with some results based with physical characteristics of the conductor and then use the observed data. The turn-to-turn transition times are given Table III.

Quenches in the coils were calculated for a variety of conditions in the two coils. A set of typical quench temperatures based on only one coil quenching are given in Fig. 7.

The resulting temperatures, though modest for magnets such as the CBA etc., are probably unacceptably high for this magnet because of the use of solder throughout the

conductor. This solder should not be allowed to melt as it might then be dispersed in the magnet by the helium pressurized by the quench. The melting or liquidus point of the solder used, and therefore the upper allowable temperature during a quench, is about 500 K. The solder enters a putty-like region at a lower temperature.

The use of shorter magnets, say 35 or 70 m would allow the energy deposited in either of the two main coils to be reduced by at least a factor of two.

For all the transitions depicted in Fig. 7 the assumption is made that either the inner coil or one half of the outer coil quenches and the rest of the magnet does not participate. In fact the system is much more complicated. What is likely to happen is that the inner coil, which is in a higher field region and more exposed to beam loss and synchrotron radiation, will quench first. As a result, as its current decays, coupling will cause the current in the outer coil to increase very slightly. Thermal conductivity and the increased current will then cause the outer coil to quench. Because of this possibly elevated current coupled with the lower field and higher effective inductance, the outer coil has more energy available during a quench that will propagate more slowly. Thus the outer coil could become slightly hotter than predicted by any of the calculations here.

In an earlier study on the 6.5 T Design A SSC dipoles[3] it was shown that the peak temperature would occur if the magnet quenched at about 80% of peak current. The result of a similar study for the Design C dipoles suggests that the peak temperature here would be at currents greater than 10,000 A. So we need not be concerned about intermediate temperature quenches.

References

1. R. Huson, "Superferric Magnet Option for the SSC," to be published in the proceedings of the 1985 Particle Accelerator Conference, Vancouver, B.C., May, 1985.

2. W. V. Hassenzahl, "Quench - Modifications and Documentation," CEN-Saclay Report 78-61, (1978)

3. G. Moritz and W. V. Hassenzahl, "Computer Studies of the Quench Behavior of an SSC Model Dipole," Appendix G.

Fig. 1. Cross Section of Design C Magnet

Fig. 2. Detailed Cross Section of Conductor Region

Fig. 3. Cross Section and Details of Conductor Alone

Fig. 4. Coodinates and Fields in the SSC Design C Dipole

Fig. 5. J_c vs. B for TAC Conductor

Fig. 6. Quench Velocity for Inner Conductor Uses Details of B vs. Position and Cross Section and J_c

Fig. 7. Temperature Development for Quenches in 140 m Coil

TABLE I

Details of the TAC SSC 3-T Dipole Conductor

Conductor cross section	(mm^2)	23.70
Conductor dimensions with insulation	(mmxmm)	2.90x7.90
Superconductor cross section	(mm^2)	3.88
Copper cross section	(mm^2)	12.85
Copper core cross section	(mm^2)	8.00
Copper in strands cross section	(mm^2)	4.85
Solder cross section	(mm^2)	2.84
Insulation cross section	(mm^2)	3.90
Helium* cross section	(mm^2)	0.23
H_{c2} at 4.2 K	(T)	10.5
T_c at B = 0	(K)	9.5
Number of strands	(mm)	24
Strand diameter	(mm)	0.67
Cu to S.C. ratio in strands		1.3

*Estimate

TABLE II

Inductances for the 3 T Superferric Design C Dipole with a Lentgh of 105 m

Coil	Field (T)	Inductance (mH)
Inner	3.0	3.6
Outer	3.0	3.3
Inner	1.6	4.6
Outer	1.6	4.9
Inner	0.5	5.5
Outer	0.5	6.2

TABLE III

Transverse or Turn-to-Turn Quench Propagation Times in the TAC005 Magnet

Current (kA)	Field (T)	Time (ms)
5.0	1.8	250
7.5	2.3	175
9.0	2.8	115

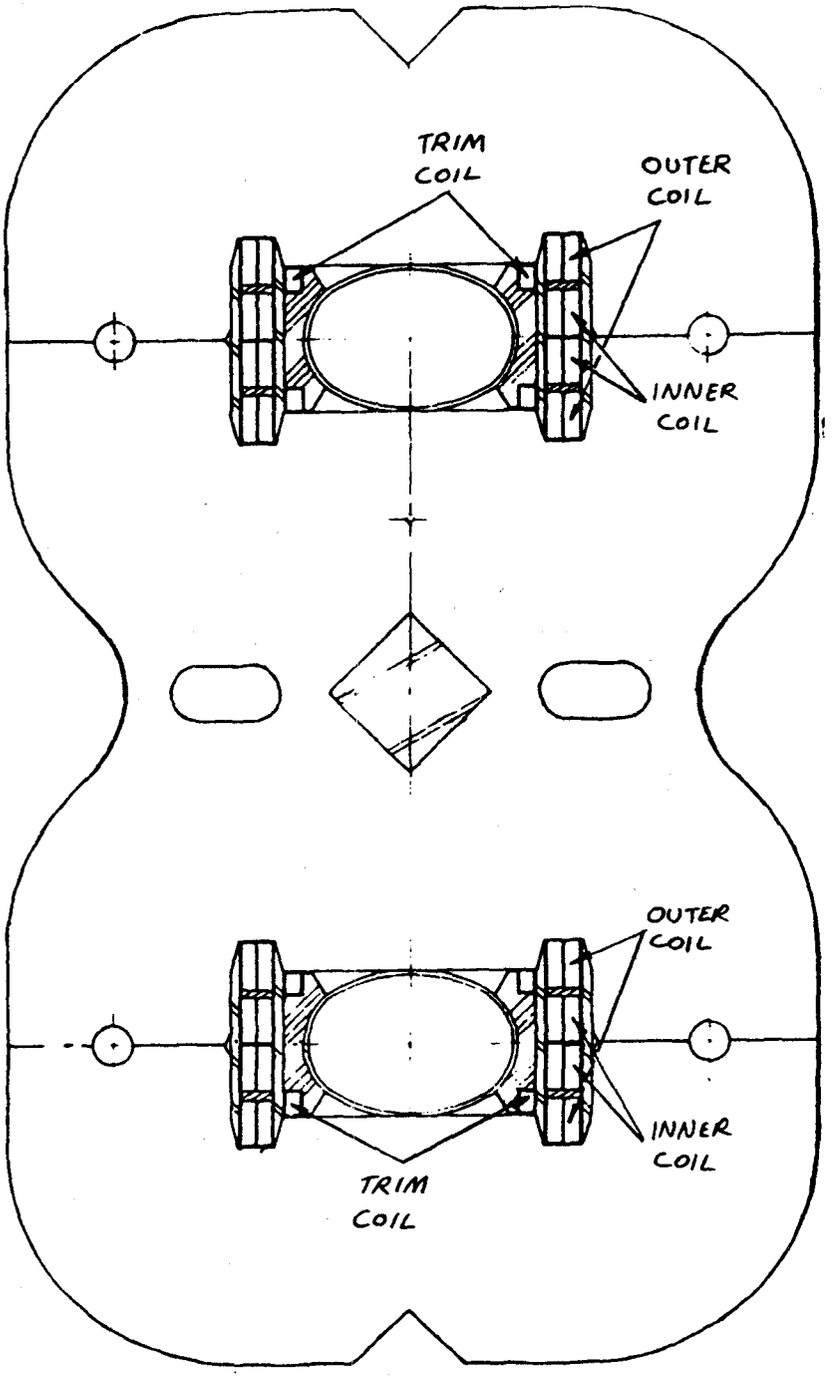
TRIM
COIL
OUTER
COIL
INNER
COIL
OUTER
COIL
INNER
COIL
TRIM
COIL

Figure 1

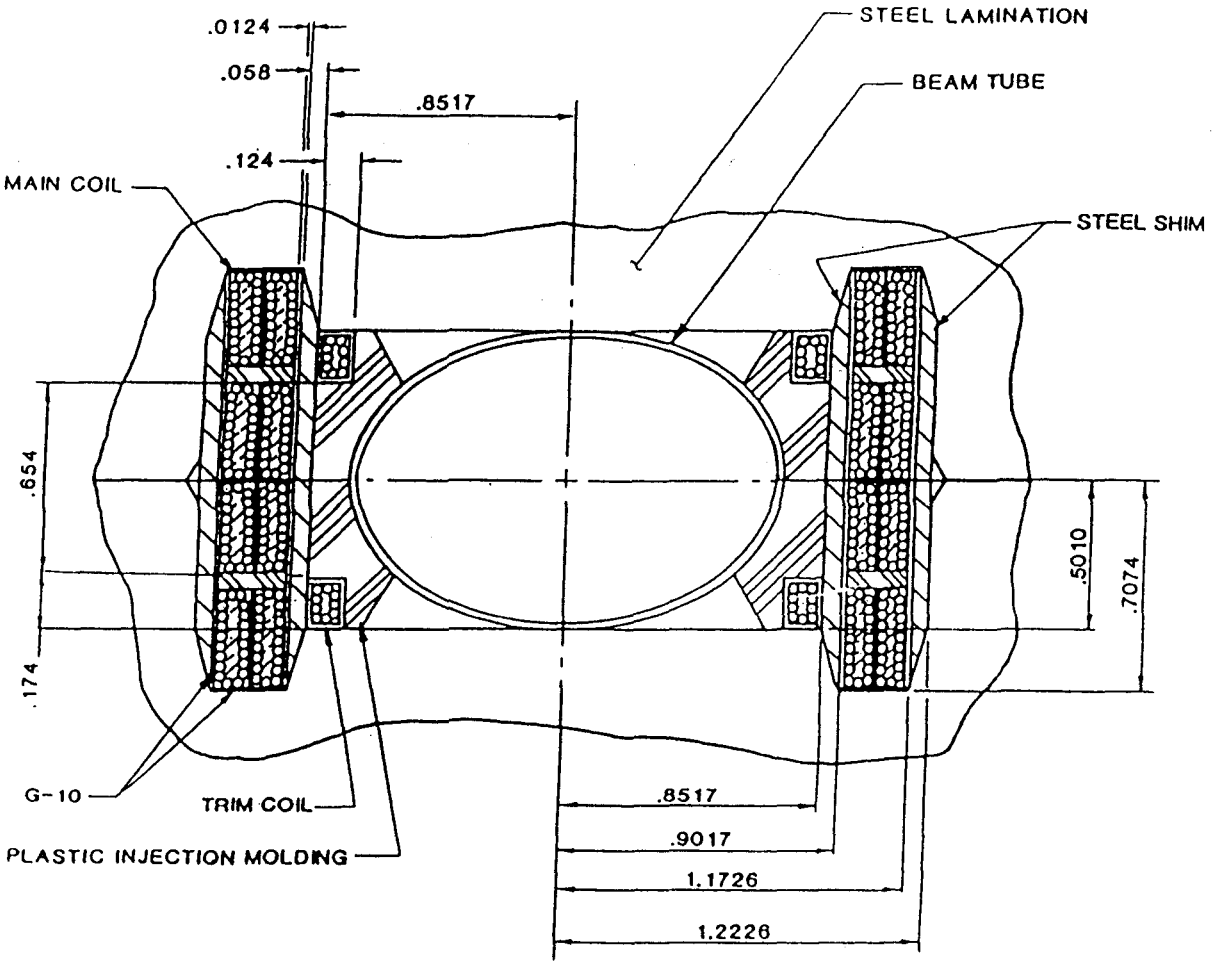

FIG.2 Cross Section of Cold Iron Dipole Magnet

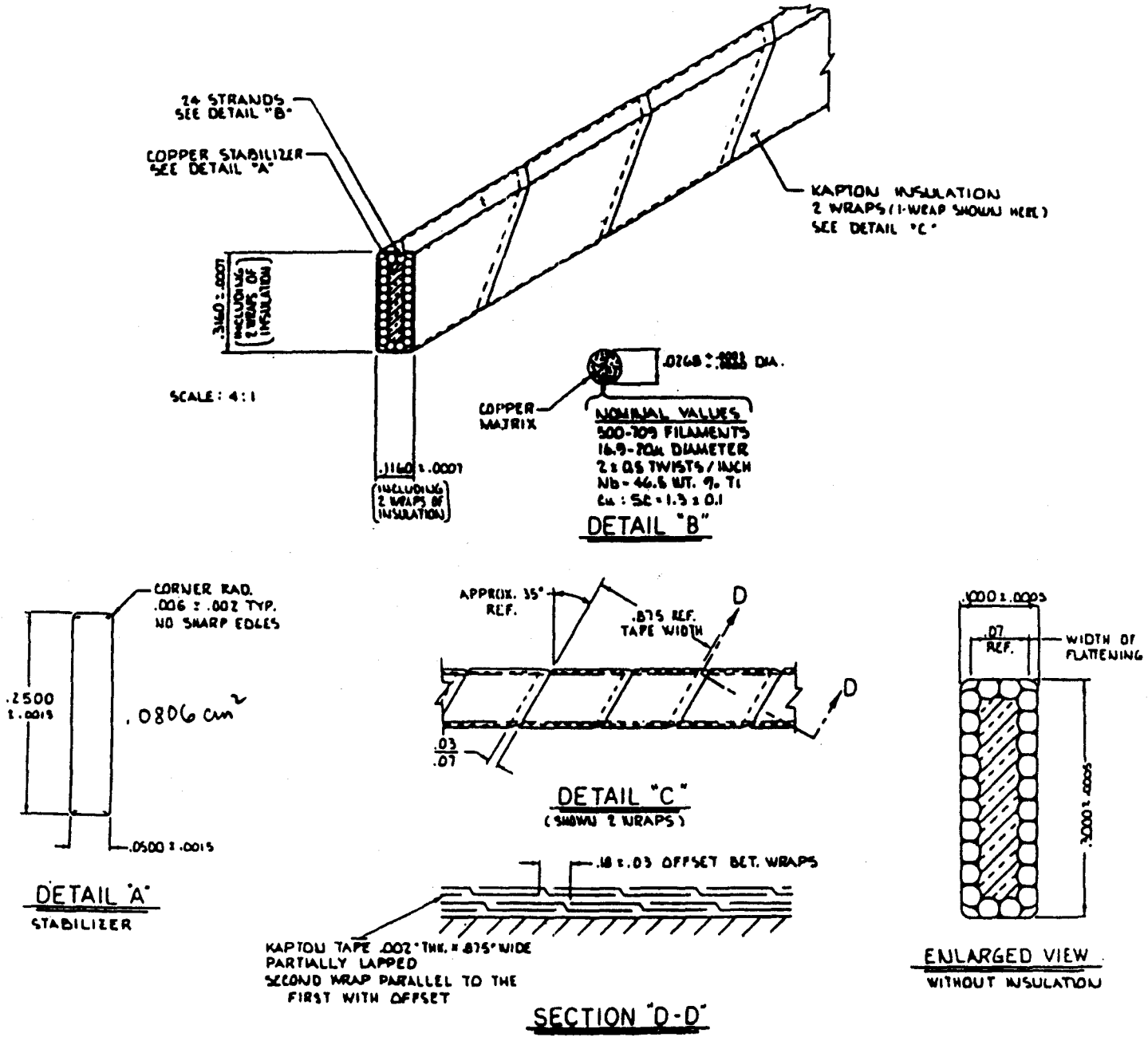

Fig.3 Cable parameters for the 3 T magnet as used in the quench calculations.

LOW FIELD, B=0.5021T

LOCATION	B(X)	B(Y)
1	71.1	-5128.1
2	102.1	-3778.1
3	1761.1	-1337.9
4	37.2	- 803.5
5	-333.2	- 92.6
6	-521.6	-5047.6
7	-781.9	-2130.5
8	-885.2	- 26.9

COORDINATES

LOCATION	X	Y
1	0.732	0.41
2	0.832	0.41
3	0.9283	0.528
4	1.0443	0.528
5	1.1443	0.528
6	0.9283	0.18114
7	1.0443	0.18114
8	1.1443	0.18114

MID FIELD, B=1.6288T

LOCATION	B(X)	B(Y)
1	497.1	-16380.1
2	505.7	-12270.1
3	3756.6	- 5078.2
4	- 594.4	- 2666.2
5	-1690.3	- 341.4
6	-1910.5	-16666.1
7	-2858.4	- 6983.0
8	-3290.8	249.6

HIGH FIELD, B=2.98T

LOCATION	B(X)	B(Y)
1	972.5	-27980.0
2	1795.2	-31147.7
3	2104.5	-23723.2
4	-1347.5	-11082.8
5	-1979.2	535.6
6	-1035.1	-30388.1
7	-1338.3	-13315.3
8	-1495.3	196.1

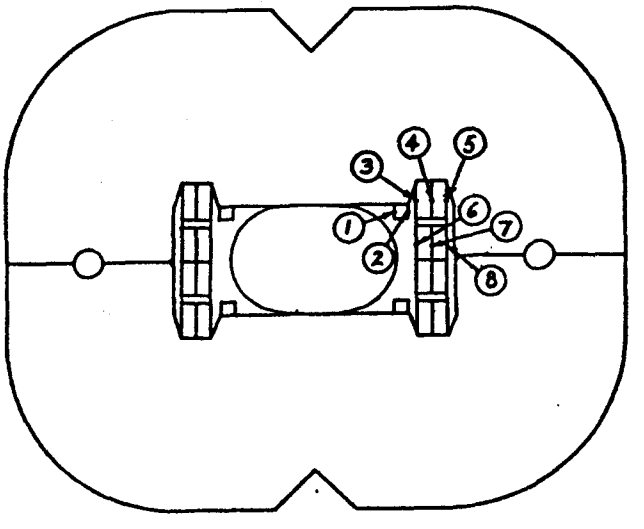

Fig. 4

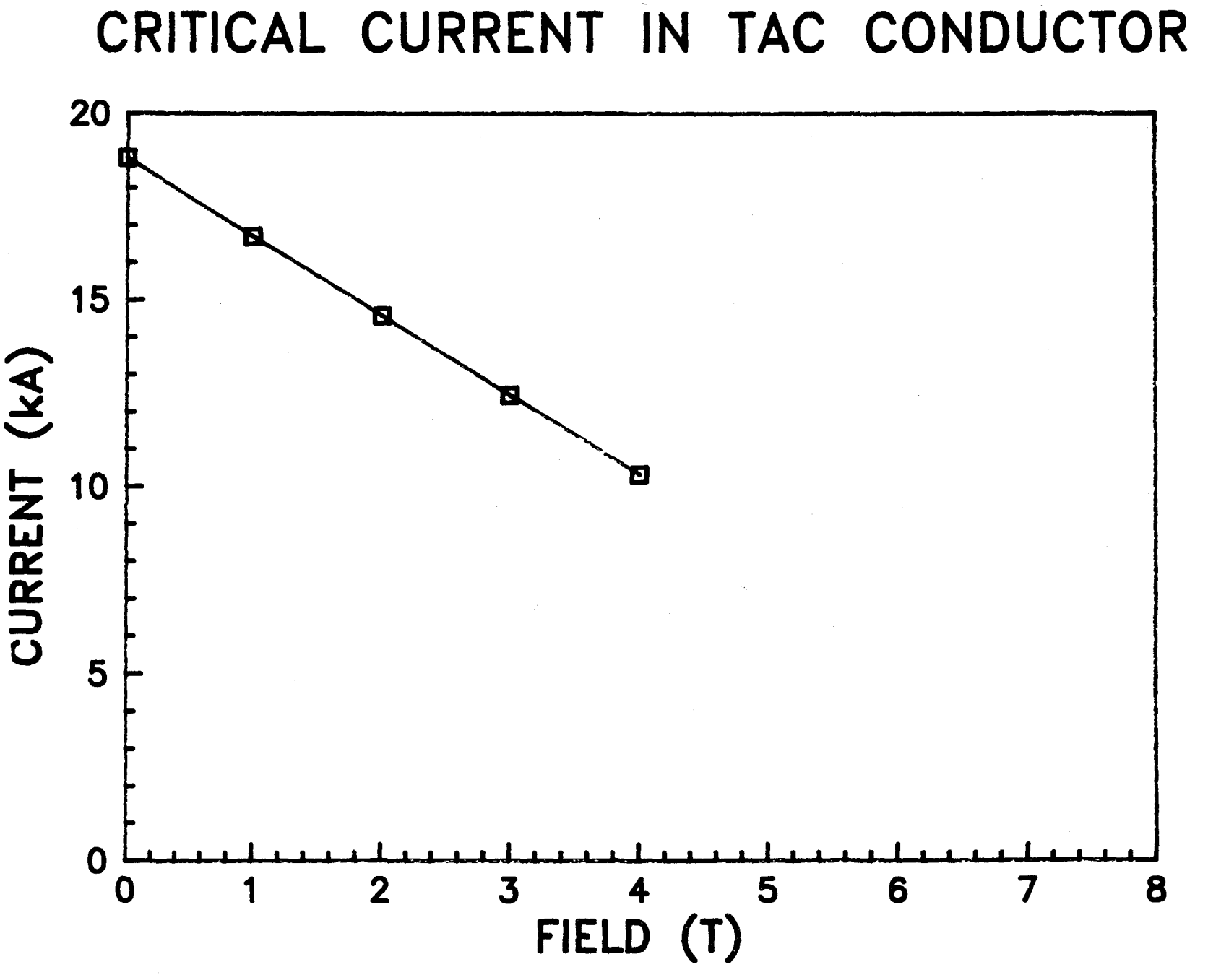
CRITICAL CURRENT IN TAC CONDUCTOR
CURRENT (kA)
20
15
10
5
0
0
1
2
3
4
5
6
7
8
FIELD (T)

Fig. 5

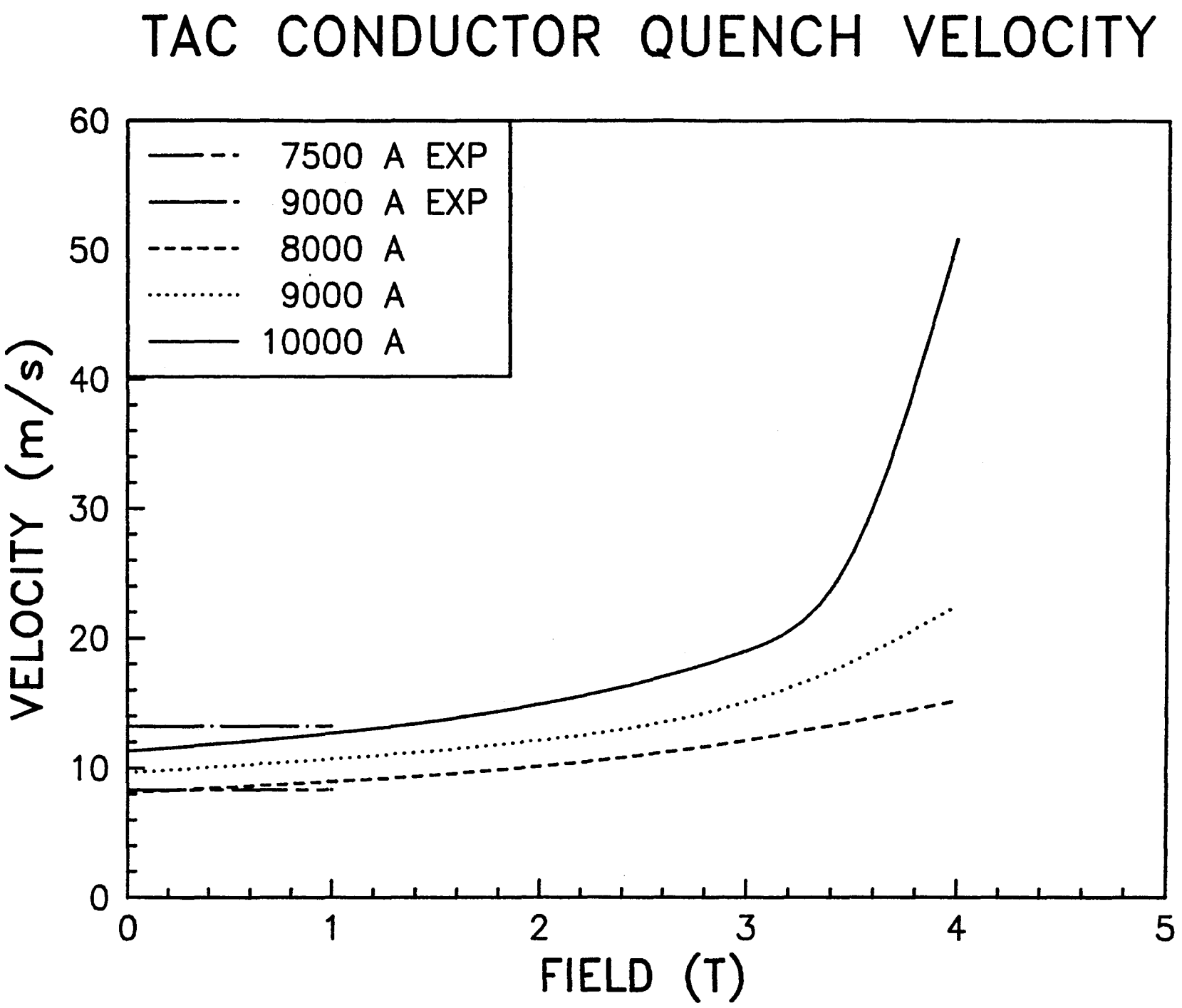
TAC CONDUCTOR QUENCH VELOCITY
7500 A EXP
9000 A EXP
8000 A
9000 A
10000 A
VELOCITY (m/s)
FIELD (T)
0
10
20
30
40
50
60
0
1
2
3
4
5

Fig. 6

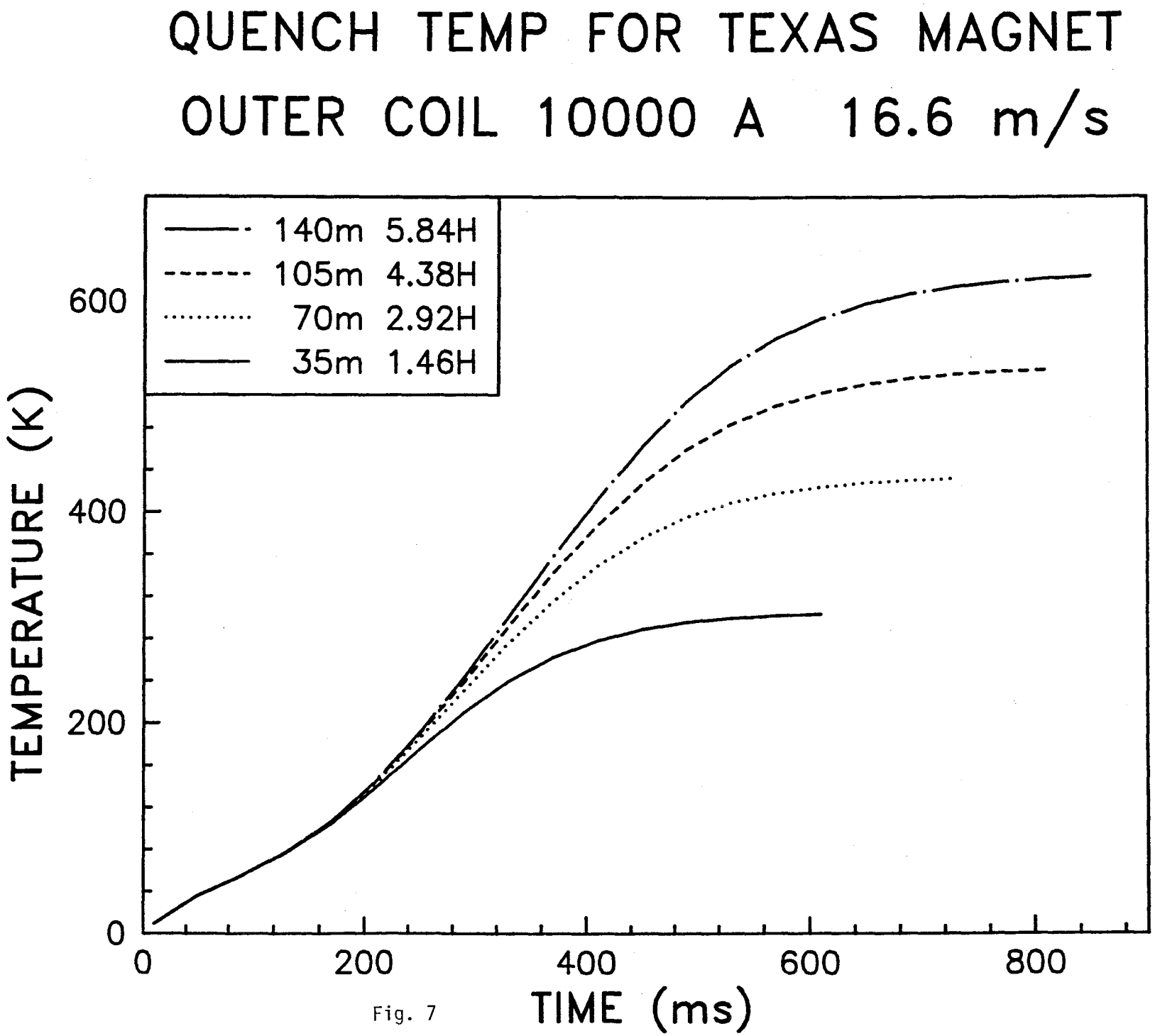
QUENCH TEMP FOR TEXAS MAGNET
OUTER COIL 10000 A 16.6 m/s
140m 5.84H
105m 4.38H
70m 2.92H
35m 1.46H
TEMPERATURE (K)
0
200
400
600
0
200
400
600
800
TIME (ms)

Fig. 7

APPENDIX F

A SIMULATION OF QUENCHES IN SSC MAGNETS WITH PASSIVE QUENCH PROTECTION

K. KOEPKE
FERMI NATIONAL ACCELERATOR LABORATORY

TM 1316 - SSC 20
SSC-N-12

A SIMULATION OF QUENCHES IN SSC MAGNETS WITH PASSIVE QUENCH PROTECTION

K.Koepke

Introduction

The relative ease of protecting an SSC magnet following a quench and the implications of quench protection on magnet reliability and operation are necessary inputs in a rational magnet selection process. As it appears likely that the magnet selection will be made prior to full scale prototype testing, an alternative means is required to ascertain the surviveability of contending magnet types. This paper attempts to provide a basis for magnet selection by calculating the peak expected quench temperatures in the 3 T Design C magnet and the 6 T Design D magnet as a function of magnet length. A passive, "cold diode" protection system has been assumed. The relative merits of passive versus active protection systems have been discussed in a previous report (1). It is therefore assumed that - given the experience gained from the Tevatron system - that an active quench protection system can be employed to protect the magnets in the eventuality of unreliable cold diode function.

Quench Model

The calculations were performed with the program TMAX. As the magnet current decays during a quench, the program updates magnetic field, quench velocity, quench resistance and quench temperature for every magnet turn and uses the results to control the magnet current. Single or multiple quenches can be started anywhere in the magnet.

The quench velocities in the program are calculated with empirical equations obtained by fit to available velocity measurements. In the case of the Design C magnet, in situ velocity measurements - longitudinal and turn-to-turn - have been made (2) and are used unaltered in the program. In the Design D magnet case, the longitudinal velocities for the inner and outer cables have been measured in a test fixture (3). It can be shown - at least in the case of test magnet SBN003 - that longitudinal velocity measurements made in a magnet and in a test fixture agree on the 10 percent level (Table 1). Turn-to-turn quench delay data was obtained by scaling from data in test magnet SBN003 (4) and test magnet RO1001 (5).

The quench temperatures are obtained by equating the change in cable heat capacity to the heat deposition in the cable due to ohmic heating, i.e., from a Miit versus temperature calculation. This calculation ignores heat transfer (adiabatic approximation) across the boundary of the cable segment and must therefore be interpreted as the maximum cable temperature possible for a given ohmic heating. The validity of this approach has been tested by comparing an in situ measurement of cable temperatures (4) with the temperatures obtained from an adiabatic calculation (Fig.1). The comparison indicates that better agreement is obtained if the cable insulation is included with the heat capacity of the cable and this has been done in all subsequent calculations. The integration has neglected the contribution of the helium to the cable heat capacity. This assumption is probably correct for the Design C magnet which has solder filled cable. Its effect on the temperature calculation for the Design D magnet is also minimal. The program uses empirical quench velocities which already include the effect of the helium. In the case of the inner cable , the helium content of the cable increases the cable Miits necessary to reach a temperature of 700 K by approximately .1 Miit.

The number and location of quenches in a passively protected magnet have a strong relation to the peak quench temperature. Graded cable and magnetic field variations result in different quench velocities. Boundary conditions such as shims, coil boundaries and splices to stabilized conductors severely limit the extent of the normal quench zone. Multiple quenches in coils protected by more than one diode can give elevated temperatures due to the bias obtained from mutual coupling of the diode loops. In recognition of this fact, quench temperatures have been calculated for locations that result in the minimum and maximum temperature. It may be argued that the quench scenarios that result in maximum temperatures are unlikely or less likely to occur during normal operation. However, the loss of operation due to magnet replacement on an even infrequent basis is probably not tolerable.

The calculations have been made with the assumption that each magnet is part of a high series-impedance string which contains a constant current. This is equivalent to the requirement that the sum of the magnet current and the

bypass current is constant during the short interval that the current switches to the diode. This condition is approximately satisfied in the Design D circuit as the quench voltage rapidly overcomes the relatively low inductive voltage that results from the dump current decay. However, the dump time constant in the Design C circuit is small enough to result in significant current decay before the magnet resistance forces the bypass diodes to conduct. Nonetheless, the calculated temperatures are probably valid in the case of maximum current in the inner and outer coil. In this particular case, the initial current decay due to the dump circuit is roughly equal to the initial current decay in the quench simulation.

Design C Magnet

The peak temperatures calculated for this magnet are shown in Fig. 2. Only the inner and outer coil temperatures were calculated as the trim coil operates at reduced current and its area and/or its composition can easily be changed if its quench temperatures are too high. Quenches were simulated in the body of the magnet where the quench is free to propagate in both longitudinal directions and also at the magnet end were the cable is spliced to the fully stabilized cable contiguous to the cold diode. The end- of-coil quench location for this magnet is critical because of the magnet's long turn-to-turn quench delay. This delay and the relatively small number of magnet turns available to the normal quench zone imply that most of the quench resistance comes from the first turn to quench. For quenches at the coil end, this quench resistance is halved. In the outer coil, the quench zone was limited to two turns. In the case of the inner coil, the third and fourth turn were simultaneously - and arbitrarily - quenched after 140 ms. The effects of intercoil quench propagation, or of multiple quenches in either or both coils were not investigated but are clearly relevant.

The cable and magnet parameters used in the quench simulation are courtesy of the TAC group. The cable cross section is shown in Fig. 3. Fig. 4 contains the calculated temperature versus Miits for this cable including the solder and insulation at 0 T and 3 T magnetic fields. The quench velocities, quench delays and coil inductances used are given in Table 2. The velocity and quench delay values for the 10.1 kA and 11.3 kA currents are extrapolated. The sizeable effect of iron saturation in this magnet has been approximated in the quench program by parameterizing the coil inductances as a function of ampere-turns.

Design D Magnet

The peak temperatures calculated for this magnet are shown in Fig. 5 thru Fig. 7 as a function of magnet length and as a function of the number of protection diodes per magnet. In the case of single diode protection, the maximum quench temperature occurs for single quenches that start in the high field turn next to the coil key. At this quench location, the quench normal zone can only expand in one azimuthal direction which compensates for the higher quench velocities. For magnets with multiple diode protection, as shown in the figures, the maximum quench temperature occurs for dual quenches at the median plane of the magnet. In general, geometrically symmetric and simultaneous quenches with mutually coupled decay circuits behave as if the coil inductance per quench is L/2 instead of L/(2+2*k) where L and k are the total magnet inductance and mutual coupling constant respectively. End-of-coil quenches for this magnet were not considered because of the relatively fast turn-to-turn quench propagation and the large number of magnet turns that contribute to the quench normal zone. This assumes that the magnet ends are of minimum size which allows a quench to rapidly exit from this location. If exagerated "dog bone" ends are used, the magnet end quench protection will need to be reevaluated.

The quench calculations assumed that the Design D magnet utilizes the cables specified for the Design A magnet of the SSC design study (6) and that the coil geometry agrees with BNL drawing no. 22-00217-4 Rev B. Fig. 8 gives the calculated temperature versus Miits for these conductors at field values of 0 T and 6 T. The Miit integration includes a .004 in. thickness of Kapton insulation per cable. The inner and outer longitudinal quench velocities used are plotted in Fig. 9 and Fig. 10. These velocities were measured in a test fixture and were furnished by B. Sampson, BNL. The turn-to-turn quench delays were obtained by scaling from measurements in test magnet SBN003 (A. Prodell, et al., BNL) and test magnet R01001 (K. Koepke, et al., FNAL) and are shown in Fig. 11. The magnet inductances were taken from SSC publication SSC-MD-104 (J. Cottingham) without any adjustment for the small iron saturation.

Adjustments

The quench temperatures calculated should be considered as a first approximation calculation as many factors present in a quenching magnet have been ignored. For example, the quench velocities were measured at constant current and field. It is known that during a quench, these velocities are increased due to eddy current heating. In fact, Tevatron dipoles quench spontaneously near short sample at 300 A/s. Other effects which may significantly alter the quench temperatures are eddy currents in the collars and cryostat - especially if constructed out of aluminum - and quench propagation between inner and outer coils. If included, these effects would tend to lower the actual quench temperature calculated. These effects, along with the asymptotic behavior of the quench velocity near short sample, are probably also responsible for the maximum in quench Miits observed in passively protected magnets, e.g., the CBA magnets. This maximum in quench Miits occurs at magnet currents well below the short sample current for the cable in the magnet.

A more realistic peak temperature estimate can be obtained by assuming a higher initial "effective quench velocity", or by evaluating the quench temperature at the magnet current at which the Miit maximum is observed, or by adjusting the calculated quench Miits by an observed correction factor. We can obtain an estimate of the current at which the quench Miits of the inner Design D coil will be at a maximum by scaling the current at which the quench Miits for the inner coil of test magnet SBN003 peaked. Scaling by cable cross section areas yields a current of 4450 A. When the inner coil Design D quench temperatures are evaluated at 4450 A, the result is equal to 78 % of the result obtained at 5906 A. This correction is probably not universal, i.e., it may depend on magnet length and certainly is different for different magnets.

Conclusions

Superconducting cable formed out of niobium-titanium with Kapton film insulation starts to show short sample degradation at a quench temperature of 800 K. Repetitive quenches in solder-filled cable may show damage at even lower temperatures. If we arbitrary set the allowed quench temperature to 700 K, this quench temperature limit and the calculated quench temperatures can be used to evaluate the relative suitability of passive quench protection for the magnets discussed.

Arbitrarily using the same correction factor for the inner and outer coils of both magnets, it appears that the 140 m long 3 T magnet and the 16.6 m long 6 T magnet are protectable with a passive quench protection system. The 3 T magnet requires a minimum of 6 diodes per half cell. This assumes that a pair of parallel diodes are needed to carry the order 10 kA currents in the inner and outer bus. A single diode for the trim winding and another for the separate quadrupole are also assumed. The 6 T magnet requires 21 diodes per 100 m half cell, i.e., 4 diodes per 16.6 m dipole and one diode for the separate quadrupole. As the 3 T ring needs to be twice as long, the 6 T ring needs approximately 2.8 times as many diodes per aperture for passive quench protection. A more complete comparison among competing SSC magnets from the viewpoint of quench detection and protection has been made in a previous report (1).

References

1. WORKSHOP ON SSC COMISSIONING AND OPERATIONS, Systems Group, "Quench Detection And Protection", K. Koepke and G.Tool
2. private communication, J. Ziegler, TAC
3. private communication, W.B. Sampson, BNL
4. private communication, A. Prodell, BNL
5. unpublished, K. Koepke, FNAL
6. SUPERCONDUCTING SUPER COLLIDER, Reference Design Study for U.S. Dept. of Energy, May 8,1984

Table 1

A comparison of the longitudinal velocities measured in a test fixture (W.B.Sampson, BNL) to the longitudinal velocities measured in test magnet SBN003 (A. Prodell, BNL). The cable in both instances was 1.3/1 high homogeneity NbTi with a cross section of .085 sqcm.

Coil Current (amps)	Average Field (tesla)	SBN003 Velocity (m/sec)	Fixture Velocity (m/sec)
Quench origin - inner coil,median plane (IMPL)			
1500	1.69	1.6	1.34
2500	2.82	2.7	3.15
3000	3.38	4.6	4.56
3500	3.94	6.3	6.02
4000	4.5	8.4	8.09
Quench origin - inner coil, median plane end (IEL)			
1500	1.69	1.5	1.34
2500	2.82	2.8	3.15
3000	3.38	5.0	4.56
4000	4.5	11.0	8.09
Quench origin - outer coil,median plane end (OEL)			
2000	.65	1.7	1.6
3000	.97	3.2	3.16
4000	1.3	5.0	5.6
5000	1.62	7.7	8.9
5500	1.79	10.0	10.5
Quench origin - outer coil,median plane (OMPL)			
2000	.65	3.6	1.6
3000	.97	6.7	3.16
4000	1.3	10.4	5.6
5000	1.62	15.4	8.9
5500	1.79	18.8	10.5

Last data set has insidious factor of 2 ?

Table 2

This table contains the parameters that were utilized to calculate the peak quench temperatures for the TAC 3 T magnet.

Magnet Current (kA)	Longitudinal Velocity (m/sec)	turn-turn delay (sec)
5.0	4.0	.248
7.5	7.9	.175
9.0	12.0	.115
10.1	15.6	.090
11.3	20.2	.070

Magnet Field (T)	Self Inductance of Magnet Coils Outer (10E-5 H/m)	Inner (10E-5 H/m)
.5	4.62	4.07
1.6	4.43	4.07
2.4	3.91	3.93
3.0	3.11	3.38

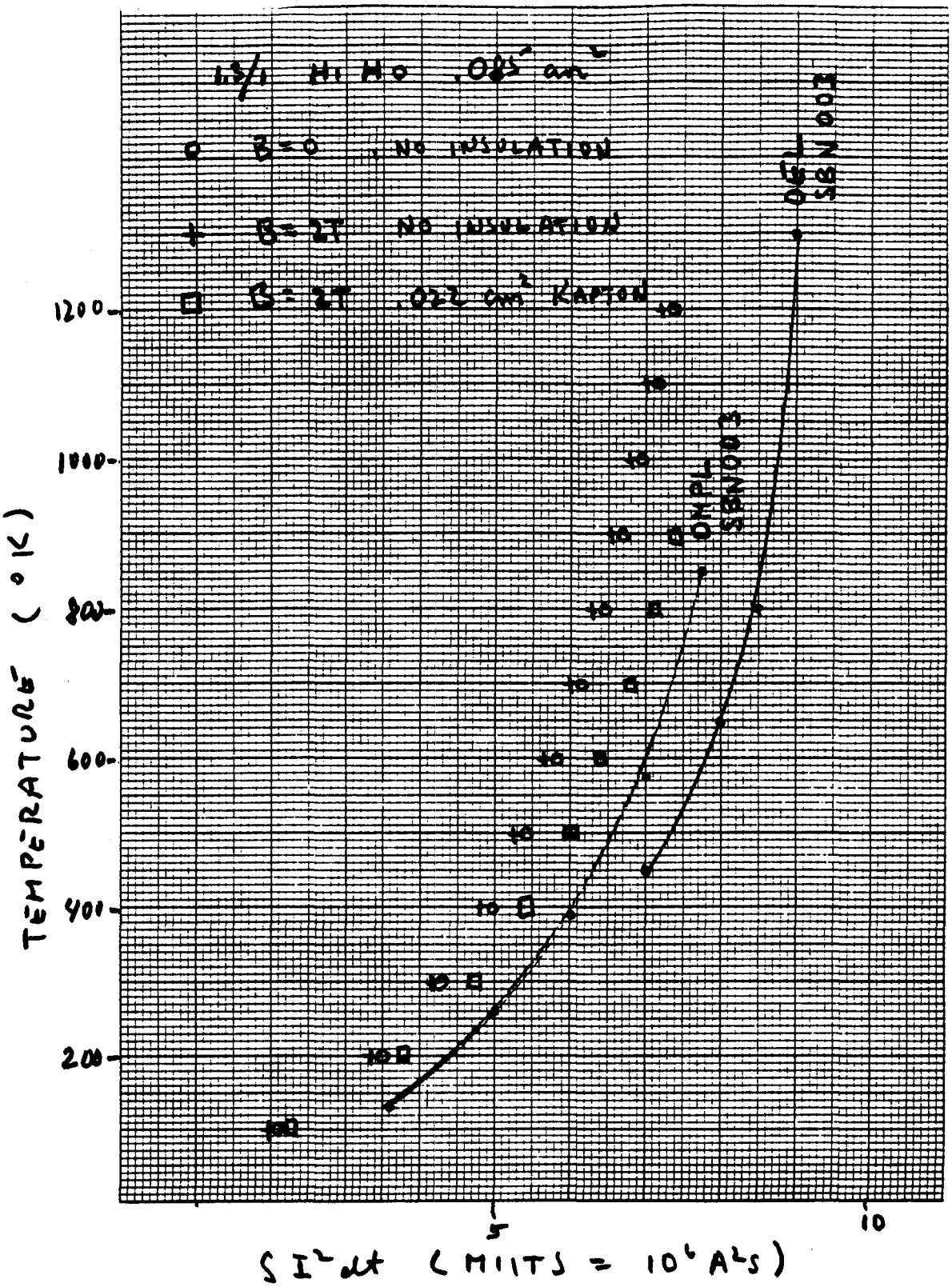

Fig.1 Calculated Temperature versus Miits values compared to the measured temperatures in magnet SBN003. The OMPL location is in the outer coil on the median plane approximately 34 in. from the end of the coil. The OEL location is the same turn but in the "dog bone" end.

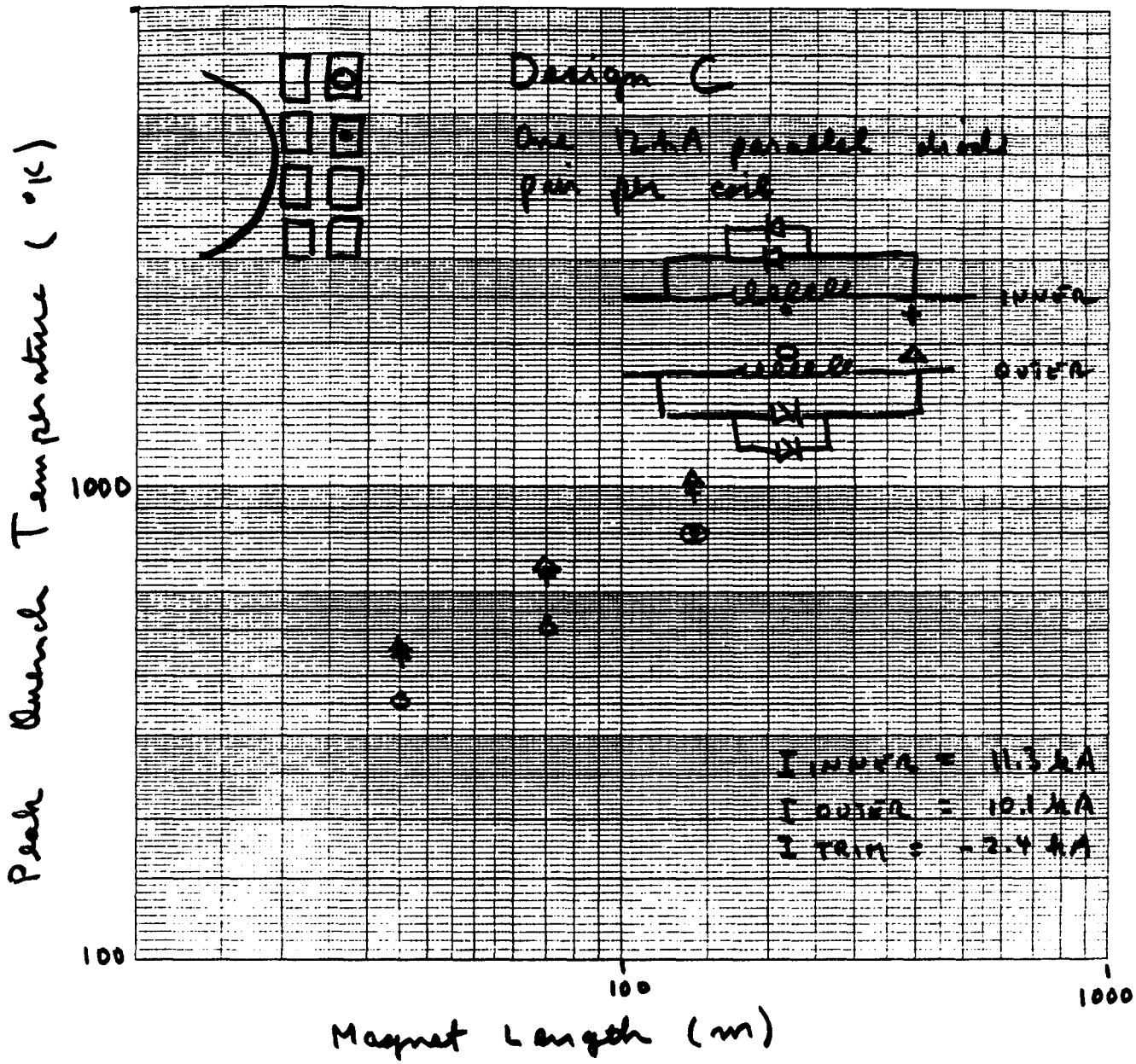

Fig.2 Calculated maximum quench temperatures for the 3 T TAC magnet. The actual quench temperatures can be expected to be lower (See "Adjustments" of text).

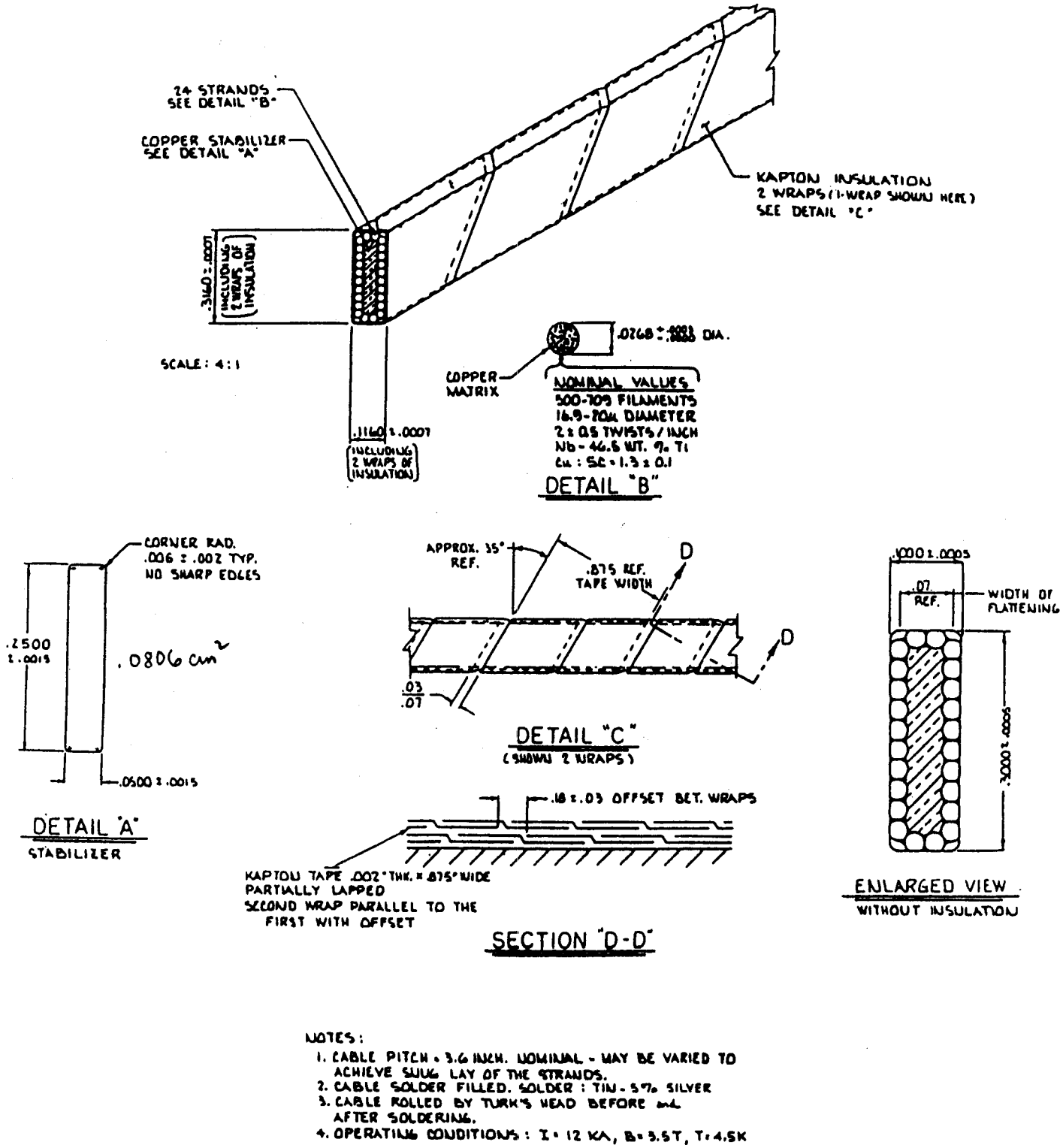

Fig.3 Cable parameters for the 3 T magnet as used in the quench calculations.

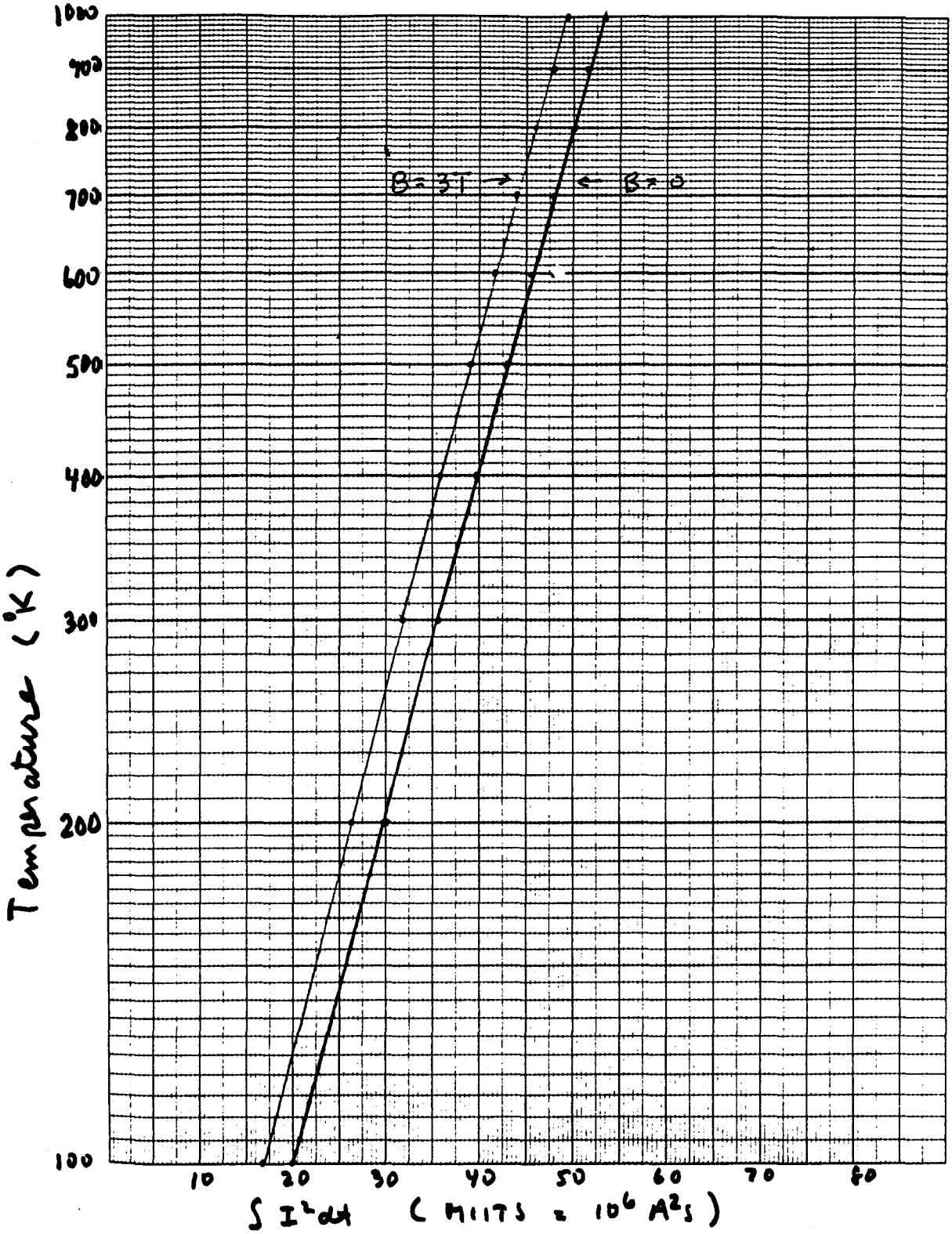

Fig.4 Predicted peak quench temperature versus Miits for the 3 T magnet cable as calculated by TMAX.

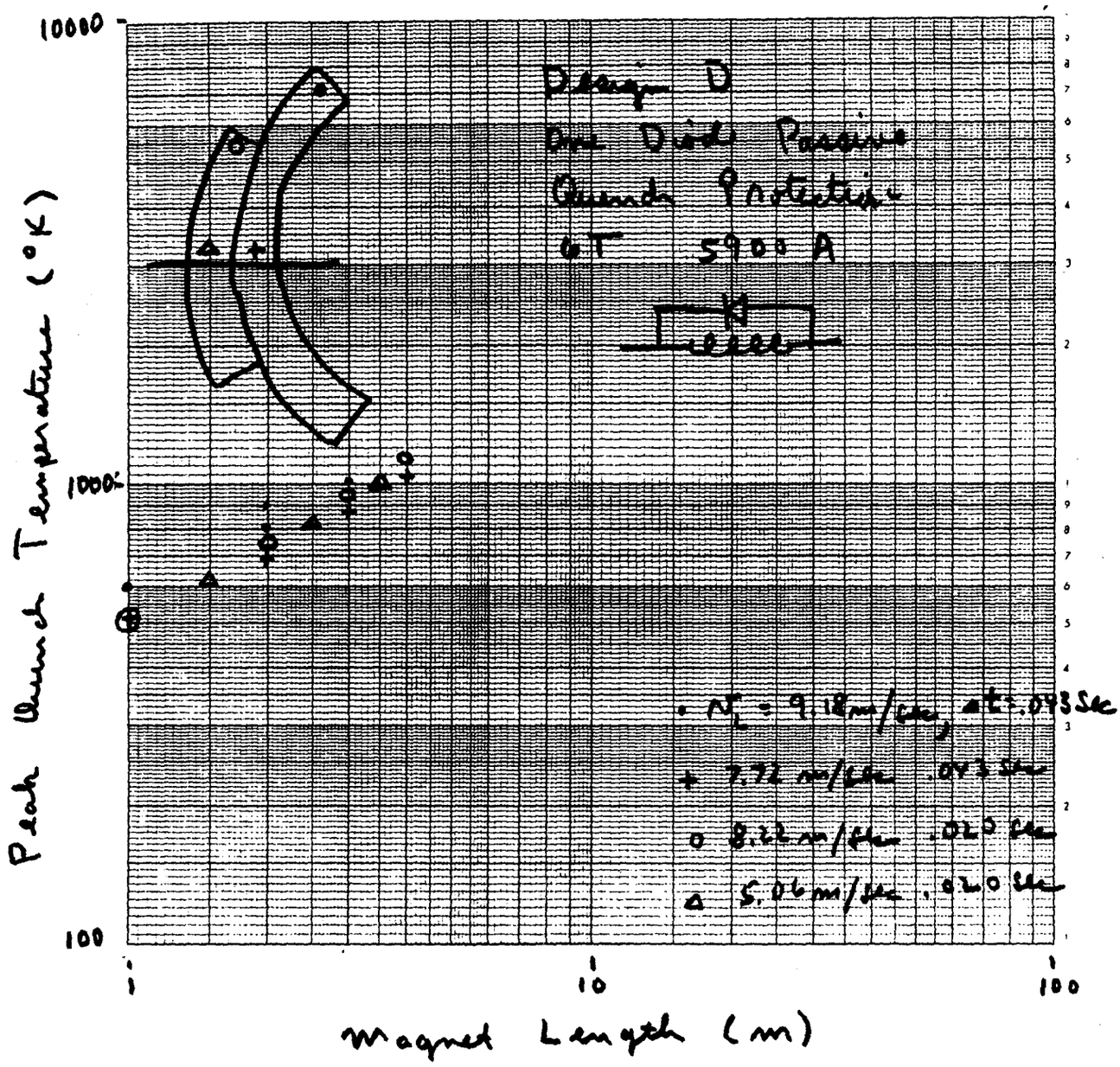

Fig.5 Calculated maximum quench temperatures for the 6 T magnet with single diode protection. The actual quench temperatures can be expected to be lower (See "Adjustments" of text).

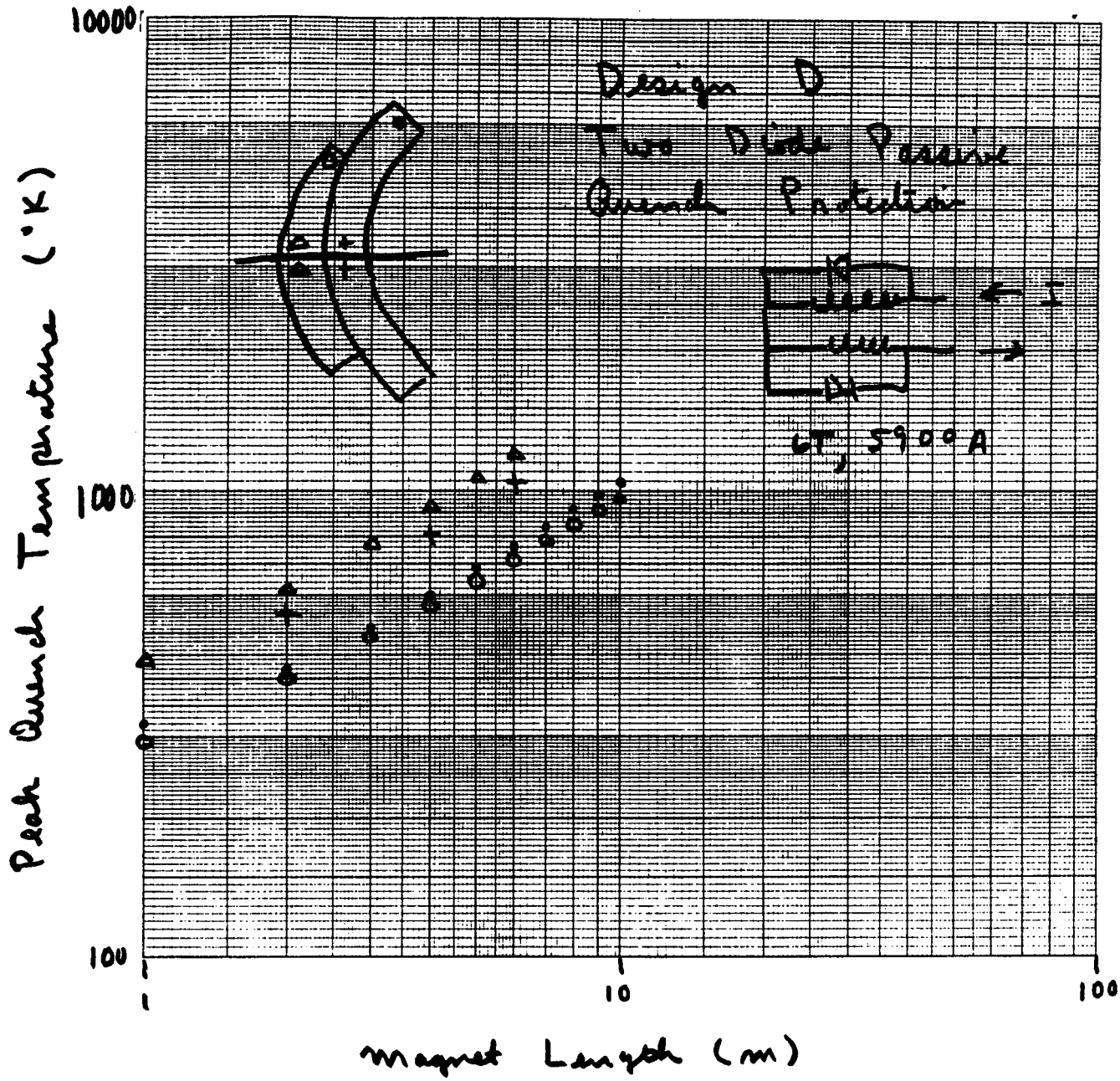

Fig.6 Calculated maximum quench temperatures for the 6 T magnet with two diode protection. The actual quench temperatures can be expected to be lower (See "Adjustments" of text).

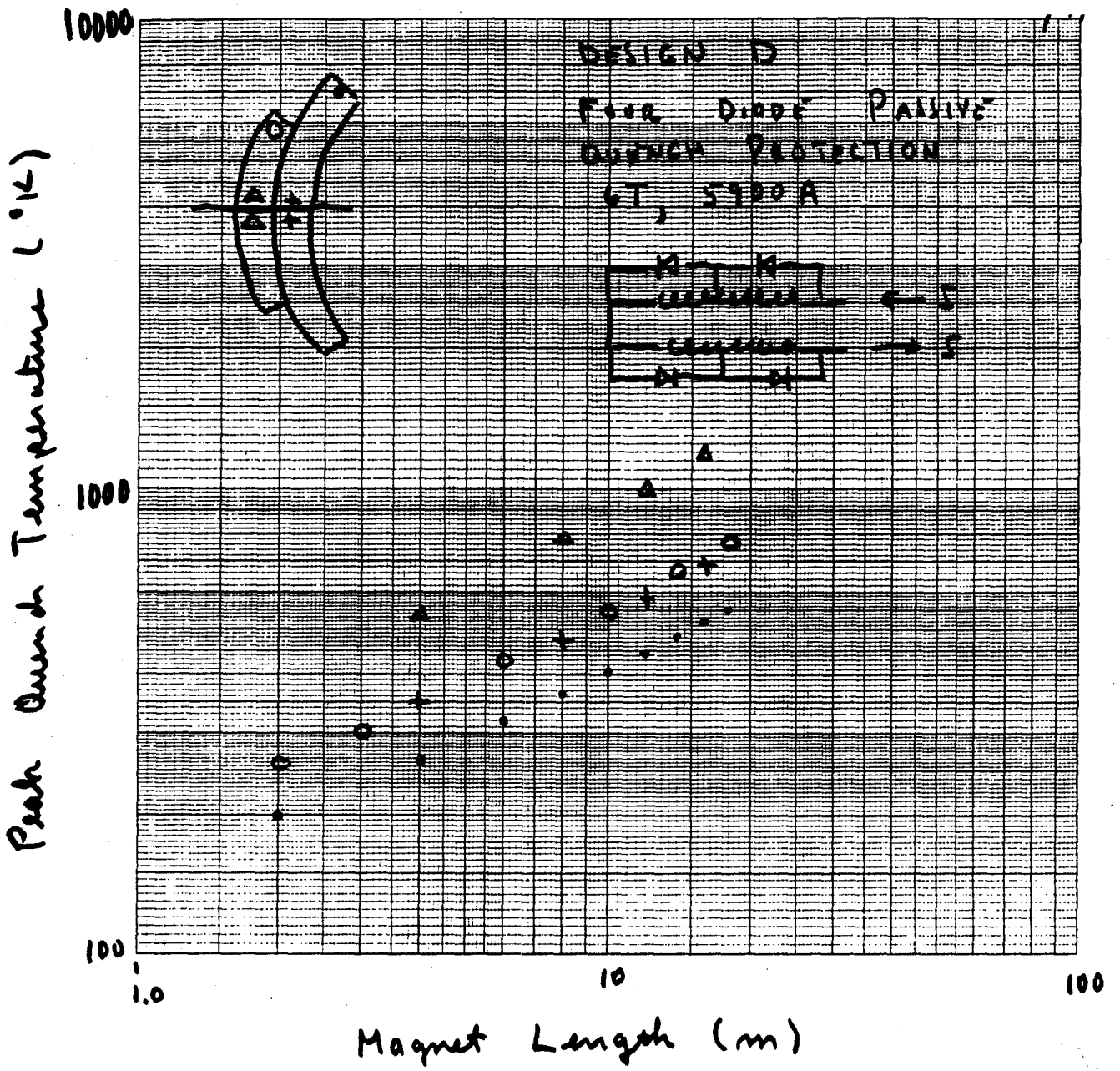

Fig.7 Calculated maximum quench temperatures for the 6 T magnet with four diode protection. The actual quench temperatures can be expected to be lower (See "Adjustments" of text).

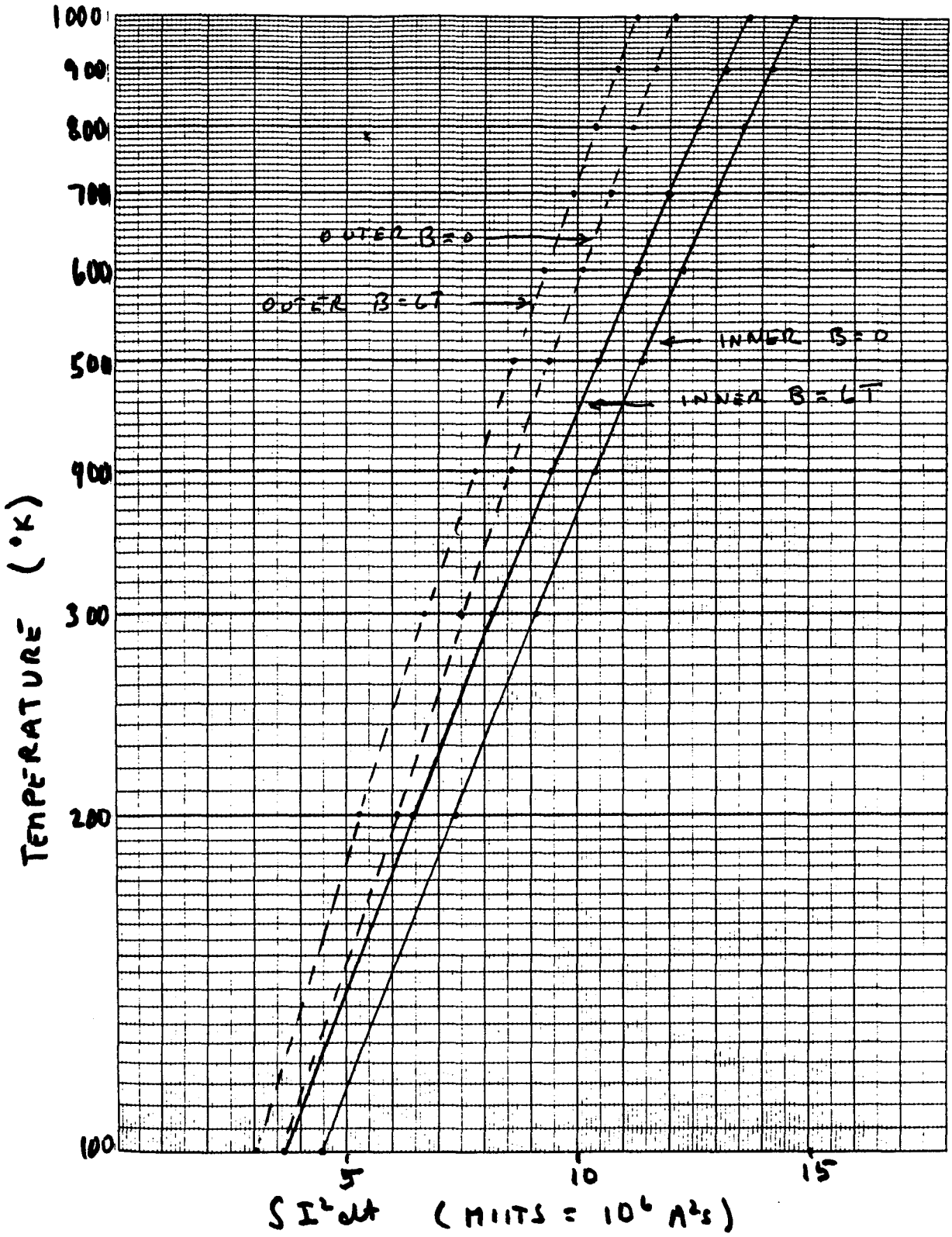

Fig.8 Predicted peak quench temperature versus Miits for the 6 T magnet cable as calculated by TMAX.

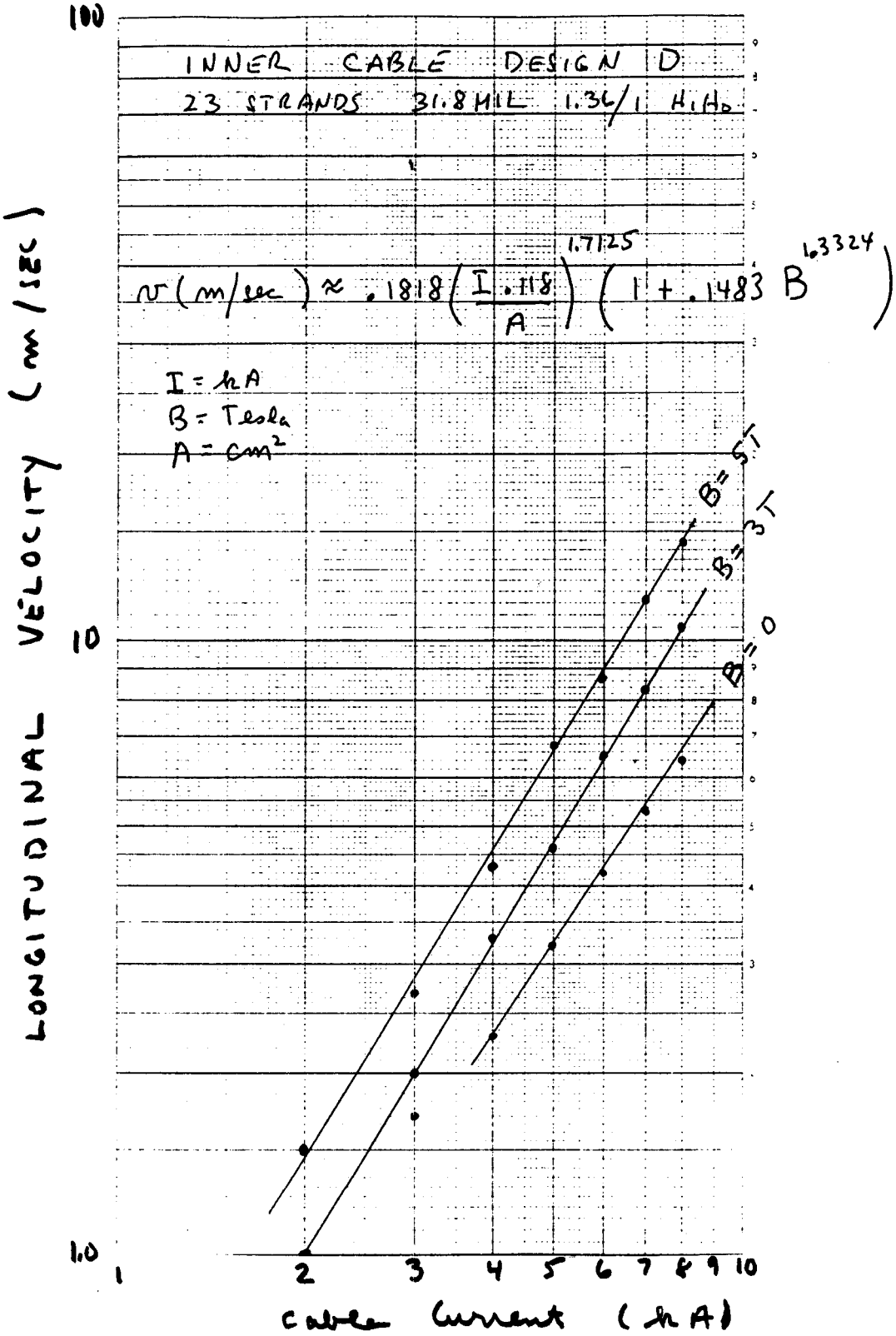

Fig.9 Quench velocities used for the inner coil of the 6 T magnet (Ref. 3)

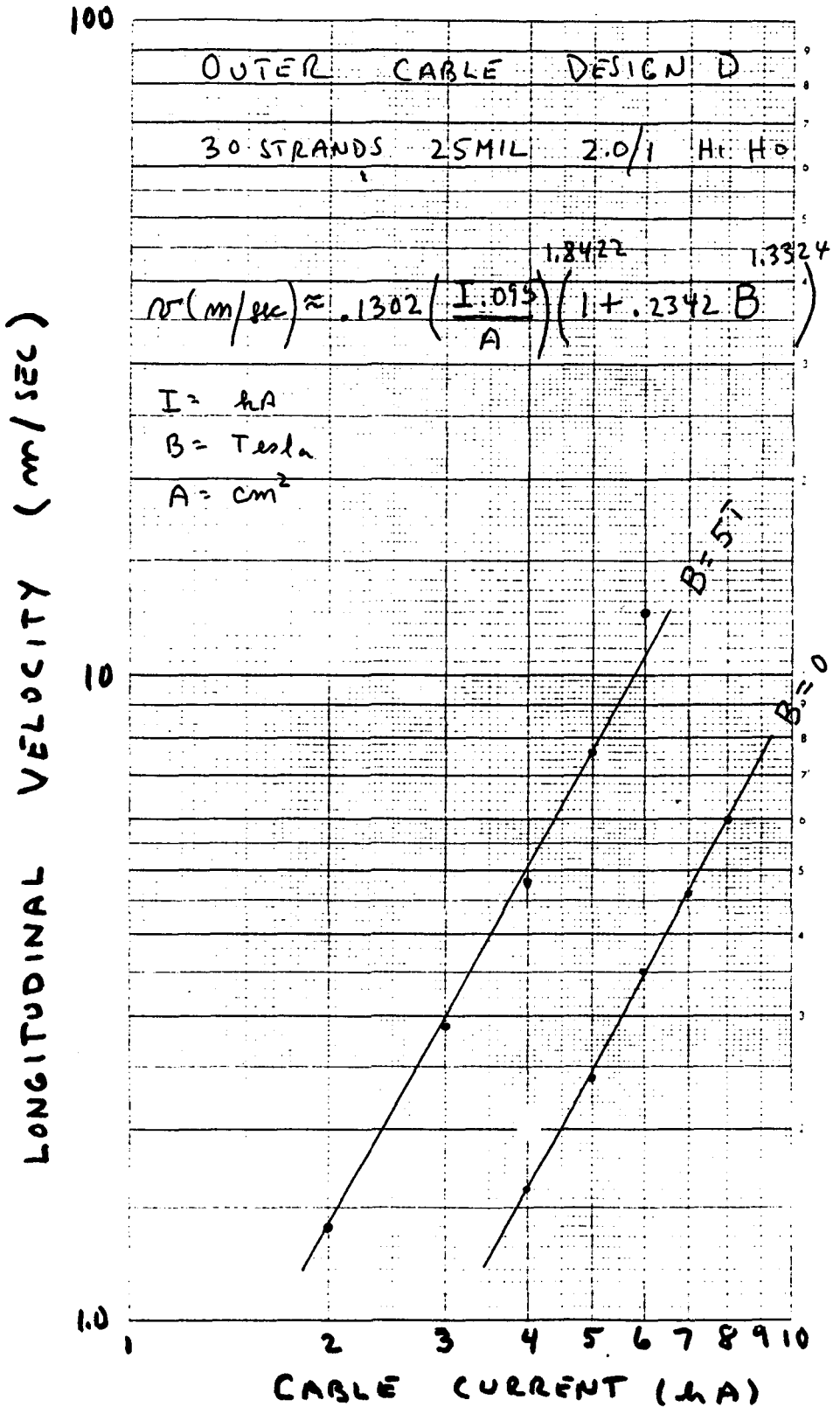

Fig.10 Quench velocities used for the outer coil of the 6 T magnet (Ref. 3).

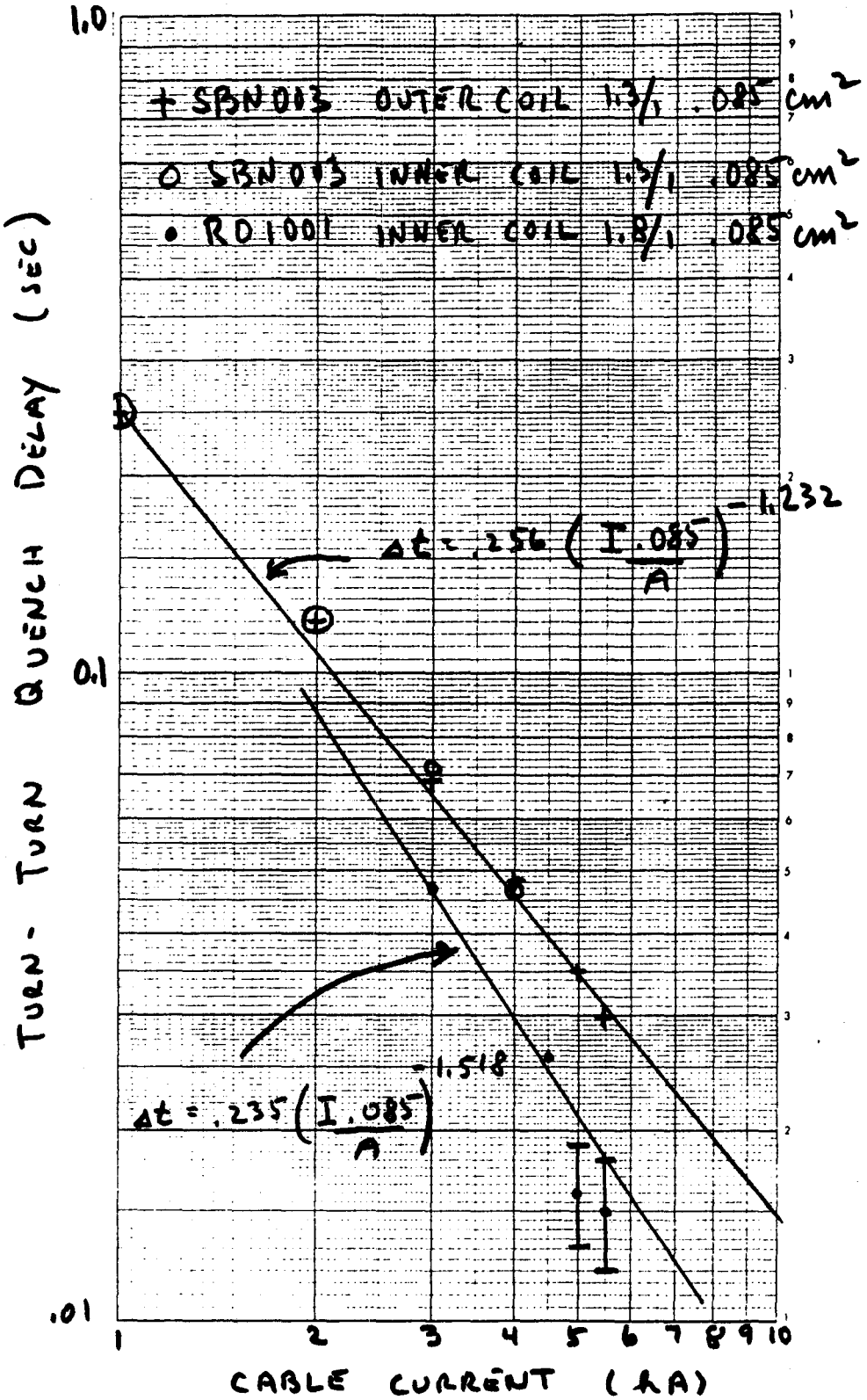

Fig.11 Turn to turn quench delays used for the inner and outer coil of the 6 T magnet (Ref. 4,5))

APPENDIX G

COMPUTER STUDIES OF THE QUENCH BEHAVIOR OF AN SSC MODEL-DIPOLE

GEBHARD MORITZ AND WILLIAM HASSENZAHL
LAWRENCE BERKELEY LABORATORY

COMPUTER STUDIES OF THE QUENCH BEHAVIOR OF AN SSC MODEL-DIPOLE*

Gebhard Moritz and William Hassenzahl

Lawrence Berkeley Laboratory
University of California
Berkeley, CA 94720

Introduction

The quench behavior of SSC dipoles is of interest for several reasons. First, the quench characteristics of the conductor will affect the design of the magnet windings. Second, if excessiv. temperatures are reached in a passive protection mode then additional accelerator components such as fast quench detection circuits, heater firing units, and heaters will be required. Third, machine operation, percent downtime, ramp rate, acceptable beam loss, etc. will depend somewhat on the quench characteristics of the various superconducting magnets in the machine. Of course all these factors influence the ultimate cost of the accelerator.

As a consequence it is desirable to understand very early on the detailed quench behavior of the SSC dipole windings. In the absence of experimental data on the magnets themselves we will attempt here to estimate the characteristics of quenches, in particular the hot spot temperature, in the SSC Reference Design A dipoles. The quenches are analyzed using the computer program QUENCH. Input data, material characterstics, are similar to those for other accelerator dipoles. We have compared calculations from the program QUENCH with actual data on quenches in the CBA magnets and the LBL model dipoles in the D-7, D-8, D-9, and D-12 series. Two "parameters", the copper resistivity at low temperatures and the effective enthalpy of the liquid helium contained in the windings were adjusted to make the temperatures and velocities calculated by QUENCH correlate with those in the actual magnets. Where

*This work was supported by the Director, Office of Energy Research, Office of High Energy and Nuclear Physics, High Energy Physics Division, U. S. Dept. of Energy, under Contract No. DE-AC03-76SF00098.

good data on the actual copper resistivity were available, the measured residual resistivity ratio was used, and only the helium fraction was adjusted. Good agreement was obtained with the available test results in all these comparisons.

These calculations are expected to be representative of quenches in the real SSC magnets, at least to the extent that they will correspond to other similar dipoles. We believe this correspondence is quite good. However, these calculations are not substitutes for hard data. Thus we recommend that as much data as possible be obtained on quenches in SSC model dipoles.

Program QUENCH

The calculations described here used the computer program QUENCH, it was first written by M.N. Wilson[1] and later modified and documented by W. Hassenzahl[2]. The specific heats of copper and superconductor and the resistivity of copper that we used are given in Figs. 1 and 2.

Because of the low copper-to-superconductor ratio in the proposed cable the windings heat up very quickly. There is no pool boiling heat transfer. Though the program would permit some of the heat from the conductor to be deposited in the helium bath, this feature is not used in these calculations. From fundamental experiments,[3] it is known that there is some transient heat transfer from the rapidly heating conductor to the small volume of helium with which it is in direct contact, which is a fraction of the helium within the insulation. This transient characteristic is taken into account by ascribing a constant specific heat C_p to helium between 4.4 and 15 K. The value used is determined by the integral $\int_{4.4K}^{15K} C_p dT$ = heat of vaporization. The maximum temperature of 15 K is used because we know that by the time the surface temperature of the conductor reaches this temperature there is essentially zero heat transfer (the film boiling limit is reached at about 5 or 6 K) to liquid helium that started at either 1.8 or 4.2 K.

Quench Velocities

The program QUENCH can calculate the quench propagation velocity or the velocity can be set by the user. If the velocity is calculated, the formula used is:

$$v_c = \frac{I(\Theta_m - 2\Theta_c)}{C} \sqrt{\frac{LT_m}{\Theta_c \, \Theta_m(\Theta_m - \Theta_c)}}$$

where: I = operating current (A/m^2)

C = specific heat (J/m^3K)

Θ_m = $(T_m - T_b)$ temperature difference between the maximum temperature of the conductor and the bath temperature

Θ_c = $(T_c - T_b)$ temperature difference between the critical temperature of the conductor and the bath temperature

L = 2.45×10^{-8} (V^2/K^2) = (Lorenz ratio)

T_c is calculated by

$$T_c = T_{cmax} - \frac{T_{cmax} - T_b}{I_c} I/I_c$$

where: T_{cmax} - maximum critical temperature for B = 0

I_c - critical current at the bath temperature (A)

Conductor and Windings

We ran quench calculations for the conductor in both the inner and outer layer of the proposed SSC-dipole. The conductors are slightly key-stoned, "Rutherford type" cables wrapped with two overlapping layers of Kapton. The Kapton has a thin layer of B-stage epoxy on one surface. The cable data for an LBL model dipole are given in Table I and those from the SSC reference design are displayed in Table II.

The coil geometry evaluated by the program QUENCH is rectangular. For small bore dipoles this approximation is not perfect, but the results of interest, namely temperature, do not depend strongly on slight variations in the overall coil dimensions. We have taken the circumferential extent of the winding at the mean radius of the conductor for one dimension, the height of the conductor for another dimension and twice the length of the coil for the other. These dimensions are also given in Tables I and II. The presently proposed geometry for the SSC model A magnet includes wedges in both layers. These may have an effect on circumferential quench propagation but the specific effect is unknown at present so these have not been included at all in the calculation.

Calculations

The program QUENCH allows the user to restrict the total normal going volume (the maximum extent of the quench) to certain regions of the coil. In our calculations the worst cases were those where only one layer, either the inner or the outer goes normal starting at the pole. The quench moves circumferentially in only one direction. For some other calculations we chose the innermost point of the inner layer in the midplane of the magnet as the point of quench initiation, i.e. B = B central. The length of the magnet is assumed to be 16 m unless otherwise specified, and no external dump resistor is used. Though some of the heat from the conductor will end up in the helium bath while the quench is in progress, the event is over so fast in general that very little

Table I

Characteristics of the D-12 Cable and Windings

	Inner Layer	Outer Layer
Bare Cable Dimension Average (in)	.371 x .0557	.383 x .0470
Insulation Thickness (in) (before squeezing)	.0022	.0022
Insulation Thickness (in) (after squeezing)	.0015	.0015
Number of Strands	23	30
Strand Diameter (in)	.0310	.0255
Copper to Superconductor Ratio	1.1	1.79
Percent of Unit Cell (%) in squeezed conductor		
Copper	44.6	52.7
Superconductors	40.5	29.5
Insulation	7.3	8.3
Void (He)	7.7	9.5
Winding Height (cm (in))	5.03 (1.98)	5.50 (2.17)
Width (cm (in))	0.93 (.37)	0.99 (.39)
Length (cm (in))	220 (87)	220 (87)

Table II

Characteristics of the SSC Reference Design Study Cable and Windings

	Inner Layer	Outer Layer
Bare Cable Dimension Average (in)	.371 x .0571	.383 x .0470
Insulation Thickness (in) (before squeezing)	.0022	.0022
Insulation Thickness (in) (after squeezing)	.0015	.0015
Number of Strands	23	30
Strand Diameter (in)	.0318	.0255
Copper to Superconductor Ratio	1.3	1.8
Percent of Unit Cell (%) in squeezed conductor		
Copper	48.1	54.0
Superconductors	37.0	30.0
Insulation	6.9	8.0
Void (He)	8.0	8.0
Winding Height (cm (in))	5.03 (1.98)	5.50 (2.17)
Width (cm (in))	0.93 (.37)	0.99 (.39)
Length (cm (in))	3220 (1268)	3320 (1268)

heat has a chance to be transferred out of the coil volume. Thus, in keeping with making a pessimistic estimate, no heat transfer to helium or any of the coil structure is taken into account.

One output of the program that is of major interest here is the time dependence of the highest temperature in the windings. The temperature increases with time and reaches its final value after 0.5 to 0.7 seconds. The final temperature depends strongly on the effective specific heat C_p of the helium in the windings through the effect of this parameter on the propagation velocity. For example, for a quench in the outer layer at the pole, the quench propagation velocity was calculated to be 13, 18, 27 and 35 m/s respectively for 7, 5, 3 and 2 percent helium, as shown in Fig. 3. To check this assumption we carried out another calculation with quench velocity as direct input to QUENCH and a helium fraction of 7 percent. In this case the enthalpy of the helium affects the temperature rise up to 15 K but not the quench velocity. These results are shown in Fig. 4. The final temperatures of this calculation are in good agreement with the results displayed in Fig. 3.

It is interesting to note, that the geometrically calculated fraction of about 7 percent helium does not give the quench velocity measured in other magnets with almost identical conductor geometry.[4] Instead, much lower percentages, about 2 percent for our model, give the experimentally observed velocity. This same effect appears to have been observed at BNL ,[5] where they measured lower velocities in "forced-flow" than in "pool-boiling" experiments. The explanation was that only a small amount of helium boils and the rest is simply forced out of the conductor with the result that the quench front "sees" only a limited volume of liquid helium. On this basis we use the percentage of helium as a knob to adjust the quench propagation velocity in the calculation so it will agree with the few known experimental values.

Figure 5 shows the final hot spot temperature for the inner and outer layers of the 1 m long D-12 magnet as a function of the operating current. A maximum is observed

at about 5000 Amps. For higher currents the stored energy increases, but the quench velocity increases even faster (Figure 6). A similar effect was observed in the CBA coils.

The predicted temperatures are well under the damage level, which we assume to be below 700 K.

Improved Superconductor

In recent months there has been a successful effort to improve the critical current density of the NbTi superconductor used in the SSC dipoles. Improved superconductor has several effects on the SSC. First, it can reduce costs. Second, it may improve accelerator reliability if a greater operating margin (ΔT) is allowed. Third, on the negative side, this increased margin will increase hysteretic losses, and induced multipoles. Fourth, the increased margin will cause the quench propagation velocity to decrease, and thereby increase the ultimate peak temperature in the windings. Figure 7 shows the critical currents of three cables; the middle curve is the quoted SSC RDS performance curve, not the design curve. The other two are actual conductors. The lower is for the conductor used in the D-12C series of magnets and the upper curve is for the most recent billets of high homogeneity conductor. Also shown in this figure is the short sample performance of the high homogeneity wire alone. In Figure 8 we see the peak magnet temperature to be expected for quenches at the layer 1 pole for 16 m SSC dipoles made of these conductors. No active protection system is used. By keeping the copper to superconductor ratio constant the improved conductor to some extent reduces the likelihood of a possibly safe coil.

Effect of Magnet Length on Temperature

The SSC coil length of 16 m, which was set rather arbitrarily for the reference design study, may be changed for a variety of reasons before the SSC is actually

constructed. One reason for shortening the coils would be the desirability of a passively safe magnet system. The peak temperature predicted in Fig. 8 occurs at about 5000 A for all the different superconductor characteristics. Using the Reference Design Study Nb-Ti critical current characteristics, and 5000 A, the effect of magnet length on peak temperature is shown in Fig. 9.

Conclusions

Preliminary calculations of the quench behavior in SSC-dipoles show that the magnets could be self-protecting and that a heater may not be necessary, depending on the conductor used. Nevertheless, in order to get more accurate results, it is necessary to measure quench propagation velocities in the model magnets and the cable temperature as a function of "MIITS" in the model magnets or in short sample experiments. Furthermore, we must pay attention to the difference between "pool-boiling" and "forced flow" cooling as this may also affect the ultimate temperature rise in the conductor. As a separate issue, not discussed above, improving the residual resistivity of the copper in the conductor will have a major effect on the final temperature.

References

(1) M.N. Wilson, "Computer Simulation of the Quenching of a Superconducting Magnet", Rutherford High Energy Lab., Report RHEL/M151.

(2) W. Hassenzahl, "QUENCH Modifications and Documentation", CEN Saclay, SUPRA/78-61 CEN

(3) D. Gentile, W. Hassenzahl, M. Polak, "A Method for Determining Temperatures and Heat Transfer Coefficients with a Superconductive Sample," J. Appl. Physics, 51(5) May 1980.

(4) S. Caspi, W.V. Hassenzahl, "The source, origin and propagation of quenches measured in superconducting dipole magnets," IEEE Transactions on Magnetics, Vol. MAG-19, No. 3, May 1983.

(5) A.J. Stevens, "Quench Studies on CBA in Forced Flow Cooling", BNL, ISABELLE Technical Note No. 381 (1982).

(6) A.J. Stevens et al, "Quench Protection Studies on CBA Magnets", IEEE Transactions on Nuclear Science, Vol. NS-30, No. 4, Aug. 1983.

(7) P.S. Martin (FNAL), Private communication.

Figure Captions

1. Specific heat of copper and NbTi superconductor used for the calculations in this report.

2. Resistivity of copper based on measurements of LBL conductor #280 used in the D12A magnet. The residual resistivity ratio is 60.

3. Quench propagation velocity affects the final quench temperature more than any other factor. In this study the effective helium content in the windings was varied to control the velocity. The initiation point of the quenches for this figure were at the inner layer midplane. No external energy dump is assumed.

4. Quench propagation velocity was a fixed input to QUENCH for this set of curves. Note that the helium content has little effect on the final temperature compared with the previous figure.

5. Estimates of maximum quench temperature for a 1-meter model magnet with graded conductor from the inner to the outer layer.

6. Estimates of quench propagation velocity as a function of current and the effective helium content within the windings.

7. Load line and critical current curves for the C-5 magnet design and three conductors. The parameters for these conductors are used to estimate the temperatures in Fig. 8.

8. Peak temperatures in a quench in an SSC dipole for different conductors. Note that the magnet made with the best conductor has the highest final temperature.

9. At the observed propagation velocities only about 5 to 7 meters of an SSC-dipole will go normal during a quench in which no heaters are used. Thus final temperature will depend on magnet length as shown here. This curve is for a 5000A quench, the highest temperature for the Reference Design Conductor of the previous figure.

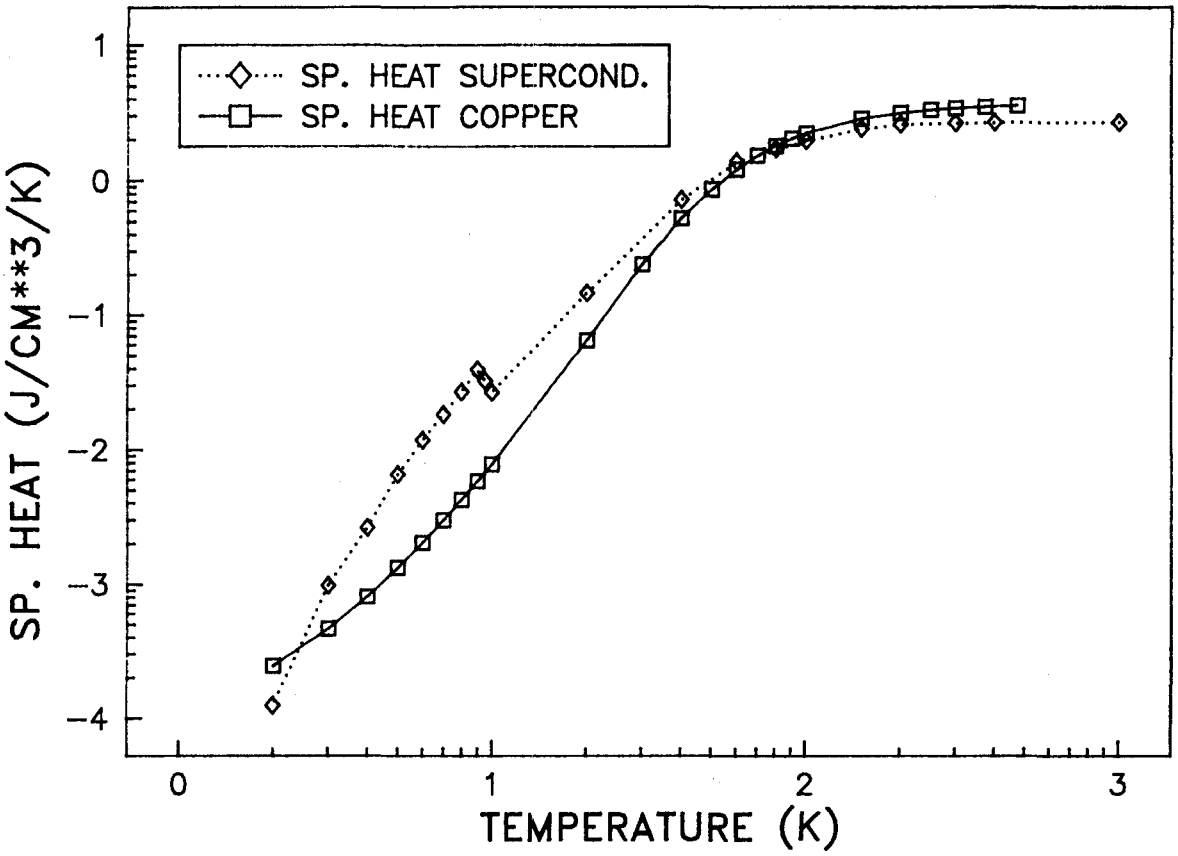

XBL 845-1735

Fig. 1

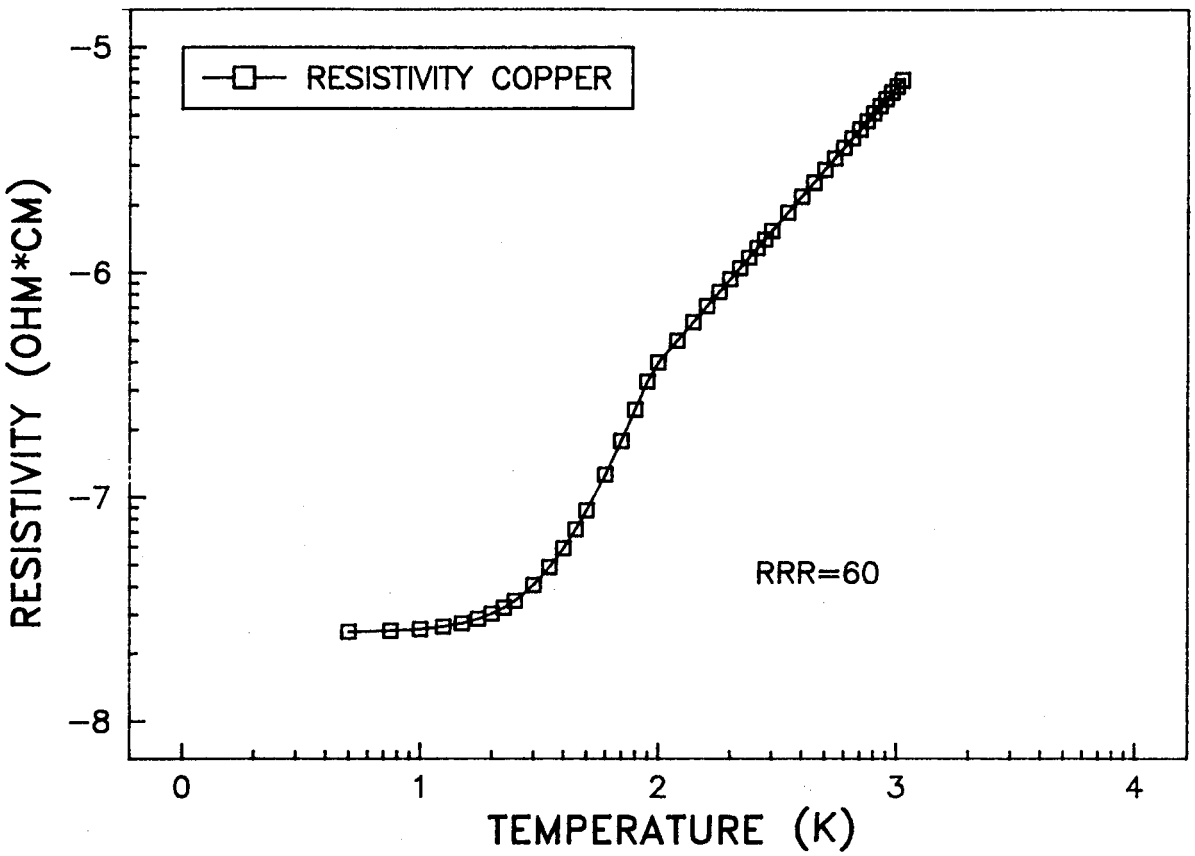

XBL 845-1734

Fig. 2

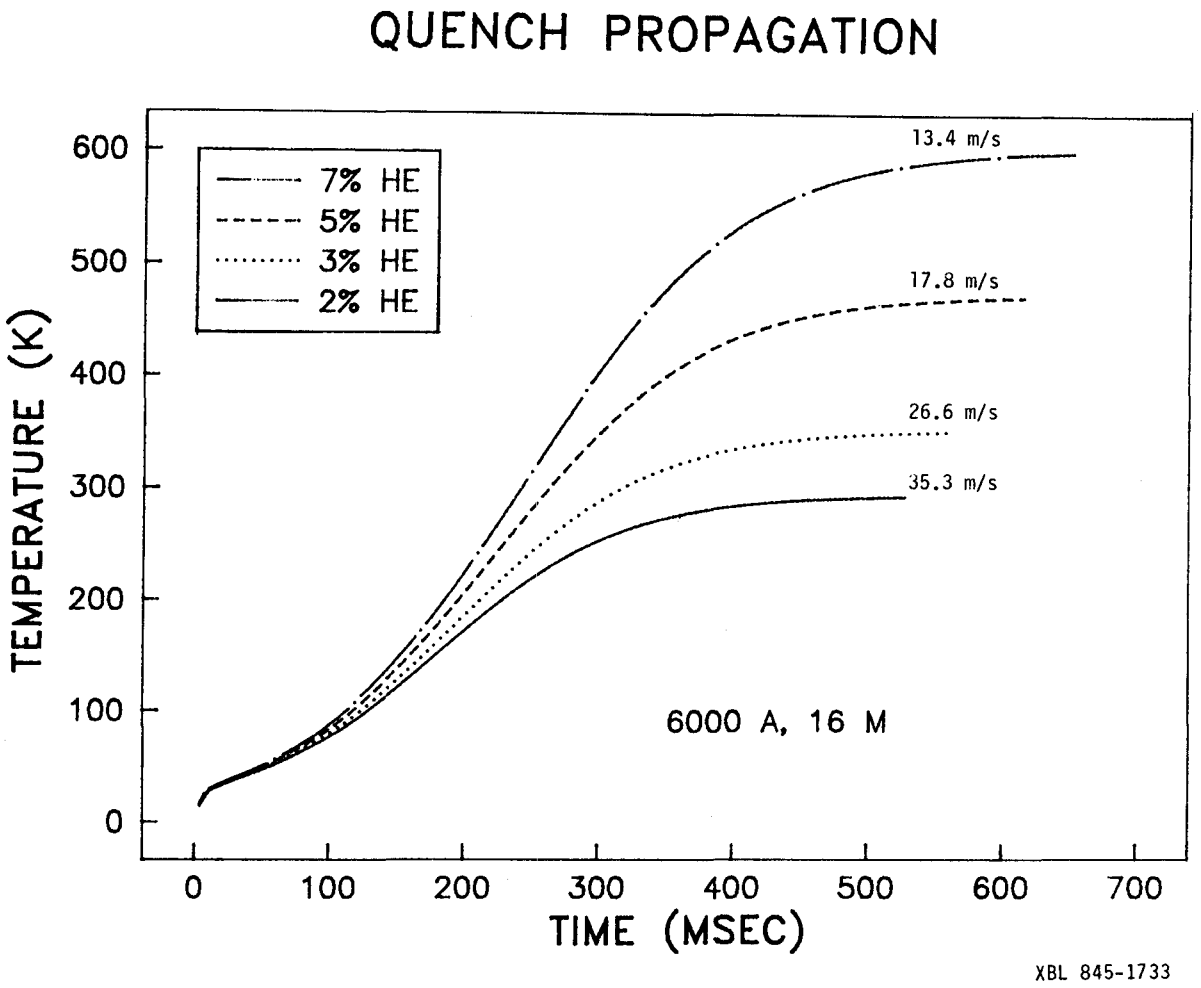
QUENCH PROPAGATION
7% HE
5% HE
3% HE
2% HE
13.4 m/s
17.8 m/s
26.6 m/s
35.3 m/s
6000 A, 16 M
TEMPERATURE (K)
TIME (MSEC)
0
100
200
300
400
500
600
700
XBL 845-1733

Fig. 3

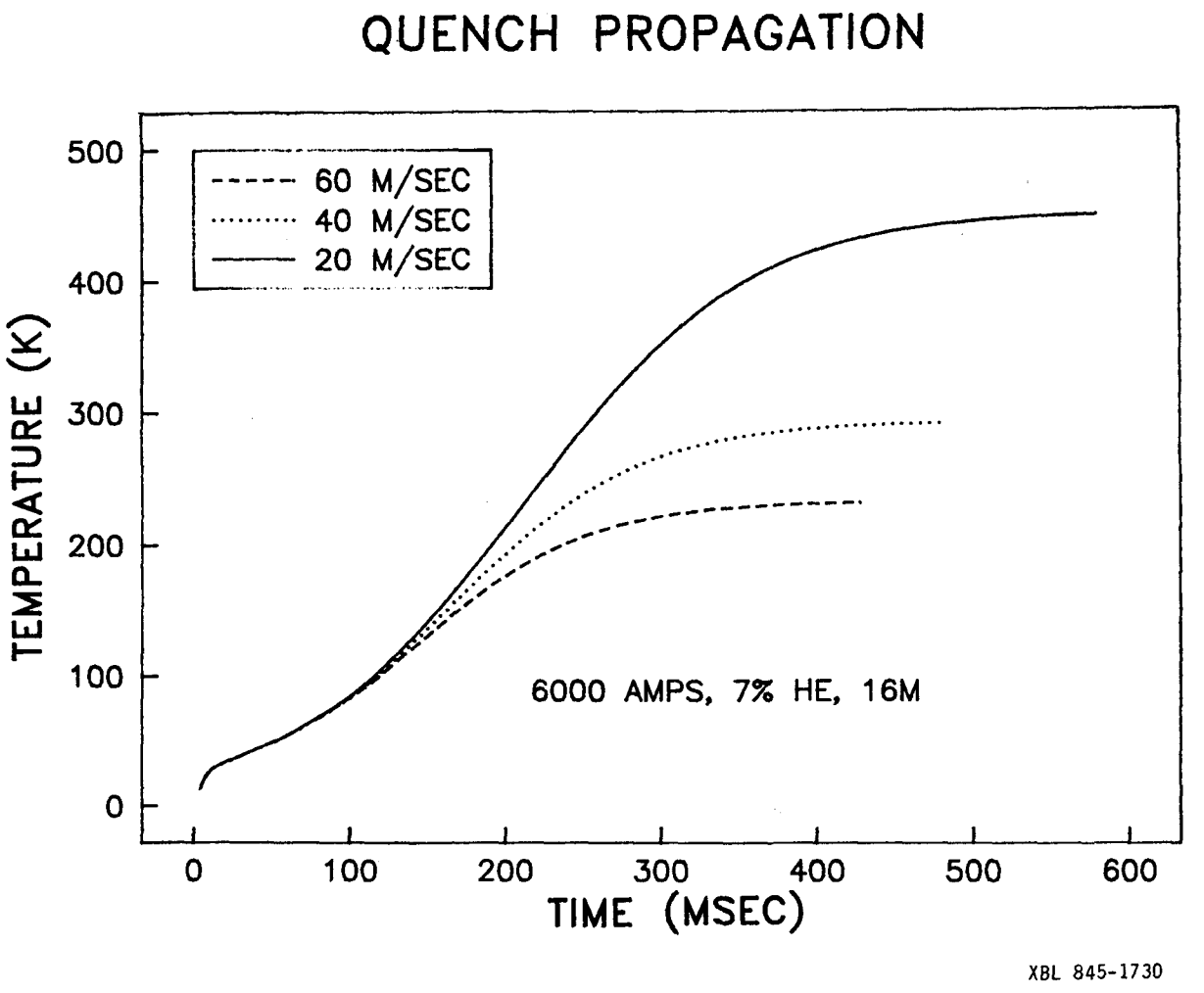
QUENCH PROPAGATION
60 M/SEC
40 M/SEC
20 M/SEC
6000 AMPS, 7% HE, 16M
TEMPERATURE (K)
TIME (MSEC)
0
100
200
300
400
500
600
XBL 845-1730

Fig. 4

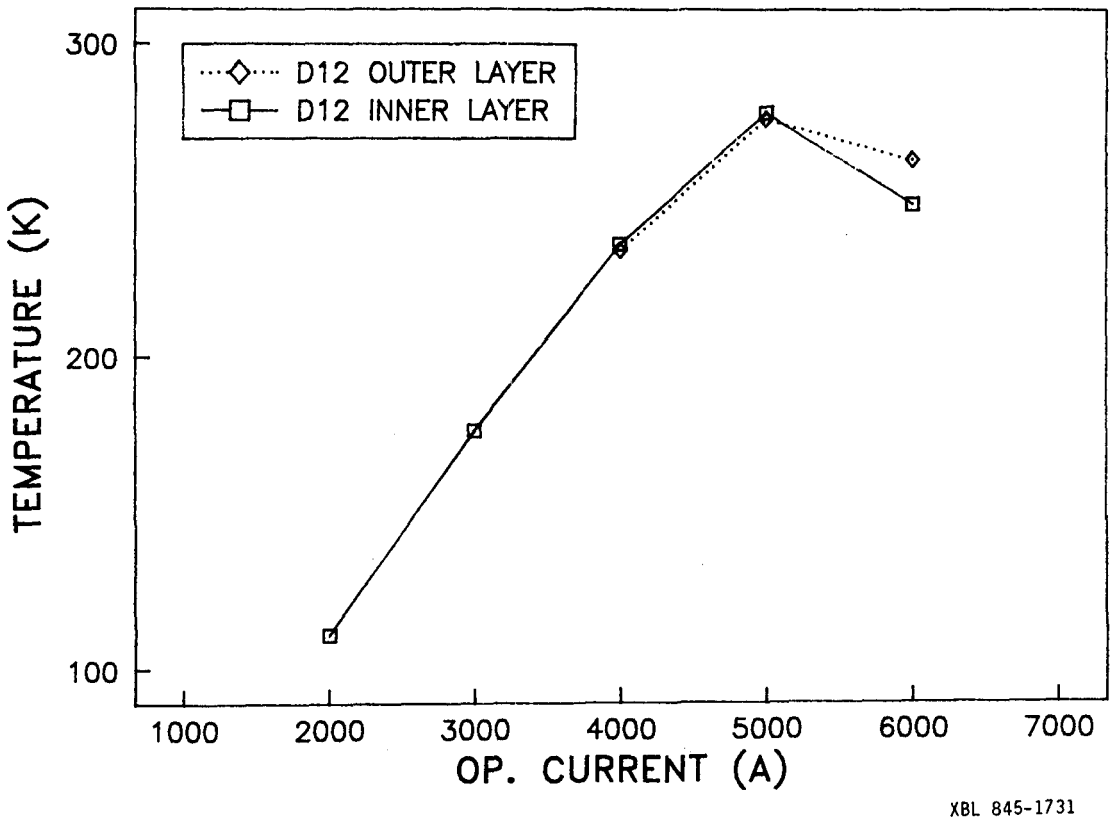
D12 OUTER LAYER
D12 INNER LAYER
TEMPERATURE (K)
300
200
100
1000
2000
3000
4000
5000
6000
7000
OP. CURRENT (A)
XBL 845-1731

Fig. 5

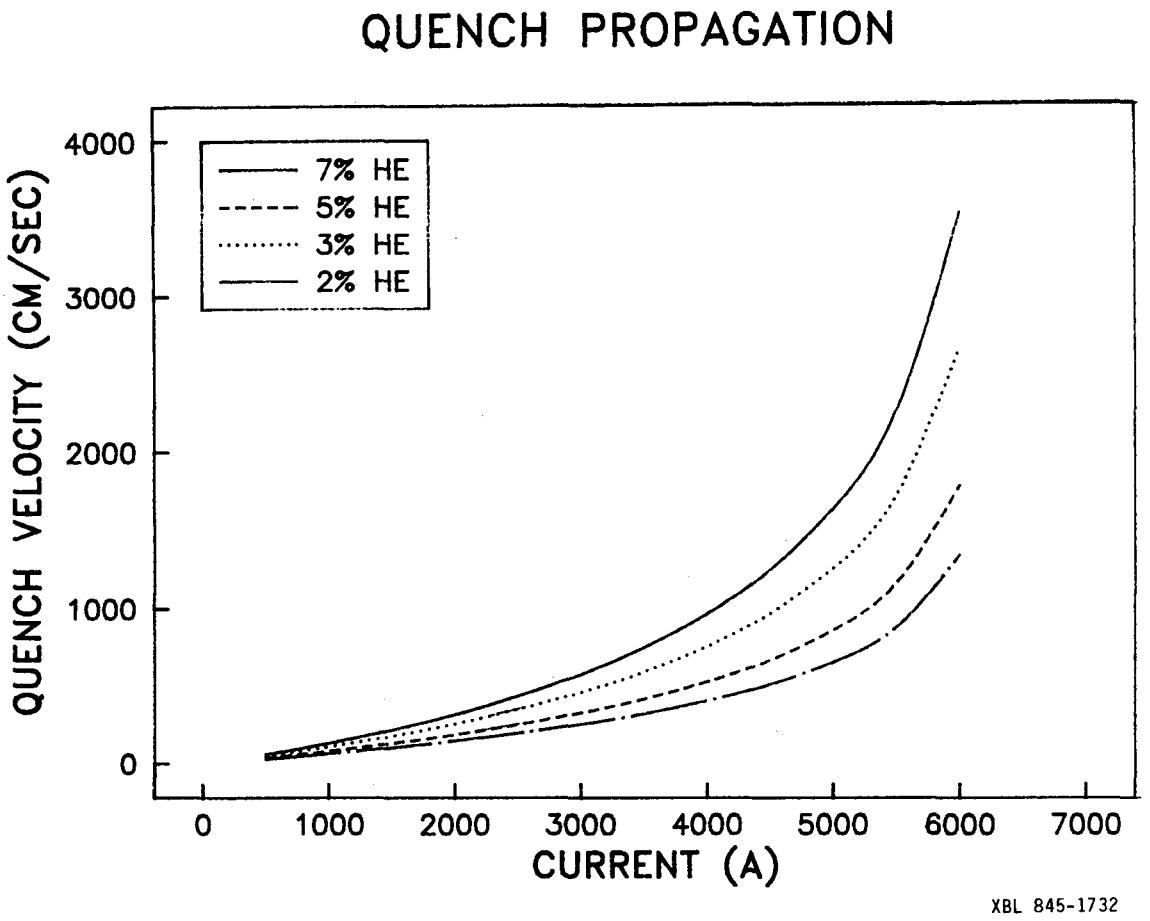
QUENCH PROPAGATION
QUENCH VELOCITY (CM/SEC)
4000
3000
2000
1000
0
7% HE
5% HE
3% HE
2% HE
0
1000
2000
3000
4000
5000
6000
7000
CURRENT (A)
XBL 845-1732

Fig. 6

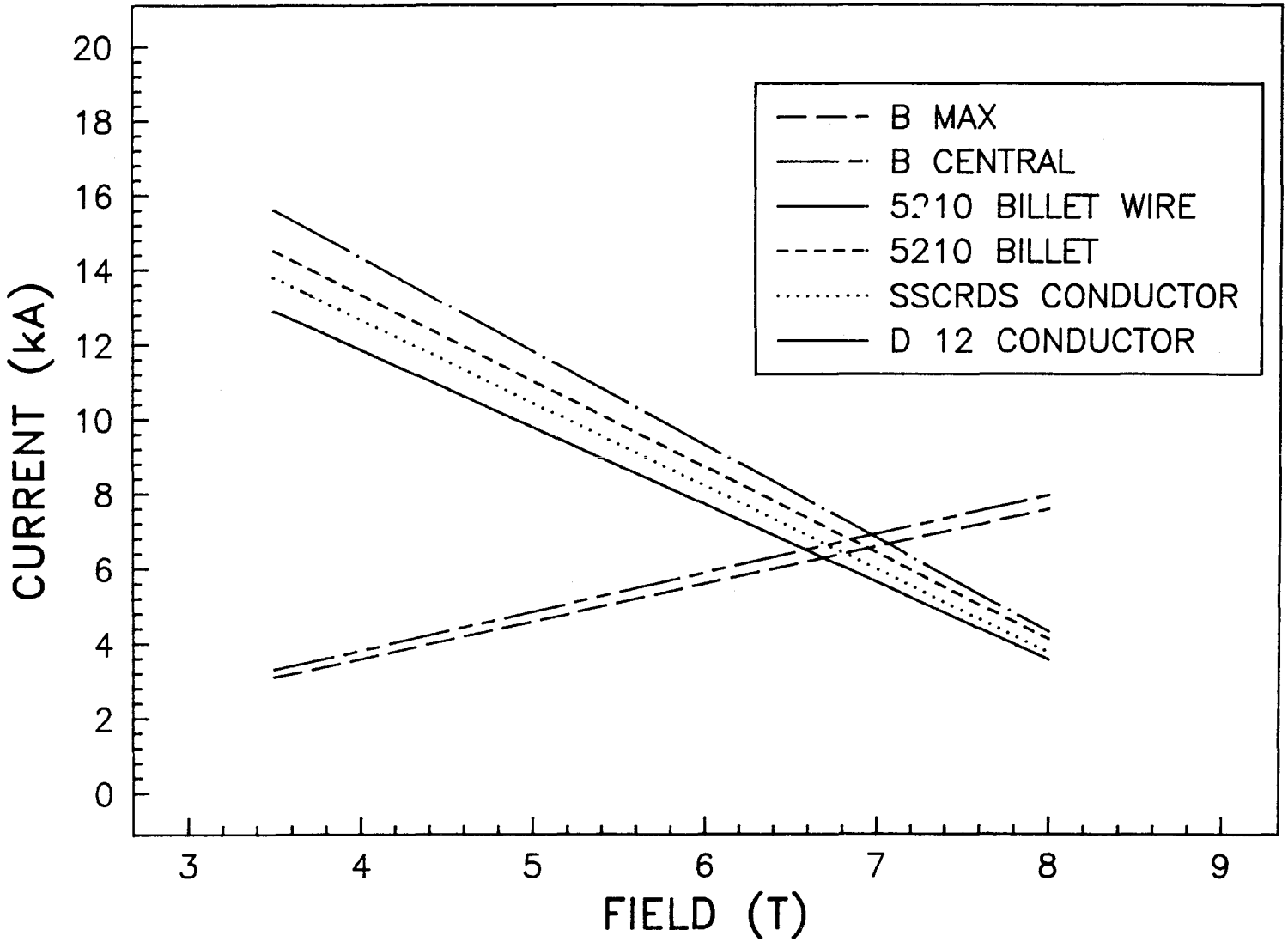

XBL 852-1276

Fig. 7

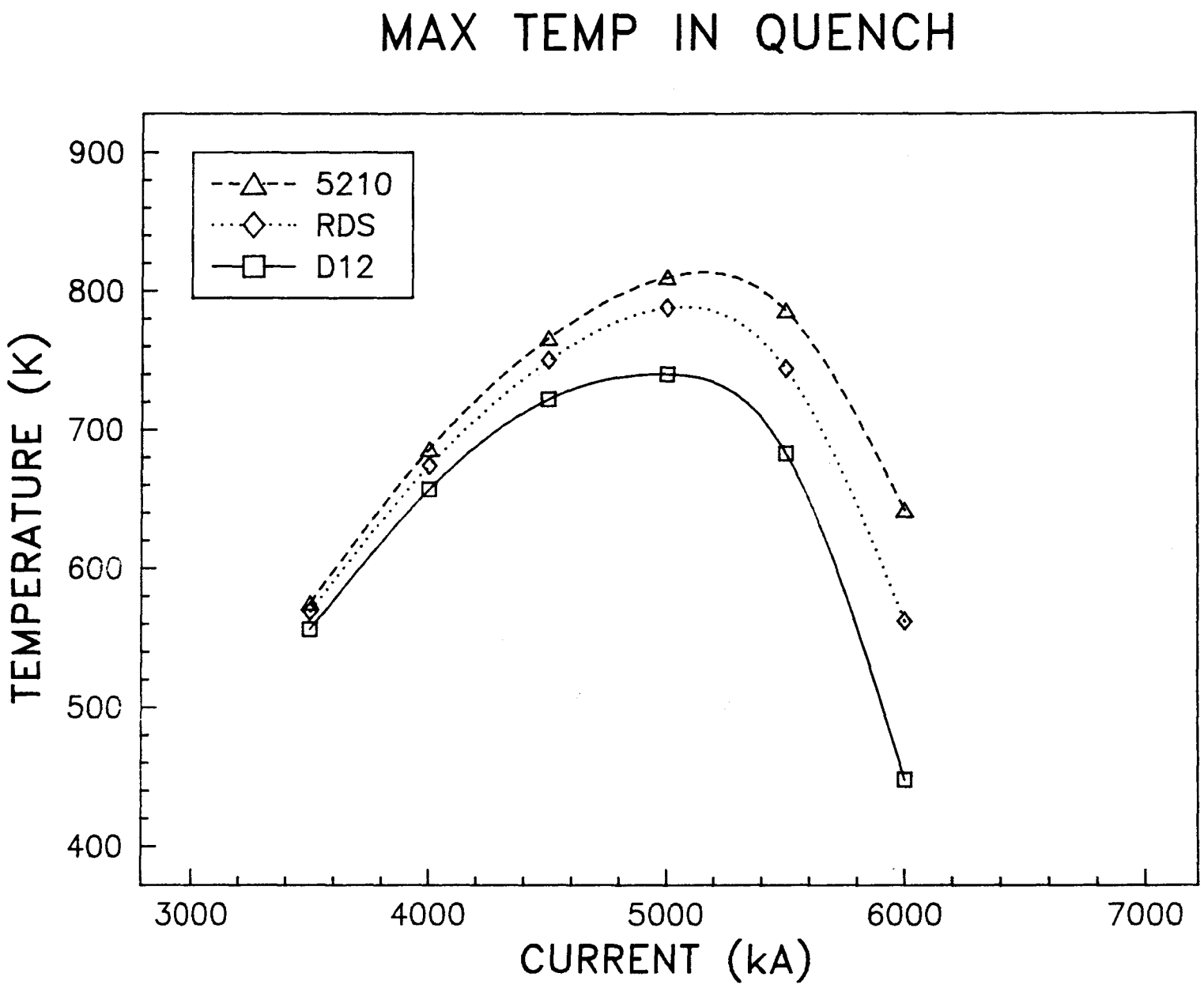

XBL 852-1275

Fig. 8

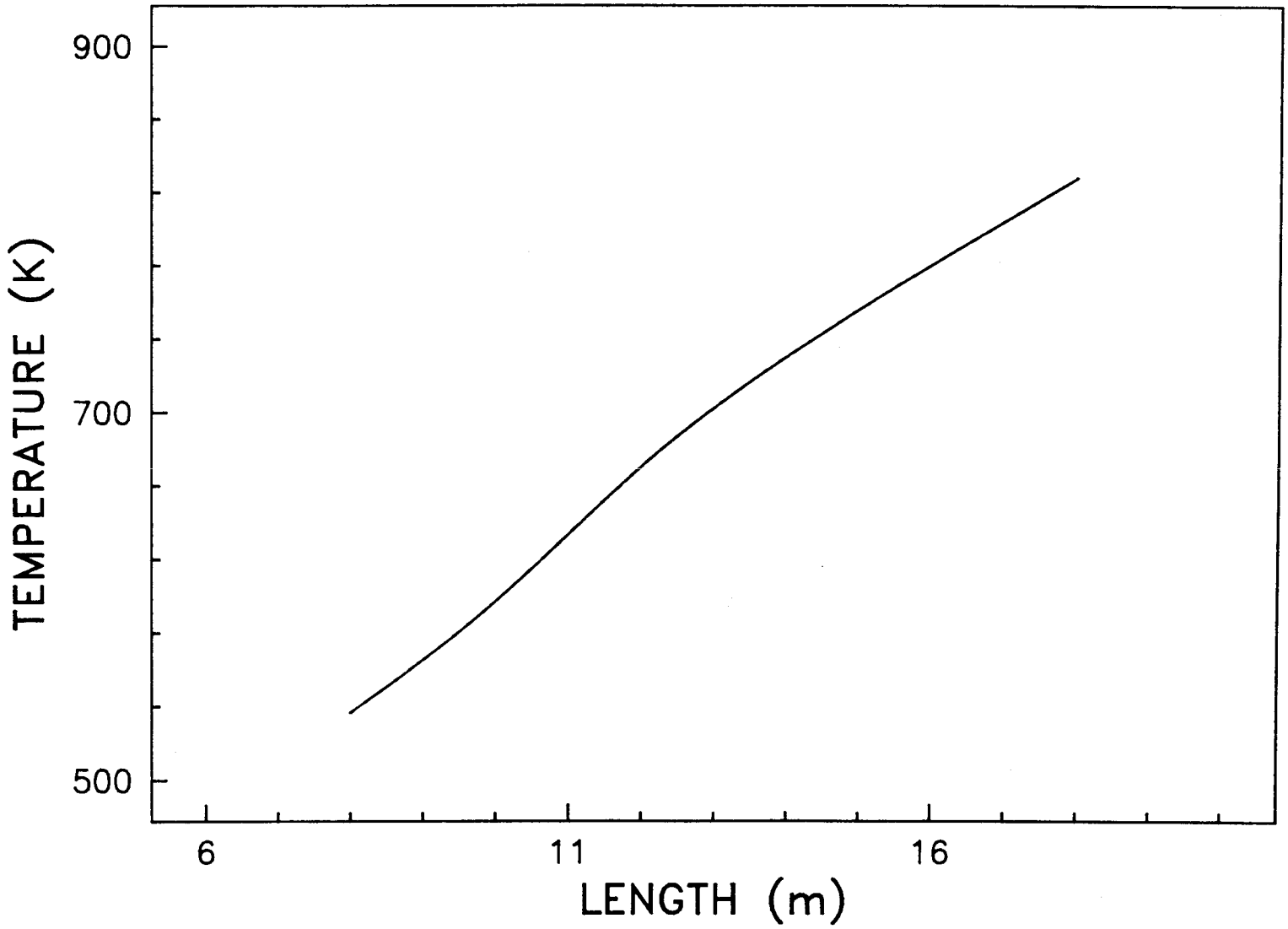

XBL 852-1277

Fig. 9

APPENDIX H

QUENCH PROTECTION FOR SSC DESIGN D MAGNETS

J.G. COTTINGHAM

Quench Protection for SSC Design D Magnets

J. G. Cottingham

Ganetis and Prodell conducted a series of experiments relating to the quench burn-out and quench propagation properties of NbTi superconducting magnets. These results are reported to the 1985 Particle Accelerator Conference and are contained in their paper entitled Results from Heater-Induced Quenches of a 4.5 m Two-in-One Superconducting R&D Dipole for the SSC.

These results can be used to upgrade the method for estimating the natural quench characteristics of the proposed full length SSC magnet which is assumed at this time to be that reported in BNL Technical Note 19.

The burn-out limit for the cable used in the experiment was estimated using a computer program which extrapolates from CBA experience. These results are tabulated below and compared with measured values.

Program predicted design limit	6.13×10^6 A^2-sec.
Measured burn-out limit	8.72 " "
800K temperature point	7.70 " "

The ratio of the A^2-sec. value for a "hot spot" temperature of 800K to that predicted by the computer program is 1.256 indicating that the program predictions are pessimistic by 25.6%. This is not surprising since the program has been known to give pessimistic results because it contains no conductive cooling correction for the "hot spot".

As has been reported before the integral I^2dt rises with quench current until it reaches a maximum then falls as the current approaches the critical current. Figure 2 in the referenced paper illustrated this typical behavior. The program used to predict quench behavior needs, as an input, the current value at which this integral peaks. The output results are a strong function of this input. In the past I have used a value of approximately 0.9 that of the planned operating current. Since the planned operating current is a judgement matter, this is a poor procedure for choosing this input parameter. The current at which the integral I^2dt peaks is a function of the quench current. Ganetis and Prodell report this current ratio to be

0.76. If I estimate the location of this peak from the design quench current using the 0.76 ratio, I obtain estimates that are lower than before. These are summarized as follows:

	Original Estimate	New Estimate
Operating Current	6530 amps	
Critical Current		5992 amps - See TN-19
Peak, Integral I^2dt	5875	4550 amps

This reduction in the current at which the integral I^2dt function peaks favorably alters the peak temperature predictions and in fact now produces a prediction that the SSC design of TN-19 is passively quench protectable. Results are summarized as follows:

Predicted Quench Characteristics for SSC Magnet Described in TN-19

	Inner Coil	Outer Coil
Predicted cable burn-out	$12.16 \times 10^6 A^2$-sec.	$10.02 \times 10^6 A^2$-sec.
Corrected cable burn-out(+25.6%)	15.27	12.58
Quench event, single diode	11.22	10.56
Quench event, double diode	9.39	8.89

If these predictions are correct, then this magnet is passively protected with only a single diode and the double diode concept becomes a backup procedure.

Clearly, small changes in certain critical inputs make significant change in the output results and in this case have radically changed the conclusion. Only tests with a full length magnet will confirm these predictions, but I believe they now represent our best estimate of quench performance and that we should now anticipate that the Magnet Design D is passively protectable.

APPENDIX I

MAGNET POWER SUPPLIES

D. HARTILL

Appendix I

MAGNET POWER SUPPLIES

Introduction

From discussions with our colleagues in the design group and after listening to our CERN colleagues describe their operating experience with SppS collider, it is clear that the quadrupole and dipole magnet currents must track within a few parts in 10^5. Requiring that the betatron tune spread be < 0.002 during acceleration (to limit particle loss) and during colliding beam operation (to limit emittance growth) implies current regulation with $dI/I < 2 \times 10^{-5}$ for the SSC. At first sight this requirement seems to provide an interesting design challenge, because in the Reference Designs Study dipole and quadrupole current was provided by 12 separate power supplies coupled together by differential transductors. Assuming that the current errors are random, each power supply must then regulate to a factor of $12^{1/2} \sim 3.5$ better than the overall regulation requirement. One way to avoid these random errors would be to connect the entire ring in series with 12 equally spaced power supplies. All except one would operate in the voltage control mode, with the remaining one operating in the current regulation mode to close the current regulation loop. For the ramp rates specified in the Reference Designs Study, the total power supply voltage requirement is less than 1360 volts for Design A (and D) and 270 volts for Design C (in both cases plus power lead drops), which is easily satisfied.

Because of the 4 volt "on" voltage for cold diodes, substantially higher voltages at low output currents are required to test the integrity of a passive quench protection system. This could be provided either by the main supplies or by separate low-power higher-voltage supplies which are switched in only during quench protection system tests. A penalty of the single-loop solution is the requirement of at least 12 high-current active and fast switches (as in the Tevatron power supply system). These must act reliably during upset conditions to limit voltage to ground by isolating the faulty sector from the circuit. Commissioning would be more difficult because the entire magnet is in series.

During a talk on overall performance of the SppS collider, Lyn Evans from CERN described the magnet power supply regulation requirements. Because of intrabeam scattering they must limit the tune spread contribution from the power supply system to less than 0.001, which implies an overall current regulation of better than 3×10^{-5}. The magnet power supply system uses separate power supplies for the vertically focusing quadrupoles, the horizontally focusing quadrupoles, and the dipoles. During normal operation, the SppS thus achieves regulation within a factor of two of that required for the SSC.

To limit the sextupole and decapole contributions to an acceptable level in the 3T magnet, the current excitation is separated into three circuits. Fig. A7.2-1 shows the coil placement for one bore in the 3T design. The eight-turn main coil is separated into two separate circuits (inner and outer) with roughly equal currents at 3T. The third circuit is a two-turn separate decapole correction winding which requires about one-third the main current. The currents in the two main sections along with the correction winding current necessary to achieve the required sextupole tolerance are shown in Fig. A7.2-2 as a function of the dipole field. Only the sum of the two currents from the two main power supplies (I_{inner}) has to be regulated to the level mentioned above, with the tolerance on the ratio being a part in a thousand. The decapole correction winding current must be regulated to one part in 10^4. The quadrupole magnets are on a separate power supply. They require 3 kA at the

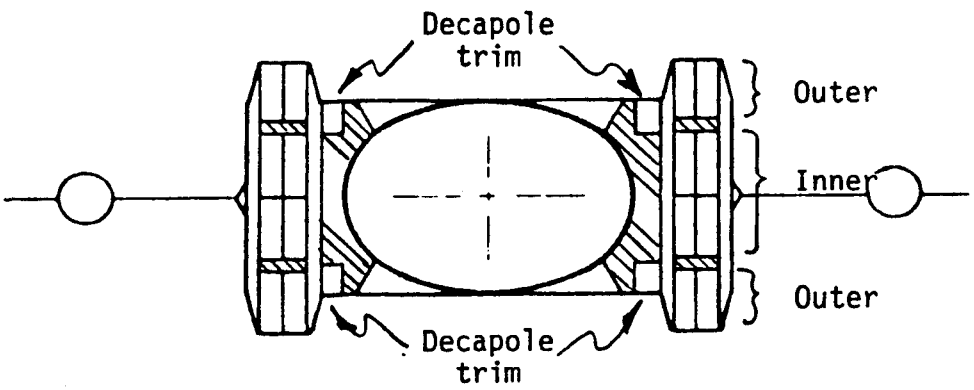

Fig. A7.2-1. Coil configuration and placement in the 3T magnet.

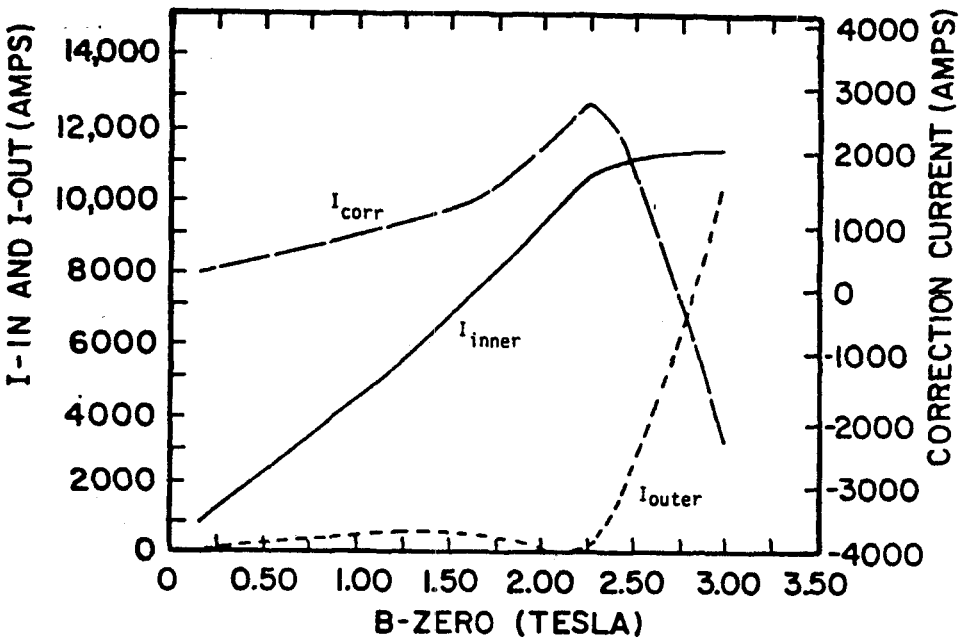

Fig. A7.2-2. I_{inner}, I_{outer}, and I_{corr} vs. magnetic field for the 3T magnet.

peak collider energy, and their current must track the dipole sum current to a few parts in 10^5.

Since the dipole magnets are in series with the quadrupole magnets in the 6T design, tracking in a sector occurs automatically except for saturation effects in the dipoles. In Reference Design A this saturation effect amounted to less than ten percent at the peak field. With the iron further away in the new Design D, the saturation should only be a few percent. It is thus possible, by increasing the strength of the correction quadrupoles, to eliminate the high current shunt around the quadrupoles, along with its additional wiring and power supply complexity.

A feature of magnet power supply systems which has often been overlooked (with painful consequences) is the transmission-line behavior of the magnet inductance and the shunt capacitance of the coil to ground. The cutoff frequency of such lines can be in excess of several tens of kHz. One of the problems in commissioning the SppS collider was a dramatic sensitivity to switching noise spikes from the power supply. These caused field spikes at the milligauss level which drove the first betatron resonance at 12 kHz. As

a transmission line, the SppS magnet has a cutoff at 50 kHz, so these noise spikes were being transmitted without attenuation by the magnet system. Installation of a low pass filter on the power supply output eliminated the spikes and improved the luminosity lifetime by 30%. A first pass analysis of transmission line effects in the SSC magnet types is given below. Propagation of signals by the line can be damped simply by including a shunt resistance across the magnets at each quench protection bypass diode. These resistors may pose a commissioning and operational difficulty when measuring coil leakage unless it is possible to disconnect them. Although it might be simpler to provide well-filtered power supplies, the shunt resistors are necessary to improve the transient response of the magnet circuit, and to assure the necessary current regulation during ramping.

A7.2.1 3T power supply system

As described in the introduction, the 3T design requires three separate high-current power supplies to assure an adequate field quality in the dipole magnets, as well as a separate high current power supply for the quadrupole magnets. Because the iron is not heavily saturated even at 3T, the three high-current circuits are tightly coupled. The self inductances per unit length of the inner (1), outer (2), and correction (3) coils are listed in Table A7.2-1 as a function of magnetic field.

Table A7.2-1

Coil inductances and coupling coefficients (3T)

Magnetic Field (Tesla)	Inner(1)	Outer(2)	Correction(3)
0.5	4.07	4.62	0.91
1.6	4.07	4.43	0.88
2.4	3.93	3.91	0.81
3.0	3.38	3.11	0.70

Coupling coefficients: K12 = 0.87 K13 = 0.813 K23 = 0.847

(Units are 10^{-5} Henrys/meter)

The tight coupling gives rise to a variety of effects during ramping and during transient events such as quenches. Preliminary indications are that the proposed 0.1 ohm dump resistors in the most recent 3T design must be reduced to 0.025 ohms to limit dI/dt to less than 3000 A s^{-1} in the outer coil, due to transformer coupling of the current decay in the correction coil. Lengthening the dump time will lead to larger temperature rises in the bypass diodes and their associated leads, and generally greater system stress. The tight coupling also means that the regulation loops will interact strongly, and, although at this time we see no fundamental difficulty with this coupling, it will certainly complicate the design and implies a delicate balancing of the loop time constants. During ramping, the voltage applied to either of the main coils divides roughly equally into charging the self inductance of the coil, and charging the mutual inductance between the coil being driven and the two other coils. The self inductance of the correction coil is small and its mutual inductance to the other coils is large. Combined with the larger dI/dt in the other coils, this results in requiring a four-quadrant power supply to provide the current. Figure A7.2-3 shows the current

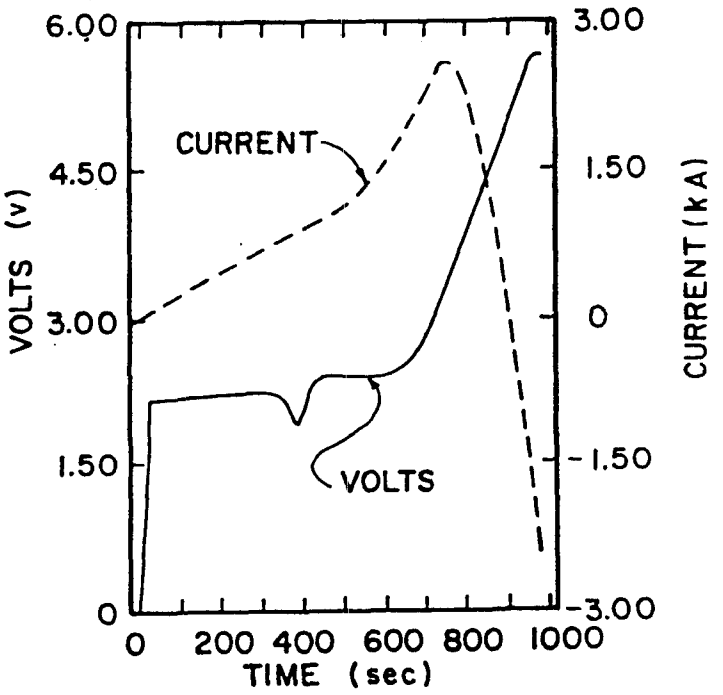

Fig. A7.2-3. Current and voltage for the 3T correction coil during ramping.

and voltage of the correction coil power supply, assuming a linear increase in the magnetic field during the ramp. A one-thousand second linear ramp is assumed. The circuit analysis program SPICE was used to calculate these data, as well as the current and voltage relationships during ramping for the other coils.

Clearly, a much more detailed analysis is required to make an accurate assessment of the likely performance of the 3T power supply system in view of the complexities disclosed by this brief study. It is certainly more complicated than the 6T supply system described in the next section.

A7.2.2 6T power supply system

The 6T magnet power supply system is simple in comparison to the one described above, since it consists of a single power supply per sector to provide the current for the series-connected dipoles and quadrupoles. As mentioned in the introduction, the present stainless-steel collared coil design for the 6T dipole magnet proposed for Design D probably places the iron far enough away from the coil to limit saturation effects to a few percent. Since the quadrupoles do not saturate, it may be possible to correct for the small dipole saturation by increasing the strength of quadrupole correction magnets, thereby eliminating the substantial current bypass shunts around the quadrupoles proposed in Reference Design A. Because of the placement of the quadrupoles in the lattice, the bus structure, as presently designed, to enable the current bypass is complex: The quads must be electrically connected at the ends of dipole strings, while they are physically distributed among the dipoles. The Design D magnet designers should be strongly encouraged to provide a design which eliminates the current bypasses. Assuming this simplification to be possible, the 6T design question reduces to that of overall current regulation of the ring due to tracking errors between the 12 sectors caused by differential current transductor errors, and lack of synchronism due to transmission line effects.

A7.2.3 Current regulation limits and transmission line effects

The ability of a power supply system of the SSC's scale to provide the current requested by the control system is limited by four main effects. The

transducer that measures the current flowing in the magnet bus has both an absolute error and a transient response error in its conversion of current to voltage. The regulation loop has finite gain, built-in offsets, and limited bandwidth. Control systems provide digital numbers, which after conversion to analog voltages are used as the inputs to error amplifiers in the regulation loops. Each compares the voltage representing the current in the magnet to the command value, and this conversion has a finite error. Finally, because of the scale of the SSC magnet structure, transmission line effects set a lower limit on the current tracking error in a sector during ramping. Because of the large inductance of the 6T magnet, this transmission line effect sets a lower limit of $dI/I > 1 \times 10^{-5}$. With the 3T design, the limit is roughly one half this value. In addition to the above effects, the 3T design has errors induced through transformer coupling, which may in fact set the higher limit on the minimum current error. The analysis of this feature is just beginning, and will be a major part of the work carried out by this group during the next several weeks. The basic regulation loop being analyzed is illustrated in Fig. A7.2-4.

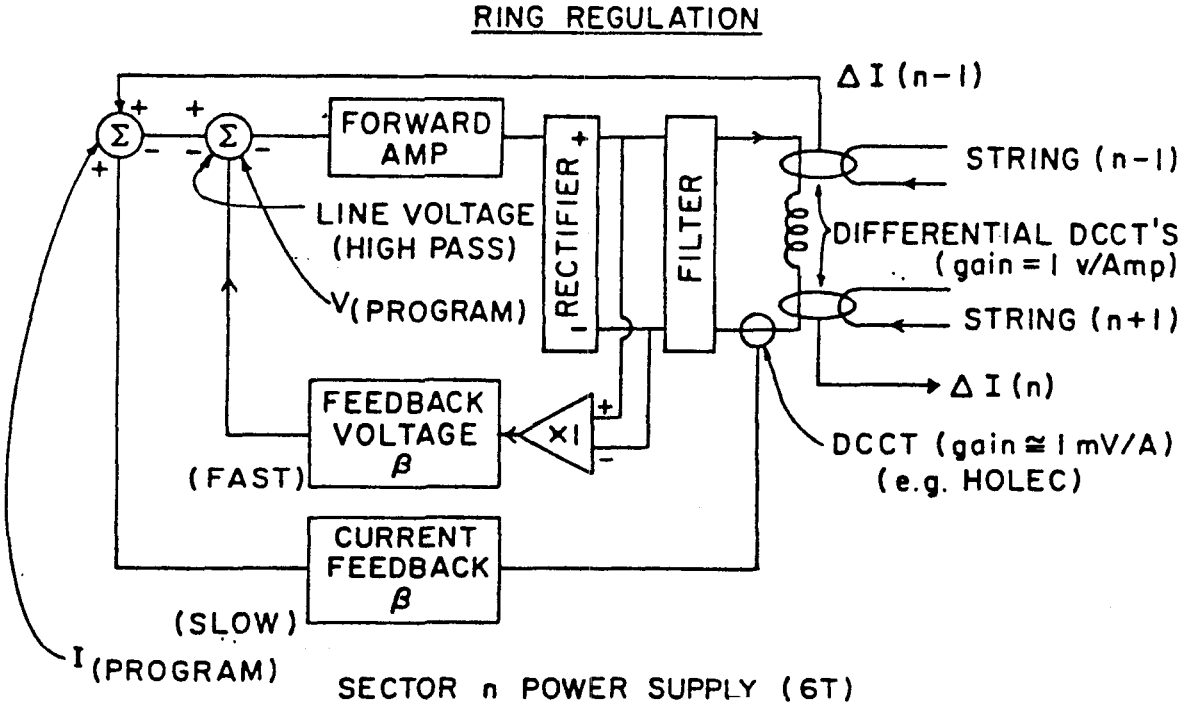

Fig. A7.2-4. Prototype regulation loop for SSC magnet power supply.

To analyze the transient response of the magnet system, the circuit analysis program SPICE has been used with input parameters of inductance and capacitance to ground as measured on the 8-meter prototype 3T magnet, and with measurements of inductance and scaled estimates of capacitance to ground for the 6T magnet. Figure A7.2-5 shows a typical equivalent circuit representing the magnet. That transmission line effects are important is dramatically illustrated in Fig. A7.2-6, which shows the magnet response to a voltage step at the power supply as a function of distance from the power supply.

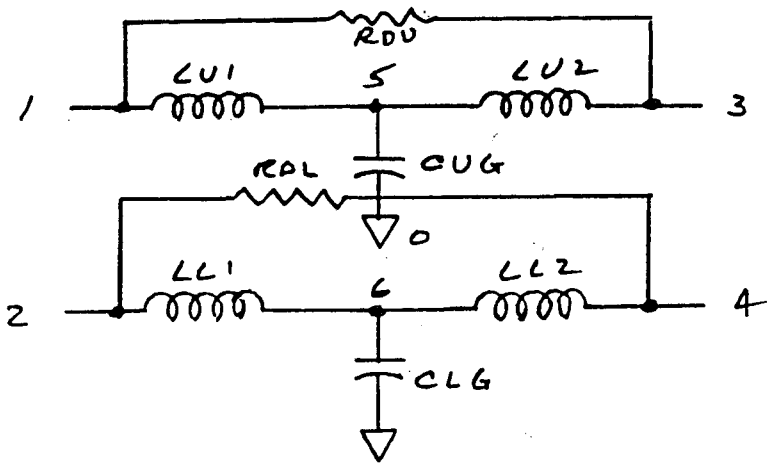

Fig. A7.2-5. Lumped constant equivalent circuit for SSC 6T Magnet.

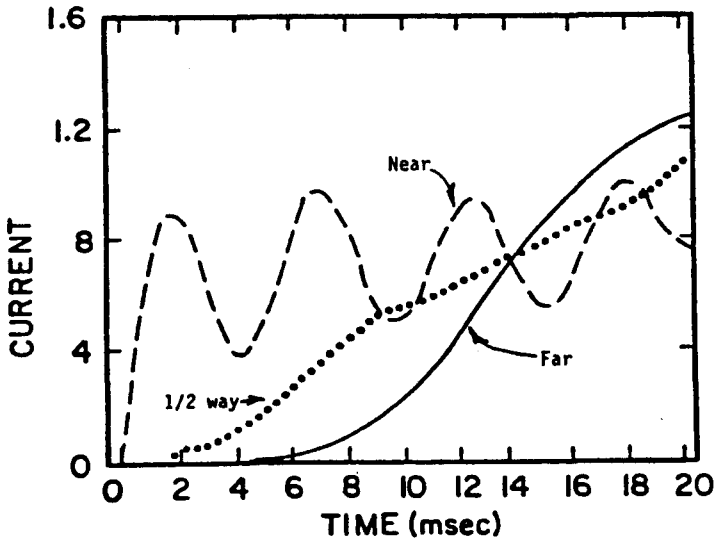

Fig. A7.2-6. Transient Response of 6T magnet to power supply voltage step.

With these features, what are the likely performance levels of the two different magnet power supply systems? The preliminary indications are that sensing the currents and providing the digital to analog command voltages are straightforward at the 10^{-5} level in each sector. Using high gain differential transductors and taking proper account of the delay line characteristics of the magnet, it appears feasible to link the individual power supply loops around the ring to achieve the required overall part in 10^5 average tracking tolerance for the 6T design. Further detailed analysis is required before the same statement can be made about the coupled 3T design. This analysis is presently under way, and, as mentioned above, a separate technical report will be issued in the near future.

As with any superconducting magnet system, the power dissipation in the magnet power supply system for the SSC occurs entirely in the room-temperature components during steady state operation. This power dissipation is dominated by the voltage drop in the necessary series filter inductance, and is typically 10 volts for a 150 microHenry 12 kA inductor. A well-designed lead system from the power supply to the magnet will have a total voltage drop of 2 volts. In addition, there is a 2-volt drop in the series switches shunting the dump resistors necessary for the quench protection system. This gives a total voltage drop of 14 volts for each power supply circuit. The total power requirement is then given simply by multiplying this 14 volt drop by the total current in each circuit and doing the sum over the circuits. Table A7.2-2 summarizes the total power requirements for the 3T and 6T designs. Since the load is resistive in steady state operation, the AC power is only slightly larger than the DC power. For DC power supplies in these current ranges, the efficiency is > 90%, taken as 100% in making Table A7.2-2. As can be seen from the Table, the 3T magnet requires an additional 4 MW of DC power to operate at 20 TeV as presently designed. This means a significantly increased operating cost. In finally designing the power supply system for the SSC, careful attention must be paid to the voltage drops in the room-temperature components to minimize such operating costs.

Table A7.2-2

AC power requirements for 3T and 6T power supplies.

Magnet	Current (kA)			DC Power (MW)
6T	I(dipole + quad)	= 5.6		1.88
3T	I(inner)	= 11.0	12.0*	4.03
	I(outer)	= 10.0		
	I(corr.)	= 2.5		0.84
	I(quad)	= 3.0		1.01
			Total	5.88

*The circuits are configured so that only one of the power supplies provides the net current at full field.

A7.2.5 Conclusions

The power supply system for the 3T design is more complex because of the two high-current and two moderate-current circuits necessary to provide the required guide-field quality. Transformer coupling of these circuits complicates the regulation loop design and dictates using smaller dump resistors to limit dI/dt during a quench in order to prevent secondary quenches in the coupled circuits. The smaller dump resistors imply a larger temperature rise in the current bypass components, and a generally higher system stress. A four-quadrant 3 kA-output power supply presents a difficult design task, and has potential reliability problems as compared to a conventional DC supply. The operating cost of the 3T power-supply system is significantly higher than the 6T system. Because of the simplicity of the single-circuit design, combined with its lower operating current, the 6T design is preferred from an operational and commissioning point of view.

APPENDIX J

ACSL STUDY OF MUTUALLY COUPLED LOOP REGULATION FOR TAC SSC DESIGN

G. TOOL & O. CALVO

Appendix J

July 5, 1985
G. Tool
O. Calvo

ACSL Study of Mutually Coupled Loop Regulation for TAC SSC Design

(Preliminary Results)

Attached are graphs from the ACSL program showing the regulation effects on each of the 3 inductively coupled circuits in the TAC SSC magnet design due to a voltage program perturbation in one of the circuits. A block diagram of the model used is shown in Figure 1, also attached. A special model having only 2 coupled circuits, shown in Figure 2 was used to simplify the demonstration of the possibility of compensating for the effect of the coupling by added networks.

GENERAL:

1. The current in each of the loops is zero, so the change due to the perturbation can be easily recognized.

2. An uncoupled reference circuit (subscript D in the graph axis labels) was included to show the difference between a loop identical to the Inner coil loop having no coupling and the actual one with coupling (subscript A in the axis labels.)

3. A unit voltage program step was used as the perturbation, resulting in displayed power supply output voltage and loop current changes. Other disturbances such as power supply output voltage steps could just as well be studied.

4. The point labels on the graph curves (i.e., A, B, etc) are placed in an order determined by the left to right order of the ordinate axis display, and do not typically correspond to similar A, B, etc subscripts used in the block diagram symbols such as EOFA.

5. Considerable effort went into understanding the power supply and load transfer functions and gain values in order to adequately demonstrate the effects of the mutual coupling in a "reasonable" regulator system, but no emphasis was placed on optimizing a regulator design. The model is similar to power supply characteristics achieved in the Energy Saver.

6. The current error in the loop into which the voltage program step is introduced becomes a steady state current error due to the finite regulator gain. The error in each of the coupled loops is a transient for some length of time, dying out to zero after the regulator for that loop responds.

Six different cases are represented in the attached graphs. Initial work was done with a sector configuration based on 1/12 of the accelerator, with nominal inductance values used in other studies in early April, 1985. The last cases have been run using presently understood inductance and coupling coefficient values and a configuration based on a power supply sector encompassing 1/4 of the total accelerator as described in John Ziegler's 6/19/85 note titled "DIPOLE POWER SUPPLY SYSTEM". The cases are numbered and described as follows:

I. Initial 1/12 ring with a voltage step at Inner coil power supply.

II. Initial 1/12 ring with a voltage step at Trim coil power supply.

III. Initial 1/12 ring, Inner & Outer only shown as reference case without any "compensation."

IV. Initial 1/12 ring, Inner & Outer only shown with a "compensation" network added to cancel effect of the coupling.

V. Current 1/4 ring, unit voltage step at Inner coil power supply.

VI. Current 1/4 ring, unit voltage step at Trim coil power supply.

SPECIFIC CASES:

I. Refer to Figure 1. Step in Inner loop. Graph I.3 shows difference between current error in an isolated loop and one coupled to the other two loops.

II. Refer to Figure 1. Step in Trim loop. In graph II.1, ignore the curve (points labeled "A") for the isolated circuit.

III. Refer to Figure 2. Reference case with no compensation circuit. Graph III.1 is plotted on a scale for direct comparison with next case.

IV. Refer to Figure 2. Note in graph IV.1 that power supply output voltage in both loops is considerably larger than in III.1; this is the price of the compensation function. Graph IV.3 clearly shows the possiblility of a much reduced effect in the loop which did not have the original disturbance. The size of the reduction would be limited in a real system by the degree to which one understands the circuit parameters and to which one can realize the compensation transfer function. Graph IV.4 is a magnified view of the coupled disturbance.

Units on graphs are volts, amps, and seconds.

V. Refer to Figure 1, but the currently understood circuit inductances and coupling coefficients are used along with a load that represents 1/4 of the accelerator and the specified circuit resistances contained in the above mentioned report from John Zeigler. Step in Inner coil circuit as in initial case I.

VI. Refer to Figure 1, but as in V above. Step in Trim coil circuit as in initial case II.

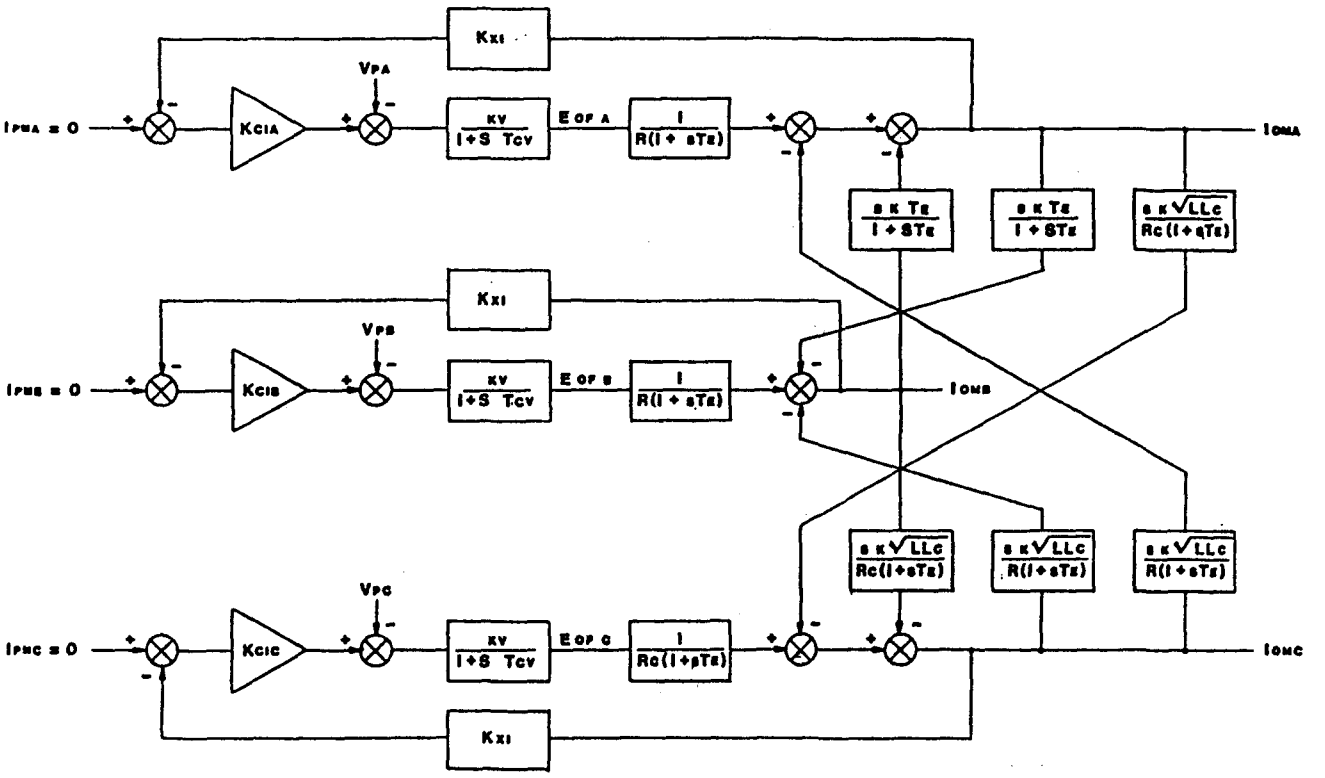

Fig. 1. Regulator Loops for 3T Magnet Power Supply

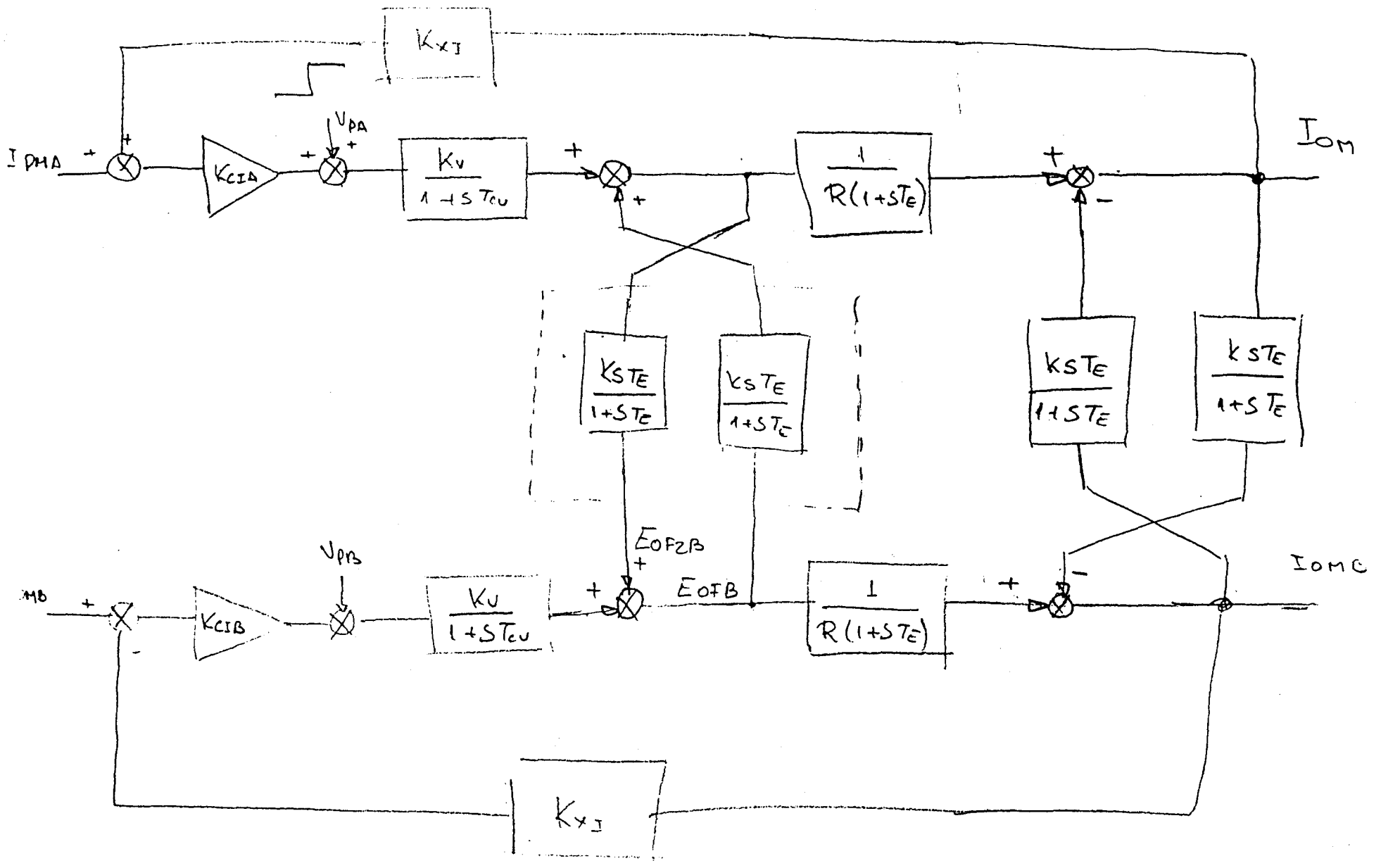

Fig. 2 - 2 coupled circuits with compensation

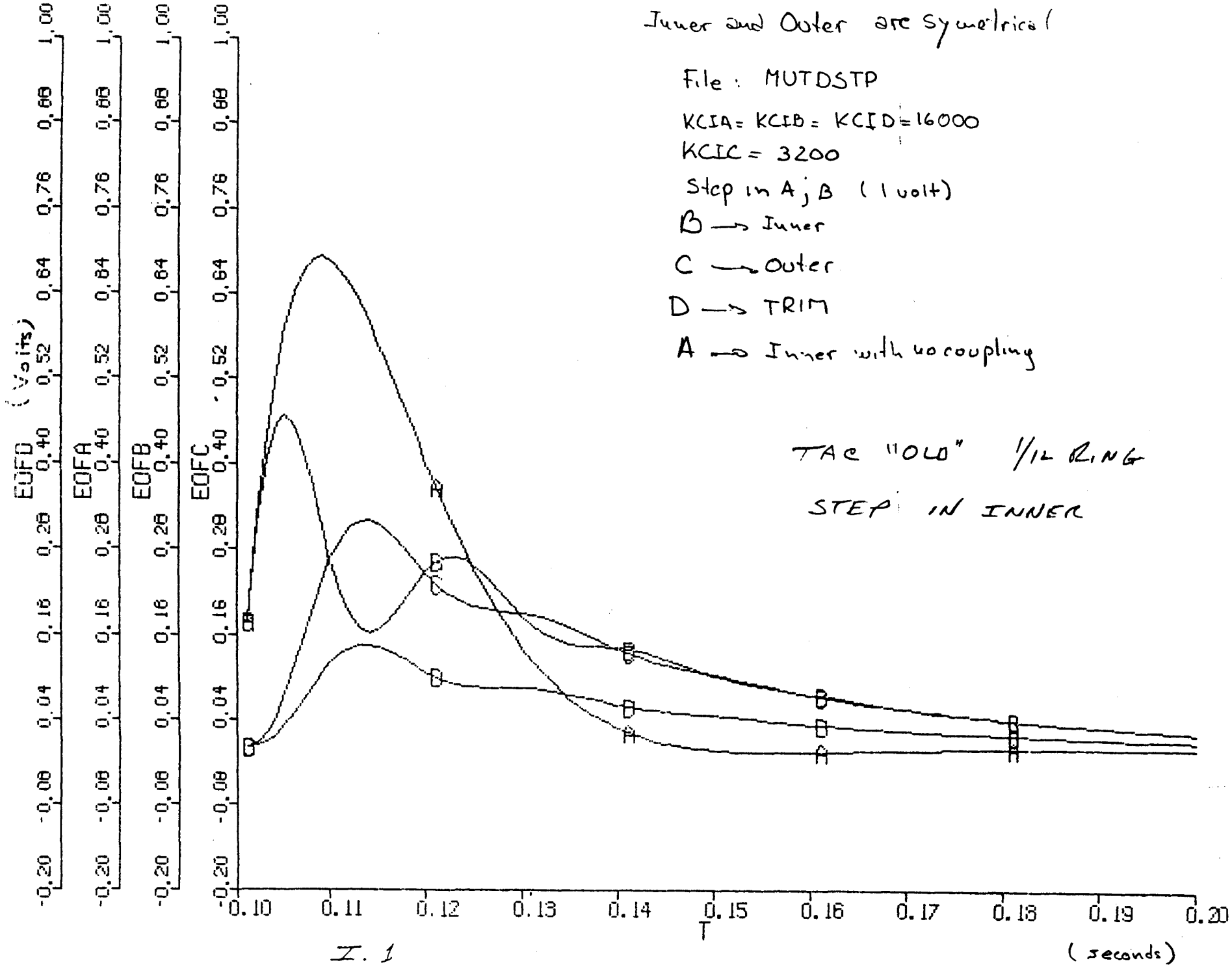
Inner and Outer are symetrical
File : MUTDSTP
KCIA = KCIB = KCID = 16000
KCIC = 3200
Step in A ; B (1 volt)
B → Inner
C → Outer
D → TRIM
A → Inner with no coupling
TAC "OLD" 1/12 RING
STEP IN INNER
EOFD
EOFA
EOFB
EOFC
(Volts)
T
(seconds)

I. 1

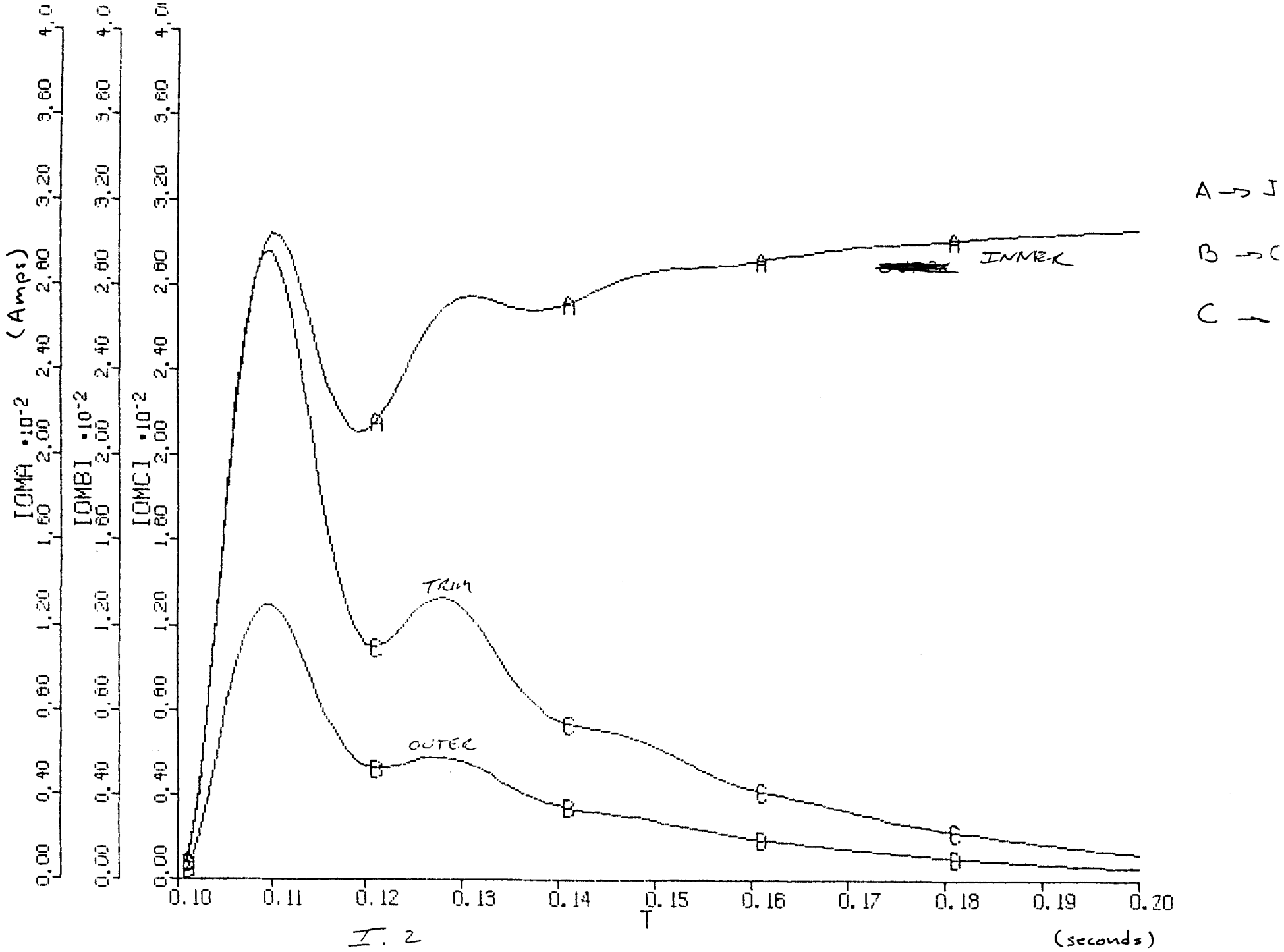
IOMA ·10^-2 (Amps)
IOMBI ·10^-2
IOMCI ·10^-2
0.00
0.40
0.80
1.20
1.60
2.00
2.40
2.80
3.20
3.60
4.0
0.10
0.11
0.12
0.13
0.14
0.15
0.16
0.17
0.18
0.19
0.20
T
(seconds)
INNER
TRIM
OUTER
A → J
B → C
C →

I. 2

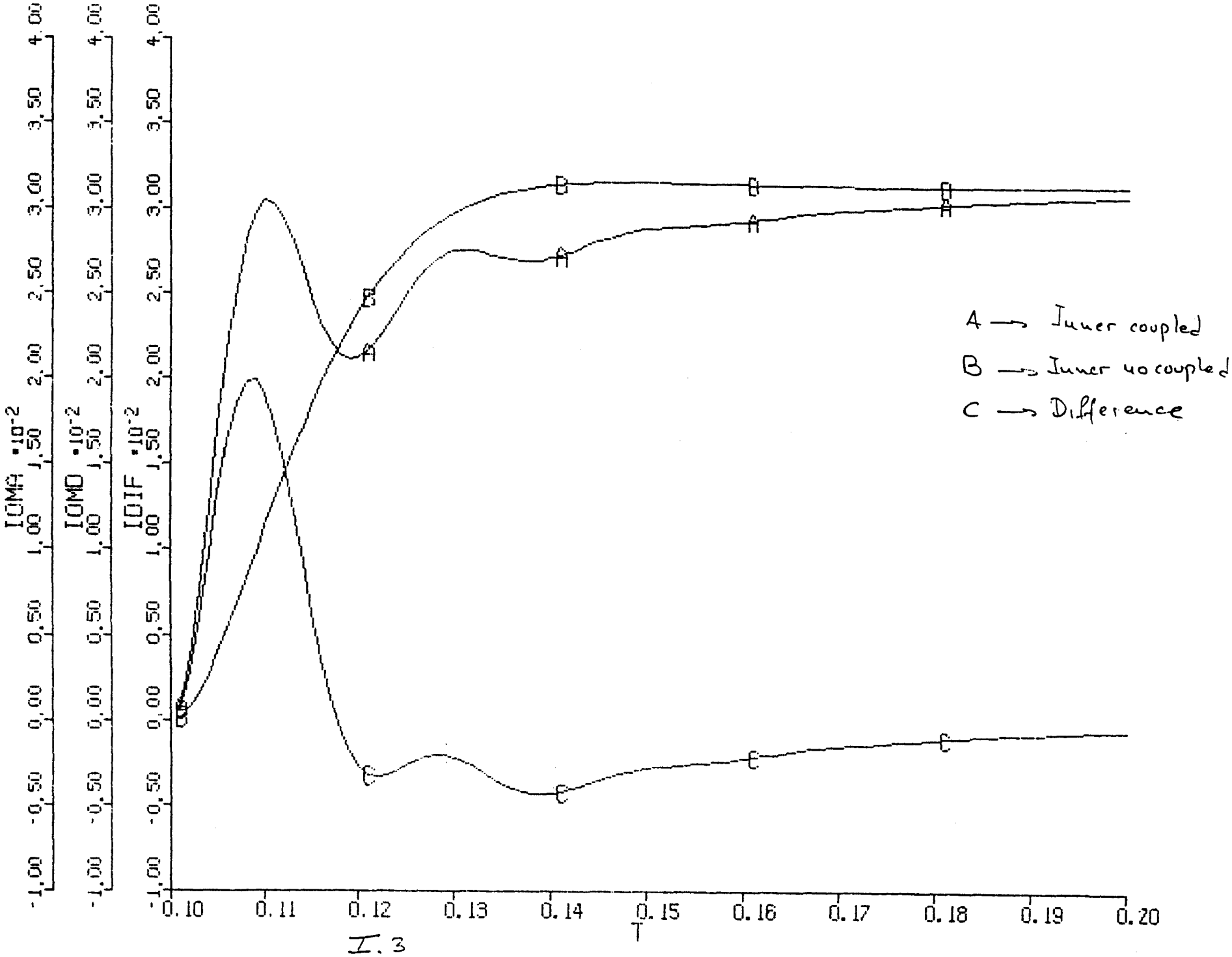
IOMA ·10^-2
IOMD ·10^-2
IOIF ·10^-2
-1.00
-0.50
0.00
0.50
1.00
1.50
2.00
2.50
3.00
3.50
4.00
0.10
0.11
0.12
0.13
0.14
0.15
0.16
0.17
0.18
0.19
0.20
T
A → Inner coupled
B → Inner no coupled
C → Difference

I.3

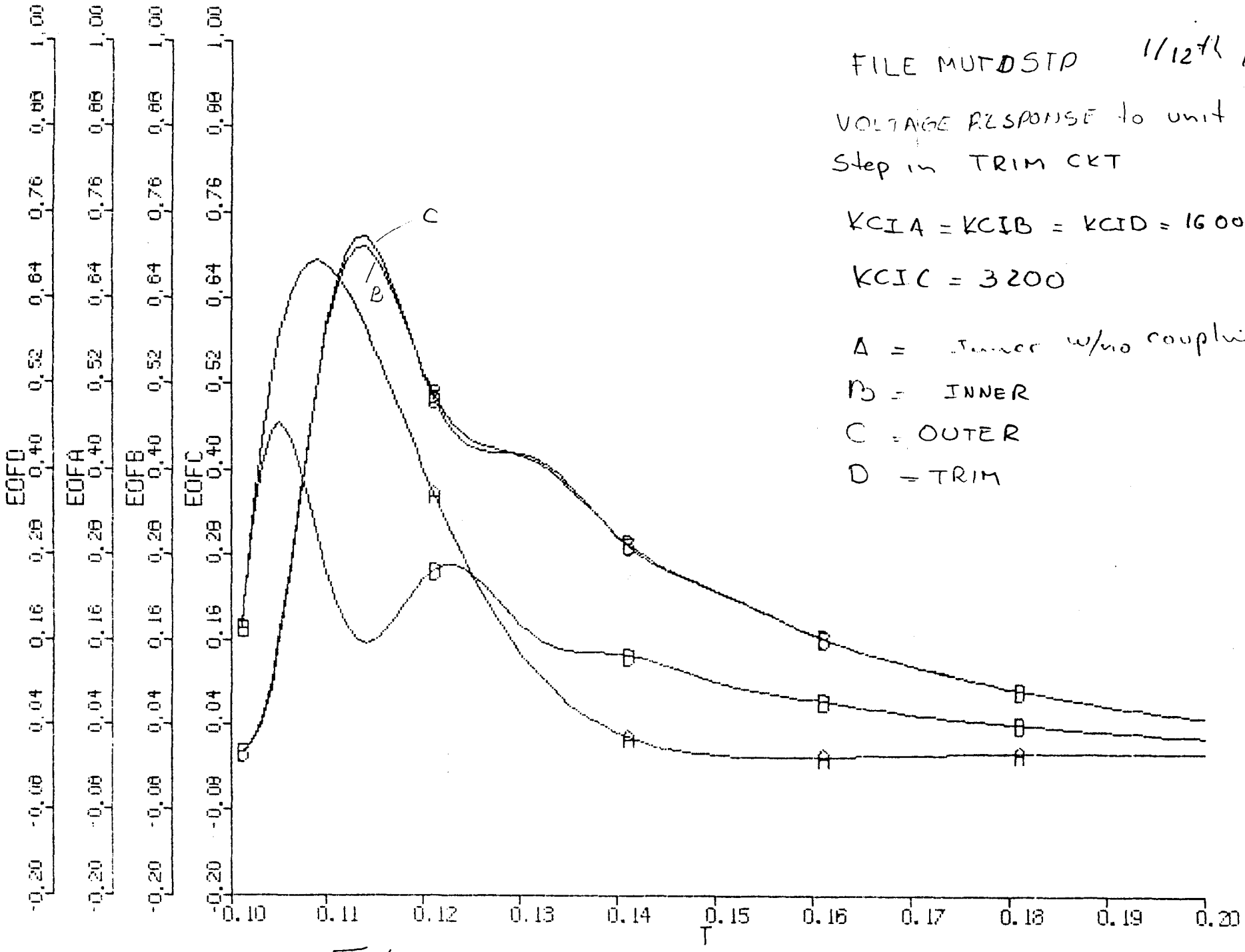
FILE MUTDSTP 1/12th min
VOLTAGE RESPONSE to unit
Step in TRIM CKT
KCIA = KCIB = KCID = 16000
KCIC = 3200
A = Inner w/no coupling
B = INNER
C = OUTER
D = TRIM
EOFD
EOFA
EOFB
EOFC
T
C
B
A
D

II.1

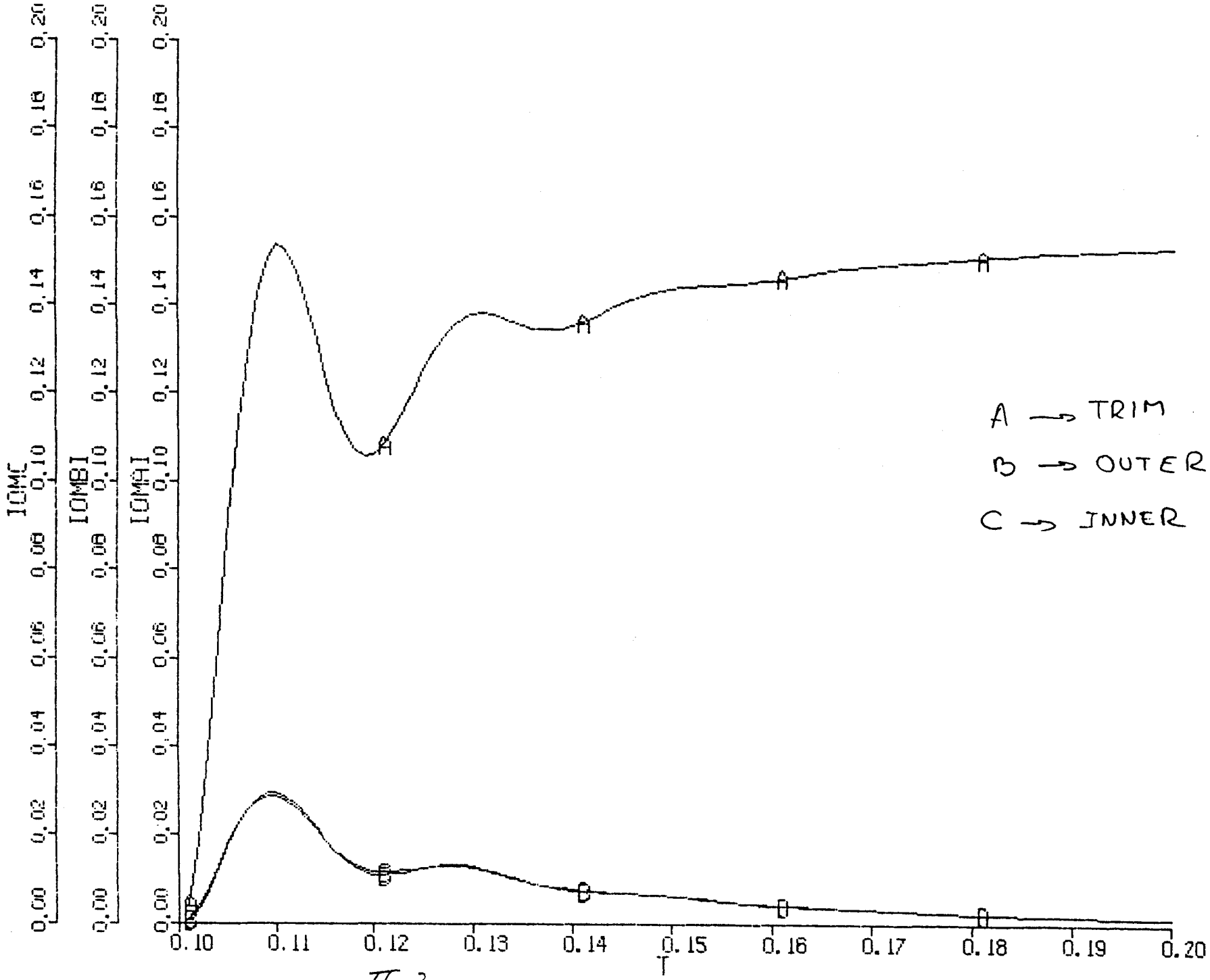
IOMC
IOMBI
IOMAI
0.00
0.02
0.04
0.06
0.08
0.10
0.12
0.14
0.16
0.18
0.20
0.10
0.11
0.12
0.13
0.14
0.15
0.16
0.17
0.18
0.19
0.20
T
A → TRIM
B → OUTER
C → INNER

II. 2

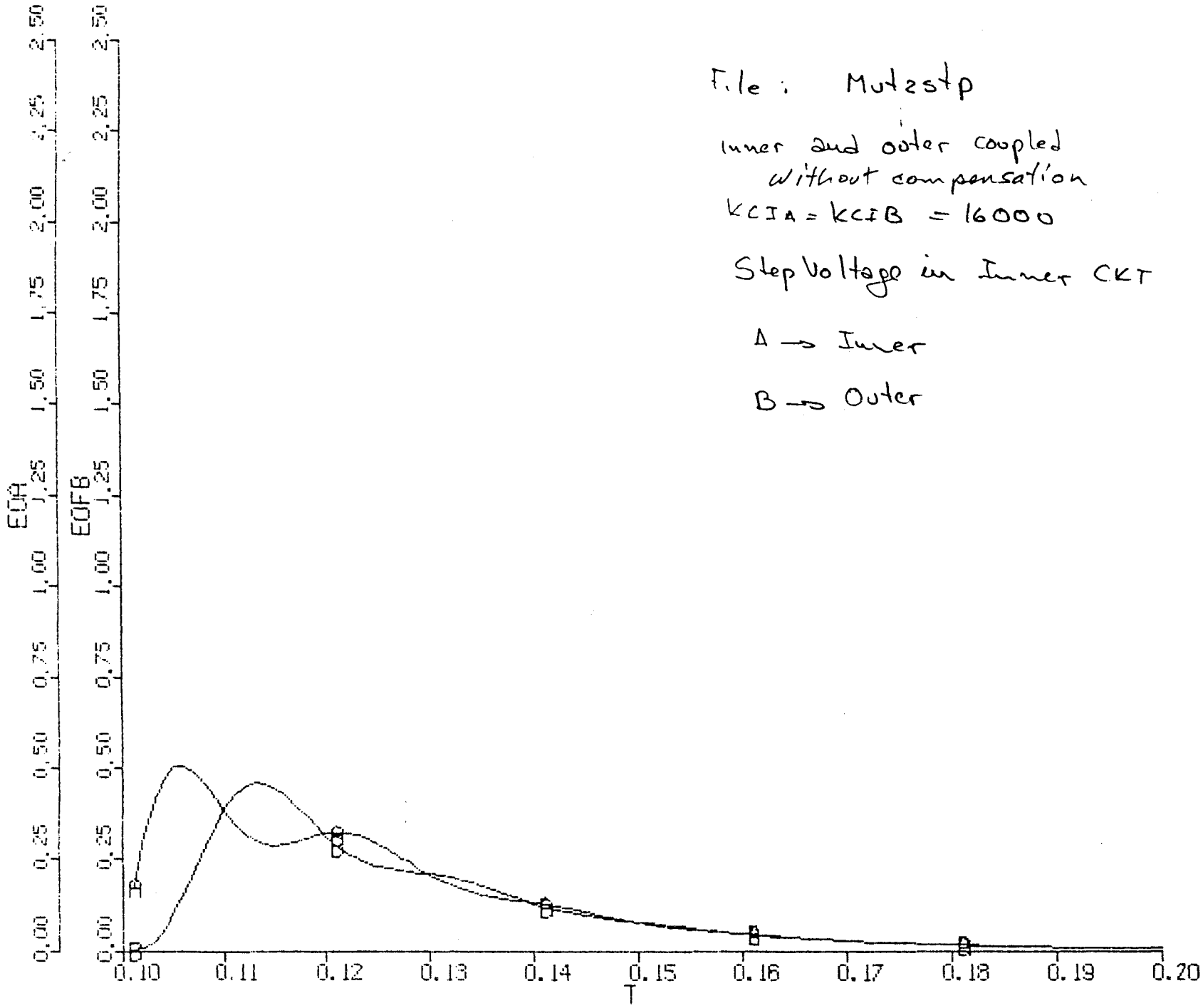
File : Mutestp
inner and outer coupled
without compensation
KCIA = KCIB = 16000
Step Voltage in Inner CKT
A → Inner
B → Outer
EOA
EOFB
0.00
0.25
0.50
0.75
1.00
1.25
1.50
1.75
2.00
2.25
2.50
0.10
0.11
0.12
0.13
0.14
0.15
0.16
0.17
0.18
0.19
0.20
T

III. 1

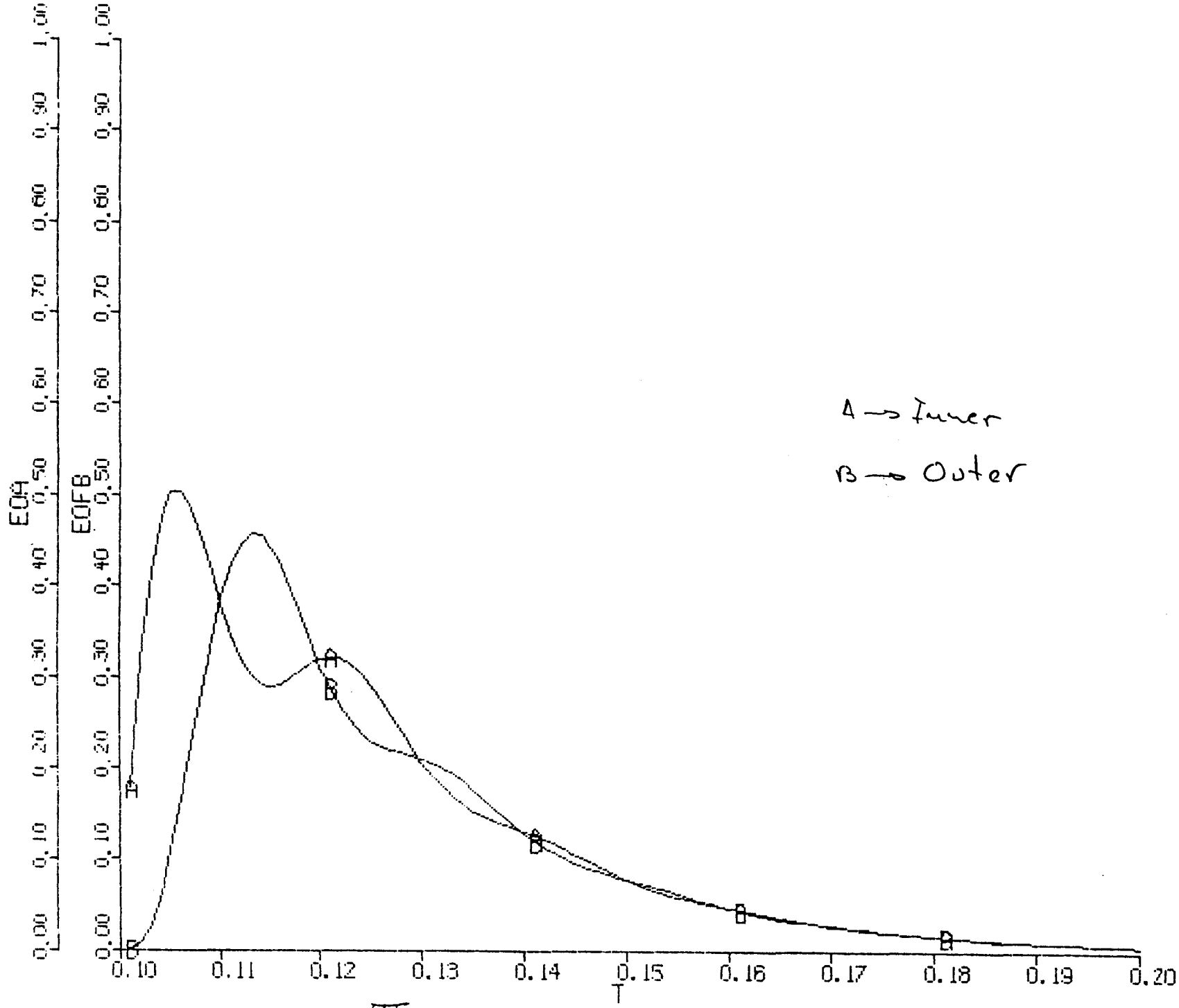
EOA
EOFB
0.00
0.10
0.20
0.30
0.40
0.50
0.60
0.70
0.80
0.90
1.00
0.10
0.11
0.12
0.13
0.14
0.15
0.16
0.17
0.18
0.19
0.20
T
A → Inner
B → Outer

III. 2

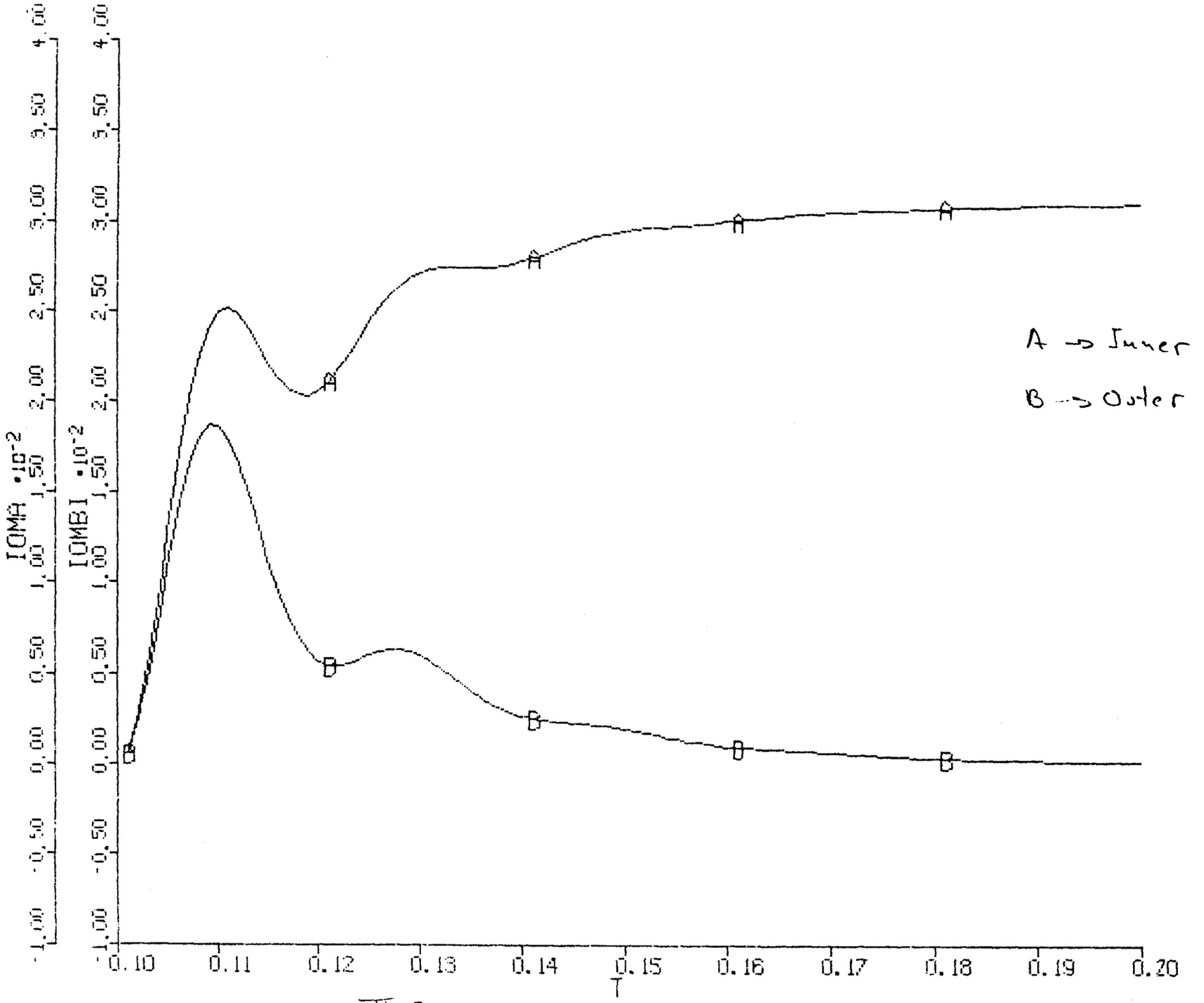
IOMA •10^-2
IOMBI •10^-2
-1.00
-0.50
0.00
0.50
1.00
1.50
2.00
2.50
3.00
3.50
4.00
0.10
0.11
0.12
0.13
0.14
0.15
0.16
0.17
0.18
0.19
0.20
T
A → Inner
B → Outer

III . 3

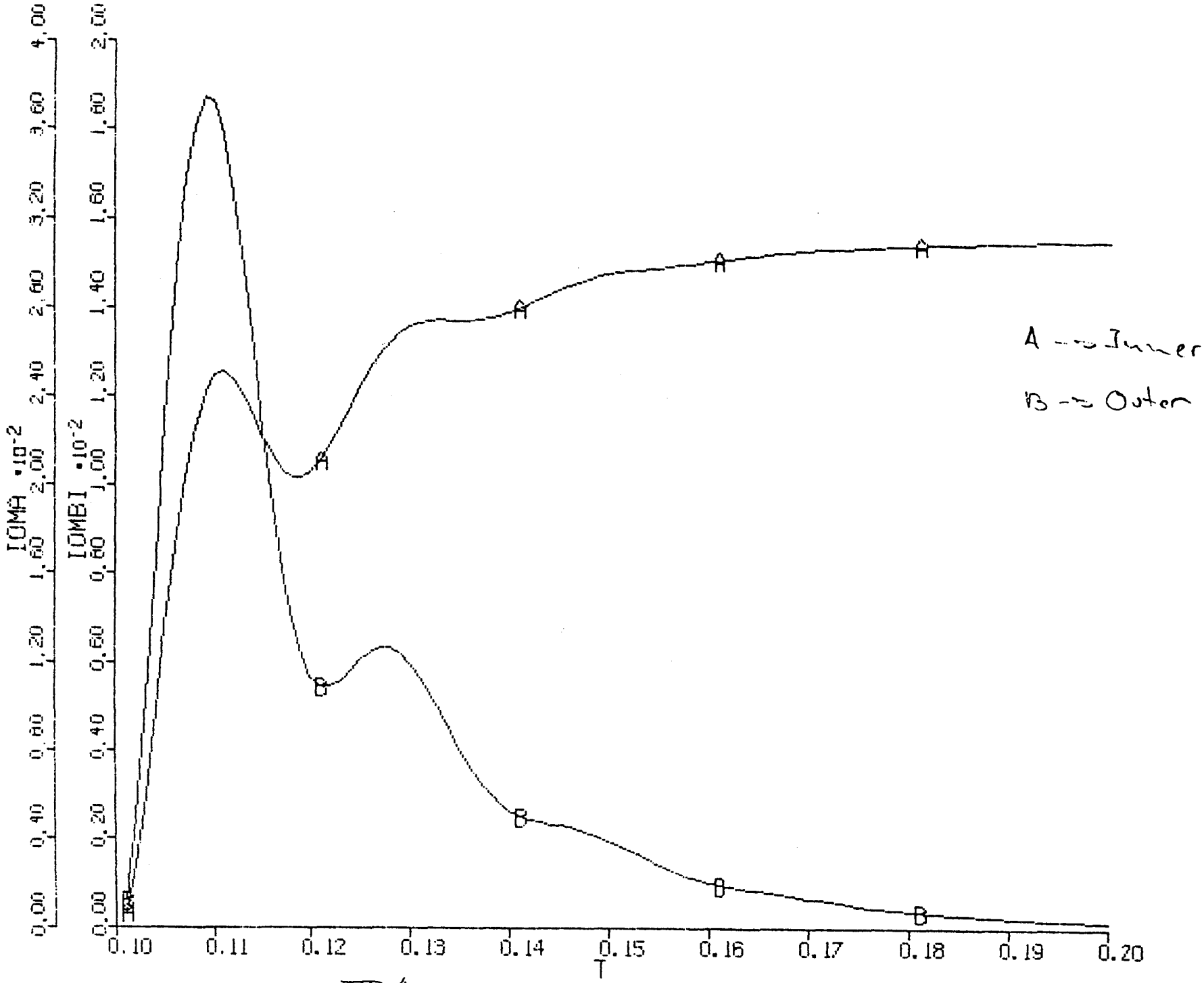
IOMA ·10^-2
IOMBI ·10^-2
0.00
0.40
0.80
1.20
1.60
2.00
2.40
2.80
3.20
3.60
4.00
0.00
0.20
0.40
0.60
0.80
1.00
1.20
1.40
1.60
1.80
2.00
0.10
0.11
0.12
0.13
0.14
0.15
0.16
0.17
0.18
0.19
0.20
T
A → Inner
B → Outer

Fig. 4

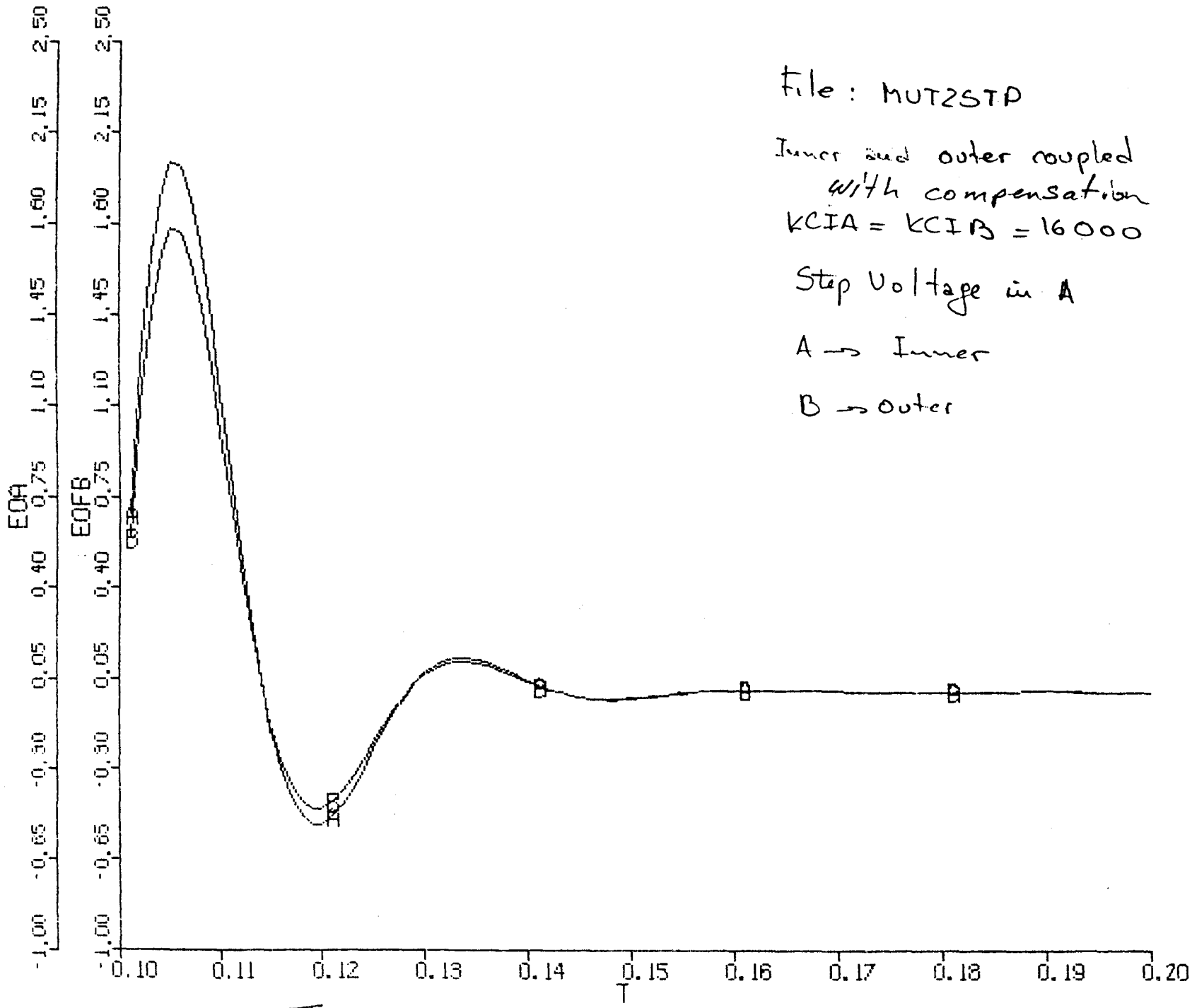

File : MUT2STP

Inner and outer coupled with compensation

KCIA = KCIB = 16000

Step Voltage in A

A → Inner

B → Outer

IV. 1

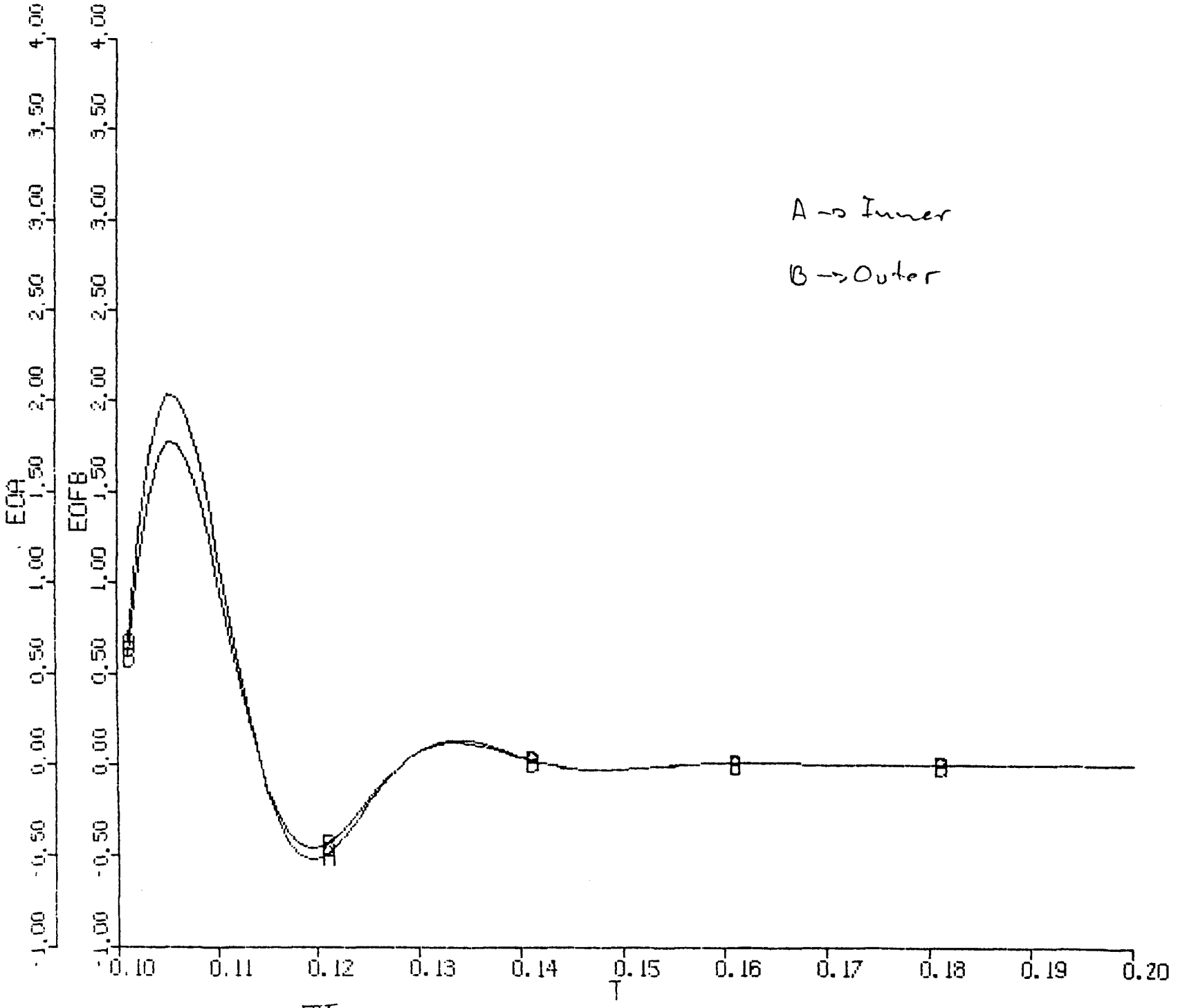
A -> Inner
B -> Outer
EOA
EOFB
T
-1.00
-0.50
0.00
0.50
1.00
1.50
2.00
2.50
3.00
3.50
4.00
0.10
0.11
0.12
0.13
0.14
0.15
0.16
0.17
0.18
0.19
0.20

IV. 2

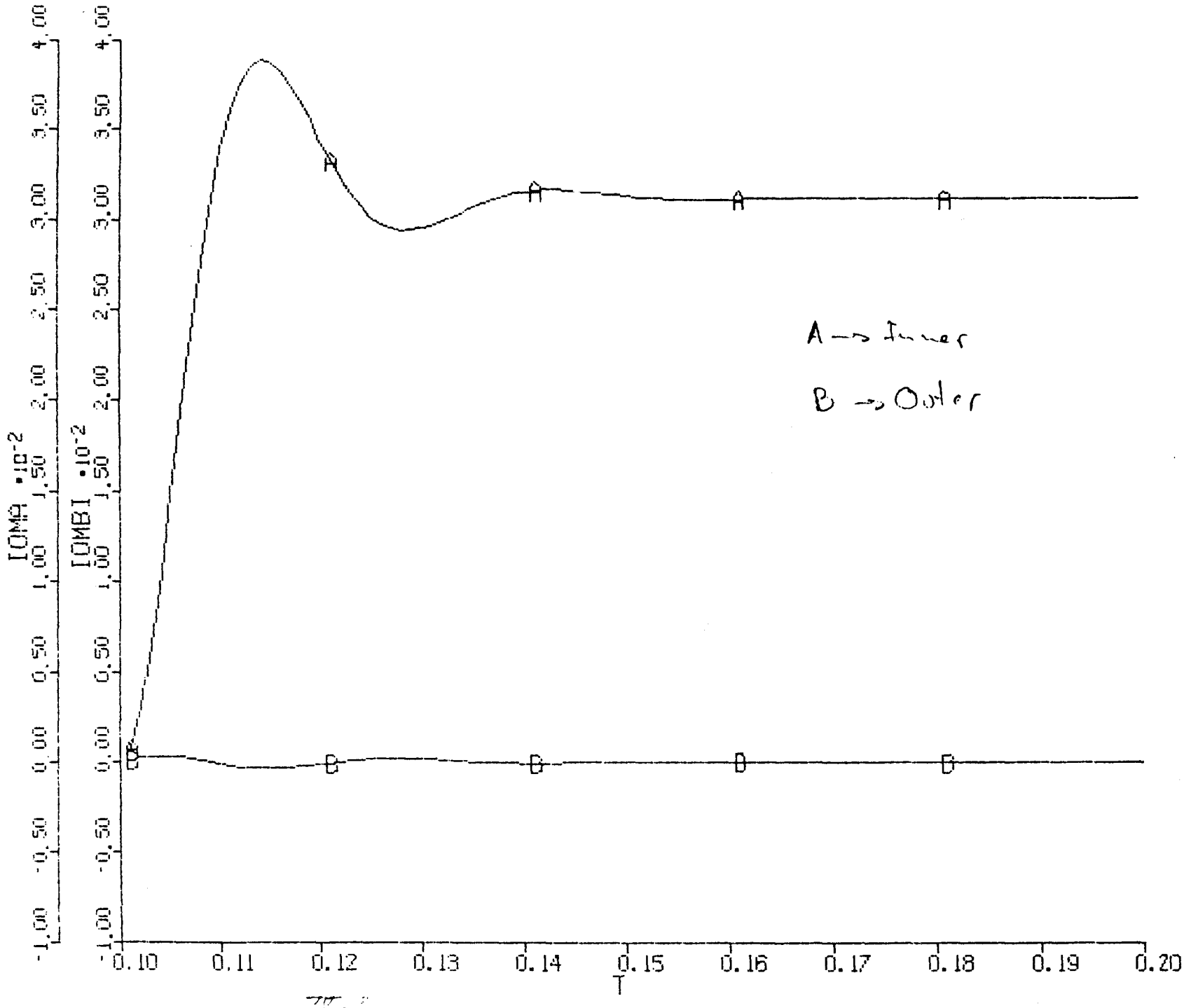
IOMA ·10^-2
IOMBI ·10^-2
4.00
3.50
3.00
2.50
2.00
1.50
1.00
0.50
0.00
-0.50
-1.00
0.10
0.11
0.12
0.13
0.14
0.15
0.16
0.17
0.18
0.19
0.20
T
A → Inner
B → Outer

FIG. 2

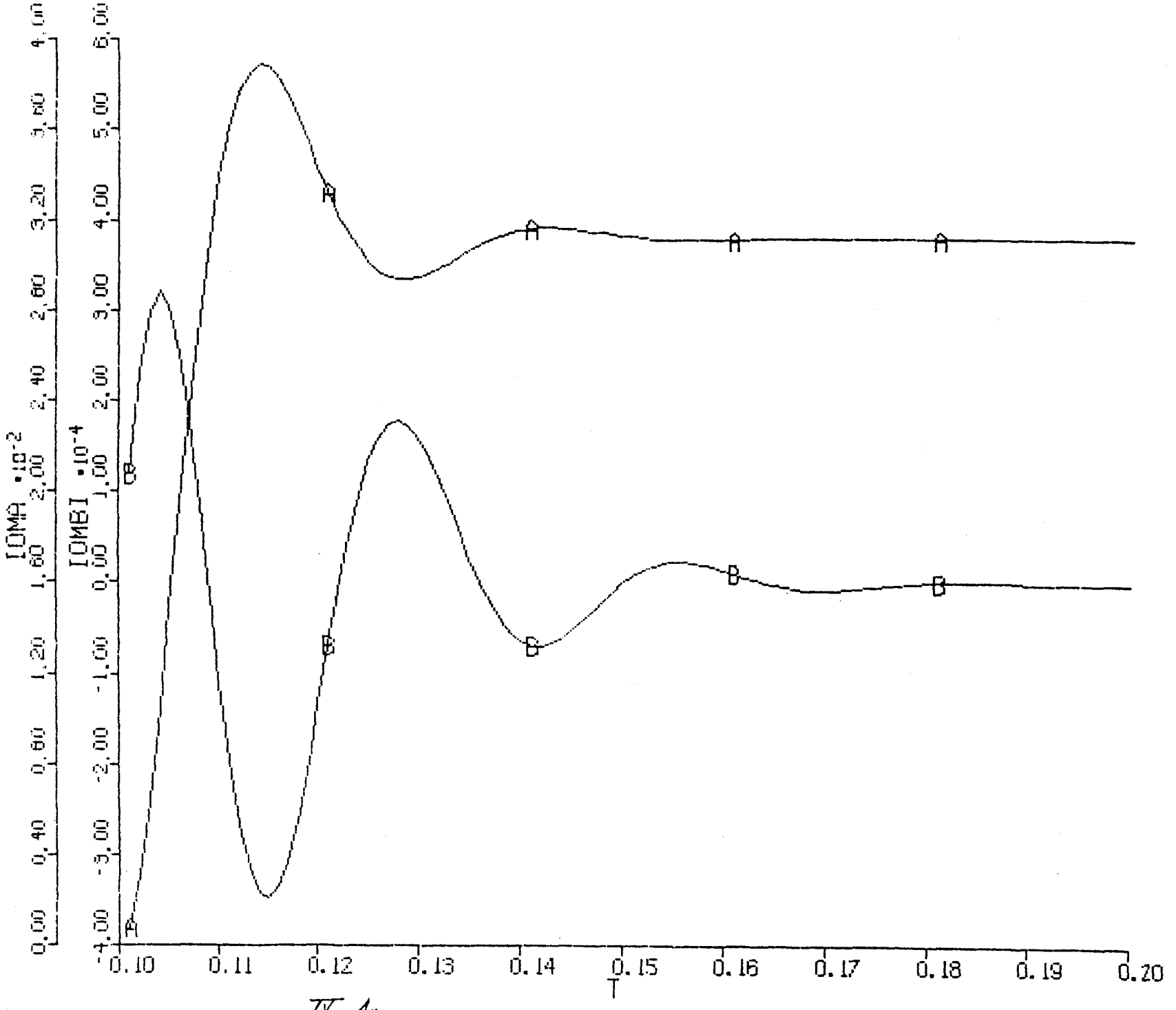
IOMA ·10^-2
IOMBI ·10^-4
0.00
0.40
0.80
1.20
1.60
2.00
2.40
2.80
3.20
3.60
4.00
-4.00
-3.00
-2.00
-1.00
0.00
1.00
2.00
3.00
4.00
5.00
6.00
0.10
0.11
0.12
0.13
0.14
0.15
0.16
0.17
0.18
0.19
0.20
T

IV. 4

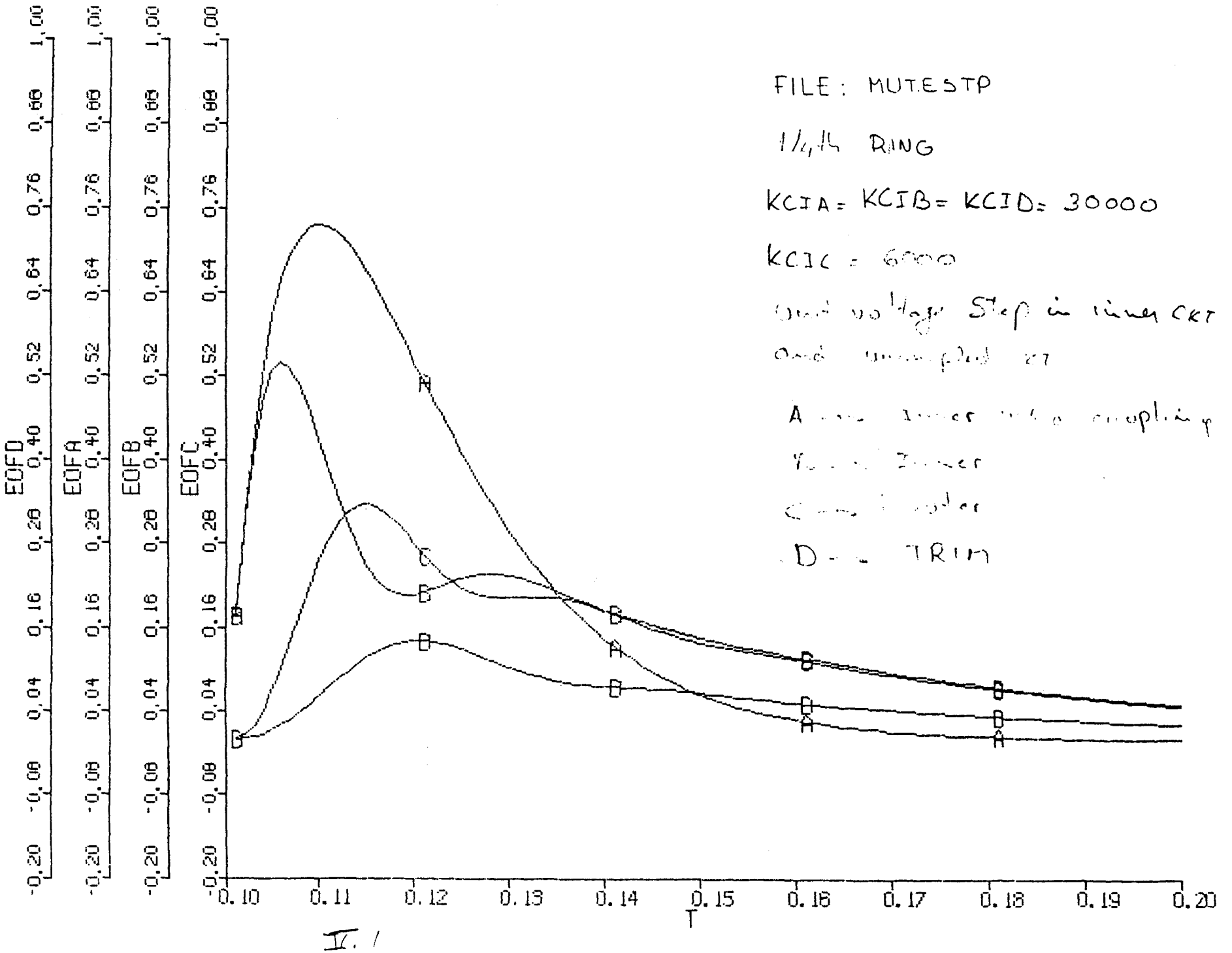
FILE: MUTESTP
1/4th RING
KCIA = KCIB = KCID = 30000
KCIC = 6000
and voltage Step in inner CKT
and unamplified
A
D - TRIM
EOFD
EOFA
EOFB
EOFC
-0.20
-0.08
0.04
0.16
0.28
0.40
0.52
0.64
0.76
0.88
1.00
0.10
0.11
0.12
0.13
0.14
0.15
0.16
0.17
0.18
0.19
0.20
T

V. 1

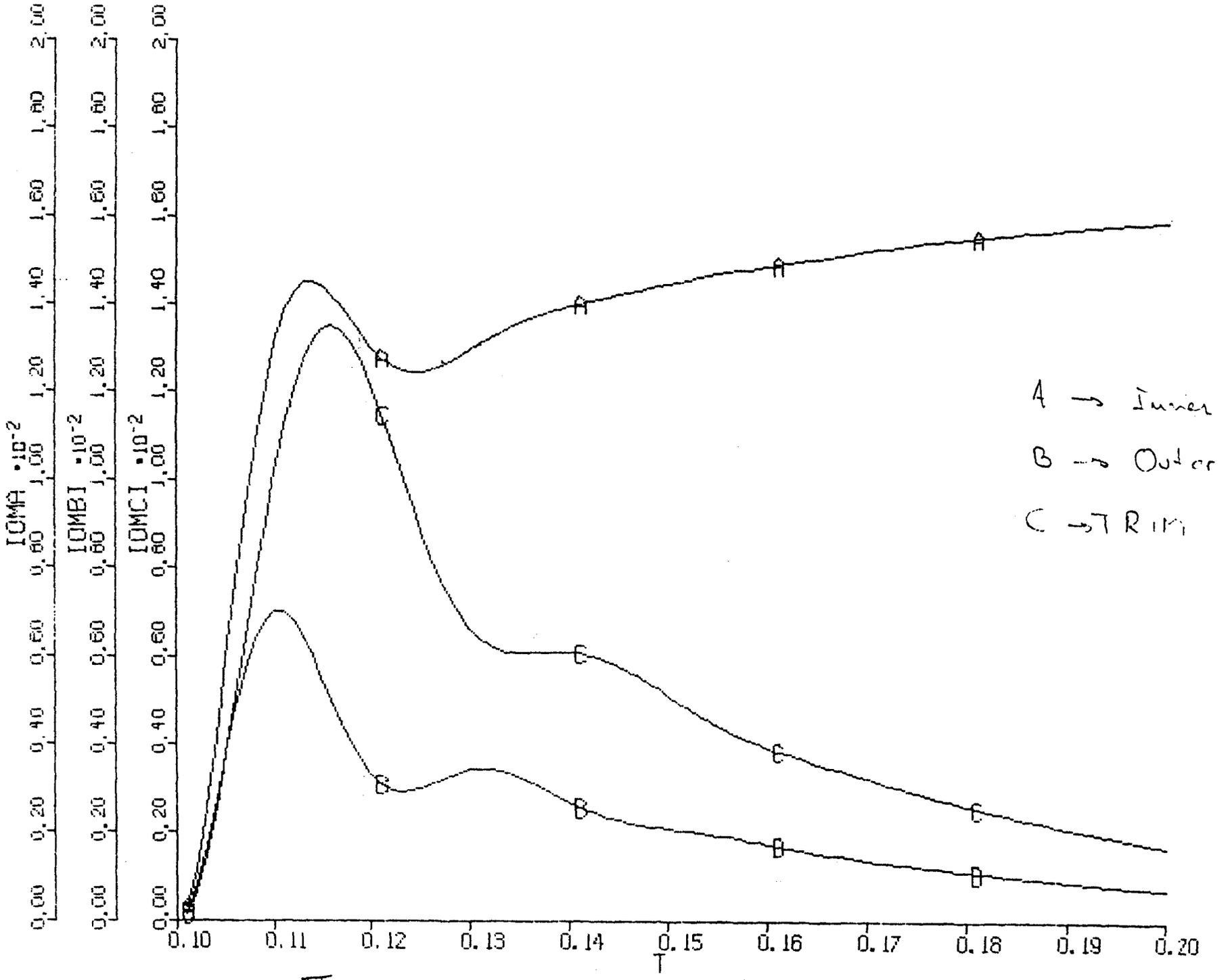
IOMA ·10⁻²
IOMBI ·10⁻²
IOMCI ·10⁻²
0.00
0.20
0.40
0.60
1.00
1.20
1.40
1.60
1.80
2.00
0.10
0.11
0.12
0.13
0.14
0.15
0.16
0.17
0.18
0.19
0.20
T
A → Inner
B → Outer
C → Rim

V.2

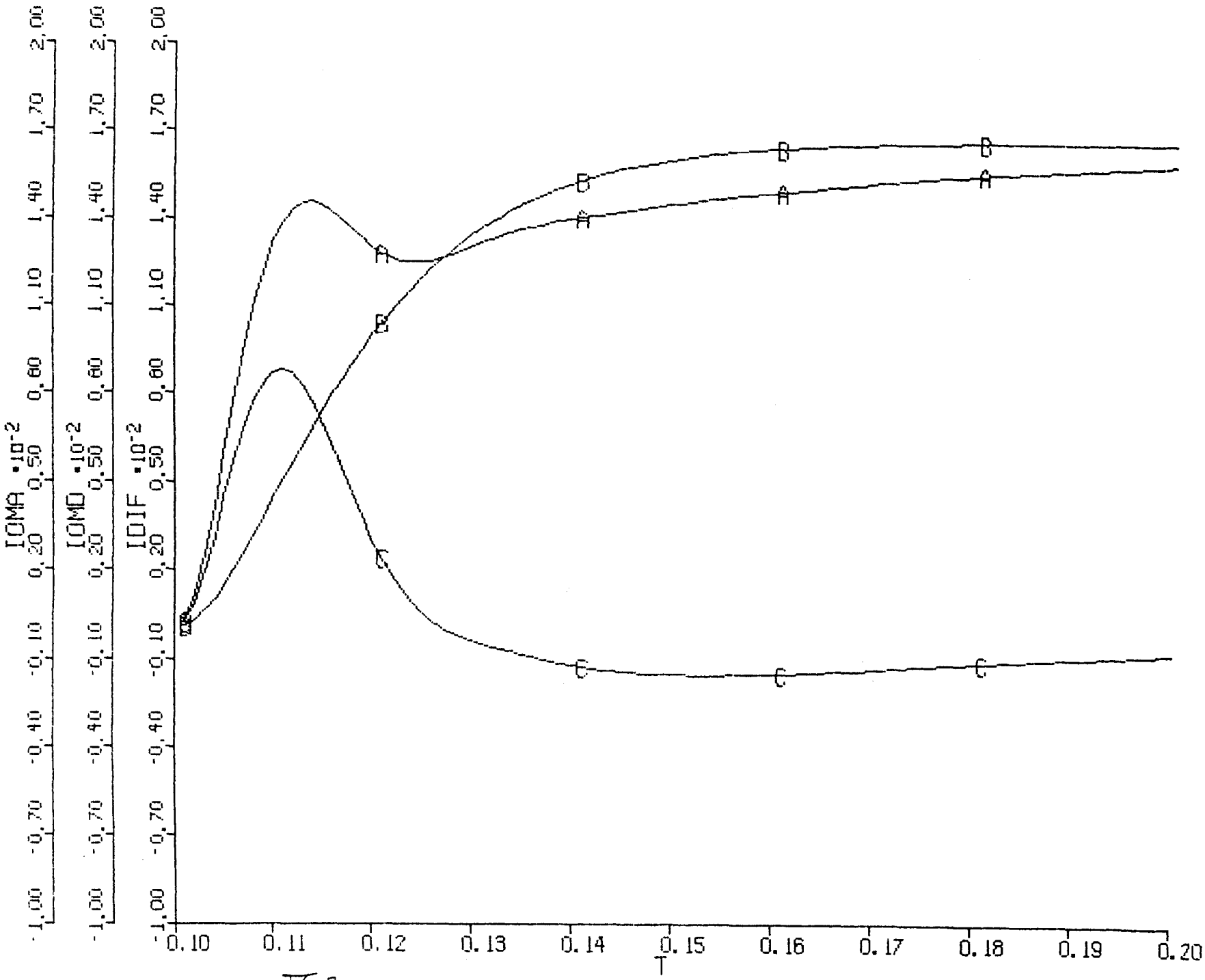
IOMA ·10^-2
IOMD ·10^-2
IOIF ·10^-2
-1.00
-0.70
-0.40
-0.10
0.20
0.50
0.60
1.10
1.40
1.70
2.00
0.10
0.11
0.12
0.13
0.14
0.15
0.16
0.17
0.18
0.19
0.20
T

V.3

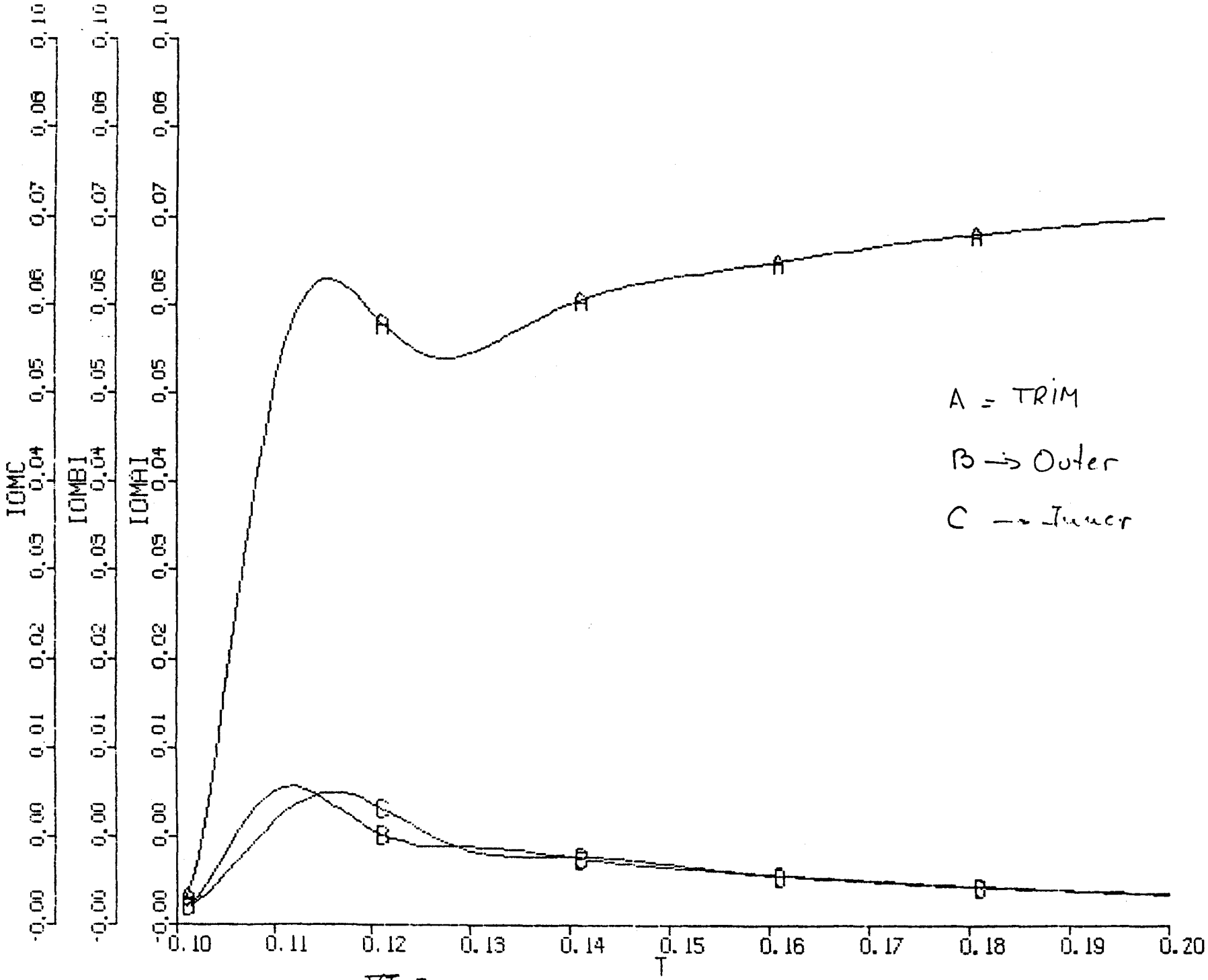
IOMC
IOMBI
IOMAI
-0.00
0.00
0.01
0.02
0.03
0.04
0.05
0.06
0.07
0.08
0.10
0.10
0.11
0.12
0.13
0.14
0.15
0.16
0.17
0.18
0.19
0.20
T
A = TRIM
B → Outer
C → Inner

VI. 2

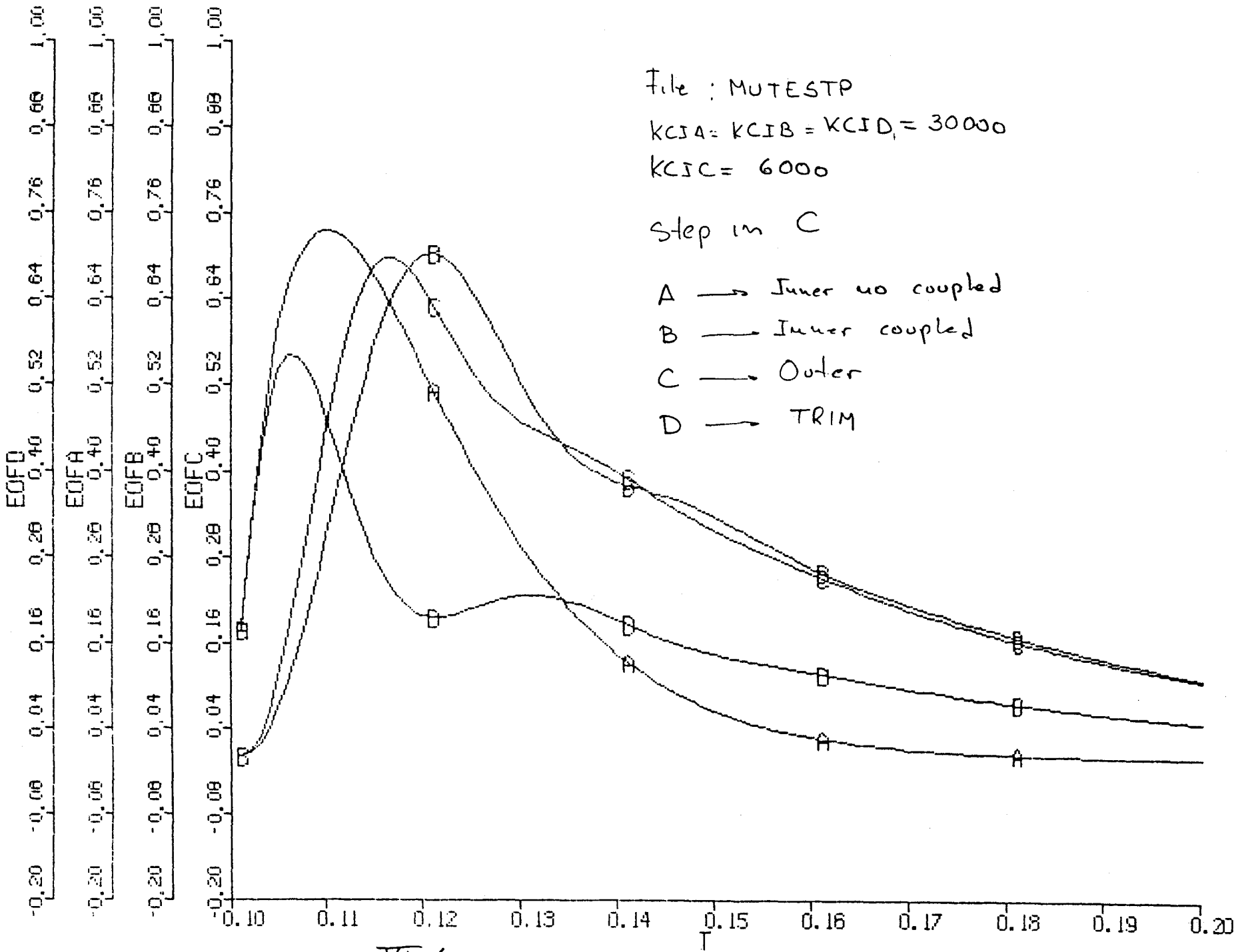
File : MUTESTP
KCIA = KCIB = KCID = 30000
KCIC = 6000
Step in C
A → Inner no coupled
B → Inner coupled
C → Outer
D → TRIM
EOFD
EOFA
EOFB
EOFC
T
-0.20
-0.08
0.04
0.16
0.28
0.40
0.52
0.64
0.76
0.88
1.00
0.10
0.11
0.12
0.13
0.14
0.15
0.16
0.17
0.18
0.19
0.20

VI. 1

APPENDIX K

DIPOLE POWER SUPPLY SYSTEM

J. ZEIGLER

6/19/85
JCZ

DIPOLE POWER SUPPLY SYSTEM

The power supply system for the Texas Accelerator Center magnet design is configured as four independent sectors per aperture. Four sectors were chosen to minimize the number of power supplies, dump switches, and current leads while maintaining adequate control of the voltages occuring during a quench. The sectors are operated independently to avoid the additional complexity of sectionalizing a series connected ring to control voltages during a full scale quench.

Each sector contains 332 half-cells consisting of a 105m dipole and either a focusing or defocusing quadrupole. The 105m dipole units are physically constructed from three 35m coil assemblies. Each coil assembly contains three coils: inner, outer, and trim. The location of these coils are shown in the cross-section of the dipole in Figure 1. The inner and outer coils generate the basic dipole field while the ratio of their currents is adjusted to correct for the sextupole field inherent to this coil geometry. The trim coil current is adjusted to correct for the decapole field which is also inherent to this coil geometry. Due to symmetry, all other lower-order multipole components are not allowed.

The major elements of the power supply system for these dipoles are shown in the schematic of Figure 2. The independent inner, outer, and trim coil currents are provided by a power supply at the center of each string of coils. The polarity of the inner coil power supply is opposite the polarity of the outer and trim coil power supplies so that the current in the common return bus is minimized.

The liquid helium refrigeration system is configured as 12 independent loops as opposed to the four sectors for the power supply system. If the power supplies for a sector are located in the service building housing a refrigerator at the center of its loop, the four main current busses must cross two refrigerator loop boundaries. This is accomplished by cryogenic feed-throughs at each end of the refrigerator loop, which correspond to the center of the string of magnets on each side of the power supply.

The power supplies are capable of ramping the magnets to the full 3 Tesla operating point in 1000 seconds. The currents required in each string of coils and the resulting return bus current during the ramp are shown in Figure 3. The inductive voltages required to provide these currents are shown in Figure 4. The stair-step effect in the voltages as calculated by the SPICE simulation package is a result of using a very coarse piece-wise-linear approximation for the current waveforms as a function of time. The actual inductive voltages would be relatively smooth curves with no discontinuities.

The current and voltage waveforms for the trim circuit require a multi-quadrant power supply to produce the desired excitation. During the first portion of the ramp the current and voltage are both positive. Near the end of the ramp, however, the current becomes negative while the voltage remains positive due to coupling from the other coils. Once steady-state operation is achieved, all inductive voltage requirements become zero and the power supply must only overcome the warm bus losses. At this point, the current remains negative while the voltage changes from positive to negative. Thus, the power supply is required to operate in three quadrants during the ramp to full field.

Dump switches are located at each power supply and at the end of each string of coils as shown in the schematic. These switches are operated each time a quench is detected in the sector, and dissipate much of the energy stored in the dipoles. The size of the dump resistors is based on the inductance of the coil strings to give a 15 to 20 second time constant for current decay in the sector. The main busses between magnets and the entire return bus are provided with enough copper stabilizer that they can withstand this current decay after a quench.

The current waveforms for a sector during a dump from full field operation are shown in Figure 5. Due to the high degree of mutual coupling between the three coils, the inner and outer coil currents decay rapidly at first as they transfer some of their energy to the trim coils. After this initial energy transfer, all three of the currents decay in a very controlled manner.

The voltage distribution across a sector for the same dump from full field operation is shown in Figure 6. In this plot, the significance of location is as follows:

LOCATION	CIRCUIT ELEMENT
0 - 5	Dump resistor at one of circuit
5 - 45	166 dipoles in series
45 - 55	Dump resistor at power supply (middle of circuit)
55 - 95	166 dipoles in series
95 - 100	Dump resistor at other end of circuit

The voltage distribution shown is at the time of maximum voltage magnitudes, occuring during the initial transfer of energy from the inner and outer coils to the trim coils. For the symmetrical dump conditions used in this case, the maximum voltage to ground is limited to less than 400 V, while the maximum voltage between coils is limited to approximately 750 V.

During a quench, individual magnets are passively protected by bypass diodes across each of the three independent coils as shown in the schematic. The trim coils require two diodes connected in inverse parallel since the current in these coils is bipolar. The bypass diodes for all three coils are installed in a liquid helium reservoir at the end of each magnet to achieve the increase in forward voltage drop associated with operation at cryogenic temperatures. As shown in Figure 7, the forward voltage drop increases as the junction temperature is decreased below 15 K. This provides a desirable characteristic requiring approximately 4 V to initiate conduction while maintaining a 1 V potential across the coil after conduction has warmed the junction temperature above 15 K.

The total installed power requirement for the main power supply system, including the quadrupole power supplies, is approximately 11 MW. The assumptions used in this calculation include:

1) All equipment is located at the surface
2) Dump switches have a 2 V drop at full current
3) Warm busses, including power leads, have a 0.5 V drop at full current
4) Power supply filters have a drop of 0.25 V/kA

Based on these assumptions, the operating power requirements at 3 Tesla are approximately 2.3 MW as shown in Figure 8. The additional power required during the 1000 second ramp is approximately 8.6 MW as shown in Figure 9. The sum of these two power requirements gives the total installed power

requirement of 11 MW for the main power supply system.

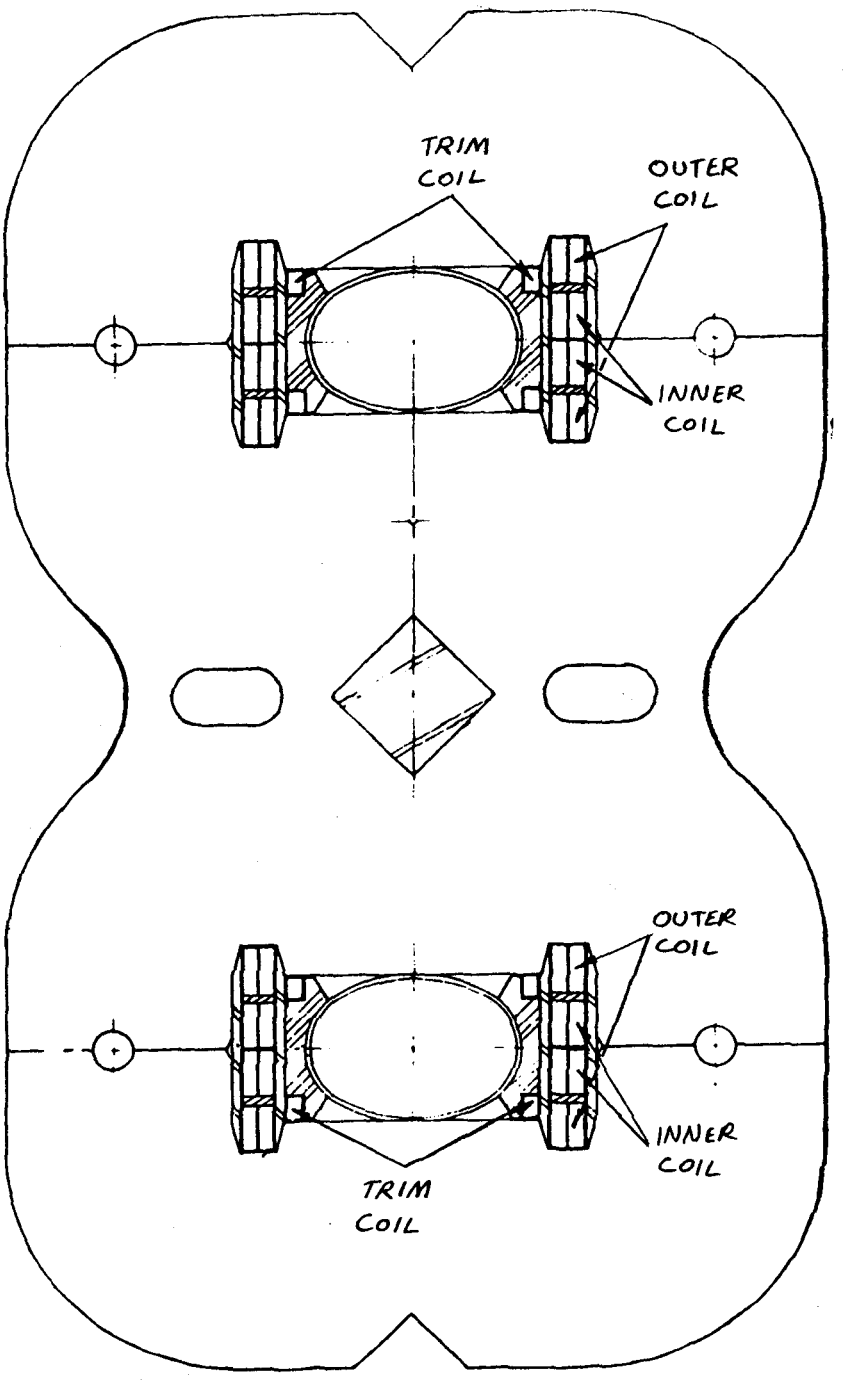

FIGURE 1. CROSS-SECTION OF DOUBLE-BORE DIPOLE

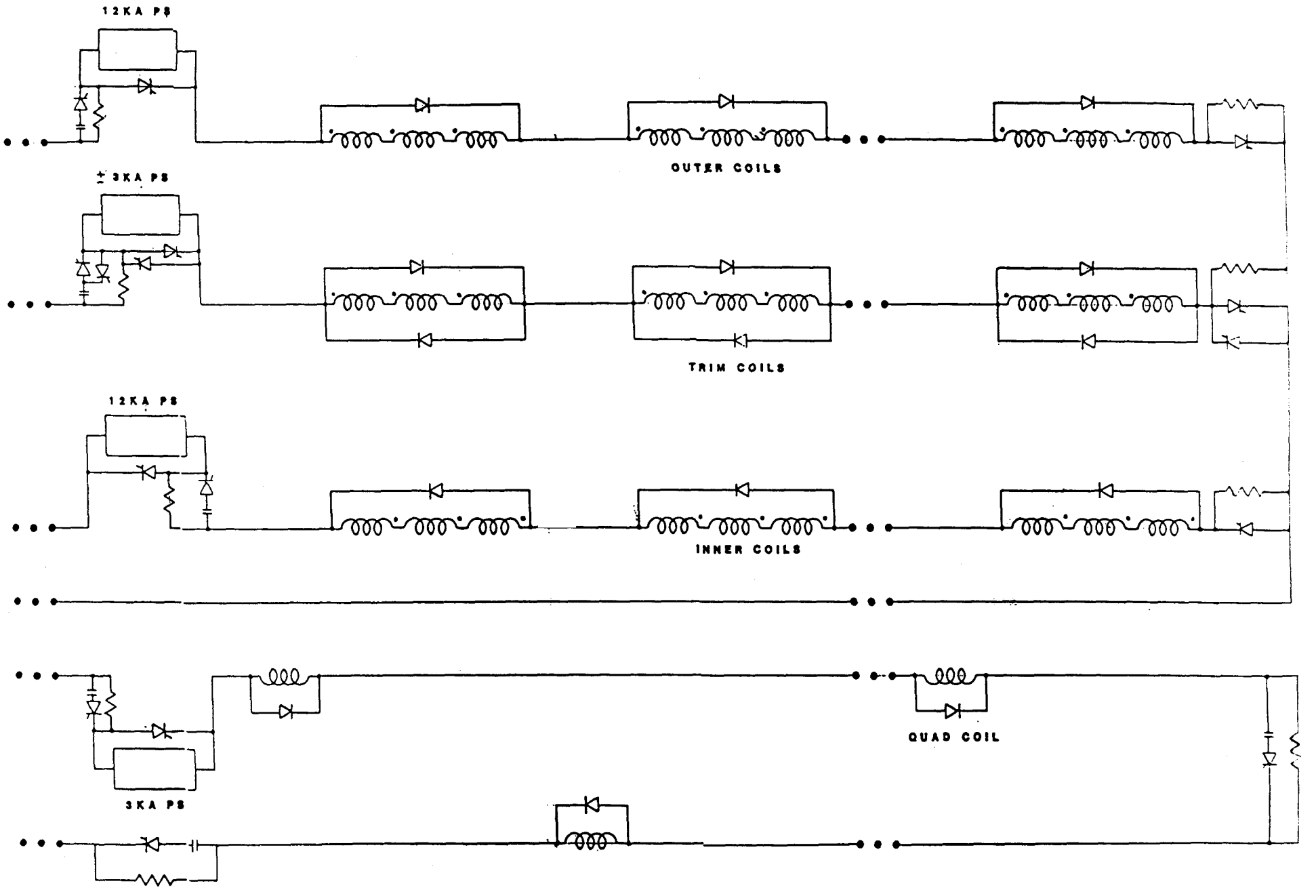

FIGURE 2. SCHEMATIC OF ONE-HALF OF POWER SUPPLY SECTOR

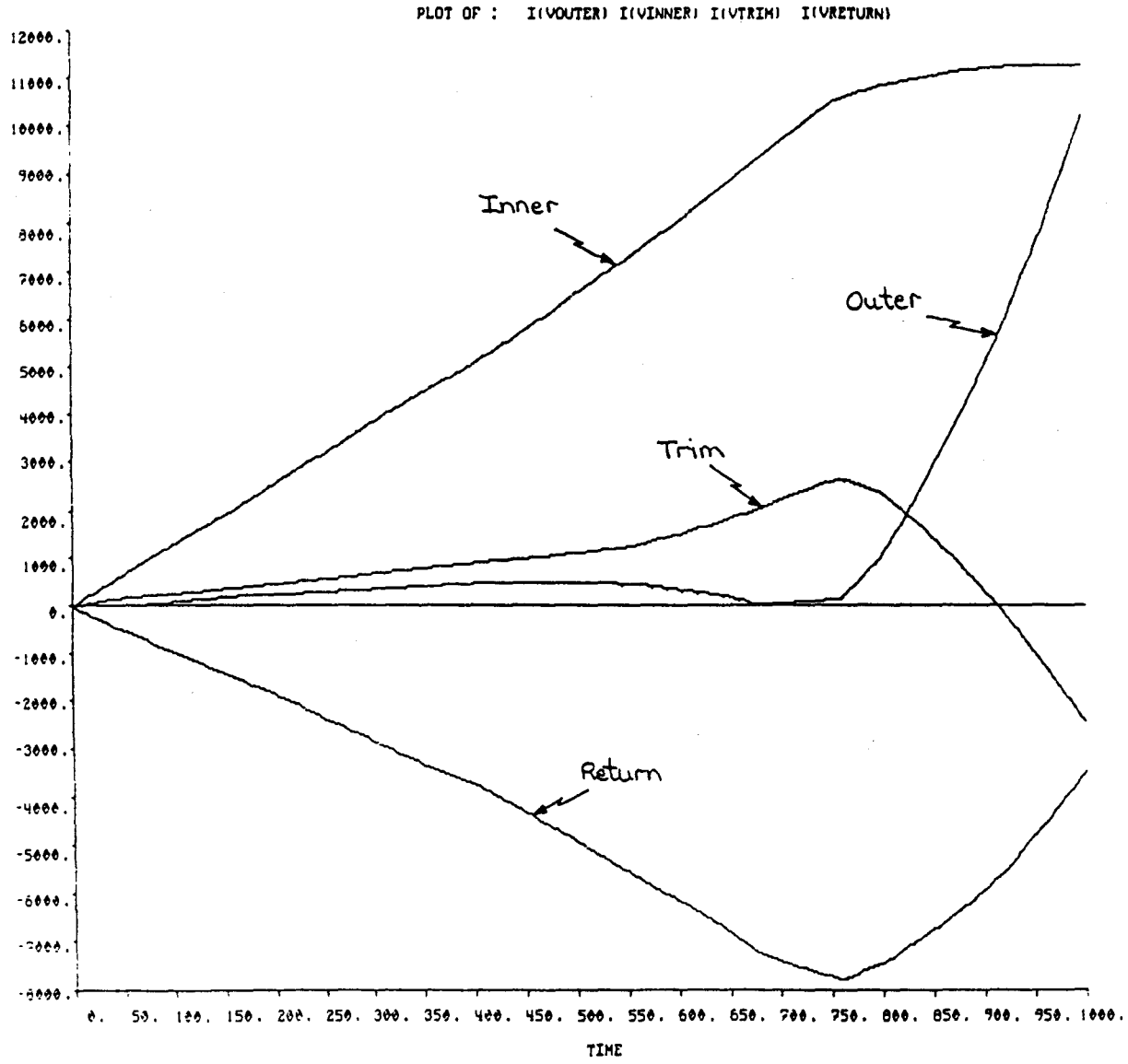

FIGURE 3. CURRENTS DURING 1000 SECOND RAMP

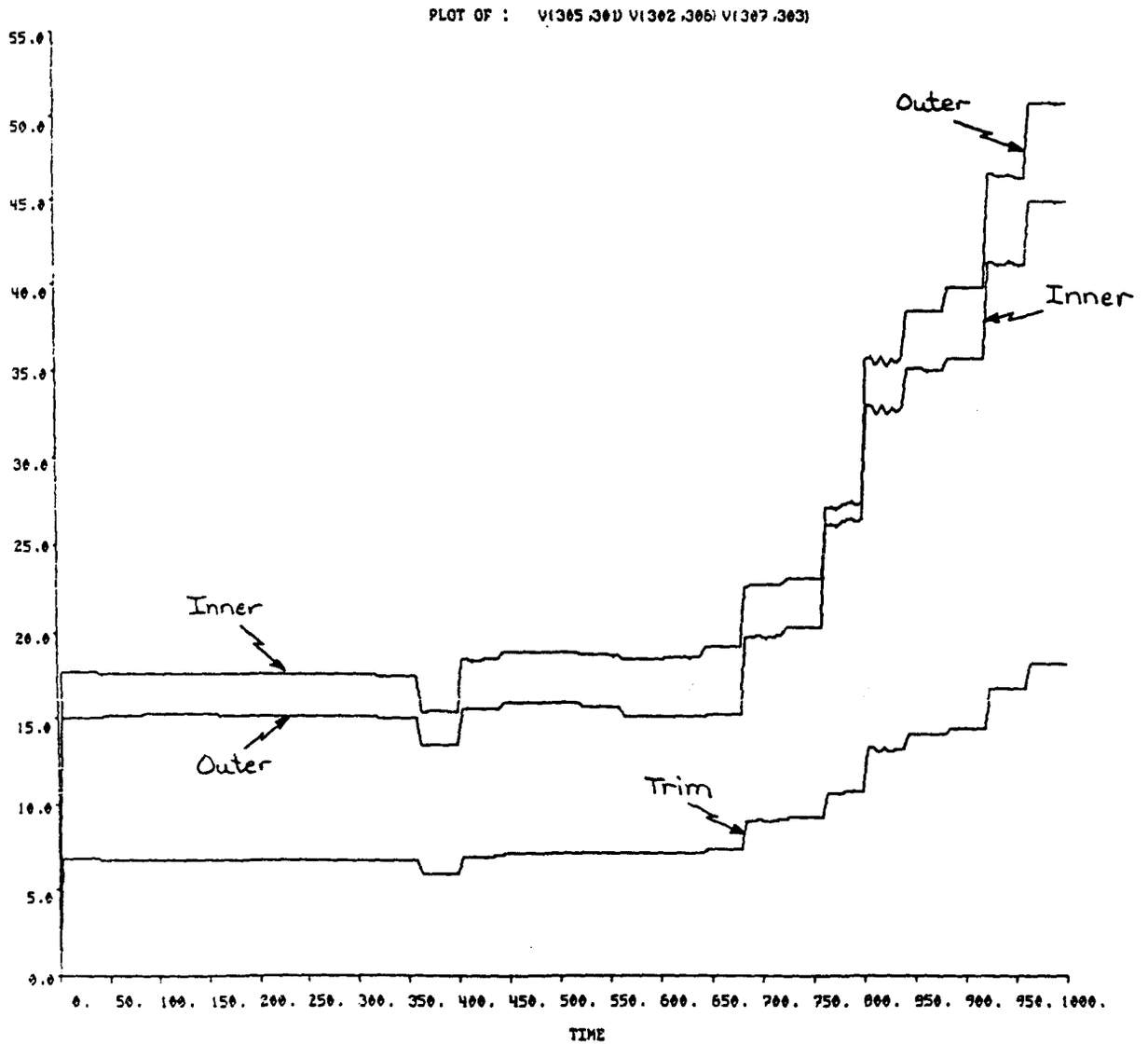

FIGURE 4. POWER SUPPLY VOLTAGES DURING 1000 SEC. RAMP

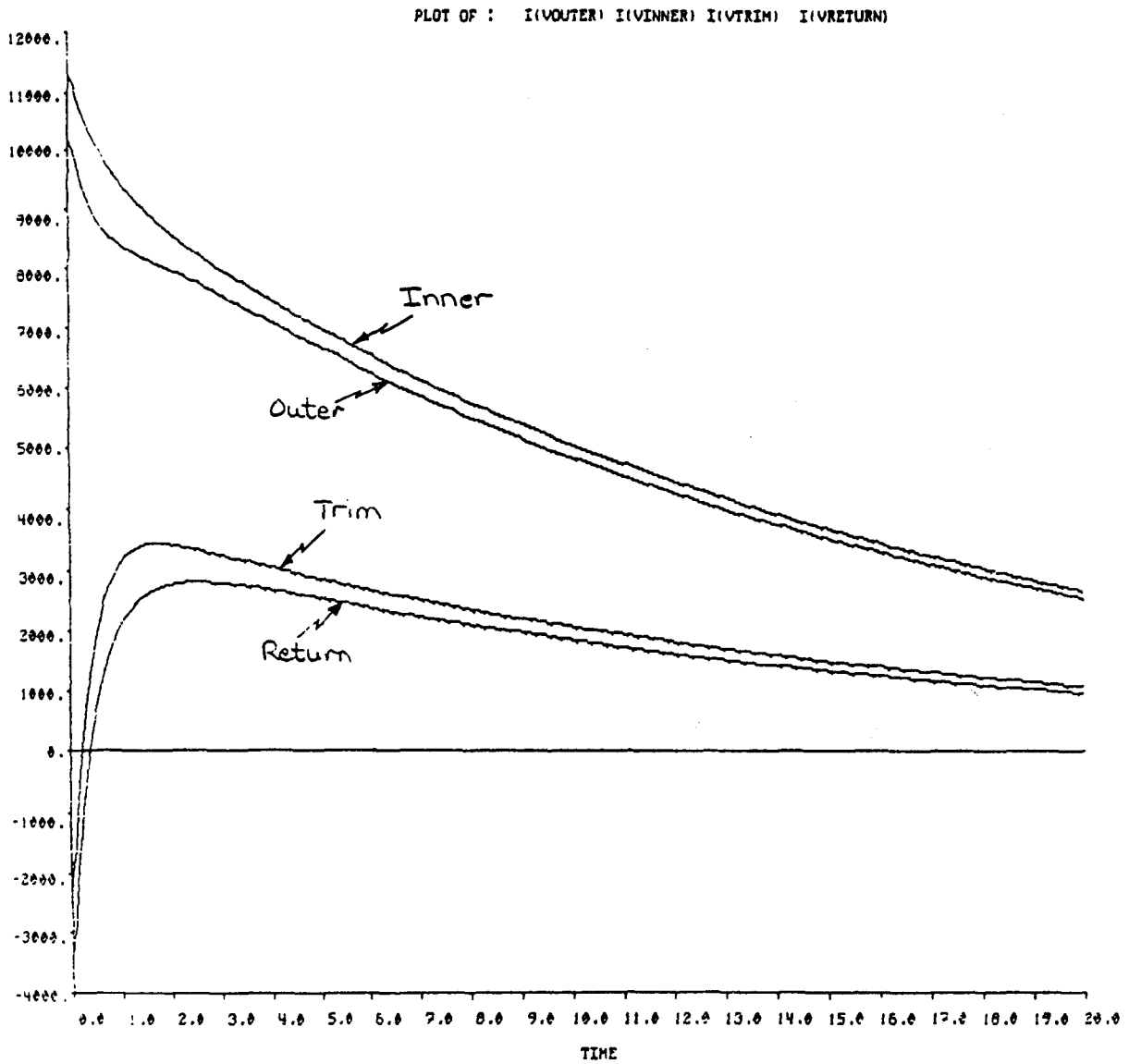

FIGURE 5. CURRENTS DURING DUMP FROM FULL FIELD OPERATION

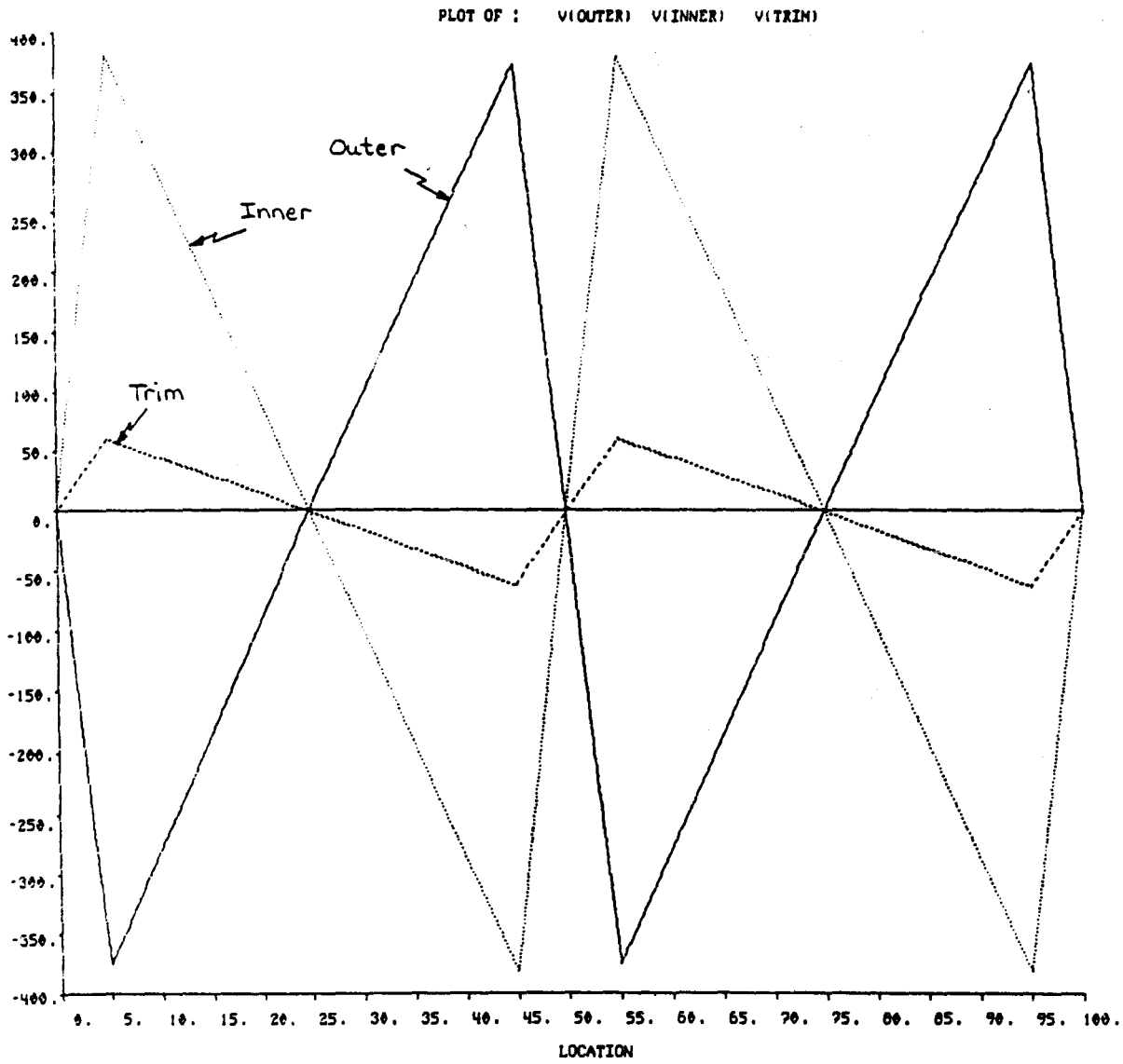

FIGURE 6. VOLTAGE DISTRIBUTION DURING DUMP FROM FULL FIELD

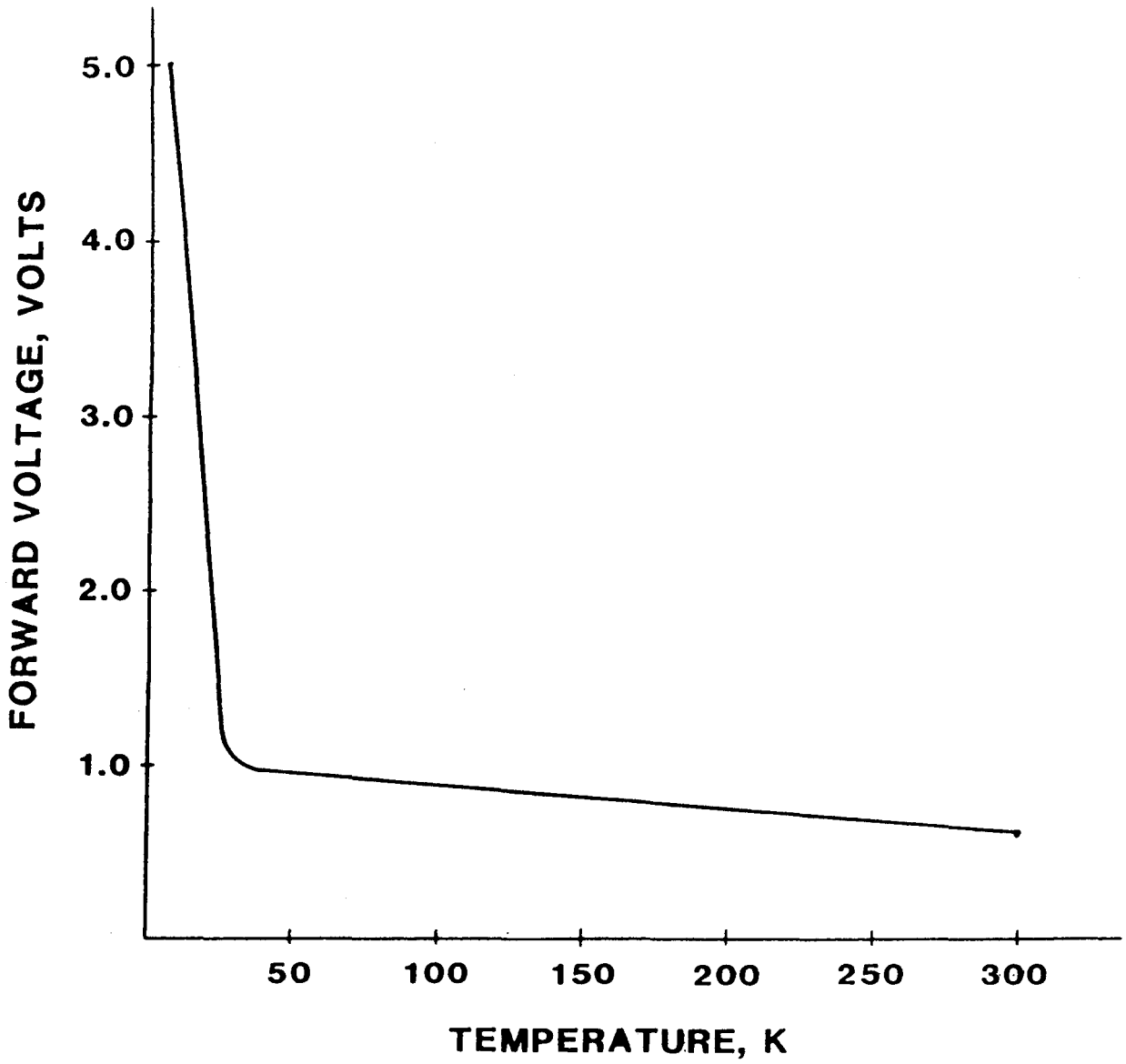

FIGURE 7. DIODE FORWARD VOLTAGE DROP

SECTOR POWER REQUIREMENTS AT 3 TESLA

COIL STRING	CURRENT (KA)	DUMP SWITCHES	WARM BUSSES	FILTERS	POWER (MW)
INNER COILS	11	3 * 2V	4 * 0.5V	1 * 2.75V	0.118
OUTER COILS	10	3 * 2V	4 * 0.5V	1 * 2.5V	0.105
TRIM COILS	2.5	3 * 2V	4 * 0.5V	1 * .625V	0.022
RETURN BUSS	3.5	-	2 * 0.5V	-	0.004
QUAD COILS	3	4 * 2V	8 * 0.5V	1 * .75V	0.038
POWER (MW)		0.165	0.063	0.059	0.287

TOTAL POWER AT 3 TESLA = 0.287 MW * 4 SECTORS * 2 BORES

= 2.3 MW

Figure 8. Power requirements during 3 Tesla operation

SECTOR POWER REQUIREMENTS DURING 1000 SEC RAMP

COIL STRING	CURRENT (KA)	INDUCTIVE VOLTAGE	POWER (MW)
INNER COILS	11	45	0.495
OUTER COILS	10	50	0.500
TRIM COILS	2.5	20	0.050
QUAD COILS	3	10	0.030
POWER (MW)			1.075

TOTAL POWER DURING 1000 SEC RAMP = 1.075 MW * 4 SECTORS * 2 BORES

= 8.6 MW

Figure 9. Power requirements during 1000 second ramp

Appendix L

Gary Cottingham
Brookhaven National Laboratory
902B, 17 Cornell
Upton, LI, New York 11973

Don Hartill
Cornell University
SSC Department
Ithaca, NY 14850

William Hassenzahl
Lawrence Berkeley Laboratory
Bldg. 46-161
Berkeley, CA 94720

Karl Koepke
Fermi National Accelerator Laboratory
P.O. Box 500
Batavia, IL 60510

Hal Krause
EG&G
P.O. Box 1625
Idaho Falls, Idaho 83401

Peter Limon
Lawrence Berkeley Laboratory
SSC-CDG
Bldg. 90-4040
Berkeley, CA 94720

Gustavo Lopez
Texas Accelerator Center
2319 Timberloch Dr.
The Woodlands, TX 77380

Al Prodell
Brookhaven National Laboratory
902B, 17 Cornell
Upton, LI, NY 11973

Gerry Tool
Fermi National Accelerator Laboratory
P.O. Box 500
Batavia, IL 60510

Toshiharu Tamanaka
Texas Accelerator Center
2319 Timberloch Dr.
The Woodlands, TX 77380

John Zeigler
Texas Accelerator Center
2319 Timberloch Dr.
The Woodlands, TX 77380

Mohamed Hilal
General Dynamics
P.O. Box 85357
San Diego, CA 92138